Motion Planning for Multi-Spacecraft Interferometric Imaging Systems

by

Islam I Hussein

A dissertation submitted in partial fulfillment
of the requirements for the degree of
Doctor of Philosophy
(Aerospace Engineering)
in The University of Michigan
2005

Doctoral Committee:

Professor Anthony M. Bloch, Co-Chair
Associate Professor Daniel J. Scheeres, Co-Chair
Professor N. Harris McClamroch
Professor David C. Hyland

Dedicated to Ibrahim, Soheir and Amira

ACKNOWLEDGEMENTS

First and foremost I wish to thank my parents, Ibrahim and Soheir, for they have endured quite a lot to secure me and my sister, Amira, the best education available to us. To all three of them that this work is dedicated. My advisors, Professors David C. Hyland, Daniel J. Scheeres, Anthony M. Bloch and Harris McClamroch, have offered me both the best mentorship a PhD student may ask for and the best moral support.

I would like express my gratitude to Professor Dennis Bernstein. It is always a great pleasure to discuss matters of science with him. I have been blessed with the academic support of Professor Brent Gillespie at the University of Michigan for his guidance and for instilling in me deeper appreciation of that most wonderful subject "Dynamics." I also wish to thank Professor Peter Crouch at Arizona State University and Professor Peter Gorham at the University of Hawaii for their scientific input.

The department staff has offered huge support over the years. I especially extend my warmest gratitude to my "Michigan Mom" Margaret Fillion. Margaret: you have and will always be a wonderful friend. Thank you! I also thank Tom, Debbie, Heidi, Denise, Michelle, Suzanne and Chris.

I also wish to thank my officemates over the years: Tobin, Suman, Rajeeva, Matt and, most recently, Sharyl. I have enjoyed wonderful discussions with them, both technical and non-technical. I have also enjoyed the company and friendship of many other graduate students at the Department of Aerospace Engineering. I wish I had

the opportunity to get acquainted with them earlier in my PhD career. I especially remember the Space Brooms, for a lack of a more descriptive name for a bunch of aerospace engineering students playing broomball! To Dan, Julie, Marci, Kooj, Steve, Erin, Rob and Matt I say "I wish we had won that last game and gone to the final." Next year is not too far away. I also wish to acknowledge others at the department: Leigh, Leo, Jesse and many others.

The financial support of NASA's Office of Space Science and the National Science Foundation is gratefully acknowledged.

TABLE OF CONTENTS

LIST OF FIGURES

Figure

LIST OF TABLES

Table

LIST OF APPENDICES

APPENDIX

CHAPTER 1

Introduction

1.1 Motivation

There is much interest in using multiple spacecraft formations for interferometric imaging. The advantages such formations offer include replacement of large monolithic telescopes, superior angular resolution and the possibility of reconfiguration for different imaging goals. These architectures can provide the order-of-magnitude advances in optical angular resolution via long baseline interferometry that are sought for various NASA missions, such as the Origins program ([1, 2, 3]), and high resolution Earth imaging.

Interferometric imaging is performed by measuring the mutual intensity (the two point correlation as defined in [4]) that results from the collection and subsequent interference of two electric field measurements of a target made at two different observation points. While moving relative to each other, the satellites collect and transmit these measurements, which are later combined at a central node using precise knowledge of their locations and timing of data collection. A least squares error estimate of the image can be reconstructed given the mutual intensity measurements, parameters of the optical system, and the physical configuration of the observatory.

To assess the quality of the reconstructed image, the reconstructed image is

Fourier transformed into a two dimensional plane of spatial frequencies (the wave number plane.) At any given point on the wave number plane, the modulation transfer function (MTF) is defined as the ratio of the estimated intensity to the true image intensity. For an interferometric imaging constellation, the MTF can be computed given the measurement history and corresponding relative position data between the light collecting spacecraft. In the wave number plane, a point with a zero MTF value implies that the system is "blind" to the corresponding spatial frequency, while a large value of the MTF implies that the image signal can be restored at that wave number via an inverse Fourier transform (see [5, 6, 4, 7].) The MTF, as a measure of the imaging system's performance, is a function of both the optical system and the configuration of the observatory in physical space.

This dissertation aims at obtaining a model for the MTF that, ultimately, relates the quality of the reconstructed image to the motion of the (multi-spacecraft) observatory's motion in space. Once such a characterization is achieved, one now has a criterion (namely, the MTF) that can be used to design the motion of the observatory to achieve improved image quality.

Multi-spacecraft formations may be classified into two categories. The first category is the set of all free-flying spacecraft formations, where the inter-spacecraft relative positions is allowed to change with time. The key question is: How do we design the motion of the formation such that the accumulated MTF is equal to or as close to unity as possible? In this dissertation, this question is posed in a geometric optimal control setting by optimizing over image quality (with the MTF as the criterion) and fuel expenditure. We do this for the general case where we have N spacecraft evolving on a general manifold in Chapters 2 and 3. In Chapters 4 and 6 we focus on the dual spacecraft problem and manage to explicitly solve for the global

optimal solution to the problem for a class of spiraling formations.

The second category is that of rigid formations, where inter-spacecraft positions are fixed in magnitude. This problem is extensively studied in Chapter 7. There we propose an N spacecraft formation in a circular Earth orbit (or any circular orbit in general.) The design is cast in a dimensionless setting and may, thus, be applied to a wide range of applications, from imaging in the radio frequency range to the visible spectrum range. Further studies explore the effect and utilization of the perturbation J_2. Due to its simplicity, this class of rigid formations has great prospects for implementation in future NASA missions under the Origins Program [1].

1.2 Literature Review

For an extensive literature survey of formation flying for imaging applications we refer the reader to the comprehensive survey paper by Scharf et. al. [8]. The dynamics and control of spacecraft formations have been given considerable attention in the past. In these studies, investigators assume certain prescribed motions that satisfy some imaging objective and then seek to achieve these motions via active control. For example, in [9] the authors derive nonlinear and linear spacecraft relative position dynamics and develop a controller design framework for linear control of spacecraft relative position dynamics with guaranteed closed-loop stability. In [10], the authors consider the full nonlinear relative position control problem using a Lyapunov-based, nonlinear, adaptive control law that guarantees global asymptotic convergence of the position tracking error in the presence of unknown, constant, or slowly-varying spacecraft masses, disturbances, and gravity forces.

The problem of rotating a satellite constellation using an adaptive controller

with actuator saturation constraints is discussed in [11]. An experimental study of synchronized rotation of multiple autonomous spacecraft with rule-based controls is presented in [12]. The authors in [13] derive control laws to synchronize formation rotation as well as to control its attitude. In [14], the problem of rotating a constellation using on/off thrusters while maintaining the relative distances within a specified tolerance is addressed. Fuel related problems, such as optimal fuel consumption during a rotation maneuver [15] or constellation reorientation with uniform fuel expenditure and conservation across the constellation [16], have also been addressed.

Natural orbital dynamics have also been exploited for interferometric observatories [17, 18, 19, 20]. In [21], the authors design a controller for formation keeping in circular orbit and in [22] for formation keeping during a spiral maneuver while in orbit. In [23] the dynamics of spacecraft formation is considered under the influence of J_2 orbit perturbations, where J_2 invariant orbits are sought for the motion. In [24] the authors design controllers for formation keeping using mean orbit elements, as opposed to spacecraft positions and velocities, as the state of the system. Finally, GPS utilization for spacecraft constellations is discussed in [25, 26] and in [27, 11, 28] the authors propose decentralized controllers for spacecraft formations.

The use of geometric control methods for spacecraft formation flying has received little attention, whereas extensive investigations have been conducted in the field of robotic path planning (for more on this issue, see Section (IV) in [8].) This work is an attempt to use geometric optimal control theory for spacecraft formation motion planning for imaging applications.

The question of which formation motions yield satisfactory imaging goals has not been discussed in any of the above mentioned research with the exception of [5, 18, 19, 20, 29]. In this paper we present a framework such that spacecraft motion

planning and controller design meet desired imaging objectives.

While extensive investigations have been conducted in the field of robotic path planning, the use of geometric control methods for spacecraft formation flying has received very little attention (see Section (IV) in [8].) We attempt in this dissertation to use geometric optimal control theory for spacecraft formation motion planning for imaging applications. Formulating the motion planning problem in an optimal control setting, we mainly rely on the use of variational approaches to analyze optimal control problems on generalized Riemannian manifolds. This approach is based on the work accomplished since the 1989 paper by Noakes et. al. [30], where they derived necessary conditions for second order dynamic optimal control problems on Lie groups. In the 1990s, Peter Crouch and his group at Arizona State University have developed this result to generic abstract manifolds for higher order dynamic problems in the papers [31], [32], [33], [34] and [35], with application to aircraft optimal control and control on compact Lie groups. In the present thesis, we build on their theoretical work and apply the results to the formation flying problem.

For a more exhaustive literature review, the reader may wish to consult the paper [8]. In addition, more references are usually provided in the main body of the thesis, where we also contextualize these results and relate them to the formation flying problem as well as other related problems in robotics, control of rigid bodies and even computer graphics.

1.3 Dissertation Outline

The dissertation is organized as follows. In Chapter 2, the basic imaging system is described in detail. The assumptions made in this work are stated and, based on the given assumptions and system model, a mathematical model for the Modulation

Transfer Function (MTF) of a multi-spacecraft formation is derived. An optimal control problem is formulated with image quality, to be maximized, directly used as an objective in the performance index. Necessary optimality conditions are derived. These necessary conditions result in a feedback control law that has image quality as a state of the system and the corresponding error in image quality (defined as the difference between the value of the MTF and a given constant function) appearing in the feedback loop. Some examples are given in one- and two-dimensions to illustrate the formulation.

Based on the inferences achieved in Chapter 2, in Chapter 3 we formulate a new class of optimal control problems called dynamic coverage optimal control. Here an optimal control problem is formulated to capture the main goals of an imaging formation: minimizing fuel expenditure, maximizing signal-to-noise ratio and maximizing coverage of the resolution disc. As opposed to being posed in terms of variables that lend themselves to image quality and the optical domain (such as the MTF), the dynamic coverage problem is posed completely in terms of the state space of the system. That is to say, maximizing signal-to-noise ratio is achieved by minimizing inter-spacecraft relative velocities. To maximize coverage of the resolution disc, we attempt to maximize the number of relative position states assumed by the formation. In this chapter, we derive the necessary conditions for optimality and show that a necessary condition for optimality of a planar formation motion is that it is symmetric about the origin.

In Chapters 4 and 6, we specialize the discussion to dual spacecraft formations. In Chapter 4 we first look at treating each spacecraft as a rigid body and formulate the dynamic coverage optimal control problem (restricted to formation maneuvers that already achieve coverage, which we call the set of "successful maneuvers.") The

cost function is generalized to include optimizing over fuel consumption, deviation of rotational and translational velocities from a given desired value and, finally, the deviation of the configuration of the spacecraft from a given desired trajectory. The analysis is performed entirely in free coordinates on the group of rigid body motions SE(3). A simple example on SE(2) that is motivated by dual spacecraft interferometry is given. This example illustrates how difficult that problem is to solve even for the two dimensional case. Still, the methodology and approach are novel and offer new results for coordinate-free trajectory tracking on SE(3).

Based on the conclusion in Chapter 4, in Chapter 5 we specialize the analysis to formations of two spacecraft, each modeled as a point particle. We derive necessary conditions for minimizing the cost function for a trajectory that evolves on a (virtual) Riemannian manifold (such as a paraboloid) and satisfies a second order differential equation together with some interpolation, smoothness and motion constraints. The cost function we consider is a weighted sum of the norm squared of the thrust (to minimize fuel expenditure) and the norm squared of the velocity (to improve signal-to-ratio.) In the mathematical literature this problem is know as the τ-elastic dynamic interpolation problem and, as we show in the chapter, is also motivated by space-based interferometric imaging applications. We define the dynamic interpolation problem, derive necessary conditions for an optimal solution and point out the interesting connection between the dynamic interpolation problem and imaging applications, which is the main contribution of this chapter.

The illustrative example we give in Chapter 5 is a dual spacecraft formation, where the collector spacecraft is constrained to evolve on a virtual spherical surface. In an imaging formation, however, the collector is required to move on a virtual paraboloidal surface [36]. Hence, in Chapter 6 we focus our attention on the dual

spacecraft formation where the collector spacecraft is constrained to evolve on a virtual paraboloidal surface (for improved optical focusing properties) while satisfying a spiraling constraint to achieve frequency domain coverage. In this chapter we first introduce a class of spiral motions that satisfies imaging objectives and seek simple solutions to the problem of motion design and control of a formation for imaging applications. Based on the observations drawn from these simple controls, an optimal control problem is formulated for the proposed class of spiral motions to achieve minimum fuel consumption, while satisfying imaging constraints. We then formulate an optimal control problem to minimize fuel consumption and further maximize image quality by minimizing the relative speed, which is proportional to the signal-to-noise ratio of the reconstructed image. We use the maximum principle to derive the necessary optimality conditions and show that they are also sufficient and that the resulting control law is unique. Finally, we apply a continuation method to solve for the unique optimal trajectory.

In Chapter 7, we propose a novel class of satellite constellations that can act as interferometric observatories in Low Earth Orbit (LEO), capable of forming high resolution images in time scales of a few hours without the need for active control. An optimization procedure is also defined that supplies m pixels of resolution with a minimum number of satellites. For the example considered, this procedure results in an observatory that is within 0-2 satellites from a lower bound of $\sqrt{m}$ satellites. We introduce a linear imaging constellation and formulate a concise 0-1 mathematical program, the solution of which is the solution to optimal aperture configuration for full coverage of the wave number plane. The effect of eccentric spacecraft trajectories and gravity field J_2 perturbations on wave-number plane coverage are then considered. Conditions for complete wave-number plane coverage are

found for certain classes of orbit perturbations. This analysis leads to design criteria for interferometric observatories that ensure wave-number plane coverage as a function of perturbation strength. We also address short-period J_2 perturbations and derive expressions for in-plane perturbations in position as a function of the orbital elements and obtain an upper bound for the magnitude of the perturbed in-plane position vector. Finally, we adjust the nominal observatory design in such a way as to guarantee full coverage of the u-v plane under general eccentricity perturbations and short-period J_2 effects.

Final remarks, conclusions and open research problems are addressed in Chapter 8.

Finally, in the appendices we provide some background information on geometric mechanics and geometric optimal control theory. In Appendix A we review basic definitions and results from geometric mechanics that are used in Chapters 3 and 5. We also make references to the necessary basic text and literature. In Appendix C, we extend the work in Chapter 5 on the dynamic interpolation problem to the case when a gravitational field is acting on the manifold. In Appendix D we investigate optimal control of under-actuated systems with application to Lie groups. An important application of the result provided in the appendix is the control of under-actuated spacecraft.

1.4 Thesis Contributions

Here are the main contributions of this thesis:

MTF and Image Quality-Dependent Feedback Control The first contribution is the derivation of the MTF and using it to directly derive a controller that is a function of image quality in the optimal feedback control law. See Chapter

2.

Dynamic Coverage Optimal Control Problem We use geometric optimal control theory to study spacecraft formation motion control for imaging applications. The problem formulated is called dynamic coverage optimal control and is treated in Chapter 3.

Constrained Optimal Trajectory Tracking on SE(3) Constrained Optimal trajectory tracking of a single rigid body on SE(3) and its subgroups is treated in Chapters 4 and 5 on $\mathbb{R}^3$ and Appendix A for SO(3).

Solving the Spiraling Dual Spacecraft Formation Problem The problem of optimally controlling a spiraling dual spacecraft formation on a paraboloid is treated in Chapter 6.

Multi-Spacecraft Earth Orbiting Observatories A novel design and analysis of a new class of interferometric observatories in Earth orbit is treated in Chapter 7.

These contributions can also be found in the following publications.

Journal Papers

1. I. I. Hussein, D. J. Scheeres, and D. C. Hyland. Interferometric observatories in earth orbit. *Journal of Guidance, Control and Dynamics*, Vol. 27, No. 2, pp. 297–301, 2004.

Conference Proceedings and Presentations

1. I. I. Hussein and A. M. Bloch. Optimal control of under-actuated systems with application to Lie groups. *2005 American Control Conference*, Portland, OR, 2005. To appear.

2. I. I. Hussein and A. M. Bloch. Dynamic coverage optimal control for interferometric imaging spacecraft formations (part II): The nonlinear case. *2005 American Control Conference*, Portland, OR, 2005. To appear.

3. I. I. Hussein, A. M. Bloch, D. J. Scheeres and N. H. McClamroch. Optimal fuel-image motion planning for a class of dual spacecraft formations. *2005 American Control Conference*, Portland, OR, 2005. To appear.

4. I. I. Hussein, D. J. Scheeres and D. C. Hyland. Optimal formation control for imaging and fuel usage. *2005 Space Flight Mechanics Meeting*, paper AAS 05-160, 2005.

5. I. I. Hussein and A. Bloch. Dynamic coverage optimal control for interferometric imaging spacecraft formations. *43rd IEEE Conference on Decision and Control*, pp. 1812-1817, December 2004.

6. I. I. Hussein and A. Bloch. Optimal control on Riemannian manifolds with potential fields. *43rd IEEE Conference on Decision and Control*, pp. 1982-1987, December 2004.

7. I. I. Hussein and A. Bloch. Dynamic interpolation on Riemannian manifolds: An application to interferometric imaging. *2004 American Control Conference*, pp. 413-418, July 2004.

8. I. I. Hussein and D. J. Scheeres. Effects of orbit perturbations on a class of earth-orbiting interferometric observatories. *2004 AAS/AIAA Space Flight Mechanics Meeting*, paper AAS 04-210, February, 2004.

9. I. I. Hussein, D. J. Scheeres, and D. C. Hyland. Control of a satellite formation for imaging applications. *2003 American Control Conference*, pp. 308-313, June 2003.

10. I. I. Hussein, D. J. Scheeres, and D. C. Hyland. Formation path planning for optimal fuel and image quality for a class of interferometric imaging missions. *2003 AAS/AIAA Space Flight Mechanics Meeting*, paper AAS 03-174, February, 2003.

11. I. I. Hussein, D. J. Scheeres, and D. C. Hyland. Interferometric observatories in earth orbit. *2003 AAS/AIAA Space Flight Mechanics Meeting*, paper AAS 03-172, February, 2003.

Journal Papers under Review

1. I. I. Hussein and D. J. Scheeres. J_2 correction for a class of Earth-orbiting interferometric observatories. *The Journal of Astronautical Sciences*, 2004.

1.5 Remarks

What is covered in this dissertation? As discussed in Chapter 2, the most important assumption made in the present work is that the target is "sufficiently" far away from the observatory. This makes the present work applicable to exo-solar imaging. Depending on the desired resolution, the formation designs proposed in this dissertation may be made applicable to, say, Earth imaging from low Earth orbits. Though the mathematical derivation is different for near-target imaging, the conceptual approach is identical and, as discussed in the present work, the proposed designs are scalable to suit various (close and far range) imaging applications. It is important to note that the proposed designs are guaranteed only for far range targets and none are provided for near range target imaging, though we do not discard this possibility.

Notation We have tried to unify notation as much as we can. For instance, we use the same variable definitions across all chapters and appendices. Bold-faced variables indicate vectors or covectors. Scalars are denoted by italic Greek and Latin symbols. Still, to every rule there is an exception and exceptions will arise due to, for example, a conflict between present notation and conventional notation used in the literature. This is especially true in Chapter 4 and A, where, in order to conform with the more than a century-long history of Lie group notation, we have opted to use, say, the italic (non-bold) symbol g to denote position in configuration space, whereas a configuration variable in the rest of the dissertation is usually denoted by the bold-faced variable $\mathbf{q}$.

Much of our analysis depends on the choice of an appropriate metric for the space under consideration. In this dissertation, we use inner products on function space,

$\mathbb{R}^n$, a Lie group G or, more generally, a manifold M. In most instances, we explicitly state or define the inner product used. Often times, we assume that the choice of inner product is inferred from the context.

CHAPTER 2

Optimal Formation Control for Imaging and Fuel Usage

The Modulation Transfer Function (MTF) is a function over the two dimensional spatial frequency domain defined as the ratio of the reconstructed image intensity to the true image intensity. Given knowledge of the MTF, we are able to obtain the true image intensity from the current reconstructed image intensity. In this chapter we precisely define and derive the MTF and show its dependence on the motion of a sparse system of N telescopes. This formulation includes a noise model to represent contamination of the optical signal and is used to define a cost function for an optimal control problem including imaging and fuel performance measures. We derive the necessary optimality conditions for a generic multi-spacecraft formation and specialize them to a two-spacecraft formation. We show that the optimal solution must be symmetric about the origin of the coordinate system and that its center of mass must be fixed in space. Simulation results are provided to further investigate this control law. This work is fundamental to current and future work related to motion path planning of separated spacecraft interferometric missions used for the imaging of astronomical targets.

In Section (2.1) of this chapter we derive the MTF of a constellation of N space-

craft interacting together in an interferometric imaging mission. In Section (2.2) we postulate a noise model to augment the derived MTF model for the measurements. In Section (2.3) we formulate an optimal control problem to maximize the MTF over the resolution disc and use the Pontryagin's maximum principle to derive the necessary optimality conditions. In Section (2.4) we specialize the result to the two spacecraft formation control problem and in Section (2.5) we give examples to test the optimal control laws and illustrate the ideas presented in earlier sections. In Section (2.6) we further specialize the analysis and provide a solution to the two spacecraft, one-dimensional problem. Finally, in Section (2.7), we conclude the chapter with a few final remarks and discuss future research directions.

2.1 The Imaging Problem and the Modulation Transfer Function

Refer to Figure (2.1). Let σ denote an extended incoherent source, whose effective dimension is given by d. Let $\mathbf{q}' = (x_Q, y_Q, 0)$ and $\mathbf{q} = (x_P, y_P, \bar{z} + \zeta_P)$ be the position vectors of a point Q on the image plane I and a point P on the observation surface O', respectively. The image plane I is the plane on which an image of σ is reconstructed and is set to be coincident with the x-y plane of our coordinate system, which is centered, say, at the geometric center of σ. On the other hand, the observation surface O' is one on which the constellation evolves and is located at a distance $\bar{z}$ from I. The observation *plane* is a plane through O', on which we project the motion of the constellation to be used in later analysis. Let D denote the effective dimension of the constellation, d denote the effective size of the target σ and A_T denote the aperture area. We need the following assumptions in this chapter.

Assumption 2.1.1. The aperture area A_T is much smaller than the size of the

constellation. In other words, $A_T \ll D^2$.

Assumption 2.1.2. The observation plane O is sufficiently far away from the target σ. In other words, $D/\bar{z} \ll 1$ and $d/\bar{z} \ll 1$.

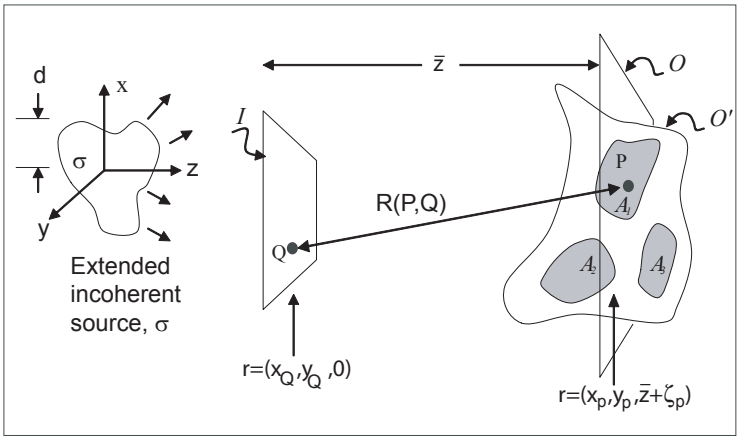

Figure 2.1: The basic imaging situation.

The main objective of the imaging constellation is to reconstruct the light intensity distribution deposited by σ on I using light collected in a set of regions $\mathcal{A}_1, \mathcal{A}_2, \ldots, \mathcal{A}_N$, which represent the entry pupils of the separated telescopes and N is the number of apertures in the system.

Consider one polarization state and let U denote some component of the electric field of a quasi-monochromatic light with mean frequency ν (corresponding to a wavelength λ) and a bandwidth $\Delta\nu$. Provided that the travel time of light rays connecting any two points within I or within O (but not connecting I and O) is much smaller than the coherence time[1] $1/\Delta\nu$, an approximate expression of the Huygens-Fresnel principle is (see page 371 of [4]):

$$U(\mathbf{q},t) = \frac{1}{\imath\lambda}\int_I \mathrm{d}^2\mathbf{q}' \frac{e^{\imath kR}}{R\,(\mathbf{q},\mathbf{q}')}\Lambda(\mathbf{q}',\mathbf{q})U(\mathbf{q}',t) \tag{2-1.1}$$

[1]Hence, the mutual path differences between points within O or within I are small compared to the coherence length; however, otherwise time delays will need to be included for path correction

apart from a phase factor, where $\Lambda(\mathbf{q}', \mathbf{q})$ is the known complex-valued inclination factor (see [4], page 371 for definition), with c being the speed of light in vacuum, $k = \frac{2\pi\nu}{c} = \frac{2\pi}{\lambda}$ and $R(\mathbf{q}, \mathbf{q}') = |\mathbf{q} - \mathbf{q}'|$ is the distance from P to Q.

To obtain the energy preserving estimate of the inverse of the field given in Equation (2-1.1) and given that light is collected over a limited entry pupil, one can reverse the time direction in the imaging situation of Figure (2.1). Treat light collectors as projectors, reverse the roles of surfaces I and O and again apply the Huygens-Fresnel principle to get:

$$U^e(\mathbf{q}', t) = -\frac{1}{\imath\lambda} \sum_{m=1}^{N} \int_{\mathcal{A}_m} \mathrm{d}^2\mathbf{q} \frac{e^{-\imath k R(\mathbf{q}, \mathbf{q}')}}{R(\mathbf{q}, \mathbf{q}')} \Lambda^*(\mathbf{q}', \mathbf{q}) U(\mathbf{q}, t). \tag{2-1.2}$$

$U^e(\mathbf{q}', t)$ is the field on the focal plane of an ideal optical instrument (consisting of physical optical processing instruments such as lenses, mirrors, beam splitters, etc) having the specified entry pupil and relying on some photo-detection process at the focal plane to acquire the image. The estimate of the image intensity, as obtained by accumulating the energy $\langle U^e(\mathbf{q}', t) U^{e*}(\mathbf{q}', t) \rangle$ over a time period $[0, t]$, is:

$$I_e(\mathbf{q}') = g \int_0^t \mathrm{d}\tau \langle U^{e*}(\mathbf{q}', t) U^e(\mathbf{q}', t) \rangle, \tag{2-1.3}$$

where g is a constant of proportionality. Using Equation (2-1.2), one gets:

$$I_e(\mathbf{q}') = \frac{g}{\lambda^2} A_p(\mathbf{q}') \int_0^t \mathrm{d}\tau \sum_{m,n} \int_{\mathcal{A}_m} \mathrm{d}^2\mathbf{q}_1 \int_{\mathcal{A}_n} \mathrm{d}^2\mathbf{q}_2 \frac{e^{-\imath k (R(\mathbf{q}_1, \mathbf{q}') - R(\mathbf{q}_2, \mathbf{q}'))}}{R(\mathbf{q}_1, \mathbf{q}') R(\mathbf{q}_2, \mathbf{q}')} \times \Lambda(\mathbf{q}', \mathbf{q}) \Lambda^*(\mathbf{q}', \mathbf{q}) J(\mathbf{q}_1, \mathbf{q}_2, \tau), \tag{2-1.4}$$

where $\mathbf{q}_i$ $(i = 1, 2)$ are integration variables,

$$J(\mathbf{q}_1, \mathbf{q}_2, t) = \langle U^*(\mathbf{q}_1, t) U(\mathbf{q}_2, t) \rangle \tag{2-1.5}$$

is the mutual intensity function, and

$$A_p(\mathbf{q}') = \begin{cases} 1 & \text{if } \mathbf{q}' \in I \text{ in within the aperture field-of-view} \\ 0 & \text{otherwise} \end{cases} \tag{2-1.6}$$

is the picture frame function used to model the restriction of the image plane to the aperture field-of-view.

Let $\mathbf{q}_i = (x_i, y_i, \bar{z} + \zeta_i)$ denote the position vector of the centroid of aperture i ($i = 1, \ldots, N$.) Assumption (2.1.1) implies that the constellation is long baseline interferometric imaging system. Moreover, Assumption (2.1.2) implies that we have:

$$\begin{aligned} R(\mathbf{q}, \mathbf{q}') &= \sqrt{(x_P - x_Q)^2 + (y_P - y_Q)^2 + \bar{z}^2} \\ &= \bar{z}\left[1 + \frac{(x_P - x_Q)^2}{2\bar{z}^2} + \frac{(y_P - y_Q)^2}{2\bar{z}^2}\right] + O\left(\frac{1}{\bar{z}^3}\right), \end{aligned} \tag{2-1.7}$$

where $\zeta_i \ll \bar{z}$ has been ignored. Hence, $R(\mathbf{q}_i, \mathbf{q}') \simeq \bar{z}$ ($i = 1, 2$) in the denominator of expression (2-1.4) but not in the exponent term since higher order terms will play a significant role when making higher order approximations of the exponential term to be made below. Assumption (2.1.2) also implies that the inclination factor varies very little with respect to the motion of the entry pupil and the position of the point $Q \in I$. Hence, $\Lambda\Lambda^* = |\Lambda|^2$ may be treated as a constant and be pulled outside the integral. Therefore, by assumptions (2.1.2) and (2.1.1) we have:

$$I_e(\mathbf{q}') = \frac{g|\Lambda|^2}{\lambda^2 \bar{z}^2} A_p(\mathbf{q}') \int_0^t \mathrm{d}\tau \sum_{m,n} \int_{\mathcal{A}_m} \mathrm{d}^2\mathbf{q}_1 \int_{\mathcal{A}_n} \mathrm{d}^2\mathbf{q}_2 e^{-\imath k(R(\mathbf{q}_1, \mathbf{q}') - R(\mathbf{q}_2, \mathbf{q}'))} J(\mathbf{q}_1, \mathbf{q}_2, \tau), \tag{2-1.8}$$

where now we use the angular position vector $\bar{\theta}$ to locate the point Q on I.

Recall that $\mathbf{q}_1$ and $\mathbf{q}_2$ are vectors specifying any two points on any of the entry pupils $\mathcal{A}_i$ ($i = 1, \ldots, N$.) With Assumption (2.1.1) one can safely treat each entry pupil as a measurement *point* (that is, $\mathcal{A}_i$ is now a point) and, hence, find that the mutual intensity function $J(\mathbf{q}_1, \mathbf{q}_2, t)$ is independent of where within the pupil the interference is made for all $\mathbf{q}_1 \in \mathcal{A}_m$ and $\mathbf{q}_2 \in \mathcal{A}_m$ and all $m, n \in \{1, \ldots, N\}$. Instead, it is now a function of the position vectors, denoted $\mathbf{q}_i$ ($i = 1, \ldots, N$), of the entry pupils; $J(\mathbf{q}_1, \mathbf{q}_2, t) = J(\mathbf{q}_m, \mathbf{q}_n, t)$ for all pairs $m, n \in \{1, \ldots, N\}$. This enables us

to drop the integrals over $\mathcal{A}_m$ and $\mathcal{A}_n$. Hence, Equation (2-1.8) can be rewritten as

$$I_e(\mathbf{q}') = \frac{g|\Lambda|^2 A_T^2}{\lambda^2 \bar{z}^2} A_p(\mathbf{q}') \int_0^t \mathrm{d}\tau \sum_{m,n} e^{-\imath k(R(\mathbf{q}_m,\mathbf{q}')-R(\mathbf{q}_n,\mathbf{q}'))} J(\mathbf{q}_m,\mathbf{q}_n,\tau), \qquad (2\text{-}1.9)$$

This gives the algorithm by which the image intensity estimate can be derived from mutual coherence measurements. This, however, does not afford an estimate of the quality of the image so obtained. To attain this, we need an expression for $I_e(\mathbf{q}')$ as a function of the "true" image intensity, $I(\mathbf{q}')$. We do this as follows. An approximate expression for $J(\mathbf{q}_m,\mathbf{q}_n)$ in terms of the true image intensity $I(\mathbf{q}')$ is given by:

$$J(\mathbf{q}_m,\mathbf{q}_n) = \frac{1}{\lambda^2\bar{z}^2}\int_I \mathrm{d}^2\mathbf{q}_1' e^{\imath k\left(R\left(\mathbf{q}_m,\mathbf{q}_1'\right)-R\left(\mathbf{q}_n,\mathbf{q}_1'\right)\right)} I(\mathbf{q}_1'), \qquad (2\text{-}1.10)$$

where this is the small angle approximation of the Huygens-Fresnel principle, obtainable by direct manipulation of Equation (2-1.1). From Equation (2-1.7), we also have

$$\begin{aligned} R(\mathbf{q}_m,\mathbf{q}) - R(\mathbf{q}_n,\mathbf{q}) &= \frac{1}{\bar{z}}\Bigg[\frac{1}{2}\Delta x_{mn}(x_m - 2x_Q + x_n) \\ &\quad + \frac{1}{2}\Delta y_{mn}(y_m - 2y_Q + y_n)\Bigg], \end{aligned} \qquad (2\text{-}1.11)$$

where $\Delta x_{mn} = x_m - x_n$ and $\Delta y_{mn} = y_m - y_n$. Substituting (2-1.10) and (2-1.11) into (2-1.9), we get

$$I_e(\mathbf{q}') = \frac{g|\Lambda|^2 A_T^2}{\lambda^4\bar{z}^4} A_p(\mathbf{q}') \sum_{m,n}\int_0^t \mathrm{d}\tau \int_I \mathrm{d}^2\mathbf{q}_1' e^{\frac{\imath k}{\bar{z}}\left(\Delta x_{mn}\left(x'-x_1'\right)+\Delta y_{mn}\left(y'-y_1'\right)\right)} I(\mathbf{q}_1'), \qquad (2\text{-}1.12)$$

where we recall the definition of $\mathbf{q}' = (x', y', 0)$ is a (fixed) point at $Q \in I$ and the definition of the variable of integration $\mathbf{q}_1' = (x_1', y_1', 0)$. Adopting a more compact notation we have

$$I_e(\mathbf{q}') = \frac{g|\Lambda|^2 A_T^2}{\lambda^4\bar{z}^4} A_p(\mathbf{q}') \sum_{m,n}\int_0^t \mathrm{d}\tau \int_I \mathrm{d}^2\mathbf{q}_1' e^{\frac{\imath k}{\bar{z}}\left(\Delta\mathbf{q}_{mn}\cdot\left(\mathbf{q}'-\mathbf{q}_1'\right)\right)} I(\mathbf{q}_1'), \qquad (2\text{-}1.13)$$

where $\Delta\mathbf{q}_{mn} = (x_m - x_n, y_m - y_n, 0)$ and "$\cdot$" is the vector inner product.

Let

$$M_{mn}(\mathbf{q}') = \int_I \mathrm{d}^2\mathbf{q}_1' I\left(\mathbf{q}_1'\right) e^{\frac{\imath k}{\bar{z}}\left(\Delta\mathbf{q}_{mn}\cdot\left(\mathbf{q}'-\mathbf{q}_1'\right)\right)} \tag{2-1.14}$$

and recall the following identities of the Fourier transform

$$\begin{aligned} \mathcal{F}(gh) &= \hat{g} * \hat{h} \\ \mathcal{F}\left[g(\mathbf{q})e^{-2\pi\imath(\mathbf{a}\cdot\mathbf{q})}\right] &= \hat{g}(\boldsymbol{\nu} - \mathbf{a}), \end{aligned} \tag{2-1.15}$$

where $\hat{g}(\boldsymbol{\nu}) = \mathcal{F}(g(\mathbf{q}))$ denotes the Fourier transform of g and $*$ denotes the convolution operator. Substituting (2-1.14) into (2-1.13), one gets:

$$I_e\left(\mathbf{q}'\right) = \frac{g\left|\Lambda\right|^2 A_T^2}{\lambda^4\bar{z}^4} \sum_{m,n} \int_0^t \mathrm{d}\tau A_p\left(\mathbf{q}'\right) M_{mn}\left(\mathbf{q}'\right). \tag{2-1.16}$$

Taking the Fourier transform of this expression and using the first of Equation (2-1.15) we get

$$\hat{I}_e\left(\boldsymbol{\nu}, t\right) = \frac{g\left|\Lambda\right|^2 A_T^2}{\lambda^4\bar{z}^4} \sum_{m,n} \int_0^t \mathrm{d}\tau \hat{A}_p\left(\boldsymbol{\nu}\right) * \hat{M}_{mn}\left(\boldsymbol{\nu}\right). \tag{2-1.17}$$

Applying the second identity in Equations (2-1.15) to Equation (2-1.14), we have

$$\hat{M}_{mn}(\boldsymbol{\nu}) = \hat{I}\left(\boldsymbol{\nu}\right)\delta\left(\boldsymbol{\nu} - \frac{\Delta\mathbf{q}_{mn}}{\lambda\bar{z}}\right). \tag{2-1.18}$$

Using the definition of a convolution, we have

$$\begin{aligned} \hat{A}_p(\boldsymbol{\nu}) * \hat{M}_{mn}(\boldsymbol{\nu}) &= \int \hat{A}_p(\boldsymbol{\nu} - \boldsymbol{\nu}')\hat{M}_{mn}(\boldsymbol{\nu}')\mathrm{d}\boldsymbol{\nu}' \\ &= \int \hat{A}_p(\boldsymbol{\nu} - \boldsymbol{\nu}')\hat{I}(\boldsymbol{\nu}')\delta\left(\boldsymbol{\nu} - \frac{\Delta\mathbf{q}_{mn}}{\lambda\bar{z}}\right)\mathrm{d}\boldsymbol{\nu}' \\ &= \hat{A}_p(\boldsymbol{\nu} - \frac{\Delta\mathbf{q}_{mn}}{\lambda\bar{z}})\hat{I}(\frac{\Delta\mathbf{q}_{mn}}{\lambda\bar{z}}). \end{aligned} \tag{2-1.19}$$

Note that the intensity can be expanded:

$$\begin{aligned} \hat{I}(\frac{\Delta\mathbf{q}_{mn}}{\lambda\bar{z}}) &= \hat{I}(\boldsymbol{\nu} + \frac{\Delta\mathbf{q}_{mn}}{\lambda\bar{z}} - \boldsymbol{\nu}) \\ &= \hat{I}(\boldsymbol{\nu}) + \frac{\partial\hat{I}}{\partial\boldsymbol{\nu}}\bigg|\left(\frac{\Delta\mathbf{q}_{mn}}{\lambda\bar{z}} - \boldsymbol{\nu}\right) + \cdots. \end{aligned}$$

If we assume that $\frac{\partial \hat{I}}{\partial \boldsymbol{\nu}}\left(\frac{\Delta \mathbf{q}_{mn}}{\lambda \bar{z}} - \boldsymbol{\nu}\right)$ and higher order terms are sufficiently small, then this, Equation (2-1.19) and Equation (2-1.17) imply

$$\hat{I}_e\left(\boldsymbol{\nu}, t\right) = \frac{g\left|\Lambda\right|^2 A_T^2}{\lambda^4 \bar{z}^4} \sum_{m,n} \int_0^t \mathrm{d}\tau \hat{A}_p \left(\boldsymbol{\nu} - \frac{\Delta \mathbf{q}_{mn}}{\lambda \bar{z}}\right) \hat{I}\left(\boldsymbol{\nu}\right). \tag{2-1.20}$$

$\frac{\partial \hat{I}}{\partial \boldsymbol{\nu}}\left(\frac{\Delta \mathbf{q}_{mn}}{\lambda \bar{z}} - \boldsymbol{\nu}\right)$ is small if either (1) the slope of $\hat{I}(\boldsymbol{\nu})$ is small for all frequencies $\boldsymbol{\nu}$ such that $\|\boldsymbol{\nu}\| < r_p$ (that is, within the region where $\hat{A}_p$ is 1), or if (2) all frequencies $\{\boldsymbol{\nu} : \|\boldsymbol{\nu}\| < r_p\}$ is such that $\left\|\boldsymbol{\nu} - \frac{\Delta \mathbf{q}_{mn}}{\lambda \bar{z}}\right\|$ is sufficiently small. The first condition is satisfied whenever the intensity varies slowly over any disk is the frequency domain whose radius is r_p and the second is satisfied whenever the effective width of the picture frame function r_p is sufficiently small. We assume that either one or both of these conditions are satisfied.

Now, let

$$\hat{M}(\boldsymbol{\nu}, t) = \beta \sum_{m,n} \int_0^t \mathrm{d}\tau \hat{A}_p \left(\boldsymbol{\nu} - \frac{\Delta \mathbf{q}_{mn}(\tau)}{\lambda \bar{z}}\right), \tag{2-1.21}$$

where $\beta = \frac{g|\Lambda|^2 A_T^2}{\lambda^4 \bar{z}^4}$, then

$$\hat{I}_e\left(\boldsymbol{\nu}, t\right) = \hat{M}(\boldsymbol{\nu}, t)\hat{I}\left(\boldsymbol{\nu}\right). \tag{2-1.22}$$

The function $\hat{M}$ is the *modulation transfer function* (MTF)[2]. Referring to Equation (2-1.21), we see that the MTF is simply the superposition of the set of "coverage" functions $\hat{A}_p$, each evaluated at $\frac{\Delta \mathbf{q}_{mn}}{\lambda \bar{z}}$.

Thus the MTF is defined as the ratio of the estimated intensity to the true image intensity. For an interferometric imaging constellation, the MTF can be computed given the measurement history and corresponding relative position data between the light collecting spacecraft. In the wave number plane, a point with a zero MTF value

---

[2]The Assumption (2.1.2) has directly led to the elimination of ζ_i from the derivation. Hence, Equation (2-1.22) presents a valid model for the system whenever $\bar{z} \gg 1$. This assumption, however, does not imply that there is a need to constrain the formation to the observation plane O.

implies that the system is "blind" to the corresponding sinusoidal pattern, while a large value of the MTF implies that the image signal can be restored at that wave number via an inverse Fourier transform (see [6, 4, 7].) The MTF, as a measure of the imaging system's performance, is a function of both the optical system and the configuration of the observatory in physical space.

Let the picture frame have a diameter $\bar{d}$ equal to the size of σ: $\bar{d} = 2d$ (with σ entirely contained in A_p.) Pixelating the image plane into an $m \times m$ grid, the size of each pixel is $L = \bar{d}/m$, and the resulting angular resolution is $\theta_r = L/\bar{z}$. Additionally, the angular extent of the desired picture frame is approximately given by $\theta_p = \bar{d}/\bar{z}$, leading to $\theta_p = m\theta_r$. Dimensions of features in the wave number plane are the reciprocals of the corresponding dimensions in the physical plane. The *resolution disc*, D_v, is a disc of diameter $\simeq 1/\theta_r$ and is the region where we desire the MTF to have nonzero values (or, equivalently, wave number plane coverage.) Making the simplifying assumption that

$$\hat{A}_p^2(\boldsymbol{\nu}) = \hat{A}_p(\boldsymbol{\nu}) = \begin{cases} 1 & \text{if } |\boldsymbol{\nu}| \leq r_p \\ 0 & \text{otherwise} \end{cases}, \tag{2-1.23}$$

where r_p is the effective radius of the true function $\hat{A}_p$. This incurs a sensible error only at the edge of the domain of $\hat{A}_p$. The *picture frame region* is a circular disc of diameter $2r_p \simeq 1/\theta_p$ that is used to approximate the effective size of $\hat{A}_p$ (equivalently, assume that $\hat{A}_p$ is a hat-shaped function.) Therefore, the diameter of the resolution disc is m times the diameter of the picture frame disc in the wave number plane (see Figure (2.2).)

As the relative projected position vector, $\Delta\mathbf{q}_{mn}$, varies in the physical plane, the picture frame disc moves in the wave number plane, where its center follows the trajectory of the vectors given by $\frac{\Delta\mathbf{q}_{mn}}{\lambda\bar{z}}$. Each satellite, by itself, will contribute

a disc that is centered at the origin with a diameter of $\simeq 1/\theta_p$, and each pair of satellites will contribute two discs of diameter $\simeq 1/\theta_p$ located 180 degrees apart with a radius of $\left|\frac{\Delta \mathbf{q}_{mn}}{\lambda \bar{z}}\right|$ from the center. This symmetry in the frequency domain is due to the fact that $\frac{\Delta \mathbf{q}_{mn}}{\lambda \bar{z}} = -\frac{\Delta \mathbf{q}_{nm}}{\lambda \bar{z}}$.

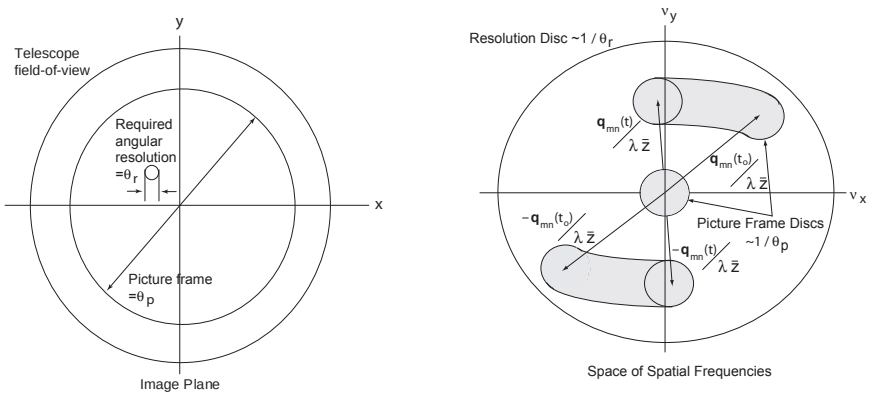

Figure 2.2: Physical and wave number plane variables. To indicate time progress, we show the trajectory on an interval $[t_0, t]$.

2.2 A Noise Model

In Section (6.3), we need to evaluate the performance of controllers for a class of spiraling maneuvers. It is desired to have a performance index that takes into account a noise model of the imaging process. Hence, we wish to augment the model in Equation (2-1.22) with a noise model. We only give a brief discussion of this topic. For a more detailed discussion, we refer the reader to the thesis by [5]. Assume that the rate of photon arrival satisfies a Poisson distribution. This incurs Poisson fluctuations in the measurement of $J(\mathbf{q}_m, \mathbf{q}_n)$. Via Equation (2-1.4), where $J(\mathbf{q}_m, \mathbf{q}_n)$ appears in the integrand, the noise in $I_e(\mathbf{q}')$ also satisfies Poisson

statistics. Let $\bar{I}$ be the average value of the signal $\hat{I}(\boldsymbol{\nu})$, which is assumed estimable beforehand. Modulated by the MTF of the constellation, the mean arrival rate is therefore proportional to $\hat{M}(\boldsymbol{\nu}, t)\,\bar{I}$. Moreover, the variance of such fluctuations is proportional to the square root of the mean arrival rate. For a more detailed discussion, see [5]. Therefore, we have:

$$\hat{I}_e(\boldsymbol{\nu}, t) \simeq \hat{M}(\boldsymbol{\nu}, t)\,\hat{I}(\boldsymbol{\nu}) + \gamma\sqrt{\hat{M}(\boldsymbol{\nu}, t)\,\bar{I}(\boldsymbol{\nu})}N(\boldsymbol{\nu}), \tag{2-2.1}$$

where $N(\boldsymbol{\nu})$ is a unit variance, white process in $\boldsymbol{\nu}$ and γ is a constant reflecting the quality of the telescope optics, detector physics... etc. Estimating $\hat{I}$ by $\bar{I}$ at each point in the $\boldsymbol{\nu}$-plane, one finds that

$$SNR \propto \frac{\hat{M}\bar{I}}{\gamma\sqrt{\hat{M}\bar{I}}} = \frac{1}{\gamma}\sqrt{\hat{M}(\boldsymbol{\nu}, t)\,\bar{I}}. \tag{2-2.2}$$

One can now introduce an imaging performance index $J = \int_0^{t_f} \mathcal{I}\mathrm{d}t$, where

$$\mathcal{I}(t) = \int_{D_v} \mathrm{d}\boldsymbol{\nu}\left(1 - \Gamma^R(\boldsymbol{\nu}, t)\right), \tag{2-2.3}$$

where R is a "risk factor" and $\Gamma(\boldsymbol{\nu}, t)$ is the ratio of the actual SNR to the desired SNR and is given by:

$$\Gamma(\boldsymbol{\nu}, t) = \frac{\text{Actual SNR}}{\text{Desired SNR}} = \begin{cases} 1 & \text{if } \alpha\hat{M}^{1/2} \geq 1 \\ \alpha\hat{M}^{1/2} & \text{otherwise} \end{cases}, \tag{2-2.4}$$

where α is inversely proportional to the desired signal-to-noise ratio and $\hat{M}$ is computed from Equation (2-1.21). The larger the risk factor R the more conservative the imaging performance measure becomes. Regions in the wave number plane where Γ is less than unity correspond to spatial frequencies of the signal that do not satisfy the desired signal-to-noise ratio, while $\Gamma = 1$ implies both coverage and achievement of the desired signal-to-noise ratio at the corresponding spatial frequency.

A final remark is in order. Since the $\hat{A}_p$ functions are evaluated at points corresponding to the trajectories of the relative position vectors, note that the rate at which the $\hat{A}_p(\boldsymbol{\nu} - \frac{\Delta \mathbf{q}_{mn}}{\lambda \bar{z}})$ function moves in the frequency domain is proportional to the relative velocity between spacecraft m and n. Hence, if the relative velocity has a large magnitude, $\hat{A}_p$ moves too fast in the frequency domain. This, in turn, may not allow for the MTF to accumulate to a satisfactory level to achieve the desired SNR (as reflected in the Γ function) and, hence, results in reduced signal strength allowing for the noise signal to overwhelm the measured signal. This results, by definition, to $\Gamma < 1$. This implies that the value of Γ and, hence,the SNR, function is inversely proportional to the square root of the relative speed between the spacecraft in the constellation. Therefore, there is a critical relative velocity v^* between any pair of spacecraft m and n such that the picture frame discs achieve $\Gamma = 1$ at the frequencies they visit and such that $\Gamma < 1$ if the relative speed $v_{mn} < v^*_{mn}$.

2.3 Multi-Spacecraft Problem: Necessary Conditions Using the Maximum Principle

In this section we derive the necessary conditions for a multi-spacecraft formation by appealing to the maximum principle (MP.) The dynamics are given by:

$$\begin{aligned} \dot{\mathbf{q}}_i(t) &= \mathbf{v}_i(t) \\ \dot{\mathbf{v}}_i(t) &= \mathbf{u}_i \end{aligned} \tag{2-3.1}$$

for all spacecraft $i = 1, \ldots, N$. The cost function to be minimized is given by:

$$\mathcal{J} = y(T) = \int_0^T \mu \left(\sum_{i=1}^{N} \|\mathbf{u}_i(t)\|^2 \right) \mathrm{d}t, \tag{2-3.2}$$

where the cost $y(t)$ satisfies the differential equation:

$$\dot{y}(t) = \mu \left(\sum_{i=1}^{N} \|\mathbf{u}_i(t)\|^2 \right). \tag{2-3.3}$$

In Equation (2-3.3), μ is a parameter introduced to study the local behavior of the resulting control law in Section (2.5). An optimal solution will be independent of the parameter μ in general. Define the normalized MTF as:

$$z(\boldsymbol{\nu},t)=\frac{1}{\beta}\hat{M}(\boldsymbol{\nu},t)-\int_0^t\sum_{n=1}^{N}\hat{A}_p\left(\boldsymbol{\nu}-\tilde{\mathbf{q}}_{nn}\right)=\int_0^t \mathrm{d}\tau\sum_{m}^{N}\sum_{n=1,\neq m}^{N}\hat{A}_p\left(\boldsymbol{\nu}-\tilde{\mathbf{q}}_{mn}(\tau)\right) \tag{2-3.4}$$

The second term after the first equality sign in the definition of z ensures that z does not include contributions due to self-interaction at the origin of the frequency domain. Hence, for the spacecraft formation z satisfies the differential equation:

$$\dot{z}(\boldsymbol{\nu},t)=\sum_{m}^{N}\sum_{n=1,\neq m}^{N}\hat{A}_p\left(\boldsymbol{\nu}-\tilde{\mathbf{q}}_{mn}(t)\right) \tag{2-3.5}$$

which we treat as a state of the system. We use $\tilde{\mathbf{q}}_{mn}$ to denote the relative position vector between spacecraft m and n:

$$\tilde{\mathbf{q}}_{mn}(t)=\frac{\mathbf{q}_m-\mathbf{q}_n}{\lambda\bar{z}}. \tag{2-3.6}$$

Previously, we used $\Delta\mathbf{q}_{mn}/(\lambda\bar{z})$ to denote $\tilde{\mathbf{q}}_{mn}$. For the rest of the thesis, we will use the latter notation.

If we let h denote the saturation function:

$$h(x)=\begin{cases} x & 0\leq x<1 \\ 1 & x\geq 1 \end{cases}$$

then we require to have the terminal condition on z be given by

$$h(z(\boldsymbol{\nu},T))=1 \tag{2-3.7}$$

for all $\boldsymbol{\nu}\in D_v$. This guarantees that $z\geq 1$ everywhere inside D_v at time T. To

summarize, initial and terminal conditions are:

$$\begin{aligned}
\mathbf{q}_i(0) &= \mathbf{q}_{i0} \\
\mathbf{v}_i(0) &= \mathbf{v}_{i0} \\
y(0) &= 0 \\
z(\boldsymbol{\nu}, 0) &= 0,\ \forall \boldsymbol{\nu} \in D_v \\
z(\boldsymbol{\nu}, T) &= 1,\ \forall \boldsymbol{\nu} \in D_v,
\end{aligned}$$

where we desire to achieve complete coverage at the terminal time T.

The problem at hand is to minimize (2-3.2) subject to the dynamics given in Equations (2-3.1), (2-3.3) and (2-3.5). We will use the maximum principle to derive the necessary conditions. Define the function:

$$\begin{aligned}
\hat{H}(t) &= \sum_{i=1}^{N} \left[\mathbf{p}_{\mathbf{q}_i} \cdot \mathbf{v}_i + \mathbf{p}_{\mathbf{v}_i} \cdot \mathbf{u}_i\right] + \mu p_y \left(\sum_{i=1}^{N} \|\mathbf{u}_i\|^2\right) \\
&\quad + \left\langle p_z(\boldsymbol{\nu}, t), \sum_{m,n=1, n\neq m}^{N} \hat{A}_p\left(\boldsymbol{\nu} - \tilde{\mathbf{q}}_{mn}\right) \right\rangle,
\end{aligned} \tag{2-3.8}$$

where $\mathbf{p}_{\mathbf{q}_i}$ and $\mathbf{p}_{\mathbf{v}_i}$ are vector Lagrange multipliers, p_y is a scalar Lagrange multiplier and $p_z : D_v \times [0, T] \to \mathbb{R}$ is a Lagrange multiplier function taken point-wise in $\boldsymbol{\nu}$. The inner product $\langle \cdot, \cdot \rangle$ in Equation (2-3.8) refers to the inner product on the vector space of real functions whose domain is the resolution disc D_v:

$$\langle f(\boldsymbol{\nu}), g(\boldsymbol{\nu}) \rangle = \int_{D_v} f(\boldsymbol{\nu}) g(\boldsymbol{\nu}) d\boldsymbol{\nu}, \tag{2-3.9}$$

for any two functions $f, g : D_v \to \mathbb{R}$.

A necessary condition for optimality is that

$$\frac{\partial \hat{H}}{\partial \mathbf{u}_i} = 0,\ i = 1, \ldots, N. \tag{2-3.10}$$

This equation implies that

$$\mathbf{u}_i = -\frac{1}{2\mu p_y} \mathbf{p}_{\mathbf{v}_i},\ i = 1, \ldots, N.$$

Hence, the Hamiltonian is given:

$$H(t) = \sum_{i=1}^{N} \left[\mathbf{p}_{\mathbf{q}_i} \cdot \mathbf{v}_i - \frac{\|\mathbf{p}_{\mathbf{v}_i}\|^2}{4\mu p_y} \right] + \left\langle p_z(\boldsymbol{\nu}, t), \sum_{m,n=1,n\neq m}^{N} \hat{A}_p \left(\boldsymbol{\nu} - \tilde{\mathbf{q}}_{mn} \right) \right\rangle . \quad (2\text{-}3.11)$$

Transversality conditions imply that (see Equation (2.3.8) in [37]):

$$\begin{aligned} \mathbf{p}_{\mathbf{q}_i}(T) &= \mathbf{p}_{\mathbf{v}_i}(T) = 0 \\ p_z(\boldsymbol{\nu}, T) &= p_z^f(\boldsymbol{\nu}) \\ p_y(T) &= 1, \end{aligned} \quad (2\text{-}3.12)$$

for some function $p_z^f D_v \to \mathbb{R}$ to be solved for.

By the maximum principle, the necessary optimality conditions are given by:

$$\begin{aligned} \dot{\mathbf{q}}_i(t) &= \frac{\partial H}{\partial \mathbf{p}_{\mathbf{q}_i}} = \mathbf{v}_i(t) \\ \dot{\mathbf{v}}_i(t) &= \frac{\partial H}{\partial \mathbf{p}_{\mathbf{v}_i}} = -\frac{\mathbf{p}_{\mathbf{v}_i}(t)}{2\mu p_y(t)} \\ \dot{y}_i(t) &= \frac{\partial H}{\partial p_y} = \sum_{i=1}^{N} \frac{\|\mathbf{p}_{\mathbf{v}_i}(t)\|^2}{4\mu p_y^2(t)} \\ \dot{z}(\boldsymbol{\nu}, t) &= \frac{\partial H}{\partial p_z} = \sum_{m,n=1,n\neq m}^{N} \hat{A}_p \left(\boldsymbol{\nu} - \tilde{\mathbf{q}}_{mn}(t) \right) \\ \dot{\mathbf{p}}_{\mathbf{q}_i}(t) &= -\frac{\partial H}{\partial \mathbf{q}_i} = \frac{1}{\lambda \bar{z}} \left\langle p_z(\boldsymbol{\nu}, t), \sum_{n=1,\neq i}^{N} \left(-\nabla \hat{A}_p(\boldsymbol{\nu} - \tilde{\mathbf{q}}_{in}(t)) + \nabla \hat{A}_p(\boldsymbol{\nu} + \tilde{\mathbf{q}}_{in}(t)) \right) \right\rangle \\ \dot{\mathbf{p}}_{\mathbf{v}_i}(t) &= -\frac{\partial H}{\partial \mathbf{v}_i} = -\mathbf{p}_{\mathbf{q}_i}(t) \\ \dot{p}_y(t) &= -\frac{\partial H}{\partial y} = 0 \\ \dot{p}_z(\boldsymbol{\nu}, t) &= -\frac{\partial H}{\partial z} = 0. \end{aligned} \quad (2\text{-}3.13)$$

From the initial and terminal conditions (2-3.8), the transversality conditions (2-3.12) and the seventh and eighth equations in (2-3.13), we find that $p_y(t) = 1$ and

$p_z(\boldsymbol{\nu}, t) = p_z^f(\boldsymbol{\nu})$ for all $t \in [0, T]$. Hence, we have:

$$\begin{aligned}
\dot{\mathbf{q}}_i(t) &= \mathbf{v}_i(t) \\
\dot{\mathbf{v}}_i(t) &= -\frac{\mathbf{p}_{\mathbf{v}_i}(t)}{2\mu} \\
\dot{y}_i(t) &= \sum_{i=1}^{N} \frac{\|\mathbf{p}_{\mathbf{v}_i}(t)\|^2}{4\mu} \\
\dot{z}(\boldsymbol{\nu}, t) &= \sum_{m,n=1, n\neq m}^{N} \hat{A}_p\left(\boldsymbol{\nu} - \tilde{\mathbf{q}}_{mn}(t)\right) \\
\dot{\mathbf{p}}_{\mathbf{q}_i}(t) &= \frac{1}{\lambda \bar{z}} \left\langle p_z^f(\boldsymbol{\nu}), \sum_{n=1, \neq i}^{N} \left(-\nabla \hat{A}_p(\boldsymbol{\nu} - \tilde{\mathbf{q}}_{in}(t)) + \nabla \hat{A}_p(\boldsymbol{\nu} + \tilde{\mathbf{q}}_{in}(t)) \right) \right\rangle \\
\dot{\mathbf{p}}_{\mathbf{v}_i}(t) &= -\mathbf{p}_{\mathbf{q}_i}(t).
\end{aligned} \tag{2-3.14}$$

In the next section we specialize the result to the two-spacecraft formation problem.

2.4 The Two Spacecraft Problem

In this section we derive the necessary conditions for a two-spacecraft formation using the MP. Since we have two degrees of freedom, instead of using the positions of the spacecraft as system states, we will use the relative position between the spacecraft and the position of the center of mass as our states. As before, let $\tilde{\mathbf{q}}$ denote the relative position vector between the spacecraft pair divided by $\lambda \bar{z}$

$$\tilde{\mathbf{q}}(t) = \frac{\mathbf{q}_2(t) - \mathbf{q}_1(t)}{\lambda \bar{z}}, \tag{2-4.1}$$

where $\mathbf{q}_i$, $i = 1, 2$, is the position vector of the two spacecraft. $\tilde{\mathbf{q}}$ corresponds to the motion of one of the picture frame discs in the frequency domain. Let $\mathbf{s}$ be the position vector of the center of mass of the formation. Then, $\mathbf{s}$ is given by

$$\mathbf{s}(t) = \frac{\mathbf{q}_2(t) + \mathbf{q}_1(t)}{2}, \tag{2-4.2}$$

where we assume unity mass for both spacecraft. The dynamics of the system are given by:

$$\begin{aligned} \dot{\tilde{\mathbf{q}}}(t) &= \mathbf{v}_{\mathbf{q}}(t) \\ \dot{\mathbf{v}}_{\mathbf{q}}(t) &= \frac{\mathbf{u}_2(t) - \mathbf{u}_1(t)}{\lambda \bar{z}} \\ \dot{\mathbf{s}}(t) &= \mathbf{v}_{\mathbf{s}}(t) \\ \dot{\mathbf{v}}_{\mathbf{s}}(t) &= \frac{\mathbf{u}_2(t) + \mathbf{u}_1(t)}{2}. \end{aligned} \tag{2-4.3}$$

The cost function to be minimized is given by:

$$\mathcal{J} = y(T), \tag{2-4.4}$$

where the cost $y(t)$ satisfies the differential equation:

$$\dot{y}(t) = \mu \left(\|\mathbf{u}_1(t)\|^2 + \|\mathbf{u}_2(t)\|^2 \right). \tag{2-4.5}$$

The normalized MTF is given by:

$$z(\boldsymbol{\nu}, t) = \frac{1}{\beta} \hat{M}(\boldsymbol{\nu}, t) - \int_0^t \mathrm{d}\tau 2 \hat{A}_p(\boldsymbol{\nu}) = \int_0^t \mathrm{d}\tau \hat{A}_p \left(\boldsymbol{\nu} - \tilde{\mathbf{q}}(\tau) \right) + \hat{A}_p \left(\boldsymbol{\nu} + \tilde{\mathbf{q}}(\tau) \right) \tag{2-4.6}$$

Hence, for the two spacecraft formation z satisfies the differential equation:

$$\dot{z}(\boldsymbol{\nu}, t) = \hat{A}_p \left(\boldsymbol{\nu} - \tilde{\mathbf{q}}(t) \right) + \hat{A}_p \left(\boldsymbol{\nu} + \tilde{\mathbf{q}}(t) \right) \tag{2-4.7}$$

and is treated as a state of the system.

Initial and terminal conditions are:

$$\begin{aligned}
\tilde{\mathbf{q}}(0) &= \tilde{\mathbf{q}}_0 \\
\mathbf{v}_{\mathbf{q}}(0) &= \mathbf{v}_{\mathbf{q}_0} \\
\mathbf{s}(0) &= \mathbf{s}_0 \\
\mathbf{v}_{\mathbf{s}}(0) &= \mathbf{v}_{\mathbf{s}_0} \\
y(0) &= 0 \\
z(\boldsymbol{\nu}, 0) &= 0,\ \forall \boldsymbol{\nu} \in D_v \\
h(z(\boldsymbol{\nu}, T)) &= 1,\ \forall \boldsymbol{\nu} \in D_v.
\end{aligned} \tag{2-4.8}$$

Again, we will use the maximum principle to derive the necessary conditions. Hence, we have:

$$\begin{aligned}
\hat{H}(t) &= \mathbf{p}_{\mathbf{q}}(t) \cdot \mathbf{v}_{\mathbf{q}}(t) + \mathbf{p}_{v_q}(t) \cdot \left(\frac{\mathbf{u}_2(t) - \mathbf{u}_1(t)}{\lambda \bar{z}} \right) \\
&\quad + \mathbf{p}_s(t) \cdot \mathbf{v}_{\mathbf{s}}(t) + \mathbf{p}_{v_s}(t) \cdot \left(\frac{\mathbf{u}_1(t) + \mathbf{u}_2(t)}{2} \right) \\
&\quad + \mu p_y(t) \left(\|\mathbf{u}_1(t)\|^2 + \|\mathbf{u}_2(t)\|^2 \right) + \left\langle p_z(\boldsymbol{\nu}, t), \hat{A}_p \left(\boldsymbol{\nu} - \tilde{\mathbf{q}}(t) \right) + \hat{A}_p \left(\boldsymbol{\nu} + \tilde{\mathbf{q}} \right) \right\rangle,
\end{aligned} \tag{2-4.9}$$

where $\mathbf{p}_{\mathbf{q}}$, $\mathbf{p}_{v_q}$, $\mathbf{p}_s$ and $\mathbf{p}_{v_s}$ are vector Lagrange multipliers, p_y is a scalar Lagrange multiplier and $p_z : D_v \times [0, T] \to \mathbb{R}$ is a Lagrange multiplier function taken point-wise in $\boldsymbol{\nu}$. A necessary condition for optimality is that

$$\frac{\partial \hat{H}}{\partial \mathbf{u}_1} = \frac{\partial \hat{H}}{\partial \mathbf{u}_2} = 0. \tag{2-4.10}$$

These equations imply that

$$\begin{aligned}
\mathbf{u}_1(t) &= \frac{1}{2\mu p_y(t)} \left[\frac{\mathbf{p}_{v_q}(t)}{\lambda \bar{z}} - \frac{\mathbf{p}_{v_s}(t)}{2} \right] \\
\mathbf{u}_2(t) &= -\frac{1}{2\mu p_y(t)} \left[\frac{\mathbf{p}_{v_q}(t)}{\lambda \bar{z}} + \frac{\mathbf{p}_{v_s}(t)}{2} \right].
\end{aligned}$$

These two equations imply

$$\begin{aligned}
\mathbf{u}_2(t) - \mathbf{u}_1(t) &= -\frac{\mathbf{p}_{v_q}(t)}{\lambda\bar{z}\mu p_y(t)} \\
\mathbf{u}_1(t) + \mathbf{u}_2(t) &= -\frac{\mathbf{p}_{v_s}(t)}{2\mu p_y(t)} \\
\|\mathbf{u}_1(t)\|^2 + \|\mathbf{u}_2(t)\|^2 &= \frac{1}{4\mu^2 p_y^2(t)}\left[\frac{2}{(\lambda\bar{z})^2}\left\|\mathbf{p}_{v_q}(t)\right\|^2 + \frac{1}{2}\left\|\mathbf{p}_{v_s}(t)\right\|^2\right].
\end{aligned}$$

Substituting these back into Equation (2-4.9), we have:

$$\begin{aligned}
H(t) &= \mathbf{p}_{\mathbf{q}}(t)\cdot\mathbf{v}_{\mathbf{q}}(t) - \frac{1}{2\mu(\lambda\bar{z})^2 p_y(t)}\left\|\mathbf{p}_{v_q}(t)\right\|^2 + \mathbf{p}_s(t)\cdot\mathbf{v}_{\mathbf{s}}(t) - \frac{1}{8\mu p_y(t)}\left\|\mathbf{p}_{v_s}(t)\right\|^2 \\
&\quad + \left\langle p_z(\boldsymbol{\nu},t), \hat{A}_p\left(\boldsymbol{\nu} - \tilde{\mathbf{q}}(t)\right) + \hat{A}_p\left(\boldsymbol{\nu} + \tilde{\mathbf{q}}\right)\right\rangle, \qquad (2\text{-}4.11)
\end{aligned}$$

Transversality conditions imply that:

$$\begin{aligned}
\mathbf{p}_{\mathbf{q}}(T) &= \mathbf{p}_{v_q}(T) = \mathbf{p}_s(T) = \mathbf{p}_{v_s}(T) = 0 \\
p_z(\boldsymbol{\nu},T) &= p_z^f(\boldsymbol{\nu}) \qquad (2\text{-}4.12) \\
p_y(T) &= 1.
\end{aligned}$$

The necessary conditions are determined as follows.

$$\begin{aligned}
\dot{\tilde{\mathbf{q}}}(t) &= \frac{\partial H}{\partial \mathbf{p_q}} = \mathbf{v_q}(t) \\
\dot{\mathbf{v}}_{\mathbf{q}}(t) &= \frac{\partial H}{\partial \mathbf{p}_{v_q}} = -\frac{\mathbf{p}_{v_q}(t)}{\mu(\lambda\bar{z})^2 p_y(t)} \\
\dot{\mathbf{s}}(t) &= \frac{\partial H}{\partial \mathbf{p}_s} = \mathbf{v_s}(t) \\
\dot{\mathbf{v}}_{\mathbf{s}}(t) &= \frac{\partial H}{\partial \mathbf{p}_{v_s}} = -\frac{\mathbf{p}_{v_s}(t)}{4\mu p_y(t)} \\
\dot{y}(t) &= \frac{\partial H}{\partial p_y} = \frac{\left\|\mathbf{p}_{v_q}(t)\right\|^2}{2\mu(\lambda\bar{z})^2 p_y^2(t)} + \frac{\|\mathbf{p}_{v_s}(t)\|^2}{8\mu p_y^2(t)} \\
\dot{z}(\boldsymbol{\nu}, t) &= \frac{\partial H}{\partial p_z} = \hat{A}_p\left(\boldsymbol{\nu} - \tilde{\mathbf{q}}(t)\right) + \hat{A}_p\left(\boldsymbol{\nu} + \tilde{\mathbf{q}}\right) \\
\dot{\mathbf{p}}_{\mathbf{q}}(t) &= -\frac{\partial H}{\partial \tilde{\mathbf{q}}} = -\left\langle p_z(\boldsymbol{\nu}, t), -\nabla\hat{A}_p\left(\boldsymbol{\nu} - \tilde{\mathbf{q}}(t)\right) + \nabla\hat{A}_p\left(\boldsymbol{\nu} + \tilde{\mathbf{q}}(t)\right)\right\rangle \\
\dot{\mathbf{p}}_{v_q}(t) &= -\frac{\partial H}{\partial \mathbf{v}_q} = -\mathbf{p_q}(t) \\
\dot{\mathbf{p}}_s(t) &= -\frac{\partial H}{\partial \mathbf{s}} = 0 \\
\dot{\mathbf{p}}_{v_s}(t) &= -\frac{\partial H}{\partial \mathbf{v}_s} = -\mathbf{p}_s(t) \\
\dot{p}_y(t) &= -\frac{\partial H}{\partial y} = 0 \\
\dot{p}_z(\boldsymbol{\nu}, t) &= -\frac{\partial H}{\partial z} = 0.
\end{aligned} \tag{2-4.13}$$

From the initial and terminal conditions (2-4.8), the transversality conditions (2-4.12) and the third, fourth, ninth and tenth equation in (2-4.13), we find that $\mathbf{p}_s(t) = \mathbf{p}_{v_s} = 0$, $\mathbf{s}(t) = \mathbf{s}_0$ and $\mathbf{v_s} = \mathbf{v}_{\mathbf{s}_0}$ for all $t \in [0, T]$. This also implies that $\mathbf{u}_1 = -\mathbf{u}_2$. Hence a necessary optimality condition is that the center of mass remains fixed in space. That is because, firstly, motion of the center of mass does not affect image quality. Secondly, any motion of the center of mass will result in additional unnecessary fuel cost. So, it is intuitive that the center of mass be fixed as an optimality necessary condition.

Finally, the transversality condition on p_y and p_z, and the eleventh and twelfth

equation in (2-4.13) imply that $p_y(t) = 1$ and $p_z(\boldsymbol{\nu}, t) = p_z^f(\boldsymbol{\nu})$ for all $t \in [0, T]$. After omitting equations related to the motion of the center of mass, the above discussion implies that the necessary conditions are:

$$\begin{aligned}
\dot{\tilde{q}}(t) &= \mathbf{v_q}(t) \\
\dot{\mathbf{v}}_{\mathbf{q}}(t) &= -\frac{\mathbf{p}_{v_q}(t)}{\mu(\lambda\bar{z})^2} \\
\dot{y}(t) &= \frac{\left\|\mathbf{p}_{v_q}(t)\right\|^2}{2\mu(\lambda\bar{z})^2} \\
\dot{z}(\boldsymbol{\nu}, t) &= \hat{A}_p\left(\boldsymbol{\nu} - \tilde{\mathbf{q}}(t)\right) + \hat{A}_p\left(\boldsymbol{\nu} + \tilde{\mathbf{q}}(t)\right) \\
\dot{\mathbf{p}}_{\mathbf{q}}(t) &= -\left\langle p_z^f(\boldsymbol{\nu}), -\nabla\hat{A}_p\left(\boldsymbol{\nu} - \tilde{\mathbf{q}}(t)\right) + \nabla\hat{A}_p\left(\boldsymbol{\nu} + \tilde{\mathbf{q}}(t)\right)\right\rangle \\
\dot{\mathbf{p}}_{v_q}(t) &= -\mathbf{p}_{\mathbf{q}}(t).
\end{aligned} \tag{2-4.14}$$

2.5 Control Law Performance

The Equations (2-4.14) are the necessary optimal conditions. These and the transversality conditions (2-4.12) represent a two point boundary value problem. These conditions, however, furnish little as far as finding a solution is concerned. Firstly, these are just necessary conditions and are not sufficient. Hence, finding a trajectory that satisfies these conditions does not mean we have found a solution to the problem. Secondly, these equations are hard to solve both analytically and numerically.

Still, these conditions are helpful in that one can study the general behavior of an optimal solution. For instance, we showed that a necessary condition for optimality in a fuel-image sense is to have the two spacecraft formation have the center of mass drift with constant velocity and the spacecraft move symmetrically about the origin of the coordinate system, which we may take to be the center of mass itself.

Moreover, we may also numerically investigate whether the control law given

above behaves as we would expect it to. We will treat the problem as an initial value problem by selecting arbitrary initial value for the adjoint variables. We perform the simulation using Matlab®. Instead of performing required integrations over D_v, we instead integrate over a rectangle containing D_v, while setting $z(\bar{u}, 0) = 1$ for all $\bar{u} \notin D_v$. The rectangle is composed of 32×32 pixels. D_v is such that it is 30 pixels in diameter. The picture frame disc is 4 pixels in diameter. We use the Matlab® function `gradient` to compute the gradient of the picture frame functions. We normalize the position vector $\bar{q}$ such that position is given in terms of number of pixels and $\bar{v}_q$ is such that it is in terms of pixels per second. The duration of the simulation is carried for 50 seconds and $\lambda\bar{z} = 1 \times 10^4$. We use these values for all simulations. We consider four numerical examples. The parameters where set as shown in Tables (2.1) and (2.2).

Example in	$\bar{q}_0$	$\bar{v}_0$	μ
Figure (2.3)	(5,10)	(-0.5,0.5)	5×10^{-4}
Figure (2.4)	(9,9)	(-1,1)	1×10^{-6}
Figure (2.5)	(13,2)	(-10,0)	1×10^{-6}
Figure (2.6)	(13,2)	(-9,0)	1×10^{-4}

Table 2.1: Variable choices for numerical examples.

Example in	$\mathbf{p_q}(0)$	$\mathbf{p}_{v_q}(0)$	$p_z^f(\boldsymbol{\nu}),\ \forall\boldsymbol{\nu}$
Figure (2.3)	-1000*(1,1)	-1000*(1,1)	-1000
Figure (2.4)	(0,0)	(0,0)	-1000
Figure (2.5)	(0,0)	(0,0)	-1000
Figure (2.6)	(0,0)	(0,0)	-1000

Table 2.2: Variable choices for numerical examples (continued.)

In Figures (2.3) and (2.4), we investigate the behavior of the picture frame disc when it gets a "head-on" impact with the boundary of the resolution disc. This behavior agrees with our intuition behind the formulation of the optimal control prob-

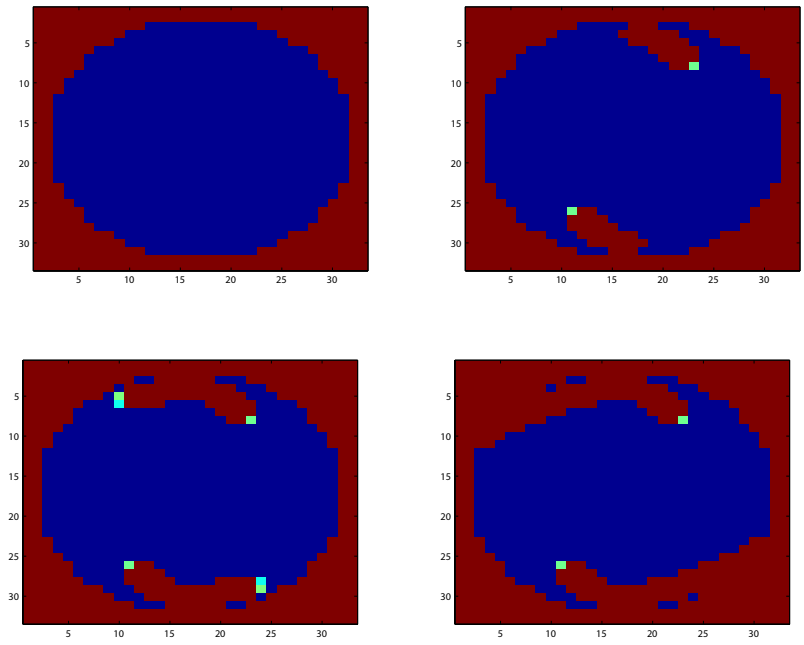

Figure 2.3: Motion of the picture frame discs in the u-v plane at $t = 0$, $t = 1.16,\ 2.33$ and 3.50 seconds.

lem in that the picture frame discs move in directions seeking to achieve $z(\boldsymbol{\nu}, T) = 1$ to satisfy the terminal condition. We note in these two examples that the choice of $p_z^f(\boldsymbol{\nu})$ greatly affects the behavior. We had to readjust its value until the desired result in the figures is obtained. This indicates that our choice for $p_z^f(\boldsymbol{\nu})$ may be close to the exact (and unknown) value. The reason for the sharper reaction by the picture frame disc in Figure (2.4) is mainly due to the fact that we have decreased the weight placed on fuel expenditure. For the former case we have $\mu = 5 \times 10^{-4}$ and $\mu = 1 \times 10^{-6}$ for the latter.

Another interesting behavior is given in Figures (2.5) and (2.6). Again the observations we make here are dependent on the choice of the value of $p_z^f(\boldsymbol{\nu})$. It seems again that our choice for $p_z^f(\boldsymbol{\nu})$ is sufficiently close to the actual optimal value that gives rise to the desired optimal behavior. In these two examples we investigate the response of the control law to the speed of the picture frame discs. Since $z(\boldsymbol{\nu}, t)$ is,

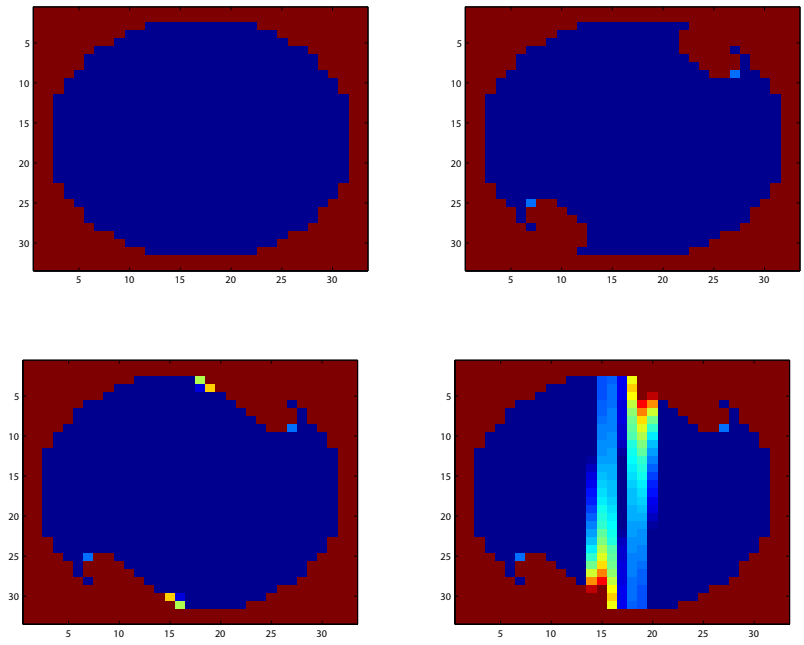

Figure 2.4: Motion of the picture frame discs in the u-v plane at $t = 0$, $t = 3.33,\ 6.66$ and 10 seconds.

by definition, equal to the amount of time the frequency point $\boldsymbol{\nu}$ spends inside the picture frame disc up to time t, then as the picture frame discs moves faster the less time it spends at a given frequency point $\boldsymbol{\nu}$. Thus, if the speed at which the picture frame disc moves is larger than the threshold value v^* (see Section (2.2)), then the value of $z(\boldsymbol{\nu}, t) < 1$ as the picture frame disc leaves $\boldsymbol{\nu}$ at time t. To meet the terminal condition on z (that is, $h(z(\boldsymbol{\nu}, T)) = 1$) we would expect that the control law apply a negative thrust to reduce the velocity of the picture frame disc (assuming we set $p_z^f(\boldsymbol{\nu})$ at the correct value.)

This is indeed what we see in Figures (2.5) and (2.6). The initial velocity is too large and we note that, with time, coverage improves as the picture frame discs move (this is observed by the fact that coverage becomes darker with time.) The initial speed in Figure (2.5) is larger than that in Figure (2.6). We note that, in the former figure, coverage converges to a darker shade of red less rapidly than that in the latter

figure. This is true assuming that we have chosen a value for $p_z^f(\boldsymbol{\nu})$ that is close enough to the desired value.

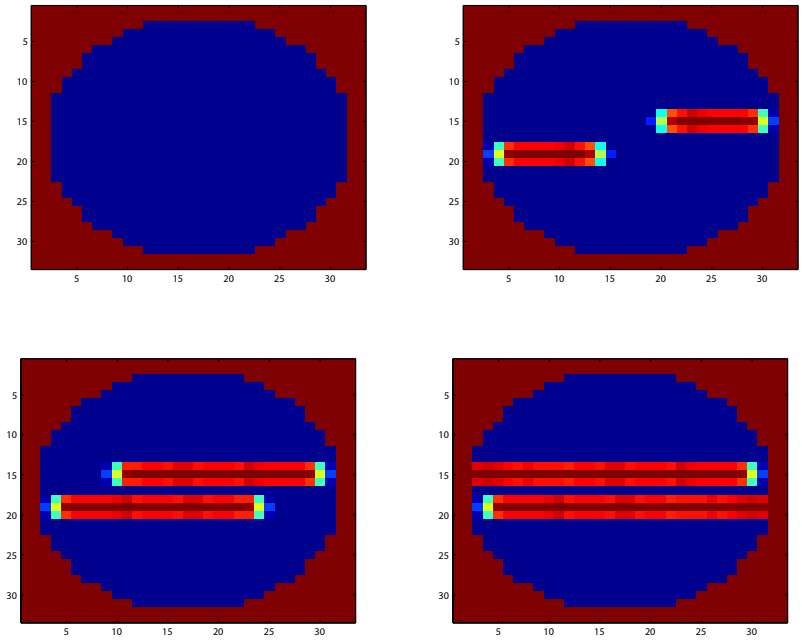

Figure 2.5: Motion of the picture frame discs in the u-v plane at $t = 0$, $t = 0.99$, 2 and 3 seconds.

2.6 The Two Spacecraft, One-Dimensional Problem

In this section we further specialize Equations (2-4.14) to the two-spacecraft, one-dimensional case. By one dimensional we mean that the wave number resolution disk D_v collapses to a wave number interval $\mathcal{L}_v = [-L_v/2, L_v/2]$, where $L_v/2$ is the bound on the frequency content of the signal to be reconstructed (that is, L_v is the width of the resolution interval.)

This simple example also has a profound theoretical implication. Note that locally the motion of any particular picture frame disc in the two-dimensional case, when linearized about any point in time t, can be approximated by a one-dimensional motion. Hence, studying the one-dimensional case gives insight into the local-time

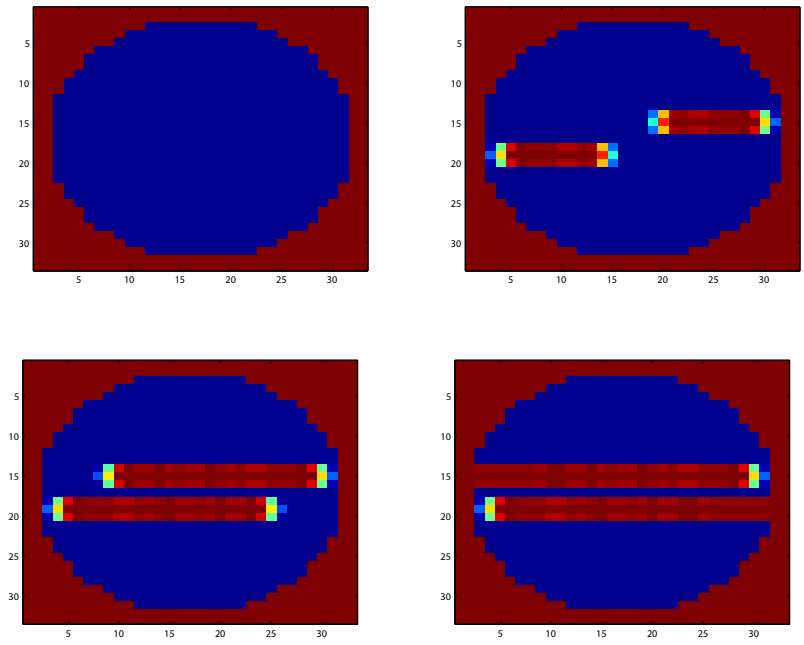

Figure 2.6: Motion of the picture frame discs in the u-v plane at $t = 0$, $t = 1.16,\ 2.33$ and 3.5 seconds.

behavior of the picture frame disc. For example, by studying how a one-dimensional picture frame disc interacts with partially covered ($z < 1$) one-dimensional intervals along the line of motion enables us to understand how a two-dimensional picture frame disc infinitesimally interacts with neighboring (2-dimensional) coverage areas.

In the one-dimensional case, the necessary conditions become:

$$\begin{aligned}
\dot{q}(t) &= v(t) \\
\dot{v}(t) &= -\frac{p_v(t)}{\mu(\lambda\bar{z})^2} \\
\dot{y}(t) &= \frac{\|p_v(t)\|^2}{2\mu(\lambda\bar{z})^2} \\
\dot{z}(\nu,t) &= \hat{A}_p\left(\nu - q(t)\right) + \hat{A}_p\left(\nu + q(t)\right) \\
\dot{p}_q(t) &= -\left\langle p_z^f(\nu), -\frac{\mathrm{d}}{\mathrm{d}\nu}\hat{A}_p\left(\nu - q(t)\right) + \frac{\mathrm{d}}{\mathrm{d}\nu}\hat{A}_p\left(\nu + q(t)\right)\right\rangle \\
\dot{p}_v(t) &= -p_q(t),
\end{aligned} \tag{2-6.1}$$

where we omit the subscript q in v_q and remove the over-bars that indicated vector-

valued variables. The inner product $\langle \cdot, \cdot \rangle$ refers to the inner product on the vector space of real functions whose domain is the resolution interval $\mathcal{L}_v$:

$$\langle f(\nu), g(\nu) \rangle = \int_{-L_v/2}^{L_v/2} f(\nu) g(\nu) \mathrm{d}\nu, \tag{2-6.2}$$

for any two functions $f, g : \mathcal{L}_v \to \mathbb{R}$. The last equation in (2-6.1) is auxiliary to the necessary conditions, and is not itself a necessary condition. The initial and terminal conditions are given:

$$\begin{aligned} q(0) &= q_0 \\ v(0) &= v_0 \\ y(0) &= 0 \\ z(\nu, 0) &= 0, \forall \nu \in \mathcal{L}_v \\ z(\nu, T) &= 1, \forall \nu \in \mathcal{L}_v \\ p_q(T) &= 0 \\ p_v(T) &= 0. \end{aligned}$$

Note also that the gradient operator changes to a simple derivative over the frequency domain. Under the model given in Equation (2-1.23), we then have

$$\begin{aligned} \hat{A}_p(\nu - q(t)) &= \begin{cases} 1 & q(t) - r_p \leq \nu \leq r_p + q(t) \\ 0 & \text{otherwise} \end{cases} \\ \hat{A}_p(\nu + q(t)) &= \begin{cases} 1 & -r_p - q(t) \leq \nu \leq r_p - q(t) \\ 0 & \text{otherwise} \end{cases} \end{aligned}$$

and, hence

$$\begin{aligned} \frac{\mathrm{d}}{\mathrm{d}\nu} \hat{A}_p(\nu - q(t)) &= \delta(\nu - (q(t) - r_p)) - \delta(\nu - (q(t) + r_p)) \\ \frac{\mathrm{d}}{\mathrm{d}\nu} \hat{A}_p(\nu + q(t)) &= \delta(\nu - (-r_p - q(t))) - \delta(\nu - (r_p - q(t))), \end{aligned}$$

where $\delta(x)$ is the Dirac delta function (assuming the picture frame function $\hat{A}_p$ assumes a Heaviside step function.)

We now postulate a trajectory and attempt to construct a solution to the above necessary conditions. Specifically, we study a trajectory such that the picture frame discs (and the spacecraft in physical space) move with a constant critical speed v_c:

$$q(t) = -v_c t + q_0. \tag{2-6.3}$$

We choose $q_0 = \frac{L_v}{2} + r_p$ such that the picture frame discs are initially located right outside the resolution interval. The critical speed v_c is the speed that guarantees that at any frequency component $\nu \in \left[-\frac{L_v}{2}, \frac{L_v}{2}\right]$ we achieve $z(\nu, T) = 1$ at the end of the maneuver with only a single passage over the resolution interval. Note that $z(\nu, t)$ is equal to the amount of time spent by the frequency ν inside one of the picture frame discs up to time t. These choices imply that we have to set $v_c = 2r_p$ to ensure that $z = 1$ at each frequency inside the resolution interval $[-L_v/2, L_v/2]$. The terminal time T is chosen such that $q(T) = 0$ (with the picture frame discs centered at the origin.) Hence, we have $T = \frac{1}{2} + \frac{(L_v/2)}{v_c}$. We will fix this terminal time value and assume it is chosen as such beforehand.

The reason behind choosing this trajectory is that at the end of the maneuver each frequency is covered such that $z(\nu, T) = 1$ and because it does not require expending any fuel to speed up or slow down the spacecraft. In fact, if the speed at any point in time is greater than the critical speed v_c, then $z(\nu, t)$ at that point will be less than unity. Hence, we set the speed at the critical value v_c to complete the mission in the required time T. A practical drawback of this motion is that the two spacecraft do not have a zero approach velocity at the terminal time T (with $q(T) = 0$ being the terminal position of both spacecraft), which leads to collision.

Equations (2-6.3) and the necessary conditions (2-6.1) imply that:

$$\begin{aligned} v(t) &= -v_c \\ p_q(t) &= 0 \\ p_v(t) &= 0 \\ p_z(\nu,t) &= p_z^f(\nu). \end{aligned}$$

Thus, we are left with

$$\begin{aligned} \dot{y} &= 0 \\ \dot{z}(\nu,t) &= \hat{A}_p\left(\nu - q(t)\right) + \hat{A}_p\left(\nu + q(t)\right) \\ 0 &= p_z^f(\nu = q(t) - r_p, t) - p_z^f(\nu = q(t) + r_p, t) \\ &\quad + p_z^f(\nu = -q(t) - r_p, t) - p_z^f(\nu = -q(t) + r_p, t),\ \forall t \in [0,T]. \end{aligned} \tag{2-6.4}$$

The first of these equations and the initial condition $y(0) = 0$ implies that $y(t) = 0$ for all $t \in [0,T]$. In particular, we have $y(T) = 0$. Hence the proposed solution achieves zero cost. Since the cost functional $\mathcal{J}$ is positive definite, then any solution that achieves zero cost and satisfies the terminal condition is then an optimal solution. We now need to show that the terminal condition is satisfied for the proposed motion. We do this as follows.

Fix a frequency point $\nu \in \mathcal{L}_v$. We now make use of the fact that the picture frame disc moves at constant speed. See Figure (2.7). We compute the time spent by the picture frame disc over ν by firstly computing the time t_1 it takes the picture frame's leading edge to touch ν and secondly by computing the time t_2 the trailing edge passes over ν. By the uniformity of the motion, the time spent by the picture frame disc over ν is simply the difference $t_2 - t_1$. By construction of our solution,

one can easily verify that

$$\begin{aligned} t_1 &= \frac{1}{2r_p}\left(\frac{L_v}{2} - \nu\right) \\ t_2 &= \frac{1}{2r_p}\left(2r_p + \frac{L_v}{2} - \nu\right). \end{aligned}$$

Hence, the difference $t_2 - t_1$ is given by

$$t_2 - t_1 = 1. \tag{2-6.5}$$

Since we do not have double passages over any frequency point ν, then at $t = T$, $z(\nu, T) = 1$, for all $\nu \in \mathcal{L}_v$. This shows that the proposed motion is indeed optimal since it achieves zero cost and satisfies the desired terminal conditions. To complete the proof, we just need to show that the third condition in Equations (2-6.4) is satisfied for all $t \in [0, T]$. Note that the function $p_z^f(\nu)$ does not influence the remaining necessary conditions. Hence, any choice for $p_z^f(\nu)$ that will set the right hand side equal to zero is a valid choice. For instance, any symmetric function $p_z^f(\nu)$ will satisfy this condition since the second term in the inner product is skew symmetric (that is, if f is symmetric and g is skew symmetric, then $\langle f, g\rangle = 0$). Indeed, if we set $p_z^f(\nu) \equiv 0$ for all $\nu \in \mathcal{L}_v$ is a valid choice. This completes the proof.

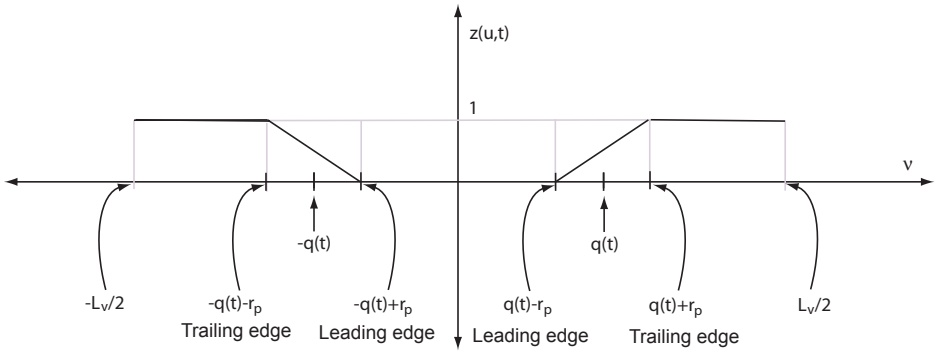

Figure 2.7: Motion under consideration in the one-dimensional case.

2.7 Conclusion

In this chapter we derived a relationship between the motion of a formation and its image quality performance via the modulation transfer function. We briefly introduced and discussed a noise model. Based on this, we formulated an optimal control problem where the objective is to minimize fuel expenditure and to maximize image quality by maximizing the normalized modulation transfer function. We used the maximum principle to derive the necessary conditions for a multi-spacecraft formation. The results are then specialized to the two-spacecraft formation. We show that necessary optimality conditions imply that the spacecraft pair move symmetrically about the origin and that the formation center of mass be fixed at the origin. We give some numerical results showing the general behavior of the resulting control law. Finally, we derive the necessary conditions and propose an optimal solution for the two spacecraft, one-dimensional problem.

CHAPTER 3

Dynamic Coverage Optimal Control for Interferometric Imaging Spacecraft Formations

In this and future chapters, we use differential geometry and geometric mechanics as the tools to analyze the formation path planning problem. If unfamiliar with these tools, for a brief background, we suggest that the reader go through Appendix A and literature referenced therein.

Dynamic coverage optimal control is a new class of optimal control problems motivated by multi-spacecraft interferometric imaging applications [38, 39]. The dynamics is composed of N second order differential equations representing N fully actuated particles. To be minimized is a cost functional that is a weighted sum of the total fuel expenditure, the relative speeds between the particles and the measure of a given set whose size is a function of the particles' trajectories. In this chapter, we first analyze the problem for formations evolving on non-linear manifolds. We derive the necessary optimality conditions and give an example of a non-rigid two spacecraft formation evolving on a paraboloidal surface. We specialize the analysis to the case when the formation is co-planar. As will be shown, one outcome of this work is that a necessary condition for a formation motion to be optimal is that it is symmetric about the origin. This chapter is concluded by giving a simple three

spacecraft planar example.

3.1 Introduction

We consider the general class of problems described by a system of N particles satisfying dynamics of the form:

$$\begin{aligned} \frac{\mathrm{D}\mathbf{q}_i}{\mathrm{d}t}(t) &= \mathbf{v}_i(t) \\ \frac{\mathrm{D}\mathbf{v}_i}{\mathrm{d}t}(t) &= \mathbf{u}_i(t) \end{aligned} \tag{3-1.1}$$

$i = 1, \ldots, N$, where $\mathbf{q}_i : [0, T] \to M$ is a curve on M, $\mathbf{v}_i(t) \in T_{\mathbf{q}_i(t)}M$ and $\mathbf{u}_i(t) \in TT_{\mathbf{q}_i(t)}M$.

Let $\mathbf{u}_i(t) \in TT_{\mathbf{q}_i(t)}M$ be given by

$$\mathbf{u}_i(t) = \sum_{j=1}^{m} u_i^j(t)\mathbf{Y}_j(\mathbf{q}_i(t)), \tag{3-1.2}$$

where $m \leq n$ and $\mathbf{Y}_j$, $j = 1, \ldots, n$, are basis vector fields that satisfy $\langle \mathbf{Y}_j, \mathbf{Y}_k \rangle = \delta_{jk}$. In other words, $\mathbf{Y}_j$ is an orthonormal set of vector fields on $T_{\mathbf{q}_i(t)}M$. Mathematically, this assumption limits the class of manifolds we consider (to parallelizable or to a local study of non-parallelizable manifolds) for the general problem formulation, but is satisfied for the special case where we deal with systems of particles in space. $m = n$ corresponds to the fully actuated system, whereas $m < n$ corresponds to the under-actuated situation. Here we only consider fully actuated systems.

Assumption 3.1.1. Each particle is fully actuated in all n directions. That is to say $m = n$.

3.2 Imaging and the Coverage Problem

Equations (3-1.1) represent the spacecraft dynamics, treating each spacecraft as a point particle. Hence, we ignore attitude dynamics and assume all spacecraft are

perfectly aligned and are pointing towards the target. In interferometric imaging, we are interested in the relative position dynamics as projected onto a plane perpendicular to the line of sight. This plane is called the observation plane, denoted by $O \subset \mathbb{R}^2$. Hence, we are interested in the *projected relative curves*:

$$\tilde{\mathbf{q}}_{ij}(t) \;=\; \frac{1}{\lambda}\mathbb{P}_O\left(\mathbf{q}_j(t) - \mathbf{q}_i(t)\right), \tag{3-2.1}$$

where λ is the optical wavelength and $\tilde{\mathbf{q}}_{ij} : [0, T] \to \tilde{O}$ are curves on $\tilde{O}$, the frequency (also known as the u-v) plane, and $\mathbb{P}_O$ is the operator that projects relative trajectories in M onto the observation plane O. Hence, O is the plane on which motion is projected and $\tilde{O}$ is the frequency plane. Let $\ll \cdot, \cdot \gg$ denote the inner product on O.

Recall that in multi-aperture interferometry there are two main imaging goals. The first is simply referred to as frequency domain coverage. We refer the reader to Chapter 2 and the thesis [5] for a detailed discussion of multi-aperture interferometric imaging. We are interested in having the resolution disc as defined by the set $\mathcal{D}_R = \left\{(\nu_x, \nu_y) : \sqrt{u^2 + v^2} \leq 1/\theta_r\right\}$ be completely covered by some ball of radius r_p centered at $\tilde{\mathbf{q}}_{ij}(t)$, for some $t \in [0, T]$, i and j, where θ_r is the angular resolution. An image is said to be successfully completed if a maneuver $\mathcal{M}$ satisfies the following condition.

Definition 3.2.1. (**Successful Imaging Maneuver**) An imaging maneuver $\mathcal{M}$ is said to be successful if, for each $(\nu_x, \nu_y) \in \mathcal{D}_R$, there exists a time $t \in [0, T]$ and some $i, j = 1, \ldots, N$ such that $(\nu_x, \nu_y) \in \bar{B}_{r_p}\left(\tilde{\mathbf{q}}_{ij}(t)\right)$, where $\bar{B}_x(\mathbf{y})$ is a *closed* ball in $\mathbb{R}^2$ of radius x centered at $\mathbf{y}$. r_p is proportional to the size of the telescope's airy disc.

The second objective is that all frequencies in $\mathcal{D}_R$ must be sampled while maximizing the signal-to-noise ratio (SNR.) SNR can be controlled by controlling the relative speeds between the spacecraft in the formation [5]. As the projected relative

speed between a spacecraft pair is minimized, so is the achievable SNR. Intuitively, as a spacecraft moves slower, it has more time spent in the neighborhood of a relative position state in space. This leads to more photon (that is, image information) collection from that neighborhood, resulting in a stronger signal. This is analogous to the notion of exposure time in photography, where the longer the shutter time, the more photons get deposited on the photographic film and the better the image gets.

3.3 Dynamic Coverage Optimal Control

Based on the above discussion, we wish to minimize three quantities: (1) the fuel expended by each spacecraft in the constellation, (2) the projected relative speeds between the spacecraft of the system and (3) the amount of uncovered points in $\mathcal{D}_R$. The constraints we have are the dynamics (3-1.1) and boundary conditions on the position and velocity vectors of each spacecraft. Motion constraints (as defined in Chapters 4 and 5, and the paper [40]) are not treated in this chapter, though they can be easily incorporated in the analysis. We now state the coverage optimal control problem considered in this chapter.

Problem 3.3.1. ***Coverage Optimal Control Problem:*** *Minimize*

$$\begin{aligned}\mathcal{J}(\mathbf{q}_i, \mathbf{u}_i, t; i = 1, \ldots, N) \;\; = \;\; & \int_0^T \frac{1}{2}\Bigg\{ \sum_{j=1}^{N} \Bigg[\langle \mathbf{u}_j, \mathbf{u}_j \rangle + \tau^2 \sum_{k=1}^{N} \ll \frac{\mathrm{d}\tilde{\mathbf{q}}_{jk}}{\mathrm{d}t}, \frac{\mathrm{d}\tilde{\mathbf{q}}_{jk}}{\mathrm{d}t} \gg \Bigg] \Bigg\} \\ & + \kappa^2 \, \mathrm{meas}\,(\Psi)\, \mathrm{d}t, \end{aligned} \tag{3-3.1}$$

where Ψ *is the mapping that returns the set of uncovered frequency points in* $\mathcal{D}_R$ *up to time* t*;* $\Psi : (t, \tilde{\mathbf{q}}_{ij}; i, j = 1, \ldots, N) \rightarrow \{(\nu_x, \nu_y) \in \mathcal{D}_R : \forall \varepsilon \in [0, t] \text{ and } \forall i, j \in 1, \ldots, N, (\nu_x, \nu_y) \notin \bar{B}_{r_p}(\tilde{\mathbf{q}}_{ij}(\varepsilon))\}$ *and the function* $\mathrm{meas}\,(\Lambda)$ *is a measure function of*

some set Λ*. The constraints are the dynamics (3-1.1), the boundary conditions*

$$\mathbf{q}_i(0) = \mathbf{q}_i^0,\ \mathbf{q}_i(T) = \mathbf{q}_i^T,\ \mathbf{v}_i(0) = \mathbf{v}_i^0,\ \mathbf{v}_i(T) = \mathbf{v}_i^T, \tag{3-3.2}$$

$i = 1, \ldots, N$*, and the relationship in Equation (3-2.1).*

In Equation (3-3.1), we have used the simple derivative $\frac{\mathrm{d}}{\mathrm{d}t}$ to differentiate the quantity $\tilde{\mathbf{q}}_{jk}$ since $\tilde{\mathbf{q}}_{jk}$ belongs to the flat space $\mathbb{R}^2$. Hence, a covariant time derivative $\frac{\mathrm{D}}{\mathrm{d}t}$ reduces to the simple derivative $\frac{\mathrm{d}}{\mathrm{d}t}$.

Note that if $\kappa = 0$, then the problem reduces to that discussed in Chapter 5 and in [40] for a two-spacecraft formation. In this case, the terminal boundary conditions alone drive the system. On the other hand if $\kappa \neq 0$, then the system is driven to also minimize the set of uncovered points in $\mathcal{D}_R$. Whenever meas (Ψ) becomes zero, the only drive is to meet the terminal conditions in (3-3.2).

The measure function meas$(\cdot)$ is simply the area covered by the set $\Psi(t, \tilde{\mathbf{q}}_{ij})$. Firstly, note that as the curves $\tilde{\mathbf{q}}_{ij} : [0, T] \to \tilde{O}$ change, the measure of Ψ at time T changes. However, if the curves $\tilde{\mathbf{q}}_{ij}$ correspond to trajectories of successful maneuvers as defined in Definition (6.5.1), then meas$(\Psi(T, \tilde{\mathbf{q}}_{ij}^*))$ is zero at time T.

Secondly, note that meas(Ψ) is a monotonically decreasing function in time t. The reason for this is illustrated in Figure (3.1), which is the situation in the frequency domain for a two spacecraft system (hence, two coverage discs), and is explained as follows. Maximum decrease rate for meas(Ψ) is when *all* balls $\bar{B}_{r_p}(\tilde{\mathbf{q}}_{ij}(t))$, $i, j = 1, \ldots, N$, are moving into uncovered territory *inside* $\mathcal{D}_R$. In Figure (3.1), this happens at time t_0 and t_3 since both coverage balls move in previously uncovered territory. The other extreme is when *all* balls $\bar{B}_{r_p}(\tilde{\mathbf{q}}_{ij}(t))$, $i, j = 1, \ldots, N$, are moving in previously covered regions or have wandered outside $\mathcal{D}_R$, which corresponds to a constant value of meas(Ψ). In Figure (3.1), this happens instantaneously at time

t_2 since both balls cover previously covered territory. Intermediate decrease rates vary between these two extremes (for example, at time t_1 as shown in the figure.) Note that the two coverage balls traverse symmetric curves. Symmetry holds for an arbitrary number of spacecraft by virtue of the condition (3-2.1).

Assumption 3.3.1. The function meas is differentiable with respect to both arguments t and $\tilde{\mathbf{q}}$.

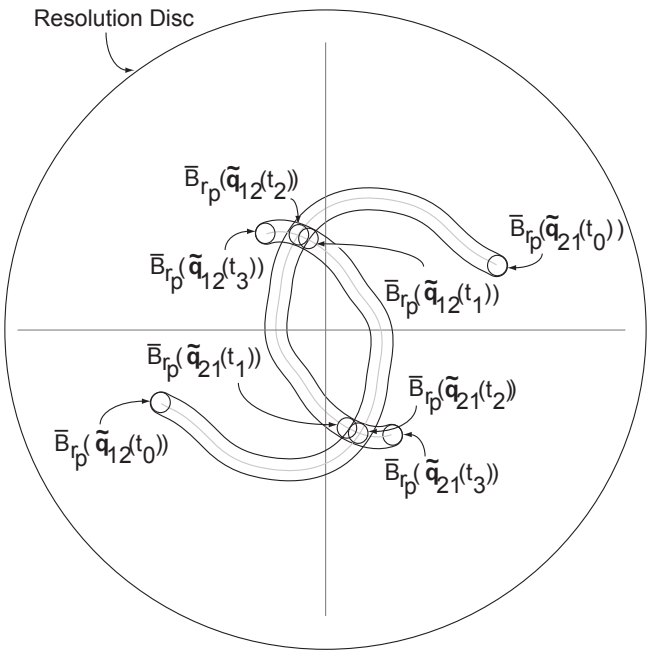

Figure 3.1: A two spacecraft illustration of motion in the frequency domain ($t_0 < t_1 < t_2 < t_3$).

Finally, note that according to the definition of the coverage optimal control problem stated above, solutions to this problem do not necessary result in successful maneuvers. As the weight κ approaches infinity, the resulting solutions will tend to

be successful maneuvers. Removing the term κ^2 meas $(\Psi(t))$ from the integrand and posing it as the terminal constraint meas $(\Psi(T)) = 0$ is another strategy that results in successful maneuvers, something we do not pursue here.

3.4 Necessary Conditions for Optimality

To obtain necessary optimality conditions we first append the dynamic constraints in Equations (3-1.1) to the Lagrangian of the cost functional (3-3.1) by introducing

$$\boldsymbol{\lambda}_1^j \left(\frac{\mathrm{D}\mathbf{q}_j}{\mathrm{d}t} - \mathbf{v}_j \right) + \boldsymbol{\lambda}_2^j \left(\frac{\mathrm{D}\mathbf{v}_j}{\mathrm{d}t} - \mathbf{u}_j \right) \tag{3-4.1}$$

into the cost functional $\mathcal{J}$, where $\boldsymbol{\lambda}_1^j$ and $\boldsymbol{\lambda}_2^j$, $j = 1, \ldots, N$, are Lagrange multipliers. Collecting terms with the same indexes, Equation (3-3.1) becomes:

$$\begin{aligned} \mathcal{J}(\mathbf{q}_i, \mathbf{u}_i) \;=\; & \int_0^T \sum_{j=1}^{N} \left[\frac{1}{2} \langle \mathbf{u}_j, \mathbf{u}_j \rangle + \boldsymbol{\lambda}_1^j \left(\frac{\mathrm{D}\mathbf{q}_j}{\mathrm{d}t} - \mathbf{v}_j \right) + \boldsymbol{\lambda}_2^j \left(\frac{\mathrm{D}\mathbf{v}_j}{\mathrm{d}t} - \mathbf{u}_j \right) \right. \\ & \left. + \frac{\tau^2}{2} \sum_{k=1}^{N} \ll \frac{\mathrm{d}\tilde{\mathbf{q}}_{jk}}{\mathrm{d}t}, \frac{\mathrm{d}\tilde{\mathbf{q}}_{jk}}{\mathrm{d}t} \gg \right] + \kappa^2 \text{ meas} \left[\Psi \left(\tilde{\mathbf{q}}_{jk}(t); j, k = 1, \ldots, N \right) \right] \mathrm{d}t. \end{aligned} \tag{3-4.2}$$

We then introduce the following one-parameter variations for the curves $\mathbf{q}_i$:

$$\begin{aligned} \mathbf{q}_i(t, 0) &= \mathbf{q}_i(t), \\ \frac{\mathrm{D}\mathbf{q}_i}{\partial \epsilon}(t, 0) &= \mathbf{W}_i(t) \\ \frac{\mathrm{D}\mathbf{q}_i}{\partial \epsilon}(0, 0) &= \frac{\mathrm{D}\mathbf{q}_i}{\partial \epsilon}(T, 0) = 0, \\ \frac{\mathrm{D}}{\mathrm{d}t} \frac{\mathrm{D}\mathbf{q}_i}{\partial \epsilon}(t, 0) &= \frac{\mathrm{D}}{\mathrm{d}t} \mathbf{W}_i(t) \text{ is continuous on } [0, T] \\ \frac{\mathrm{D}}{\mathrm{d}t} \frac{\mathrm{D}\mathbf{q}_i}{\partial \epsilon}(0, 0) &= \frac{\mathrm{D}}{\mathrm{d}t} \frac{\mathrm{D}\mathbf{q}_i}{\partial \epsilon}(T, 0) = 0, \end{aligned} \tag{3-4.3}$$

$i = 1, \ldots, N$. Likewise, we may define variations in $\mathbf{v}_i(t)$, $\mathbf{u}_i(t)$ and $\boldsymbol{\lambda}_k^i(t)$, $k = 1, 2$, $i = 1, \ldots, N$, by $\mathbf{v}_i(t, \epsilon)$, $\mathbf{u}_i(t, \epsilon)$ and $\boldsymbol{\lambda}_k^i(t, \epsilon)$, $k = 1, 2$, $i = 1, \ldots, N$, as follows:

$$\begin{aligned}
\mathbf{u}_i(t, \epsilon) &= \sum_{j=1}^{m} u_i^j(t, \epsilon) \mathbf{Y}_j(\mathbf{q}_i(t, \epsilon)) \in TT_{\mathbf{q}_i(t,\epsilon)} M \\
\mathbf{v}_i(t, \epsilon) &= \sum_{j=1}^{n} v_i^j(t, \epsilon) \mathbf{Y}_j(\mathbf{q}_i(t, \epsilon)) \in T_{\mathbf{q}_i(t,\epsilon)} M \\
\boldsymbol{\lambda}_k^i(t, \epsilon) &= \sum_{j=1}^{n} \boldsymbol{\lambda}_k^{ij}(t, \epsilon) \omega_j(\mathbf{q}_i(t, \epsilon)) \in T^*_{\mathbf{q}_i(t,\epsilon)} M
\end{aligned}$$

where $\boldsymbol{\omega}_j$, $j = 1, \ldots, n$, are co-vector fields such that $\boldsymbol{\omega}_l(\mathbf{Y}_j) = \delta_{lj}$. Taking variations in $\mathbf{u}_i$ and $\mathbf{v}_i$, we have:

$$\begin{aligned}
\left.\frac{\mathrm{D}\mathbf{u}_i}{\partial \epsilon}(t, \epsilon)\right|_{\epsilon=0} &= \delta \mathbf{u}_i(t) + \left(\mathbf{B}\left(\mathbf{W}_i, \mathbf{u}_i\right)\right)\left(\mathbf{q}_i(t)\right) \in TTM \\
\left.\frac{\mathrm{D}\mathbf{v}_i}{\partial \epsilon}(t, \epsilon)\right|_{\epsilon=0} &= \delta \mathbf{v}_i(t) + \left(\mathbf{B}\left(\mathbf{W}_i, \mathbf{u}_i\right)\right)\left(\mathbf{q}_i(t)\right) \in TTM
\end{aligned}$$

where, for instance,

$$\delta \mathbf{u}_i(t) = \sum_{j=1}^{m} \frac{\partial u_i^j}{\partial \epsilon}(t, 0) \mathbf{Y}_j(\mathbf{q}_i(t))$$

and

$$\left(\mathbf{B}\left(\mathbf{W}_i, \mathbf{u}_i\right)\right)\left(\mathbf{q}_i(t)\right) = \sum_{j=1}^{m} u_i^j(t) \left(\nabla_{\mathbf{W}_i} \mathbf{Y}_j\right)\left(\mathbf{q}_i(t)\right).$$

Similar expressions can be obtained for $\frac{\mathrm{D}\mathbf{v}_i}{\partial \epsilon}$ and $\frac{\mathrm{D}\boldsymbol{\lambda}_i^j}{\partial \epsilon}$, $j = 1, 2$, $i = 1, \ldots, N$. $\mathbf{B}(\cdot, \cdot)$ is a bilinear form that we introduce in order to be able to separate variations in the components of $\mathbf{u}_i$, $\mathbf{v}_i$ and $\boldsymbol{\lambda}_i^j$, $i = 1, \ldots, N$, $j = 1, 2$, from variations in the basis vector fields. It is important to separate these terms since the variations $\delta \mathbf{u}_i$, $\delta \mathbf{v}_i$ and $\delta \boldsymbol{\lambda}_j^i$, $i = 1, \ldots, N$, $j = 1, 2$, are independent from each other as well as from $\mathbf{W}_i$ –a fact which has significant importance in deriving necessary conditions.

For variations in $\tilde{\mathbf{q}}_{ij}(t)$, let

$$\tilde{\mathbf{q}}_{ij}(t, \epsilon) = \sum_{k=1}^{2} \tilde{q}_{ij}^k(t, \epsilon) \mathbf{Z}_k(\tilde{\mathbf{q}}_{ij}(t, \epsilon)) \in T_{\tilde{\mathbf{q}}_{ij}(t,\epsilon)} \tilde{O},$$

where $\mathbf{Z}_k$, $k = 1, 2$, is an orthonormal set of vector fields on $T_{\tilde{\mathbf{q}}_{ij}(t,\epsilon)}\tilde{O}$. The set $\mathbf{Z}_k$, $k = 1, 2$, may be taken to be the standard set of vector fields spanning $\mathbb{R}^2$.

The spacecraft are free to move on some given non-flat surface M. Such surfaces are usually dictated by some further imaging specifications. For example, having the formation evolve on a virtual paraboloid surface provides improved focusing properties. One good example is the ST-3 formation discussed in [36].

Thus, for $i, j = 1, \ldots, N$ we have

$$\begin{aligned}
\tilde{\mathbf{q}}_{ij}(t,0) &= \tilde{\mathbf{q}}_{ij}(t) = \frac{1}{\lambda}\mathbb{P}_O\left(\mathbf{q}_j(t) - \mathbf{q}_i(t)\right), \\
\frac{\mathrm{D}\tilde{\mathbf{q}}_{ij}}{\partial\epsilon}(t,0) &= \frac{1}{\lambda}\frac{\partial\mathbb{P}_O}{\partial\mathbf{q}} \cdot \left(W_j(t) - W_i(t)\right) \\
\frac{\mathrm{D}\tilde{\mathbf{q}}_{ij}}{\partial\epsilon}(0,0) &= \frac{\mathrm{D}\tilde{\mathbf{q}}_{ij}}{\partial\epsilon}(T,0) = 0, \\
\frac{\mathrm{D}}{\mathrm{d}t}\frac{\mathrm{D}\tilde{\mathbf{q}}_{ij}}{\partial\epsilon}(t,0) &= \frac{1}{\lambda}\frac{\mathrm{D}}{\mathrm{d}t}\left[\frac{\partial\mathbb{P}_O}{\partial\mathbf{q}} \cdot \left(W_j(t) - W_i(t)\right)\right] \\
\frac{\mathrm{D}}{\mathrm{d}t}\frac{\mathrm{D}\tilde{\mathbf{q}}_{ij}}{\partial\epsilon}(0,0) &= \frac{\mathrm{D}}{\mathrm{d}t}\frac{\mathrm{D}\tilde{\mathbf{q}}_{ij}}{\partial\epsilon}(T,0) = 0
\end{aligned} \tag{3-4.4}$$

where $\frac{\partial\mathbb{P}_O}{\partial\mathbf{q}} : M \to \mathbb{R}^2$ is viewed as a matrix transformation (tensor) on M. Hence, the right hand sides of the second and fourth equations represent the *projected* variational vector fields (that is, the components of the variational vector fields along O.)

Remark 3.4.1. $\tilde{\mathbf{q}}_{ij}$ belongs to a flat space O. Then

$$\frac{\mathrm{D}}{\partial\epsilon}\frac{\mathrm{D}\tilde{\mathbf{q}}}{\partial t} = \frac{\mathrm{D}}{\partial t}\frac{\mathrm{D}\tilde{\mathbf{q}}}{\partial\epsilon} + \tilde{R}\left(\frac{\mathrm{D}\tilde{\mathbf{q}}}{\partial\epsilon}, \frac{\mathrm{D}\tilde{\mathbf{q}}}{\partial t}\right)\frac{\mathrm{D}\tilde{\mathbf{q}}}{\partial t} = \frac{\mathrm{D}}{\partial t}\frac{\mathrm{D}\tilde{\mathbf{q}}}{\partial\epsilon} \tag{3-4.5}$$

because the curvature of O $\tilde{R} \equiv 0$.

We now have the first result of our chapter.

Theorem 3.4.1. *Under Assumptions (3.1.1) and (3.3.1), taking first order varia-*

tions of the expression in Equation (3-4.2) leads to the following relationship:

$$\frac{\partial \mathcal{J}}{\partial \epsilon}(\mathbf{q}_i(t,\epsilon),\mathbf{u}_i(t,\epsilon),t;i=1,\ldots,N)\Big|_{\epsilon=0} = \int_0^T \sum_{j=1}^N \langle \mathbf{u}_j, \mathbf{B}\left(\mathbf{W}_j,\mathbf{u}_j\right)\rangle - \frac{\mathrm{D}\boldsymbol{\lambda}_1^j}{\mathrm{d}t}\left(W_j\right)$$

$$-\boldsymbol{\lambda}_1^j\left(\mathbf{B}\left(\mathbf{W}_j,\mathbf{v}_j\right)\right) - \boldsymbol{\lambda}_2^j\left(\mathbf{B}\left(\mathbf{W}_j,\mathbf{u}_j\right)\right) + \boldsymbol{\lambda}_2^j\left(R\left(\mathbf{W}_j,\mathbf{v}_j\right)\mathbf{v}_j\right) - \frac{\mathrm{D}\boldsymbol{\lambda}_2^j}{\mathrm{d}t}\left(\mathbf{B}\left(\mathbf{W}_j,\mathbf{v}_j\right)\right)$$

$$+\sum_{k=1}^N \frac{\tau^2}{\lambda} \ll \frac{\mathrm{d}^2\tilde{\mathbf{q}}_{jk}}{\mathrm{d}t^2}, \frac{\partial \mathbb{P}_O}{\partial \mathbf{q}} W_j \gg -\frac{\kappa^2}{\lambda}\frac{\partial \mathrm{meas}}{\partial \tilde{\mathbf{q}}_{jk}}\left(\frac{\partial \mathbb{P}_O}{\partial \mathbf{q}} W_j\right)\mathrm{d}t \tag{3-4.6}$$

$$+\int_0^T \sum_{j,k=1}^N -\frac{\tau^2}{\lambda} \ll \frac{\mathrm{d}^2\tilde{\mathbf{q}}_{jk}}{\mathrm{d}t^2}, \frac{\partial \mathbb{P}_O}{\partial \mathbf{q}} W_k \gg +\frac{\kappa^2}{\lambda}\frac{\partial \mathrm{meas}}{\partial \tilde{\mathbf{q}}_{jk}}\left(\frac{\partial \mathbb{P}_O}{\partial \mathbf{q}} W_k\right)\mathrm{d}t$$

$$+\int_0^T \sum_{j=1}^N -\boldsymbol{\lambda}_2^j(\delta\mathbf{u}_j) + \langle \mathbf{u}_j, \delta\mathbf{u}_j\rangle\,\mathrm{d}t + \int_0^T \sum_{j=1}^N -\boldsymbol{\lambda}_1^j\left(\delta\mathbf{v}_j\right) - \frac{\mathrm{D}\boldsymbol{\lambda}_2^j}{\mathrm{d}t}\left(\delta\mathbf{v}_j\right)\mathrm{d}t.$$

Proof In Equation (3-4.2), we replace $\tilde{\mathbf{q}}_{jk}(t)$, $\mathbf{u}_j(t)$ and $\mathbf{v}_j(t)$ with the perturbed variables $\tilde{\mathbf{q}}_{jk}(t,\epsilon)$, $\mathbf{u}_j(t,\epsilon)$ and $\mathbf{v}_j(t,\epsilon)$, respectively. To prove the theorem, we compute $\partial\mathcal{J}/\partial\epsilon$ on a term by term basis as follows. First, we have:

$$\frac{\partial}{\partial \epsilon}\int_0^T \frac{1}{2}\langle \mathbf{u}_j(t,\epsilon),\mathbf{u}_j(t,\epsilon)\rangle\,\mathrm{d}t\Big|_{\epsilon=0} = \int_0^T \langle \mathbf{u}_j, \delta\mathbf{u}_j + \mathbf{B}\left(\mathbf{W}_j,\mathbf{u}_j\right)\rangle\,\mathrm{d}t, \tag{3-4.7}$$

where a summation over j is understood. For the fourth term in Equation (3-4.2), we use the fourth identity in Equations (3-6.1) and integrate by parts to obtain

$$\begin{aligned}\frac{\partial}{\partial \epsilon}\int_0^T \frac{\tau^2}{2} \ll \frac{\mathrm{d}\tilde{\mathbf{q}}_{jk}}{\mathrm{d}t}, \frac{\mathrm{d}\tilde{\mathbf{q}}_{jk}}{\mathrm{d}t} \gg \mathrm{d}t\Big|_{\epsilon=0} &= \int_0^T \frac{\tau^2}{\lambda} \ll \frac{\mathrm{d}\tilde{\mathbf{q}}_{jk}}{\mathrm{d}t}, \frac{\mathrm{d}}{\mathrm{d}t}\left[\frac{\partial \mathbb{P}_O}{\partial \mathbf{q}}\left(W_k - W_j\right)\right] \gg \mathrm{d}t \\ &= -\int_0^T \frac{\tau^2}{\lambda} \ll \frac{\mathrm{d}^2\tilde{\mathbf{q}}_{jk}}{\mathrm{d}t^2}, \frac{\partial \mathbb{P}_O}{\partial \mathbf{q}}\left(W_k - W_j\right) \gg \mathrm{d}t \\ &\quad + \frac{\tau^2}{\lambda} \ll \frac{\mathrm{d}\tilde{\mathbf{q}}_{jk}}{\mathrm{d}t}, \frac{\partial \mathbb{P}_O}{\partial \mathbf{q}}\left(W_k - W_j\right) \gg \Big|_0^T,\end{aligned}$$

for all $j,k = 1,\ldots,N$, where use has been made of Equation (3-4.5). The second term vanishes due to the fixed boundary conditions as expressed in Equations (3-4.3). Thus, for the fourth term in Equation (3-4.2) we have

$$\frac{\partial}{\partial \epsilon}\int_0^T \frac{\tau^2}{2}\sum_{j,k=1}^N \ll \frac{\mathrm{d}\tilde{\mathbf{q}}_{jk}}{\mathrm{d}t}, \frac{\mathrm{d}\tilde{\mathbf{q}}_{jk}}{\mathrm{d}t} \gg \mathrm{d}t\Big|_{\epsilon=0} =$$

$$-\int_0^T \frac{\tau^2}{\lambda}\sum_{j,k=1}^N \ll \frac{\mathrm{d}^2\tilde{\mathbf{q}}_{jk}}{\mathrm{d}t^2}, \frac{\partial \mathbb{P}_O}{\partial \mathbf{q}}\left(W_k - W_j\right) \gg \mathrm{d}t. \tag{3-4.8}$$

For the second term, we have

$$\frac{\partial}{\partial\epsilon}\int_0^T \boldsymbol{\lambda}_1^j\left(\frac{\mathrm{D}\mathbf{q}_j}{\mathrm{d}t}-\mathbf{v}_j\right)\mathrm{d}t=\int_0^T \boldsymbol{\lambda}_1^j\left(\frac{\mathrm{D}}{\mathrm{d}t}\mathbf{W}_j-\delta\mathbf{v}_j-\mathbf{B}\left(\mathbf{W}_j,\mathbf{v}_j\right)\right)\mathrm{d}t.$$

For the first term in the parenthesis, we integrate by parts to obtain

$$\int_0^T \boldsymbol{\lambda}_1^j\left(\frac{\mathrm{D}}{\mathrm{d}t}\mathbf{W}_j\right)\mathrm{d}t=\boldsymbol{\lambda}_1^j\left(\mathbf{W}_j\right)\Big|_0^T-\int_0^T\frac{\mathrm{D}\boldsymbol{\lambda}_1^j}{\mathrm{d}t}\left(\mathbf{W}_j\right)\mathrm{d}t.$$

The first term on the right hand side vanishes by virtue of the boundary conditions (3-4.3) imposed on $\mathbf{W}_j$. We then obtain

$$\frac{\partial}{\partial\epsilon}\int_0^T \boldsymbol{\lambda}_1^j\left(\frac{\mathrm{D}\mathbf{q}_j}{\mathrm{d}t}-\mathbf{v}_j\right)\mathrm{d}t=\int_0^T -\frac{\mathrm{D}\boldsymbol{\lambda}_1^j}{\mathrm{d}t}\left(\mathbf{W}_j\right)-\boldsymbol{\lambda}_1^j\left(\delta\mathbf{v}_j+\mathbf{B}\left(\mathbf{W}_j,\mathbf{v}_j\right)\right)\mathrm{d}t. \quad (3\text{-}4.9)$$

For the third term in Equation (3-4.2), first recall the identity (page 52 in [41]):

$$\frac{\mathrm{D}}{\partial\epsilon}\frac{\mathrm{D}}{\partial t}\mathbf{Y}-\frac{\mathrm{D}}{\partial t}\frac{\mathrm{D}}{\partial\epsilon}\mathbf{Y}=R\left(\frac{\mathrm{D}\mathbf{q}}{\partial\epsilon},\frac{\mathrm{D}\mathbf{q}}{\partial t}\right)\mathbf{Y},$$

where $\mathbf{Y}$ is a vector field along a trajectory $\mathbf{q}(t)$. Then

$$\begin{aligned}\frac{\partial}{\partial\epsilon}\int_0^T \boldsymbol{\lambda}_2^j\left(\frac{\mathrm{D}\mathbf{v}_j}{\mathrm{d}t}-\mathbf{u}_j\right)\mathrm{d}t &= \int_0^T \boldsymbol{\lambda}_2^j\left(R(\mathbf{W}_j,\mathbf{v}_j)\mathbf{v}_j+\frac{\mathrm{D}^2\mathbf{v}_j}{\partial t\partial\epsilon}-\delta\mathbf{u}_j-\mathbf{B}\left(\mathbf{W}_j,\mathbf{v}_j\right)\right)\mathrm{d}t\\ &= \int_0^T \boldsymbol{\lambda}_2^j\left(R(\mathbf{W}_j,\mathbf{v}_j)\mathbf{v}_j-\delta\mathbf{u}_j-\mathbf{B}\left(\mathbf{W}_j,\mathbf{v}_j\right)\right)\\ &- \frac{\mathrm{D}\boldsymbol{\lambda}_2^j}{\mathrm{d}t}\left(\delta\mathbf{v}_j+\mathbf{B}\left(\mathbf{W}_j,\mathbf{v}_j\right)\right)\mathrm{d}t \qquad (3\text{-}4.10)\end{aligned}$$

where integration by parts has been used to arrive at the last equation. Finally, under Assumption 3.3.1, for the last term we have

$$\begin{aligned}\frac{\partial}{\partial\epsilon}\int_0^T \kappa^2\mathrm{meas}\left[\Psi\right]\mathrm{d}t &= \int_0^T\sum_{j,k=1}^N \kappa^2\frac{\partial\mathrm{meas}}{\partial\tilde{\mathbf{q}}_{jk}}\frac{\partial\tilde{\mathbf{q}}_{jk}}{\partial\epsilon}\mathrm{d}t\\ &= \int_0^T\sum_{j,k=1}^N \frac{\kappa^2}{\lambda}\frac{\partial\mathrm{meas}}{\partial\tilde{\mathbf{q}}_{jk}}\left[\frac{\mathrm{D}\mathbb{P}_O}{\mathrm{d}\mathbf{q}}\left(W_k-W_j\right)\right]\mathrm{d}t, \qquad (3\text{-}4.11)\end{aligned}$$

where it is understood that the meas function is applied to the set $\Psi\left(\tilde{\mathbf{q}}_{jk}\right)$ for all $j,k=1,\ldots,N$. Finally, from equations (3-6.3-3-6.7), by separating terms involving the coefficients $\mathbf{W}_j$, $\mathbf{W}_k$, $\delta\mathbf{v}_j$ and $\delta\mathbf{u}_j$, we obtain the expression (3-6.2) and, hance, proving the theorem.

■

Remark 3.4.2. Note that $\frac{\partial \text{meas}}{\partial \tilde{\mathbf{q}}_{jk}}$ constitute the components of the differential form $\mathrm{d}\,(\text{meas}) \in T^*O$, the cotangent space on O. Hence, the notation $\frac{\partial \text{meas}}{\partial \tilde{\mathbf{q}}_{jk}}(\mathbf{X})$ denotes this form operating on $\mathbf{X} \in TO$.

From Theorem (3.6.1) one can extract the necessary optimality conditions as the following theorem states.

Theorem 3.4.2. *Under Assumptions (3.1.1) and (3.3.1), a set of optimal trajectories $\tilde{\mathbf{q}}_i$, $i = 1, \ldots, N$, that minimize $\mathcal{J}$ while satisfying the dynamic constraints (3-1.1) and the boundary conditions (3-3.2) satisfy the following necessary conditions for an arbitrary vector field $\mathbf{X}$:*

$$\begin{aligned}
\frac{\mathrm{D}\mathbf{q}_i}{\mathrm{d}t} &= \mathbf{v}_i \\
\frac{\mathrm{D}\mathbf{v}_i}{\mathrm{d}t} &= \left(\boldsymbol{\lambda}_2^j\right)^{\#}, \\
\frac{\mathrm{D}\boldsymbol{\lambda}_1^j}{\mathrm{d}t}(\mathbf{X}) &= \left(R\left(\mathbf{u}_j, \mathbf{v}_j\right)\mathbf{v}_j\right)^{\flat}(\mathbf{X}) \\
\frac{\mathrm{D}\boldsymbol{\lambda}_2^j}{\mathrm{d}t}(\mathbf{X}) &= -\boldsymbol{\lambda}_1^j(\mathbf{X}) \\
\mathbf{u}_j &= \left(\boldsymbol{\lambda}_2^j\right)^{\#} \\
0 &= \sum_{k=1}^{N} \tau^2 \left(\frac{\mathrm{D}^2\tilde{\mathbf{q}}_{jk}}{\mathrm{d}t^2}\right)^{\flat}(\mathbf{X}) - \kappa^2 \frac{\partial \text{meas}}{\partial \tilde{\mathbf{q}}_{jk}}(\mathbf{X})
\end{aligned}$$

for $j = 1, \ldots, N$ and where $\mathbf{Y}^{\flat}(\mathbf{X}) = \langle \mathbf{Y}, \mathbf{X} \rangle$, with $\flat$ denoting the flat operator (see [42] for definition of $\flat$ and $\sharp$).

Proof The first equation follows immediately from Equation (3-1.1). For an optimal solution, the first order necessary condition is that

$$\frac{\partial \mathcal{J}}{\partial \epsilon}(\mathbf{q}_i(t,\epsilon), \mathbf{u}_i(t,\epsilon), t; i = 1, \ldots, N)\Big|_{\epsilon=0} = 0. \tag{3-4.12}$$

The rest of the proof relies on this condition and the fact that $\mathbf{W}_j$, $\mathbf{W}_k$, $\delta\mathbf{u}_j$ and $\delta\mathbf{v}_j$ are independent for all $j, k = 1, \ldots, N$. The fourth equation follows immediately from the last integral in Equation (3-6.2) and the independence of $\delta\mathbf{v}_j$, $j = 1, \ldots, N$. The fifth equation follows immediately from condition (3-6.9), the third integral in Equation (3-6.2) and the independence of $\delta\mathbf{u}_j$, $j = 1, \ldots, N$. The last (algebraic) equation is obtained by studying the second integral in Equation (3-6.2). Since $\mathbf{W}_k$, $k = 1, \ldots, N$, are independent, we then have

$$\sum_{j=1}^{N} \tau^2 \left(\frac{\mathrm{d}^2 \tilde{\mathbf{q}}_{jk}}{\mathrm{d}t^2} \right)^{\flat} (\mathbf{X}) - \kappa^2 \frac{\partial \mathrm{meas}}{\partial \tilde{\mathbf{q}}_{jk}} (\mathbf{X}) = 0,$$

$\forall k = 1, \ldots, N$. Since $\mathbf{u}_j = \left(\boldsymbol{\lambda}_2^j\right)^{\#}$ and by interchanging indices ($j \to k$ and $k \to j$), we obtain the last (algebraic) condition. Hence, the last term under the first integral in Equation (3-6.2) is zero. the third equation in the theorem is obtained from this, the fourth Equation in the theorem, the first integral in Equation (3-6.2) and the independence of $\mathbf{W}_j$, $j = 1, \ldots, N$. The second equation follows from Equation (3-1.1) and the fifth condition in the theorem.

■

Remark 3.4.3. In the proof for Theorem (3.6.1) we have not taken variations in the multipliers $\boldsymbol{\lambda}_i^j$, $i = 1, 2$, $j = 1, \ldots, N$. This is standard practice and the justification can found in Remark (C.2.1) in Appendix C and Section 2 of [43].

3.5 Example: Dual-Spacecraft Interferometry

In this section we demonstrate the above ideas for a two spacecraft formation. We first derive a single degree of freedom version of the necessary conditions of Theorem (3.4.2), which only apply to fully actuated multi-spacecraft systems. Since in the present example one spacecraft is fixed (and not free) in space, the symmetries

exhibited in Theorem (3.4.2) are broken (specifically, the fifth algebraic condition in the theorem.) Hence, the result presented in this section is not a simple special case of Theorem (3.4.2).

The curve $\mathbf{q}(t) \in M$ corresponds to the trajectory of the collector spacecraft on the manifold and $\mathbf{v}(t) \in TM$ corresponds to the relative velocity vector field between the parent and collector spacecraft. The projected relative position is given by $\tilde{\mathbf{q}} = (1/\lambda)\mathbb{P}_O(\mathbf{q})$ while the projected relative velocity is given by $\tilde{\mathbf{v}} = (1/\lambda)\frac{\mathrm{d}}{\mathrm{d}t}\mathbb{P}_O(\mathbf{q}) = \mathbb{P}_O^v(\mathbf{q}, \mathbf{v})$, where $\mathbb{P}_O^v : M \times TM \to \mathbb{E}^2$ is a continuously differentiable function on the tangent bundle to M and where $\mathbb{E}^2$ is the tangent space to $\mathbb{R}^2$. Hence, $\tilde{\mathbf{v}} \in \mathbb{E}^2$.

The cost functional to be minimized is given by:

$$\mathcal{J} \;=\; \int_0^T \frac{1}{2}\langle \mathbf{u}, \mathbf{u}\rangle + \frac{\tau^2}{2} \ll \tilde{\mathbf{v}}, \tilde{\mathbf{v}} \gg + \kappa^2 \mathrm{meas}\left(\Psi(\tilde{\mathbf{q}})\right) \mathrm{d}t.$$

One now follows a procedure similar to that found in Section (3.4) by appending the Lagrangian with $\boldsymbol{\lambda}_1(\dot{\mathbf{q}} - \mathbf{v}) + \boldsymbol{\lambda}_2\left(\frac{\mathrm{D}\mathbf{v}}{\mathrm{d}t} - \mathbf{u}\right)$. We only derive the expression:

$$\begin{aligned}
\frac{\partial}{\partial \epsilon}\int_0^T \frac{\tau^2}{2} \ll \tilde{\mathbf{v}}, \tilde{\mathbf{v}} \gg \mathrm{d}t \;&=\; \int_0^T \tau^2 \ll \tilde{\mathbf{v}}, \frac{\partial}{\partial \epsilon}\mathbb{P}_O^v(\mathbf{q}, \mathbf{v}) \gg \mathrm{d}t \\
&=\; \int_0^T \tau^2 \ll \tilde{\mathbf{v}}, \frac{\partial \mathbb{P}_O^v}{\partial \mathbf{q}}(\mathbf{W}) + \frac{\partial \mathbb{P}_O^v}{\partial \mathbf{v}}\left(\frac{\partial \mathbf{v}}{\partial \epsilon}\right) \gg \mathrm{d}t \\
&=\; \int_0^T \tau^2 \Bigg[\left\langle \left(\frac{\partial \mathbb{P}_O^v}{\partial \mathbf{q}}\right)^T \tilde{\mathbf{v}}, \mathbf{W} \right\rangle \\
&\qquad + \left\langle \left(\frac{\partial \mathbb{P}_O^v}{\partial \mathbf{v}}\right)^T \tilde{\mathbf{v}}, \delta\mathbf{v} + \mathbf{B}(\mathbf{W}, \mathbf{v}) \right\rangle \Bigg] \mathrm{d}t, \qquad \text{(3-5.1)}
\end{aligned}$$

where $\mathbf{W} \in TM$ is the variation vector field corresponding to the curve $\mathbf{q}$ and $\frac{\partial \mathbb{P}_O^v}{\partial \mathbf{q}}$ and $\frac{\partial \mathbb{P}_O^v}{\partial \mathbf{q}}$ are viewed as the components of the differential form: $\mathrm{d}\mathbb{P}_O^v \in T^*TM$. The T in the superscript corresponds to the adjoint (transpose) operation. In obtaining the above expression we have used integration by parts and the fact that $\mathbf{W}(0) = \mathbf{W}(T) = 0$. The inner product on the last line corresponds to the metric on M. The

remainder of the derivation is similar to that obtained in Section (3.4). We obtain the following:

$$\begin{aligned}
\left.\frac{\partial \mathcal{J}}{\partial \epsilon}\right|_{\epsilon=0} &= \int_0^T \langle \mathbf{u}, \delta\mathbf{u}\rangle - \boldsymbol{\lambda}_2(\delta\mathbf{u})\,\mathrm{d}t \\
&\quad + \int_0^T -\boldsymbol{\lambda}_1(\delta\mathbf{v}) - \frac{\mathrm{D}\boldsymbol{\lambda}_2}{\mathrm{d}t}(\delta\mathbf{v}) + \tau^2\left\langle \left(\frac{\partial \mathbb{P}_O^v}{\partial \mathbf{v}}\right)^T \tilde{\mathbf{v}}, \delta\mathbf{v}\right\rangle \mathrm{d}t \\
&\quad + \int_0^T \langle \mathbf{u}, \mathbf{B}(\mathbf{W},\mathbf{u})\rangle + \tau^2\left\langle \left(\frac{\partial \mathbb{P}_O^v}{\partial \mathbf{q}}\right)^T \tilde{\mathbf{v}}, \mathbf{W}\right\rangle \\
&\quad + \kappa^2 \frac{\partial \mathrm{meas}}{\partial \mathbf{q}}(\mathbf{W}) - \frac{\mathrm{D}\boldsymbol{\lambda}_1}{\mathrm{d}t}(\mathbf{W}) - \boldsymbol{\lambda}_1(\mathbf{B}(\mathbf{W},\mathbf{v})) \\
&\quad - \boldsymbol{\lambda}_2(\mathbf{B}(\mathbf{W},\mathbf{u})) - \frac{\mathrm{D}\boldsymbol{\lambda}_2}{\mathrm{d}t}(\mathbf{B}(\mathbf{W},\mathbf{v})) \\
&\quad + \boldsymbol{\lambda}_2(R(\mathbf{W},\mathbf{v})\mathbf{v}) + \tau^2\left\langle \left(\frac{\partial \mathbb{P}_O^v}{\partial \mathbf{v}}\right)^T \tilde{\mathbf{v}}, \mathbf{B}(\mathbf{W},\mathbf{v})\right\rangle \mathrm{d}t. \qquad \text{(3-5.2)}
\end{aligned}$$

We are now in a position to extract the necessary conditions. These are as follows:

$$\begin{aligned}
\dot{\mathbf{q}} &= \mathbf{v} \\
\frac{\mathrm{D}\mathbf{v}}{\mathrm{d}t} &= \boldsymbol{\lambda}_2^\sharp \\
\left(\frac{\mathrm{D}\boldsymbol{\lambda}_1}{\mathrm{d}t}\right)^\sharp &= R(\mathbf{u},\mathbf{v})\mathbf{v} - \tau^2\left(\frac{\partial \mathbb{P}_O^v}{\partial \mathbf{q}}\right)^T \tilde{\mathbf{v}} + \kappa^2 \frac{\partial \mathrm{meas}}{\partial \mathbf{q}} \\
\frac{\mathrm{D}\boldsymbol{\lambda}_2}{\mathrm{d}t} &= -\boldsymbol{\lambda}_1 + \tau^2\left(\frac{\partial \mathbb{P}_O^v}{\partial \mathbf{v}}\right)^T \tilde{\mathbf{v}}^\flat \\
\mathbf{u} &= \boldsymbol{\lambda}_2^\sharp.
\end{aligned}$$

These necessary conditions for the problem when $\kappa = 0$ are obtained in local coordinates (the arc length q_1) in Chapter 6 and in [44].

We now look at a class of two-spacecraft formations, where one spacecraft, the "parent", is fixed at the origin and the second, the "collector", is restricted to move along a spiral embedded in a two-dimensional paraboloidal surface. Hence, this system is a one degree of freedom system.

We model each spacecraft as a point mass, each with unity mass. The choice of a paraboloid surface is made because of its improved focusing properties. This

type of formation belongs to a class of formations known by Space Technology 3 (ST-3) as one of NASA's Origin's missions. For more on this class of formations, we refer the reader to [36]. Moreover, the collector spacecraft follows a spiral trajectory along the paraboloid. The spiral is designed to ensure that the resulting maneuver is successful in the sense of Definition (6.5.1). Hence, the spiral embedded on the paraboloid surface will be considered as our one-dimensional manifold M with $n = 1$.

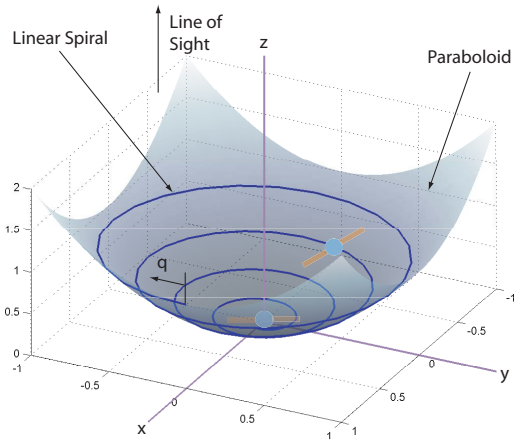

Figure 3.2: The basic interferometer.

Refer to figure (3.2). Let $\mathbf{q} = q$ be the single coordinate we choose to work. We choose q to be the arc length traversed along the spiral. Therefore, $\partial_q = \frac{\partial}{\partial q}$ is the basis vector for T_qM. The velocity vector field is then given by $\mathbf{v} = v_1\partial_q$. The control vector $\mathbf{u} = u_1\partial_q$ is restricted to the tangent space to TM. That is, $\mathbf{u} \in TTM$. In rectangular coordinates, the paraboloid is given by

$$z = \frac{1}{2}\left(\frac{\rho^2}{\beta^2} - \beta^2\right), \tag{3-5.3}$$

where $\rho = \sqrt{x^2 + y^2}$ and β is a parameter that controls the depth of the paraboloid. Note that vertex of the paraboloid is located at the point $(0, 0, -\beta^2/2)$ in $\mathbb{R}^3$.

In this section we give a brief account for the spiral maneuver. We refer the

reader to Chapter 6 and to [45] for further details and background information. In the x-y plane, the projected position may be given in terms of polar coordinates (ρ, θ). One way to ensure full coverage of the resolution disc $\mathcal{D}_R$ is to initialize the second spacecraft such that at $t = 0$ we have $(\rho = \frac{\lambda(m+1)}{2\theta_p}, \theta = 0)$, make it follow a linear spiral as a function of θ, and to impose the terminal condition that at $t = T$ we have $\rho = 0, \theta = \frac{(m+1)\pi}{2}$), where T is the terminal maneuver time. m is an integer that is equal to the number of pixels in the reconstructed image and θ_p is a parameter such that $\theta_p = m\theta_r$. This motion implies that the two coverage balls $\bar{B}_{r_p}(\tilde{\mathbf{p}}_{12})$ and $\bar{B}_{r_p}(\tilde{\mathbf{p}}_{21})$ are initialized such that they lie outside the resolution disc $\mathcal{D}_R$ and move spirally inwards till they overlap the central (fixed) ball $\bar{B}_{r_p}(\tilde{\mathbf{p}}_{00}) = \bar{B}_{r_p}(0, 0)$. Thus ρ and θ are constrained to satisfy

$$\rho(\theta) = k_1 (k_2\pi - \theta), \ \theta \in \left[0, \frac{(m+1)\pi}{2}\right], \tag{3-5.4}$$

where $k_1 = \frac{\lambda}{\pi\theta_p}$ and $k_2 = \frac{(m+1)}{2}$.

If we let $\mathbf{r}$ be the position vector of the collector spacecraft, then the constraints (3-5.3) and (3-5.4) imply that

$$\begin{aligned} \mathbf{r} &= (x, y, z) \qquad (3\text{-}5.5) \\ &= \left((k_1(k_2\pi - \theta)\cos\theta, k_1(k_2\pi - \theta)\sin\theta, \frac{1}{2}\left(\frac{k_1^2}{\beta^2}(k_2\pi - \theta)^2 - \beta^2\right)\right). \end{aligned}$$

The arc length q is obtained as a function of θ using the definition of the arc length of curve in space:

$$q(\theta) = h(\theta) = \int_0^\theta \left\| \frac{\partial \mathbf{r}(\theta')}{\partial \theta'} \right\| \mathrm{d}\theta'. \tag{3-5.6}$$

The functional form of h can be obtained explicitly, which we omit for the sake of brevity. By the geometry of the problem described in previous paragraphs, it is easy to see that the function h is both one-to-one and onto (for each θ there is one and

only one corresponding q value.) Hence, given a value for θ, one can uniquely solve for q using

$$\theta = h^{-1}(q). \tag{3-5.7}$$

The metric on the tangent space is determined by computing the line element $\mathrm{d}s^2$ in terms of the coordinate q. Since q is the distance traveled on M, then $\mathrm{d}s^2 = \mathrm{d}q^2$ and the single element of the metric g is simply given by

$$g(q) = 1. \tag{3-5.8}$$

With this, one is now in a position to compute the connection coefficients. The single connection coefficient (or the Christoffel symbol) is given by

$$\Gamma = \frac{1}{2g}\frac{\partial g}{\partial q} = 0. \tag{3-5.9}$$

This and the fact that M is a one-dimensional manifold, then the curvature tensor R is identically zero everywhere on M.

To compute $\tilde{\mathbf{v}}$ in terms of q and $v = \dot{q}_1$, we first need to obtain an expression for $\dot{\theta}$ in terms of q and $\dot{q}_1$. Differentiating Equation (3-5.6), we obtain

$$v = \dot{q}_1 = \frac{\partial h}{\partial \theta}\dot{\theta} = r(q)\dot{\theta}, \tag{3-5.10}$$

where $r(q) = \frac{\partial h}{\partial \theta}\big|_{\theta = h^{-1}(q)}$ using the relation (3-5.7). Using this and Equations (3-5.5) and (3-5.7), we have:

$$\tilde{\mathbf{v}} = \mathbb{P}_O^v = \dot{x}\partial_x + \dot{y}\partial_y = P_x(q,v)\partial_x + P_y(q,v)\partial_y, \tag{3-5.11}$$

where

$$\begin{aligned} P_x(q,v) &= \frac{v}{r(q)}\Big[- k_1 \cos\left(h^{-1}(q)\right) - k_1\left(k_2\pi - h^{-1}(q)\right)\sin\left(h^{-1}(q)\right)\Big] \\ P_y(q,v) &= \frac{v}{r(q)}\Big[- k_1 \sin\left(h^{-1}(q)\right) + k_1\left(k_2\pi - h^{-1}(q)\right)\cos\left(h^{-1}(q)\right)\Big]. \end{aligned}$$

Finally, after quite an involved computation, one can show that for such "scripted" (that is, pre-determined) maneuvers, the meas function that ensues from the spiral motion is given in terms of $\theta = h^{-1}(q)$ by:

$$\begin{aligned}
\text{meas}(\theta) &= \frac{\pi}{4\theta_p^2} + \frac{1}{2}\left[\frac{m\theta^2}{2\pi\theta_p^2} - \frac{\theta^3}{3\pi^2\theta_p^2}\right],\ \theta \in [0,\pi] \\
\text{meas}(\theta) &= \frac{\pi(3m+1)}{12\theta_p^2} + \frac{1}{\theta_p^2}\left[\frac{(m+1)(\theta-\pi)}{2} - \frac{\theta^2-\pi^2}{2\pi}\right],\ \theta \in \left[\pi, \frac{\pi(m-1)}{2}\right] \\
\text{meas}(\theta) &= \frac{\pi\,(3m^2-7)}{24\theta_p^2} + \frac{1}{2\theta_p^2}\left[\frac{(m+3)(m+1)}{4}\left(\theta - \frac{(m-1)\pi}{2}\right)\right. \\
&\quad \left. -\frac{(m+2)}{2\pi}\left(\theta^2 - \frac{(m-1)^2\pi^2}{4}\right) + \frac{1}{3\pi^2}\left(\theta^3 - \frac{(m-1)^3\pi^3}{8}\right)\right], \\
&\quad \theta \in [\frac{\pi(m-1)}{2}, \frac{\pi(m+1)}{2}].
\end{aligned}$$

The meas may now be obtained in terms of q by the relation $\theta = h^{-1}(\theta)$.

3.6 The Planar Case

In this section, we make the assumption that the manifold M is identical to O; the formation is constrained to evolve on the observation plane O. This assumption simplifies the analysis and offers further insight into the necessary properties of an optimal formation motion.

Assumption 3.6.1. Let $M = O \subset \mathbb{R}^2$. In other words, the surfaces M and O coincide.

Under Assumption (3.6.1), the projection $\mathbb{P}_O$ is the identity operator. This implies that all the derivatives $\mathrm{D}/\mathrm{d}t$ could be replaced by regular derivatives in $\mathbb{R}^2$. However, we will retain the former notation because it is very convenient, especially in the case when one works with non-rectangular coordinates (such as polar coordi-

nates.) Thus, for $i, j = 1, \ldots, N$ we have

$$\begin{aligned}
\tilde{\mathbf{q}}_{ij}(t,0) &= \tilde{\mathbf{q}}_{ij}(t) = \frac{\mathbf{q}_j(t) - \mathbf{q}_i(t)}{\lambda}, \\
\frac{\mathrm{D}\tilde{\mathbf{q}}_{ij}}{\partial\epsilon}(t,0) &= \frac{1}{\lambda}\left[W_j(t) - W_i(t)\right] \\
\frac{\mathrm{D}\tilde{\mathbf{q}}_{ij}}{\partial\epsilon}(0,0) &= \frac{\mathrm{D}\tilde{\mathbf{q}}_{ij}}{\partial\epsilon}(T,0) = 0, \\
\frac{\mathrm{D}}{\mathrm{d}t}\frac{\mathrm{D}\tilde{\mathbf{q}}_{ij}}{\partial\epsilon}(t,0) &= \frac{1}{\lambda}\frac{\mathrm{D}}{\mathrm{d}t}\left[W_j(t) - W_i(t)\right] \text{ cont. on } [0,T] \\
\frac{\mathrm{D}}{\mathrm{d}t}\frac{\mathrm{D}\tilde{\mathbf{q}}_{ij}}{\partial\epsilon}(0,0) &= \frac{\mathrm{D}}{\mathrm{d}t}\frac{\mathrm{D}\tilde{\mathbf{q}}_{ij}}{\partial\epsilon}(T,0) = 0.
\end{aligned} \tag{3-6.1}$$

Theorem 3.6.1. *Under Assumptions (3.1.1), (3.3.1) and (3.6.1), taking first order variations of the expression in Equation (3-4.2) leads to the following relationship:*

$$\begin{aligned}
&\frac{\partial\mathcal{J}}{\partial\epsilon}(\mathbf{q}_i(t,\epsilon), \mathbf{u}_i(t,\epsilon), t; i = 1, \ldots, N)\Big|_{\epsilon=0} \\
&= \int_0^T \sum_{j=1}^N \left\langle \mathbf{u}_j, \mathbf{B}\left(\mathbf{W}_j, \mathbf{u}_j\right)\right\rangle - \frac{\mathrm{D}\boldsymbol{\lambda}_1^j}{\mathrm{d}t}\left(W_j\right) \\
&-\boldsymbol{\lambda}_1^j\left(\mathbf{B}\left(\mathbf{W}_j, \mathbf{v}_j\right)\right) - \boldsymbol{\lambda}_2^j\left(\mathbf{B}\left(\mathbf{W}_j, \mathbf{u}_j\right)\right) + \boldsymbol{\lambda}_2^j\left(R\left(\mathbf{W}_j, \mathbf{v}_j\right)\mathbf{v}_j\right) - \frac{\mathrm{D}\boldsymbol{\lambda}_2^j}{\mathrm{d}t}\left(\mathbf{B}\left(\mathbf{W}_j, \mathbf{v}_j\right)\right) \\
&+ \sum_{k=1}^N \frac{\tau^2}{\lambda^2}\left\langle \mathbf{u}_k - \mathbf{u}_j, W_j\right\rangle - \frac{\kappa^2}{\lambda}\frac{\partial \mathrm{meas}}{\partial\tilde{\mathbf{q}}_{jk}}\left(W_j\right)\mathrm{d}t \\
&+ \int_0^T \sum_{j,k=1}^N -\frac{\tau^2}{\lambda^2}\left\langle \mathbf{u}_k - \mathbf{u}_j, W_k\right\rangle + \frac{\kappa^2}{\lambda}\frac{\partial \mathrm{meas}}{\partial\tilde{\mathbf{q}}_{jk}}\left(W_k\right)\mathrm{d}t \\
&+ \int_0^T \sum_{j=1}^N -\boldsymbol{\lambda}_2^j(\delta\mathbf{u}_j) + \left\langle \mathbf{u}_j, \delta\mathbf{u}_j\right\rangle \mathrm{d}t + \int_0^T \sum_{j=1}^N -\boldsymbol{\lambda}_1^j\left(\delta\mathbf{v}_j\right) - \frac{\mathrm{D}\boldsymbol{\lambda}_2^j}{\mathrm{d}t}\left(\delta\mathbf{v}_j\right)\mathrm{d}t.
\end{aligned} \tag{3-6.2}$$

Proof In Equation (3-4.2), we replace $\tilde{\mathbf{q}}_{jk}(t)$, $\mathbf{u}_j(t)$ and $\mathbf{v}_j(t)$ with the perturbed variables $\tilde{\mathbf{q}}_{jk}(t,\epsilon)$, $\mathbf{u}_j(t,\epsilon)$ and $\mathbf{v}_j(t,\epsilon)$, respectively. To prove the theorem, we compute $\partial\mathcal{J}/\partial\epsilon$ on a term by term basis as follows. First, we have:

$$\frac{\partial}{\partial\epsilon}\int_0^T \frac{1}{2}\left\langle \mathbf{u}_j(t,\epsilon), \mathbf{u}_j(t,\epsilon)\right\rangle \mathrm{d}t\Big|_{\epsilon=0} = \int_0^T \left\langle \mathbf{u}_j, \delta\mathbf{u}_j + \mathbf{B}\left(\mathbf{W}_j, \mathbf{u}_j\right)\right\rangle \mathrm{d}t, \tag{3-6.3}$$

where a summation over j is understood. For the fourth term in Equation (3-4.2),

we use the fourth identity in Equations (3-6.1) and integrate by parts to obtain

$$\begin{aligned}
&\frac{\partial}{\partial\epsilon}\int_0^T \frac{\tau^2}{2}\sum_{j=1}^N\sum_{k=1}^N \left\langle \frac{\mathrm{D}\tilde{\mathbf{q}}_{jk}}{\mathrm{d}t}, \frac{\mathrm{D}\tilde{\mathbf{q}}_{jk}}{\mathrm{d}t}\right\rangle \mathrm{d}t\bigg|_{\epsilon=0} \\
&= \int_0^T \frac{\tau^2}{\lambda}\sum_{j=1}^N\sum_{k=1}^N \left\langle \frac{\mathrm{D}\tilde{\mathbf{q}}_{jk}}{\mathrm{d}t}, \frac{\mathrm{D}}{\mathrm{d}t}\left[W_k - W_j\right]\right\rangle \mathrm{d}t \\
&= -\int_0^T \frac{\tau^2}{\lambda}\sum_{j=1}^N\sum_{k=1}^N \left\langle \frac{\mathrm{D}^2\tilde{\mathbf{q}}_{jk}}{\mathrm{d}t^2}, W_k - W_j\right\rangle \mathrm{d}t + \sum_{j=1}^N\sum_{m=1}^N \frac{\tau^2}{\lambda}\left\langle \frac{\mathrm{D}\tilde{\mathbf{q}}_{jk}}{\mathrm{d}t}, W_k - W_j\right\rangle\Bigg|_0^T.
\end{aligned}$$

The second term vanishes due to the fixed boundary conditions (3-4.3). Under Assumption (3.6.1), we have

$$\frac{\mathrm{D}^2\tilde{\mathbf{q}}_{jk}}{\mathrm{d}t^2} = \frac{1}{\lambda}\left(\mathbf{u}_k - \mathbf{u}_j\right).$$

Thus, for the fourth term in Equation (3-4.2) we have

$$\frac{\partial}{\partial\epsilon}\int_0^T \frac{\tau^2}{2}\sum_{j,k=1}^N \left\langle \frac{\mathrm{D}\tilde{\mathbf{q}}_{jk}}{\mathrm{d}t}, \frac{\mathrm{D}\tilde{\mathbf{q}}_{jk}}{\mathrm{d}t}\right\rangle \mathrm{d}t\bigg|_{\epsilon=0} = -\int_0^T \frac{\tau^2}{\lambda^2}\sum_{j,k=1}^N \left\langle \mathbf{u}_k - \mathbf{u}_j, W_k - W_j\right\rangle \mathrm{d}t. \tag{3-6.4}$$

For the second term, we have

$$\frac{\partial}{\partial\epsilon}\int_0^T \boldsymbol{\lambda}_1^j\left(\frac{\mathrm{D}\mathbf{q}_j}{\mathrm{d}t} - \mathbf{v}_j\right)\mathrm{d}t = \int_0^T \boldsymbol{\lambda}_1^j\left(\frac{\mathrm{D}}{\mathrm{d}t}\mathbf{W}_j - \delta\mathbf{v}_j - \mathbf{B}\left(\mathbf{W}_j, \mathbf{v}_j\right)\right)\mathrm{d}t.$$

For the first term in the parenthesis, we integrate by parts to obtain

$$\int_0^T \boldsymbol{\lambda}_1^j\left(\frac{\mathrm{D}}{\mathrm{d}t}\mathbf{W}_j\right)\mathrm{d}t = \boldsymbol{\lambda}_1^j\left(\mathbf{W}_j\right)\Big|_0^T - \int_0^T \frac{\mathrm{D}\boldsymbol{\lambda}_1^j}{\mathrm{d}t}\left(\mathbf{W}_j\right)\mathrm{d}t.$$

The first term on the right hand side vanishes by virtue of the boundary conditions (3-4.3). We then obtain

$$\frac{\partial}{\partial\epsilon}\int_0^T \sum_{j=1}^N \boldsymbol{\lambda}_1^j\left(\frac{\mathrm{D}\mathbf{q}_j}{\mathrm{d}t} - \mathbf{v}_j\right)\mathrm{d}t = \int_0^T \sum_{j=1}^N -\frac{\mathrm{D}\boldsymbol{\lambda}_1^j}{\mathrm{d}t}\left(\mathbf{W}_j\right) - \boldsymbol{\lambda}_1^j\left(\delta\mathbf{v}_j + \mathbf{B}\left(\mathbf{W}_j, \mathbf{v}_j\right)\right)\mathrm{d}t. \tag{3-6.5}$$

For the third term in Equation (3-4.2), first recall the identity (page 52 in [41]):

$$\frac{\mathrm{D}}{\partial\epsilon}\frac{\mathrm{D}}{\partial t}\mathbf{Y} - \frac{\mathrm{D}}{\partial t}\frac{\mathrm{D}}{\partial\epsilon}\mathbf{Y} = R\left(\frac{\mathrm{D}\mathbf{q}}{\partial\epsilon}, \frac{\mathrm{D}\mathbf{q}}{\partial t}\right)\mathbf{Y}.$$

Then, we have

$$\begin{aligned}\frac{\partial}{\partial\epsilon}\int_0^T \boldsymbol{\lambda}_2^j\left(\frac{\mathrm{D}\mathbf{v}_j}{\mathrm{d}t}-\mathbf{u}_j\right)\mathrm{d}t &= \int_0^T \boldsymbol{\lambda}_2^j\Big(R(\mathbf{W}_j,\mathbf{v}_j)\mathbf{v}_j+\frac{\mathrm{D}^2\mathbf{v}_j}{\partial t\partial\epsilon}-\delta\mathbf{u}_j-\mathbf{B}\left(\mathbf{W}_j,\mathbf{v}_j\right)\Big)\mathrm{d}t \\ &= \int_0^T \boldsymbol{\lambda}_2^j\Big(R(\mathbf{W}_j,\mathbf{v}_j)\mathbf{v}_j-\delta\mathbf{u}_j-\mathbf{B}\left(\mathbf{W}_j,\mathbf{v}_j\right)\Big) \\ &\quad -\frac{\mathrm{D}\boldsymbol{\lambda}_2^j}{\mathrm{d}t}\left(\delta\mathbf{v}_j+\mathbf{B}\left(\mathbf{W}_j,\mathbf{v}_j\right)\right)\mathrm{d}t \qquad (3\text{-}6.6)\end{aligned}$$

where integration by parts has been used to arrive at the last equation. Finally, under Assumption 3.3.1, for the last term we have

$$\begin{aligned}\frac{\partial}{\partial\epsilon}\int_0^T \kappa^2\mathrm{meas}\left[\Psi\right]\mathrm{d}t &= \int_0^T\sum_{j,k=1}^N \kappa^2\frac{\partial\mathrm{meas}}{\partial\tilde{\mathbf{q}}_{jk}}\frac{\partial\tilde{\mathbf{q}}_{jk}}{\partial\epsilon}\mathrm{d}t \\ &= \int_0^T\sum_{j,k=1}^N \frac{\kappa^2}{\lambda}\frac{\partial\mathrm{meas}}{\partial\tilde{\mathbf{q}}_{jk}}\left(\mathbf{W}_k-\mathbf{W}_j\right)\mathrm{d}t, \qquad (3\text{-}6.7)\end{aligned}$$

where it is understood that the meas function is applied to the set $\Psi\left(\tilde{\mathbf{q}}_{jk}\right)$ for all $j,k=1,\ldots,N$. Finally, from equations (3-6.3-3-6.7), by separating terms involving the coefficients $\mathbf{W}_j$, $\mathbf{W}_k$, $\delta\mathbf{v}_j$ and $\delta\mathbf{u}_j$, we obtain the expression (3-6.2) and, hance, proving the theorem.

■

Theorem 3.6.2. *Under Assumptions (3.1.1), (3.3.1) and (3.6.1), a set of optimal trajectories $\tilde{\mathbf{q}}_i$, $i=1,\ldots,N$, that minimize $\mathcal{J}$ while satisfying the dynamic constraints (3-1.1) and the boundary conditions (3-3.2) satisfies the following necessary*

conditions for an arbitrary vector field $\mathbf{X}$*:*

$$\begin{aligned}
&\frac{\mathrm{D}\mathbf{q}_i}{\mathrm{d}t} = \mathbf{v}_i \\
&\frac{\mathrm{D}\mathbf{v}_i}{\mathrm{d}t} = \left(\boldsymbol{\lambda}_2^j\right)^{\#}, \\
&\frac{\mathrm{D}\boldsymbol{\lambda}_1^j}{\mathrm{d}t}(\mathbf{X}) = \left(R\left(\mathbf{u}_j, \mathbf{v}_j\right)\mathbf{v}_j\right)^{\flat}(\mathbf{X}) \\
&\frac{\mathrm{D}\boldsymbol{\lambda}_2^j}{\mathrm{d}t}(\mathbf{X}) = -\boldsymbol{\lambda}_1^j(\mathbf{X}) \\
&\mathbf{u}_j = \left(\boldsymbol{\lambda}_2^j\right)^{\#} \\
&0 = \sum_{k=1}^{N} \frac{\tau^2}{\lambda^2}\left(\boldsymbol{\lambda}_2^k(\mathbf{X}) - \boldsymbol{\lambda}_2^j(\mathbf{X})\right) - \frac{\kappa^2}{\lambda}\frac{\partial \mathrm{meas}}{\partial \tilde{\mathbf{q}}_{jk}}(\mathbf{X})
\end{aligned} \tag{3-6.8}$$

for $j = 1, \ldots, N$ *and where* $\mathbf{Y}^{\flat}(\mathbf{X}) = \langle \mathbf{Y}, \mathbf{X} \rangle$*, with* $\flat$ *denoting the flat operator [42].*

Proof The first equation follows immediately from Equation (3-1.1). For an optimal solution, the first order necessary condition is that

$$\frac{\partial \mathcal{J}}{\partial \epsilon}(\mathbf{q}_i(t,\epsilon), \mathbf{u}_i(t,\epsilon), t; i = 1, \ldots, N)\Big|_{\epsilon=0} = 0. \tag{3-6.9}$$

The rest of the proof relies on this condition and the fact that $\mathbf{W}_j$, $\mathbf{W}_k$, $\delta\mathbf{u}_j$ and $\delta\mathbf{v}_j$ are independent for all $j, k = 1, \ldots, N$. The fourth equation follows immediately from the last integral in Equation (3-6.2) and the independence of $\delta\mathbf{v}_j$, $j = 1, \ldots, N$. The fifth equation follows immediately from condition (3-6.9), the third integral in Equation (3-6.2) and the independence of $\delta\mathbf{u}_j$, $j = 1, \ldots, N$. The last (algebraic) equation in (4.11) is obtained by studying the second integral in Equation (3-6.2). Since $\mathbf{W}_k$, $k = 1, \ldots, N$, are independent, we then have

$$\sum_{j=1}^{N} -\frac{\tau^2}{\lambda^2}\left(\mathbf{u}_k - \mathbf{u}_j\right) + \frac{\kappa^2}{\lambda}\frac{\partial \mathrm{meas}(\boldsymbol{\Psi})}{\partial \tilde{\mathbf{q}}_{jk}} = 0, \ \forall k = 1, \ldots, N.$$

Since $\mathbf{u}_j = \left(\boldsymbol{\lambda}_2^j\right)^{\#}$ and by interchanging indices ($j \to k$ and $k \to j$), we obtain the last (algebraic) condition in (4.11). Hence, the last term under the first integral in

Equation (3-6.2) is zero. This, the fact that $\frac{\mathrm{D}\boldsymbol{\lambda}_2^j}{\mathrm{d}t} = -\boldsymbol{\lambda}_1^j$ and the independence of $\mathbf{W}_j$, $j = 1, \ldots, N$, in the first integral in Equation (3-6.2) give the third equation in the theorem. The second equation follows from Equation (3-1.1) and the fifth condition in equation (4.11).

■

Studying the last (algebraic) necessary condition gives further insight into the optimal trajectory. Note that one can write these N conditions in a matrix form:

$$\mathbf{AU} = \frac{\kappa^2 \lambda}{\tau^2}\mathbf{M}, \tag{3-6.10}$$

where

$$\mathbf{A} = \begin{bmatrix} N-1 & -1 & \cdots & -1 \\ -1 & N-1 & & -1 \\ \vdots & & \ddots & \vdots \\ -1 & \cdots & -1 & N-1 \end{bmatrix}$$

is an $N \times N$ matrix, $\mathbf{U}$ is the $N \times 1$ column matrix whose j^{th} entry is $\mathbf{u}_j$ and $\mathbf{M}$ is the $N \times 1$ column matrix whose j^{th} entry is $\sum_{k=1}^{N} \frac{\partial \text{meas}(\boldsymbol{\Psi})}{\partial \tilde{\mathbf{q}}_{jk}}$. Let a_{ij} be the ij^{th} element of $\mathbf{A}$. Note that $a_{Nj} = -\sum_{i=1}^{N-1} a_{ij}$. Hence, the last row is dependent on the first $N-1$ rows. In fact, one can show that $\mathbf{A}$ has rank exactly equal to $N-1$. The homogenous solution to the above equation is found to be $\mathbf{u}_1^h = \mathbf{u}_2^h = \cdots = \mathbf{u}_N^h$. The homogeneous solution corresponds to the motion of the center of mass of the formation in the plane. Since it is desired to minimize fuel, then we may set the homogeneous solution to zero: $\mathbf{u}_1^h = \mathbf{u}_2^h = \cdots = \mathbf{u}_N^h = \mathbf{0}$.

What really matters in this situation is the particular solution, if one exists. Indeed, we now show that the matrix $\mathbf{M}$ lies in the range space of the matrix $\mathbf{A}$ and, hence, a particular solution exists. First, append $\mathbf{M}$ to $\mathbf{A}$ to form the new matrix

$\tilde{\mathbf{A}} = [\mathbf{A}\ \mathbf{M}]$. Recall that $\mathbf{A}$ has rank equal to $N-1$. If we can show that $\tilde{\mathbf{A}}$ also has rank $N-1$, then $\mathbf{M}$ lies in the range space of $\mathbf{A}$. Let $\tilde{\mathbf{M}}$ be the matrix whose elements are given by $\tilde{M}_{ij} = \frac{\partial \text{meas}}{\partial \tilde{\mathbf{q}}_{ij}}$. With $\tilde{\mathbf{q}}_{ij} = -\tilde{\mathbf{q}}_{ji}$ and $\tilde{\mathbf{q}}_{ii} = \mathbf{0}$ is fixed at the origin, then $\frac{\partial \text{meas}}{\partial \tilde{\mathbf{q}}_{ii}} = 0$ and $\tilde{\mathbf{M}}$ is skew symmetric. Next, note that the N^{th} element of $\mathbf{M}$ is given by

$$\begin{aligned}\sum_{j=1}^{N-1} \frac{\partial \text{meas}}{\partial \tilde{\mathbf{q}}_{Nj}} &= \sum_{j=1}^{N-1} \frac{\partial \text{meas}}{\partial \tilde{\mathbf{q}}_{Nj}} + \sum_{j,k=1}^{N-1} \frac{\partial \text{meas}}{\partial \tilde{\mathbf{q}}_{kj}} \\ &= \sum_{j=1}^{N-1}\sum_{k=1}^{N} \frac{\partial \text{meas}}{\partial \tilde{\mathbf{q}}_{kj}} = -\sum_{j=1}^{N-1}\sum_{k=1}^{N} \frac{\partial \text{meas}}{\partial \tilde{\mathbf{q}}_{jk}},\end{aligned}$$

where the second term after the first equality sign is zero since $\tilde{\mathbf{M}}$ is skew symmetric. The term after the last equality sign is nothing but the sum of all the first $N-1$ elements of the matrix $\mathbf{M}$. This and the fact that $a_{Nj} = -\sum_{i=1}^{N-1} a_{ij}$ show that the last row of $\tilde{\mathbf{A}}$ is equal to the sum of the first $N-1$ rows of $\tilde{\mathbf{A}}$. Since $\mathbf{A}$ has rank $N-1$, then so must $\tilde{\mathbf{A}}$. Hence, $\mathbf{M}$ must in fact be in the range space of $\mathbf{A}$ and a particular solution must exist ([46], pp. 116-121.)

For $N = 2$, the condition (3-6.10) is equivalent to $\mathbf{u}_1 - \mathbf{u}_2 = \frac{\kappa^2\lambda}{\tau^2}\frac{\partial \text{meas}}{\partial \tilde{\mathbf{q}}_{12}}$. Hence, for a two spacecraft formation, a necessary optimality condition is that the relative thrusting between the two spacecraft is in the direction of descent of the measure of the uncovered set of frequency points. For $N = 3$, the condition (3-6.10) is equivalent to:

$$\begin{aligned}\mathbf{u}_1 - \mathbf{u}_2 &= \frac{1}{3}\frac{\kappa^2\lambda}{\tau^2}\left[\frac{\partial \text{meas}}{\partial \tilde{\mathbf{q}}_{13}} + 2\frac{\partial \text{meas}}{\partial \tilde{\mathbf{q}}_{12}} + \frac{\partial \text{meas}}{\partial \tilde{\mathbf{q}}_{32}}\right] \\ \mathbf{u}_1 - \mathbf{u}_3 &= \frac{1}{3}\frac{\kappa^2\lambda}{\tau^2}\left[\frac{\partial \text{meas}}{\partial \tilde{\mathbf{q}}_{12}} + 2\frac{\partial \text{meas}}{\partial \tilde{\mathbf{q}}_{13}} + \frac{\partial \text{meas}}{\partial \tilde{\mathbf{q}}_{23}}\right],\end{aligned}$$

where now a necessary optimality condition is that the relative thrusting between the three spacecraft is a weighted sum of the direction of descent of the measure of the uncovered set of frequency points.

Hence, each spacecraft's motion and control effort is affected by the amount of area of $\mathcal{D}_R$ that has not been covered by the formation as it involves summations over motions of all the other spacecraft. Therefore, the resulting control law is in some sense decentralized: Given knowledge of the motions of the other spacecraft, the above necessary conditions command each spacecraft to move in directions that attempt to minimize the cost function $\mathcal{J}$.

Remarks:

1. Note that $\frac{\partial \text{meas}}{\partial \tilde{\mathbf{q}}_{jk}}$ constitute the components of the differential form $\mathrm{d}\,(\text{meas})$. Hence, the notation $\frac{\partial \text{meas}}{\partial \tilde{\mathbf{q}}_{jk}}\,(\mathbf{X})$ denotes this form operating on $\mathbf{X}$.

3.7 Example: A Three-Spacecraft Formation

In this section we state the necessary conditions for a three-spacecraft, rigidly-connected, co-planar formation. The necessary conditions for a general one degree of freedom system are slightly different from those of Theorem (3.6.2). Since we only have a single degree of freedom, a single control vector field suffices to drive the system. Hence, the condition (3-6.10) will vanish. Instead, the effect of the measure function $\text{meas}\,(\mathbf{\Psi})$ on the closed loop system appears in the dynamics governing the Lagrange multipliers. This result governs other single degree of freedom systems with different numbers of spacecraft and configurations.

The formation we study is shown in Figure (3.3). The formation assumes the shape of an equilateral triangle. Formations such as this one appear in previous literature. See for example the formation used in [47]. Let the side of the triangle be given by a and each spacecraft is at a distance r from the center of mass CM, where $r = a/\sqrt{3}$. To guarantee that the resulting motion results in a successful maneuver, we impose the condition that $a = 2r_p\lambda$. Moreover, assume the resolution disc D_R has

a radius of $1/\theta_r = 3r_p$. These conditions and the rigidity of the formation guarantee that the resulting six picture frame discs (as defined in Section 3.2) are centered such that each scans an annulus about the central disc. After the formation rotates by an angle of 60°, the maneuver is completed, resulting in a successful maneuver. The motion in the frequency plane is shown in Figure (3.3) (right.)

Since this is a single degree of freedom system evolving on the unit circle S^1, let the angular position, $\theta(t)$, describe the state of the system as shown in Figure (3.3). Hence, $\theta(0) = 0$ and $\theta(T) = \pi/3$. For this example, an approximation of the measure function is given by

$$\text{meas}\left(\Psi(\theta(t))\right) = -24r_p^2\theta(t) + 8\pi r_p^2. \tag{3-7.1}$$

One can also check that $\text{meas}\left(\Psi(\theta = 0)\right) = 8\pi r_p^2$ (that is, the area of the initial uncovered annulus) and that $\text{meas}(\Psi\left(\theta = \pi/3\right)) = 0$ as one expects at the end of a successful maneuver.

If we let the mass of each spacecraft be given by m_s and the torque applied to each spacecraft be given by F, then the equations of motion are given by the equation

$$\frac{\mathrm{D}\theta}{\mathrm{d}t} = \omega, \ \frac{\mathrm{D}\omega}{\mathrm{d}t} = u, \tag{3-7.2}$$

where $u = \frac{F}{m_s}$. The cost function to be minimized is

$$\mathcal{J} = \int_0^T \frac{1}{2}\left\langle u, u\right\rangle + \frac{\tau'^2 a^2}{2\lambda^2}\left\langle \omega, \omega\right\rangle + \kappa^2 \text{meas}(\theta)\mathrm{d}t, \tag{3-7.3}$$

where the absolute linear velocity of the discs is given by $\frac{a}{\lambda}\frac{\mathrm{D}\theta}{\mathrm{d}t} = 2r_p\frac{\mathrm{D}\theta}{\mathrm{d}t}$. Appending $\mathcal{J}$ by the terms $\boldsymbol{\lambda}_1\left(\frac{\mathrm{D}\theta}{\mathrm{d}t} - \omega\right)$ and $\boldsymbol{\lambda}_2\left(\frac{\mathrm{D}\omega}{\mathrm{d}t} - u\right)$, and following a procedure similar to

that used to derive Theorems (3.6.1) and (3.6.2), we obtain Equations (3-7.2) and

$$\begin{aligned}
\frac{\mathrm{D}\boldsymbol{\lambda}_1}{\mathrm{d}t}(\mathbf{X}) &= \kappa^2 \frac{\partial \mathrm{meas}}{\partial \theta}(\mathbf{X}) + \langle R(u,\omega)\omega, \mathbf{X}\rangle \\
\frac{\mathrm{D}\boldsymbol{\lambda}_2}{\mathrm{d}t}(\mathbf{X}) &= -\boldsymbol{\lambda}_1(\mathbf{X}) + \tau^2 \langle \omega, \mathbf{X}\rangle \\
u &= \boldsymbol{\lambda}_2^{\#},
\end{aligned}$$

as necessary conditions, where $\partial \mathrm{meas}/\partial\theta = -24 r_p^2$ and $\mathbf{X} \in TM$ is any arbitrary vector field. We note here that the algebraic condition on $\boldsymbol{\lambda}_2$ vanishes since the system has only one degree of freedom. Instead, an additional term is added to the $\frac{\mathrm{D}\boldsymbol{\lambda}_1}{\mathrm{d}t}$ equation.

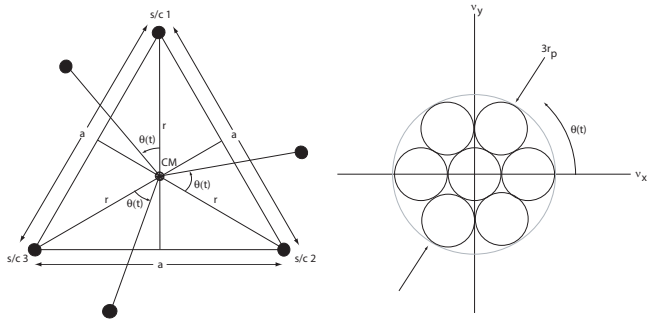

Figure 3.3: A three-spacecraft, rigidly-connected, co-planar formation (left) and the motion in the frequency plane (right.)

3.8 Conclusion

In this chapter we studied the dynamic coverage optimal control problem. The problem is motivated by interferometric imaging spacecraft formations. An optimal control problem is defined to achieve maneuvers optimal in both imaging and fuel senses. Optimality conditions were derived and a two spacecraft example was given to illustrate our results for a one degree of freedom case. The result was further simplified to co-planar formations. Optimality conditions show that a necessary

optimality feature of a spacecraft formation is that its motion must exhibit a form of symmetry about the formation's center of mass. A simple three co-planar spacecraft formation was given to illustrate our results.

CHAPTER 4

Constrained Optimal Trajectory Tracking on the Group of Rigid Body Motions

In the previous section, we studied a formation composed of a group of N *particles*. In this chapter and Chapters 5 and 6, we specialize the discussion to a class of two-spacecraft formations. We will also omit the coverage component of the cost function since the formation motion will already be restricted to successful maneuvers as defined in Chapter 3. In this chapter, we treat each spacecraft in the formation as a rigid body evolving on SE(3), while in Chapters 5 and 6 we assume they are point masses to simplify the analysis.

The ultimate goal of this chapter is to study *constrained optimal trajectory tracking* on SE(3). To do so, we begin first by studying simple optimal control problems on SE(3), including deriving the equations of motion of a rigid body (i.e., Euler's equations) by formulating it as a constrained variational optimal control problem. We recommend the reader go through the material in Appendices A and B first before proceeding with this chapter.

4.1 Optimal Control of a Single Rigid Body on SE(3)

4.1.1 Metric on $\mathfrak{se}(3)$

For SE(3) there does not exist a bilinear form on $\mathfrak{se}(3)$ that is both positive definite and Ad-invariant. However, one can consider two bilinear forms defined on $\mathfrak{se}(3)$. However, more generally, lets consider a class of left invariant metrics.

A matrix form for a family of left-invariant metrics on $\mathfrak{se}(3)$, parameterized by 3 scalars α, β and γ, is expressed as [48]:

$$\mathbf{G} = \begin{bmatrix} \alpha I_3 & \beta I_3 \\ \beta I_3 & \gamma I_3 \end{bmatrix}.$$

Setting $\beta = \gamma = 0$ results in the Killing form. The corresponding inner product is given by: $\alpha \langle \boldsymbol{\omega}_1, \boldsymbol{\omega}_2 \rangle$. Setting $\alpha = \gamma = 0$ results in the Klein form with inner product that is given by: $\beta (\langle \boldsymbol{\omega}_2, \mathbf{v}_1 \rangle + \langle \boldsymbol{\omega}_1, \mathbf{v}_2 \rangle)$. Hence, the metric given above is a linear combination of the Killing and Klein forms where γ is set to zero. Finally, there is the decoupled Park [48] form where $\beta = 0$, which is a weighted quadratic combination of the linear and angular velocities: $\alpha \langle \boldsymbol{\omega}_1, \boldsymbol{\omega}_2 \rangle + \gamma \langle \mathbf{v}_1, \mathbf{v}_2 \rangle$ and which reduces to the standard metric on $\mathbb{R}^6$ when $\alpha = \gamma = 1$ [48].

The two bilinear forms one may consider are [49]:

1. A linear combination of Klein and Killing form: the most generic Ad-invariant form on $\mathfrak{se}(3)$ is given by

   $$\langle \mathbf{V}_1, \mathbf{V}_2 \rangle_{\mathfrak{se}(3)} = \alpha \langle \boldsymbol{\omega}_1, \boldsymbol{\omega}_2 \rangle_{\mathbb{R}^3} + \beta (\langle \boldsymbol{\omega}_1, \mathbf{v}_2 \rangle_{\mathbb{R}^3} + \langle \boldsymbol{\omega}_2, \mathbf{v}_1 \rangle_{\mathbb{R}^3}),$$

   where $\langle \boldsymbol{\omega}_1, \boldsymbol{\omega}_2 \rangle_{\mathbb{R}^3}$ is the standard inner product on $\mathbb{R}^3$ and $\alpha, \beta \in \mathbb{R}$.

2. The standard inner product on $\mathfrak{se}(3) = \mathbb{R}^6$: discard the Lie algebra structure of $\mathfrak{se}(3)$ and set

   $$\langle \mathbf{V}_1, \mathbf{V}_2 \rangle_{\mathbb{R}^6} = \langle \boldsymbol{\omega}_1, \boldsymbol{\omega}_2 \rangle_{\mathbb{R}^3} + \langle \mathbf{v}_1, \mathbf{v}_2 \rangle_{\mathbb{R}^3} = \langle \boldsymbol{\Omega}_1, \boldsymbol{\Omega}_2 \rangle + \langle \mathbf{v}_1, \mathbf{v}_2 \rangle_{\mathbb{R}^3}.$$

In [49], the authors select the standard inner product on $\mathbb{R}^6$, $\langle \cdot, \cdot \rangle_{\mathbb{R}^6}$, to work with. Since positive definiteness is crucial in an optimal control context (we must have a positive definite cost function), we elect to work with the standard inner product on $\mathbb{R}^6$.

4.1.2 Free Rigid Body Equations of Motion as a Constrained Optimal Control Problem

EOMs in body-fixed frame

In this section we derive the rigid body equations of motion (both translational and rotational equations of motion) in the body-fixed frame starting with the kinematic equations of motion:

$$\dot{g} = g\mathbf{V}^b \in \mathrm{T}_g\mathrm{SE}(3), \tag{4-1.1}$$

where $g = (R, p) \in \mathrm{SE}(3)$ and $\mathbf{V}^b = (\mathbf{\Omega}^b, \mathbf{v}^b) \sim (\boldsymbol{\omega}^b, \mathbf{v}^b) \in \mathfrak{se}(3)$ are as described in Appendix B, with $\mathbf{\Omega}^b = \hat{\boldsymbol{\omega}}^b$.

We begin by making a few observations. Equation (4-1.1) can be re-written as an expression over $\mathfrak{se}(3)$ as: $g^{-1}\dot{g} - \mathbf{V}^b = 0$ with g and $\mathbf{V}^b$ given by equation (B-1.2). The inverse g^{-1} is given by:

$$g^{-1} = \begin{bmatrix} R^T & -R^T p \\ 0 & 1 \end{bmatrix} \in \mathrm{SE}(3). \tag{4-1.2}$$

Hence, we have:

$$g^{-1}\dot{g} = \begin{bmatrix} R^T\dot{R} & R^T\dot{p} \\ 0 & 0 \end{bmatrix} \in \mathfrak{se}(3), \tag{4-1.3}$$

such that the following kinematic equations hold:

$$\begin{aligned} \dot{R} &= R\mathbf{\Omega}^b \\ \dot{p} &= R\mathbf{v}^b. \end{aligned} \tag{4-1.4}$$

Finally, for a perturbed element $g_\epsilon(t,\epsilon) = (R_\epsilon(t,\epsilon), p_\epsilon(t,\epsilon))$ that satisfies $g_\epsilon(t,0) = g(t)$, we have an analogous expression to (4-1.1) as follows (see [50], page 41):

$$\left.\frac{\partial g_\epsilon}{\partial \epsilon}\right|_{\epsilon=0} = g\mathbf{W} = \begin{bmatrix} R\mathbf{W}_1^b & R\mathbf{w}_2^b \\ 0 & 0 \end{bmatrix} \in \mathrm{T}_g\mathrm{SE}(3) \tag{4-1.5}$$

where

$$\mathbf{W} = \begin{bmatrix} \mathbf{W}_1^b & \mathbf{w}_2^b \\ 0 & 0 \end{bmatrix} \in \mathfrak{se}(3)$$

and $\mathbf{W}_1^b \in \mathfrak{so}(3)$ and $\mathbf{w}_1^b \in \mathbb{R}^3$ such that

$$\begin{aligned} \left.\frac{\partial R_\epsilon}{\partial \epsilon}\right|_{\epsilon=0} &= R\mathbf{W}_1^b \\ \left.\frac{\partial p_\epsilon}{\partial \epsilon}\right|_{\epsilon=0} &= R\mathbf{w}_2^b. \end{aligned} \tag{4-1.6}$$

Here we view the pair $(\mathbf{W}_1^b, \mathbf{w}_2^b) \in \mathfrak{se}(3)$ the perturbation vector fields expressed in the body fixed frame just as we view the pair $(\mathbf{\Omega}^b, \mathbf{v}^b) \in \mathfrak{se}(3)$ as the angular and translational velocities in the body fixed frame. In addition we have the following result.

Lemma 4.1.1. *Let $g_\epsilon \in \mathrm{SE}(3)$ and $\mathbf{W} \in \mathfrak{se}(3)$ be defined as above, then we have*

$$\left.\frac{\partial g_\epsilon^{-1}}{\partial \epsilon}\right|_{\epsilon=0} = -\mathbf{W}g^{-1}.$$

Proof Since $g_\epsilon^{-1} g_\epsilon = \mathrm{Id}$, then $\frac{\partial}{\partial \epsilon}\left(g_\epsilon^{-1} g_\epsilon\right)\big|_{\epsilon=0} = \left.\frac{\partial g_\epsilon^{-1}}{\partial \epsilon}\right|_{\epsilon=0} g + g^{-1} g\mathbf{W} = 0$ and, hence, $\left.\frac{\partial g_\epsilon^{-1}}{\partial \epsilon}\right|_{\epsilon=0} = -\mathbf{W}g^{-1}$.

■

For SE(3), it is important to note that, unlike the SO(3) case, $\langle [\mathbf{A}, \mathbf{B}], \mathbf{C} \rangle \neq \langle \mathbf{A}, [\mathbf{B}, \mathbf{C}] \rangle$, $\mathbf{A}, \mathbf{B}, \mathbf{C} \in \mathfrak{se}(3)$. Instead we have the following lemma, which is easily proven.

Lemma 4.1.2. *Let* $\mathbf{A} = (\mathbf{\Omega}_a, \mathbf{v}_a), \mathbf{B} = (\mathbf{\Omega}_b, \mathbf{v}_b), \mathbf{C} = (\mathbf{\Omega}_c, \mathbf{v}_c) \in \mathfrak{se}(3)$. *Then we have*

$$\langle [\mathbf{A}, \mathbf{B}], \mathbf{C}] \rangle_{\mathbb{R}^6} = \langle \mathbf{A}, [\mathbf{B}, \mathbf{C}] + [[\mathbf{B}, \mathbf{C}]] \rangle_{\mathbb{R}^6} ,$$

where $[\mathbf{A}, \mathbf{B}] = \mathbf{AB} - \mathbf{BA}$ *is the Lie bracket on SE(3) and* $[[\mathbf{B}, \mathbf{C}]]$ *is given by*

$$[[\mathbf{B}, \mathbf{C}]] = \begin{bmatrix} \widehat{\mathbf{v}_b \times \mathbf{v}_c} & \mathbf{\Omega}_c \mathbf{v}_b \\ 0 & 0 \end{bmatrix} \in \mathfrak{se}(3).$$

Proof

$$\begin{aligned} \langle [\mathbf{A}, \mathbf{B}], \mathbf{C}] \rangle_{\mathbb{R}^6} &= \langle [\mathbf{\Omega}_a, \mathbf{\Omega}_b], \mathbf{\Omega}_c \rangle + \langle \mathbf{\Omega}_a \mathbf{v}_b - \mathbf{\Omega}_b \mathbf{v}_a, \mathbf{v}_c \rangle_{\mathbb{R}^3} \\ &= \langle \mathbf{\Omega}_a, [\mathbf{\Omega}_b, \mathbf{\Omega}_c] \rangle + \left\langle \mathbf{\Omega}_a, \widehat{\mathbf{v}_b \times \mathbf{v}_c} \right\rangle + \langle \mathbf{v}_a, \mathbf{\Omega}_b \mathbf{v}_c \rangle_{\mathbb{R}^3} \\ &= \langle \mathbf{A}, [\mathbf{B}, \mathbf{C}] + [[\mathbf{B}, \mathbf{C}]] \rangle_{\mathbb{R}^6} , \end{aligned}$$

where we have used the facts that: $\langle \mathbf{\Omega}_a \mathbf{v}_b, \mathbf{v}_c \rangle_{\mathbb{R}^3} = \mathbf{v}_c \cdot (\boldsymbol{\omega}_a \times \mathbf{v}_b) = \boldsymbol{\omega}_a \cdot (\mathbf{v}_b \times \mathbf{v}_c) = \langle \boldsymbol{\omega}_a, \mathbf{v}_b \times \mathbf{v}_c \rangle_{\mathbb{R}^3} = \left\langle \mathbf{\Omega}_a, \widehat{\mathbf{v}_b \times \mathbf{v}_c} \right\rangle$ and $- \langle \mathbf{\Omega}_b \mathbf{v}_a, \mathbf{v}_c \rangle_{\mathbb{R}^3} = -\mathbf{v}_c \cdot (\boldsymbol{\omega}_b \times \mathbf{v}_a) = -\mathbf{v}_a \cdot (\mathbf{v}_c \times \boldsymbol{\omega}_b) = \mathbf{v}_a \cdot (\boldsymbol{\omega}_b \times \mathbf{v}_c) = \langle \mathbf{v}_a, \mathbf{\Omega}_b \mathbf{v}_c \rangle_{\mathbb{R}^3}$.

■

If we view SO(3) as a subgroup of SE(3), then Lemma (4.1.2) reduces to the standard result on SO(3): $\langle [\mathbf{A}, \mathbf{B}], \mathbf{C} \rangle = \langle \mathbf{A}, [\mathbf{B}, \mathbf{C}] \rangle$.

To derive a rigid body's equations of motion, we minimize the kinetic energy:

$$\mathcal{J} = \int_0^T \frac{1}{2} \left\langle \mathbf{V}^b, \tilde{\mathbf{J}}(\mathbf{V}^b) \right\rangle_{\mathbb{R}^6} \mathrm{d}t \tag{4-1.7}$$

subject to the constraint given by equation (4-1.1) and the boundary conditions:

$$\begin{aligned} g(0) &= g_0 = (R_0, p_0), \\ \mathbf{V}^b(0) &= \mathbf{V}_0^b = (\boldsymbol{\omega}_0^b, \mathbf{v}_0^b), \\ g(T) &= g_T = (R_T, p_T), \\ \mathbf{V}^b(T) &= \mathbf{V}_T^b = (\boldsymbol{\omega}_T^b, \mathbf{v}_T^b), \end{aligned} \tag{4-1.8}$$

where $\tilde{\mathbf{J}} : \mathfrak{se}(3) \to \mathfrak{se}(3)$ is the symmetric, positive definite, and, hence, invertible operator defined by:

$$\tilde{\mathbf{J}}(\mathbf{V}) = \begin{bmatrix} \mathbf{J}(\boldsymbol{\Omega}) & m\mathbf{v} \\ 0 & 0 \end{bmatrix}, \ \forall \mathbf{V} = (\boldsymbol{\omega}, \mathbf{v}) \in \mathfrak{se}(3) \tag{4-1.9}$$

where $\mathbf{J}$ is as defined in Section (B.4.2) and m is the mass of the body. By our definition of inner product on $\mathbb{R}^6$ in Section (4.1.1), the integrand in the cost functional (4-1.7) corresponds to the total kinetic energy: $\frac{1}{2}\left\langle \boldsymbol{\Omega}^b, \mathbf{J}(\boldsymbol{\Omega}^b)\right\rangle + \frac{1}{2}\left\langle \mathbf{v}^b, m\mathbf{v}^b\right\rangle_{\mathbb{R}^3}$.

First, we form the modified cost functional:

$$\mathcal{J} \ = \ \int_0^T \frac{1}{2}\left\langle \mathbf{V}^b, \tilde{\mathbf{J}}(\mathbf{V}^b)\right\rangle_{\mathbb{R}^6} + \left\langle \boldsymbol{\Lambda}^b, g^{-1}\dot{g} - \mathbf{V}^b\right\rangle_{\mathbb{R}^6} \mathrm{d}t, \tag{4-1.10}$$

where

$$\boldsymbol{\Lambda}^b = \begin{bmatrix} \boldsymbol{\Lambda}_1^b & \boldsymbol{\lambda}_2^b \\ 0 & 0 \end{bmatrix} \in \mathfrak{se}(3)$$

is the Lagrange multiplier with $\boldsymbol{\Lambda}_1^b = \hat{\boldsymbol{\lambda}}_1^b \in \mathfrak{so}(3)$ and $\boldsymbol{\lambda}_2^b \in \mathbb{R}^3$. Then we have:

$$\left.\frac{\partial \mathcal{J}}{\partial \epsilon}\right|_{\epsilon=0} = \int_0^T \left\langle \left.\frac{\mathrm{D}\mathbf{V}_\epsilon^b}{\partial \epsilon}\right|_{\epsilon=0}, \tilde{\mathbf{J}}\left(\mathbf{V}^b\right) - \boldsymbol{\Lambda}^b \right\rangle + \left\langle \boldsymbol{\Lambda}^b, \left[\mathbf{V}^b, \mathbf{W}^b\right] + \frac{\mathrm{D}\mathbf{W}^b}{\mathrm{d}t} \right\rangle \mathrm{d}t.$$

Integrating $\left\langle \boldsymbol{\Lambda}^b, \left[\mathbf{V}^b, \mathbf{W}^b\right] + \frac{\mathrm{D}\mathbf{W}^b}{\mathrm{d}t} \right\rangle$ by parts and using Lemma (4.1.2), we find that

$$\left.\frac{\partial \mathcal{J}}{\partial \epsilon}\right|_{\epsilon=0} = \int_0^T \left\langle \left.\frac{\mathrm{D}\mathbf{V}_\epsilon^b}{\partial \epsilon}\right|_{\epsilon=0}, \tilde{\mathbf{J}}\left(\mathbf{V}^b\right) - \boldsymbol{\Lambda}^b \right\rangle - \left\langle \mathbf{W}^b, \left[\mathbf{V}^b, \boldsymbol{\Lambda}^b\right] + \left[\left[\mathbf{V}^b, \boldsymbol{\Lambda}^b\right]\right] + \frac{\mathrm{D}\boldsymbol{\Lambda}^b}{\mathrm{d}t} \right\rangle \mathrm{d}t.$$

Hence, the necessary optimality conditions are given by

$$\begin{aligned} \boldsymbol{\Lambda}^b \ &= \ \tilde{\mathbf{J}}\left(\mathbf{V}^b\right) \\ \frac{\mathrm{D}\boldsymbol{\Lambda}^b}{\mathrm{d}t} \ &= \ \left[\boldsymbol{\Lambda}^b, \mathbf{V}^b\right] - \left[\left[\mathbf{V}^b, \boldsymbol{\Lambda}^b\right]\right]. \end{aligned}$$

Expanding this expression, we get:

$$\begin{aligned} \frac{\mathrm{D}\mathbf{M}^b}{\mathrm{d}t} \ &= \ \left[\mathbf{M}^b, \boldsymbol{\Omega}^b\right], \ \mathbf{M}^b = \boldsymbol{\Lambda}_1^b = \mathbf{J}(\boldsymbol{\Omega}^b) \\ \frac{\mathrm{D}\mathbf{l}^b}{\mathrm{d}t} \ &= \ \mathbf{l}_2^b \times \boldsymbol{\omega}^b, \ \mathbf{l}^b = \boldsymbol{\lambda}_2^b = m\mathbf{v}, \end{aligned} \tag{4-1.11}$$

which are the equations of motion for a rigid body in space.

To verify the above result, let us view SE(3) as SO(3)$\times\mathbb{R}^3$ and use the definition for the metric on SE(3) given above. When differentiating the perturbed cost function

$$\begin{aligned}\mathcal{J}_\epsilon &= \int_0^T \frac{1}{2}\left\langle \boldsymbol{\Omega}^b, \mathbf{J}(\boldsymbol{\Omega}^b)\right\rangle + \frac{1}{2}\left\langle \mathbf{v}^b, m\mathbf{v}^b\right\rangle_{\mathbb{R}^3} \\ &\quad + \left\langle \boldsymbol{\Lambda}_1^b, R^T\dot{R} - \boldsymbol{\Omega}^b\right\rangle + \left\langle \boldsymbol{\lambda}_2^b, R^T\dot{p} - \mathbf{v}^b\right\rangle_{\mathbb{R}^3} \mathrm{d}t, \end{aligned} \tag{4-1.12}$$

with respect to ϵ, the first and third terms give identical expressions to those given by equation (B-4.8). We now focus our attention on the second and fourth terms:

$$\begin{aligned}\frac{\partial}{\partial\epsilon}\int_0^T \frac{1}{2}\left\langle \mathbf{v}^b, m\mathbf{v}^b\right\rangle_{\mathbb{R}^3} &+ \left\langle \boldsymbol{\lambda}_2^b, R^T\dot{p} - \mathbf{v}^b\right\rangle_{\mathbb{R}^3}\mathrm{d}t \\ &= \int_0^T \left\langle \delta\mathbf{v}^b, m\mathbf{v}^b - \boldsymbol{\lambda}_2^b\right\rangle_{\mathbb{R}^3} + \left\langle \boldsymbol{\lambda}_2^b, \frac{\partial}{\partial\epsilon}\bigg|_{\epsilon=0}\left(R^T\dot{p}\right)\right\rangle_{\mathbb{R}^3}\mathrm{d}t \\ &= \int_0^T \left\langle \delta\mathbf{v}^b, m\mathbf{v}^b - \boldsymbol{\lambda}_2^b\right\rangle_{\mathbb{R}^3} \\ &\quad + \left\langle \boldsymbol{\lambda}_2^b, \left(\mathbf{W}_1^b\right)^T\mathbf{v}^b + \boldsymbol{\Omega}^b\mathbf{w}_2^b + \frac{\partial\mathbf{w}_2^b}{\partial t}\right\rangle_{\mathbb{R}^3}\mathrm{d}t \\ &= \int_0^T \left\langle \delta\mathbf{v}^b, m\mathbf{v}^b - \boldsymbol{\lambda}_2^b\right\rangle_{\mathbb{R}^3} + \left\langle \mathbf{W}_1^b\boldsymbol{\lambda}_2^b, \mathbf{v}^b\right\rangle_{\mathbb{R}^3} + \left\langle \boldsymbol{\lambda}_2^b, \boldsymbol{\Omega}^b\mathbf{w}_2^b\right\rangle_{\mathbb{R}^3} \\ &\quad - \left\langle \frac{\mathrm{d}\boldsymbol{\lambda}_2^b}{\mathrm{d}t}, \mathbf{w}_2^b\right\rangle_{\mathbb{R}^3}\mathrm{d}t \\ &= \int_0^T \left\langle \delta\mathbf{v}^b, m\mathbf{v}^b - \boldsymbol{\lambda}_2^b\right\rangle_{\mathbb{R}^3} + \left\langle \boldsymbol{\lambda}_2^b\times\mathbf{v}^b, \mathbf{w}_1^b\right\rangle_{\mathbb{R}^3} - \left\langle \boldsymbol{\Omega}^b\boldsymbol{\lambda}_2^b, \mathbf{w}_2^b\right\rangle_{\mathbb{R}^3} \\ &\quad - \left\langle \frac{\mathrm{d}\boldsymbol{\lambda}_2^b}{\mathrm{d}t}, \mathbf{w}_2^b\right\rangle_{\mathbb{R}^3}\mathrm{d}t \end{aligned}$$

since $\mathbf{W}_1^b, \boldsymbol{\Omega}^b \in \mathfrak{so}(3)$ is skew symmetric with $\hat{\mathbf{w}}_1^b = \mathbf{W}_1^b$ and $\hat{\boldsymbol{\omega}}^b = \boldsymbol{\Omega}^b$. To obtain the above expressions we have used the identities: $\langle x, \mathbf{A}y\rangle_{\mathbb{R}^3} = x\cdot(\mathbf{A}y) = (\mathbf{A}^Tx)\cdot y = \left\langle \mathbf{A}^Tx, y\right\rangle_{\mathbb{R}^3}$ for all $\mathbf{A}\in\mathbb{R}^{3\times3}$ and $x, y\in\mathbb{R}^3$. In particular, if $\mathbf{A}$ is skew symmetric we have $\langle x, \mathbf{A}y\rangle_{\mathbb{R}^3} = -\langle \mathbf{A}x, y\rangle_{\mathbb{R}^3}$. We also needed the identity: $\left\langle \mathbf{W}_1^b\boldsymbol{\lambda}_2^b, \mathbf{v}^b\right\rangle_{\mathbb{R}^3} = \left\langle \mathbf{w}_1^b\times\boldsymbol{\lambda}_2^b, \mathbf{v}^b\right\rangle_{\mathbb{R}^3} = (\mathbf{w}_1^b\times\boldsymbol{\lambda}_2^b)\cdot\mathbf{v}^b = (\boldsymbol{\lambda}_2^b\times\mathbf{v}^b)\cdot\mathbf{w}_1^b = \left\langle \mathbf{w}_1^b, \boldsymbol{\Lambda}_2^b\mathbf{v}^b\right\rangle_{\mathbb{R}^3}$. From this and

equation (B-4.8) we obtain

$$\begin{aligned}\frac{\partial}{\partial\epsilon}\mathcal{J}_\epsilon &= \int_0^T \left\langle \frac{\mathrm{D}\boldsymbol{\Omega}^b}{\mathrm{d}\epsilon}\Big|_{\epsilon=0}, \mathbf{J}(\boldsymbol{\Omega}^b) - \boldsymbol{\Lambda}_1^b \right\rangle \mathrm{d}t \left\langle -\frac{\mathrm{D}\boldsymbol{\Lambda}_1^b}{\mathrm{d}t} + [\boldsymbol{\Lambda}_1^b, \boldsymbol{\Omega}^b], \mathbf{W}_1^b \right\rangle \mathrm{d}t \\ &+ \int_0^T \left\langle \delta\mathbf{v}^b, m\mathbf{v}^b - \boldsymbol{\lambda}_2^b \right\rangle_{\mathbb{R}^3} + \left\langle \boldsymbol{\lambda}_2^b \times \mathbf{v}^b, \mathbf{w}_1^b \right\rangle_{\mathbb{R}^3} \\ &- \left\langle \boldsymbol{\Omega}^b \boldsymbol{\lambda}_2^b, \mathbf{w}_2^b \right\rangle_{\mathbb{R}^3} - \left\langle \frac{\mathrm{d}\boldsymbol{\lambda}_2^b}{\mathrm{d}t}, \mathbf{w}_2^b \right\rangle \mathrm{d}t. \end{aligned} \tag{4-1.13}$$

Note that $\mathbf{W}_1^b = \hat{\mathbf{w}}_1^b$ appears in both the second and third integrals, which seemingly couples both terms together. First observe that by the independence of $\delta\mathbf{v}^b$ from $\delta\boldsymbol{\Omega}^b$, $\mathbf{W}_1^b$ and $\mathbf{w}_2^b$, the first term in the third integral implies that $\boldsymbol{\lambda}_2^b = m\mathbf{v}^b$, which is easily identified as the linear momentum of the rigid body's center of mass. Since $\boldsymbol{\lambda}_2^b = m\mathbf{v}^b$, then $\boldsymbol{\lambda}_2^b \times \mathbf{v}^b = m\mathbf{v}^b \times \mathbf{v}^b = 0$ and the second term under the third time integral is zero. Therefore, the second and third time integrals are now decoupled (the apparent coupling was due to the variable $\mathbf{W}_1^b = \hat{\mathbf{w}}_1^b$ appearing in both integrals.) The third and fourth terms under the third integral imply that $\dot{\boldsymbol{\lambda}}_2^{\,b} = -\boldsymbol{\Omega}^b\boldsymbol{\lambda}_2^b = -\boldsymbol{\omega}^b \times \boldsymbol{\lambda}_2^b = \boldsymbol{\lambda}_2^b \times \boldsymbol{\omega}^b$. These facts and the result obtained in Section (B.4.2) imply that

$$\begin{aligned}\frac{\mathrm{D}\mathbf{M}^b}{\mathrm{d}t} &= \left[\mathbf{M}^b, \boldsymbol{\Omega}^b\right], \ \mathbf{M}^b = \boldsymbol{\Lambda}_1^b = \mathbf{J}(\boldsymbol{\Omega}^b) \\ \frac{\mathrm{D}\mathbf{l}^b}{\mathrm{d}t} &= \mathbf{l}_2^b \times \boldsymbol{\omega}^b, \ \mathbf{l}^b = \boldsymbol{\lambda}_2^b = m\mathbf{v}, \end{aligned} \tag{4-1.14}$$

which are identical to equations (4-1.11). Recall the relation between the time derivative of an arbitrary variable $s(t)$ in a body fixed frame, $\frac{\mathrm{d}'s}{\mathrm{d}t}$, with the space fixed frame time derivative $\frac{\mathrm{d}s}{\mathrm{d}t}$: $\frac{\mathrm{d}s}{\mathrm{d}t} = \frac{\mathrm{d}'s}{\mathrm{d}t} + \boldsymbol{\omega} \times s$. Equation (4-1.14) then implies that the rate of change of the linear momentum $\boldsymbol{\lambda}_2^b$ in the space fixed frame is zero: $\frac{\mathrm{d}\boldsymbol{\lambda}_2^s}{\mathrm{d}t} = \frac{\mathrm{d}'\boldsymbol{\lambda}_2^b}{\mathrm{d}t} + \boldsymbol{\omega}^b \times \boldsymbol{\lambda}_2^b = \boldsymbol{\lambda}_2^b \times \boldsymbol{\omega}^b + \boldsymbol{\omega}^b \times \boldsymbol{\lambda}_2^b = 0$ as one expects since no external forces are applied at the center of mass of the rigid body. Similarly we have $\frac{\mathrm{d}m^s}{\mathrm{d}t} = \frac{\mathrm{d}'m^b}{\mathrm{d}t} + \boldsymbol{\omega}^b \times m^b = 0$, where again $\mathbf{M}^b = \hat{m}^b$.

EOMs in space-fixed frame

In this section we derive the corresponding equations of motion in a space fixed frame. The kinematic equation is given by $\dot{g} = \mathbf{V}^s g$. In the space-fixed case, we have:

$$\dot{g}g^{-1} = \begin{bmatrix} \dot{R}R^T & -\dot{R}R^T p + \dot{p} \\ 0 & 0 \end{bmatrix} = \begin{bmatrix} \boldsymbol{\Omega}^s & \mathbf{v}^s \\ 0 & 0 \end{bmatrix} \in \mathfrak{se}(3). \tag{4-1.15}$$

Hence, the following kinematic equations are:

$$\begin{aligned} \dot{R} &= \boldsymbol{\Omega}^s R \\ \dot{p} &= \mathbf{v}^s + \boldsymbol{\Omega}^s p. \end{aligned} \tag{4-1.16}$$

Since $\dot{p} = R\mathbf{v}^b = \mathbf{v}^s + \boldsymbol{\Omega}^s p$, then $\mathbf{v}^b = R^T\mathbf{v}^s + R^T\boldsymbol{\Omega}^s p$. The cost functional becomes:

$$\mathcal{J} = \int_0^T \frac{1}{2} \left\langle \boldsymbol{\Omega}^s, RJR^T\boldsymbol{\Omega}^s + \boldsymbol{\Omega}^s RJR^T \right\rangle + \frac{m}{2} \left\langle \mathbf{v}^s + \boldsymbol{\Omega}^s p, \mathbf{v}^s + \boldsymbol{\Omega}^s p \right\rangle_{\mathbb{R}^3} \mathrm{d}t.$$

Appending the cost by the terms $\left\langle \boldsymbol{\Lambda}_1^s, \dot{R}R^T - \boldsymbol{\Omega}^s \right\rangle + \langle \boldsymbol{\lambda}_2^s, \dot{p} - \mathbf{v}^s - \boldsymbol{\Omega}^s p \rangle$ we find that:

$$\begin{aligned} \left.\frac{\partial \mathcal{J}_\epsilon}{\partial \epsilon}\right|_{\epsilon=0} = & \int_0^T \left\langle \frac{\mathrm{D}\boldsymbol{\Omega}^s}{\mathrm{d}\epsilon}\Big|_{\epsilon=0}, \left(RJR^T\boldsymbol{\Omega}^s + \boldsymbol{\Omega}^s RJR^T\right) - \boldsymbol{\Lambda}_1^s \right\rangle \mathrm{d}t - \int_0^T \left\langle \frac{\mathrm{D}\boldsymbol{\Lambda}_1^s}{\mathrm{d}t}, \mathbf{W}_1^s \right\rangle \mathrm{d}t \\ & + m \left\langle \delta\mathbf{v}^s, -\boldsymbol{\lambda}_2 + m(\mathbf{v}^s + \boldsymbol{\Omega}^s p) \right\rangle_{\mathbb{R}^3} + \left\langle m(\mathbf{v}^s + \boldsymbol{\Omega}^s p) - \boldsymbol{\lambda}_2^s, \delta\boldsymbol{\Omega}^s p \right\rangle_{\mathbb{R}^3} \\ & + \left\langle -\frac{\mathrm{D}\boldsymbol{\lambda}_2^s}{\mathrm{d}t}, \mathbf{w}_2^s \right\rangle + \left\langle -\boldsymbol{\lambda}_2^s + m(\mathbf{v}^s + \boldsymbol{\Omega}^s p), \boldsymbol{\Omega}^s \mathbf{w}_2^s \right\rangle_{\mathbb{R}^3} \mathrm{d}t. \end{aligned}$$

The above equation implies that the first order necessary conditions are:

$$\begin{aligned} \frac{\mathrm{D}\mathbf{M}^s}{\mathrm{d}t} &= 0, \\ \frac{\mathrm{D}\boldsymbol{\lambda}_2^s}{\mathrm{d}t} &= 0 \end{aligned} \tag{4-1.17}$$

where, as before, $\mathbf{M}^s := \boldsymbol{\Lambda}_2^s = RJR^T\boldsymbol{\Omega}^s + \boldsymbol{\Omega}^s RJR^T$ and $\boldsymbol{\lambda}_2^s = m(\mathbf{v}^s + \boldsymbol{\Omega}^s p)$. This result expresses conservation of angular and linear momenta (in a space-fixed frame) for the free rigid body.

4.1.3 Second Order Optimal Control Problem on SE(3)

In body-fixed frame

We now study the minimum control problem in body-fixed variables, minimizing

$$\mathcal{J} = \int_0^T \frac{1}{2} \left\langle \mathbf{U}^b, \mathbf{U}^b \right\rangle_{\mathbb{R}^6} \mathrm{d}t \tag{4-1.18}$$

subject to the second order dynamics:

$$\begin{aligned} \dot{g} &= g\mathbf{V}^b \\ \frac{\mathrm{D}\tilde{\mathbf{J}}\left(\mathbf{V}^b\right)}{\mathrm{d}t} &= \left[\tilde{\mathbf{J}}\left(\mathbf{V}^b\right), \mathbf{V}^b\right] - \left[[\mathbf{V}^b, \tilde{\mathbf{J}}\left(\mathbf{V}^b\right)]\right] + \mathbf{U}^b \end{aligned} \tag{4-1.19}$$

and the boundary conditions:

$$g(0) = g_0,\ \mathbf{V}^b(0) = \mathbf{V}_0^b,\ g(T) = g_T,\ \mathbf{V}^b(T) = \mathbf{V}_T^b, \tag{4-1.20}$$

where $\mathbf{U}^b = \left(\hat{\boldsymbol{\tau}}^b, \mathbf{u}^b\right) \in \mathfrak{se}(3)$ is the control vector field in body fixed coordinates.

We first form the modified cost functional:

$$\begin{aligned} \mathcal{J} &= \int_0^T \frac{1}{2} \left\langle \mathbf{U}^b, \mathbf{U}^b \right\rangle + \left\langle \boldsymbol{\Lambda}_1^b, g^{-1}\dot{g} - \mathbf{V}^b \right\rangle \\ &\quad + \left\langle \boldsymbol{\Lambda}_2^b, \frac{\mathrm{D}\tilde{\mathbf{J}}\left(\mathbf{V}^b\right)}{\mathrm{d}t} - \left[\tilde{\mathbf{J}}\left(\mathbf{V}^b\right), \mathbf{V}^b\right] + \left[[\mathbf{V}^b, \tilde{\mathbf{J}}\left(\mathbf{V}^b\right)]\right] - \mathbf{U}^b \right\rangle \mathrm{d}t, \end{aligned}$$

where $\boldsymbol{\Lambda}_1^b = \left(\boldsymbol{\Lambda}_{11}^b, \boldsymbol{\lambda}_{12}^b\right) \in \mathfrak{se}(3)$ and $\boldsymbol{\Lambda}_2^b = \left(\boldsymbol{\Lambda}_{21}^b, \boldsymbol{\lambda}_{22}^b\right) \in \mathfrak{se}(3)$, with $\boldsymbol{\Lambda}_{11}^b, \boldsymbol{\Lambda}_{21}^b \in \mathfrak{so}(3)$ and $\boldsymbol{\lambda}_{12}^b, \boldsymbol{\lambda}_{22}^b \in \mathbb{R}^3$, are Lagrange multipliers. After a lengthy computation, we find that

$$\begin{aligned} \left.\frac{\partial \mathcal{J}}{\partial \epsilon}\right|_{\epsilon=0} &= \int_0^T \left\langle \left.\frac{\mathrm{D}\mathbf{U}^b}{\partial \epsilon}\right|_{\epsilon=0}, \mathbf{U}^b - \boldsymbol{\Lambda}_2^b \right\rangle \\ &\quad + \left\langle \mathbf{W}^b, \tilde{\mathbf{R}}\left(\tilde{\mathbf{J}}\left(\boldsymbol{\Lambda}_2^b\right), \mathbf{V}^b\right)\mathbf{V}^b - \left[\mathbf{V}^b, \boldsymbol{\Lambda}_1^b\right] - \left[[\mathbf{V}^b, \boldsymbol{\Lambda}_1^b]\right] - \frac{\mathrm{D}\boldsymbol{\Lambda}_1^b}{\mathrm{d}t} \right\rangle \\ &\quad + \left\langle \left.\frac{\mathrm{D}\mathbf{V}^b}{\partial \epsilon}\right|_{\epsilon=0}, \tilde{\mathbf{J}}\left(\left[\boldsymbol{\Lambda}_2^b, \mathbf{V}^b\right]\right) - \left[\boldsymbol{\Lambda}_2^b, \tilde{\mathbf{J}}\left(\mathbf{V}^b\right)\right] - \left[[\boldsymbol{\Lambda}_2^b, \tilde{\mathbf{J}}\left(\mathbf{V}^b\right)]\right] \right. \\ &\quad \left. - \frac{\mathrm{D}\tilde{\mathbf{J}}\left(\boldsymbol{\Lambda}_2^b\right)}{\mathrm{d}t} - \boldsymbol{\Lambda}_1^b \right\rangle \mathrm{d}t, \end{aligned}$$

where $\tilde{\mathbf{R}}$ is the curvature tensor associated with SE(3). This gives our next theorem.

Theorem 4.1.1. *The necessary optimality conditions for the problem of minimizing (4-1.18) subject to the dynamics (4-1.19) and the boundary conditions (4-1.20) are given by*

$$\begin{aligned} \boldsymbol{\Lambda}_2^b &= \mathbf{U}^b \\ \frac{\mathrm{D}\boldsymbol{\Lambda}_1^b}{\mathrm{d}t} &= \tilde{\mathbf{R}}\left(\tilde{\mathbf{J}}\left(\boldsymbol{\Lambda}_2^b\right), \mathbf{V}^b\right)\mathbf{V}^b - \left[\mathbf{V}^b, \boldsymbol{\Lambda}_1^b\right] - \left[\left[\mathbf{V}^b, \boldsymbol{\Lambda}_1^b\right]\right] \\ \frac{\mathrm{D}\tilde{\mathbf{J}}\left(\boldsymbol{\Lambda}_2^b\right)}{\mathrm{d}t} &= \tilde{\mathbf{J}}\left(\left[\boldsymbol{\Lambda}_2^b, \mathbf{V}^b\right]\right) - \left[\boldsymbol{\Lambda}_2^b, \tilde{\mathbf{J}}\left(\mathbf{V}^b\right)\right] - \left[\left[\boldsymbol{\Lambda}_2^b, \tilde{\mathbf{J}}\left(\mathbf{V}^b\right)\right]\right] - \boldsymbol{\Lambda}_1^b. \end{aligned} \tag{4-1.21}$$

In obtaining the above result we used the fact that the vector fields $\mathbf{V}^b$ and $\mathbf{W}^b$ are left-invariant vector fields. In the process of obtaining Theorem (4.1.1), the curvature tensor is evaluated at a point $g_\epsilon(t) \neq \mathrm{Id}$, that is we get $\tilde{\mathbf{R}}_{g_\epsilon}\left(\frac{\partial g_\epsilon}{\partial \epsilon}, \frac{\partial g_\epsilon}{\partial t}\right)\mathbf{V}^b$. Evaluating this at $\epsilon = 0$ we get: $\tilde{\mathbf{R}}_g\left(g\mathbf{W}^b, g\mathbf{V}^b\right)\mathbf{V}^b$. Since $g\mathbf{W}^b$ and $g\mathbf{V}^b$ are left-invariant vector fields at the group element $g(t)$, then by virtue of the identification $\mathrm{T}_g\mathrm{SE}(3) \simeq \mathfrak{se}(3)$ (see Theorem (5.27) on page 266 in [51] and pages 84-85 in [52]), we have $\tilde{\mathbf{R}}_g\left(g\mathbf{W}^b, g\mathbf{V}^b\right)\mathbf{V}^b = \tilde{\mathbf{R}}\left(\mathbf{W}^b, \mathbf{V}^b\right)\mathbf{V}^b$, which is the curvature tensor evaluated at the identity element. The result directly follows using the properties of the curvature tensor and Lemma (4.1.2).

Though the curvature tensor for a compact semi-simple Lie group (such as SO(3)), with respect to a bi-invariant metric) is well known [41], it is not clear what the curvature tensor for a non-compact Lie group, such as SE(3), is. One may conjecture that $\tilde{\mathbf{R}}$ is the curvature tensor over the product space $\mathrm{SO}(3) \times \mathbb{R}^3$. We show this by reformulating the optimal control problem on the product space $\mathrm{SO}(3) \times \mathbb{R}^3$ and re-derive the necessary conditions on the product space. By comparing this result with Theorem (4.1.1), we are then able to read out an expression for the curvature

tensor on SE(3). The dynamics are now written as components of $\mathrm{SO}(3)\times\mathbb{R}^3$ as:

$$\begin{aligned} \dot{R} &= R\boldsymbol{\Omega}^b \\ \dot{p} &= R\mathbf{v}^b \\ \frac{\mathrm{D}\mathbf{M}^b}{\mathrm{d}t} &= \left[\mathbf{M}^b, \boldsymbol{\Omega}^b\right] + \hat{\boldsymbol{\tau}}^b \\ \frac{\mathrm{D}\mathbf{l}^b}{\mathrm{d}t} &= \mathbf{l}^b \times \boldsymbol{\omega}^b + \mathbf{u}^b, \end{aligned} \tag{4-1.22}$$

where $\hat{\boldsymbol{\tau}}^b \in \mathfrak{so}(3)$ is the skew symmetric form of the torque vector $\boldsymbol{\tau}^b \in R^3$, $\mathbf{u} \in \mathbb{R}^3$ is the control force, and $\mathbf{M}^b = \mathbf{J}(\boldsymbol{\Omega}^b)$ and $\mathbf{l}^b = m\mathbf{v}^b$ denote the angular and linear momenta as expressed in a body-fixed frame. We follow the same procedure as before by first formulating the appended cost functional:

$$\begin{aligned} \mathcal{J} = \int_0^T & \frac{1}{2}\left\langle \hat{\boldsymbol{\tau}}^b, \hat{\boldsymbol{\tau}}^b \right\rangle + \frac{1}{2}\left\langle \mathbf{u}^b, \mathbf{u}^b \right\rangle_{\mathbb{R}^3} + \left\langle \boldsymbol{\Lambda}_{11}^b, R^T\dot{R} - \boldsymbol{\Omega}^b \right\rangle + \left\langle \boldsymbol{\lambda}_{12}^b, R^T\dot{p} - \mathbf{v}^b \right\rangle_{\mathbb{R}^3} \\ & + \left\langle \boldsymbol{\Lambda}_{21}^b, \frac{\mathrm{D}\mathbf{M}^b}{\mathrm{d}t} - \left[\mathbf{M}^b, \boldsymbol{\Omega}^b\right] - \hat{\boldsymbol{\tau}}^b \right\rangle + \left\langle \boldsymbol{\lambda}_{22}^b, \frac{\mathrm{D}\mathbf{l}^b}{\mathrm{d}t} - \mathbf{l}^b \times \boldsymbol{\omega}^b - \mathbf{u}^b \right\rangle_{\mathbb{R}^3} \mathrm{d}t. \end{aligned}$$

Computing $\partial\mathcal{J}_\epsilon/\partial\epsilon\big|_{\epsilon=0}$, we get:

$$\begin{aligned} \left.\frac{\partial\mathcal{J}}{\partial\epsilon}\right|_{\epsilon=0} = & \int_0^T \left\langle \frac{\mathrm{D}\hat{\boldsymbol{\tau}}^b}{\mathrm{d}\epsilon}, \hat{\boldsymbol{\tau}}^b - \boldsymbol{\Lambda}_{21}^b \right\rangle \mathrm{d}t + \int_0^T \left\langle \frac{\mathrm{D}\mathbf{u}^b}{\mathrm{d}\epsilon}, \mathbf{u}^b - \boldsymbol{\lambda}_{22}^b \right\rangle_{\mathbb{R}^3} \mathrm{d}t \\ & + \int_0^T \left\langle \mathbf{W}_1^b, -[\boldsymbol{\Omega}^b, \boldsymbol{\Lambda}_{11}^b] - \frac{\mathrm{D}\boldsymbol{\Lambda}_{11}^b}{\mathrm{d}t} + \mathbf{R}\left(\mathbf{J}\left(\boldsymbol{\Lambda}_{21}^b\right), \boldsymbol{\Omega}^b\right)\boldsymbol{\Omega}^b - \widehat{\mathbf{v}^b \times \boldsymbol{\lambda}_{12}^b} \right\rangle \mathrm{d}t \\ & + \int_0^T \left\langle \mathbf{w}_2, -\frac{\mathrm{D}\boldsymbol{\lambda}_{12}^b}{\mathrm{d}t} + \boldsymbol{\lambda}_{12}^b \times \boldsymbol{\omega}^b \right\rangle_{\mathbb{R}^3} \mathrm{d}t \\ & + \int_0^T \left\langle \frac{\mathrm{D}\boldsymbol{\Omega}^b}{\mathrm{d}\epsilon}, -\boldsymbol{\Lambda}_{11}^b - \frac{\mathrm{D}}{\mathrm{d}t}\mathbf{J}\left(\boldsymbol{\Lambda}_{21}^b\right) \right. \\ & \left. -\mathbf{J}\left(\left[\boldsymbol{\Omega}^b, \boldsymbol{\Lambda}_{21}^b\right]\right) + \left[\mathbf{M}^b, \boldsymbol{\Lambda}_{21}^b\right] - \widehat{\boldsymbol{\lambda}_{22}^b \times \mathbf{l}^b} \right\rangle \mathrm{d}t \\ & + \int_0^T \left\langle \delta\mathbf{v}^b, -\boldsymbol{\lambda}_{12}^b - m\frac{\mathrm{D}\boldsymbol{\lambda}_{22}^b}{\mathrm{d}t} - m\boldsymbol{\omega}^b \times \boldsymbol{\lambda}_{22}^b \right\rangle_{\mathbb{R}^3} \mathrm{d}t, \end{aligned} \tag{4-1.23}$$

where $\mathbf{R}$ is the curvature tensor associated with SO(3). Hence, the necessary opti-

mality conditions are:

$$\begin{aligned}
\hat{\boldsymbol{\tau}}^b &= \boldsymbol{\Lambda}_{21}^b \\
\mathbf{u}^b &= \boldsymbol{\lambda}_{22}^b \\
\frac{\mathrm{D}\boldsymbol{\Lambda}_{11}^b}{\mathrm{d}t} &= -[\boldsymbol{\Omega}^b, \boldsymbol{\Lambda}_{11}^b] + \mathbf{R}(\mathbf{J}\left(\boldsymbol{\Lambda}_{21}^b\right), \boldsymbol{\Omega}^b)\boldsymbol{\Omega}^b - \widehat{\mathbf{v}^b \times \boldsymbol{\lambda}_{12}^b} \\
\frac{\mathrm{D}\boldsymbol{\lambda}_{12}^b}{\mathrm{d}t} &= \boldsymbol{\lambda}_{12}^b \times \boldsymbol{\omega}^b \\
\frac{\mathrm{D}\mathbf{J}(\boldsymbol{\Lambda}_{21}^b)}{\mathrm{d}t} &= [\mathbf{M}^b, \boldsymbol{\Lambda}_{21}^b] - \boldsymbol{\Lambda}_{11}^b - \mathbf{J}(\left[\boldsymbol{\Omega}^b, \boldsymbol{\Lambda}_{21}^b\right]) - \widehat{\boldsymbol{\lambda}_{22}^b \times \mathbf{l}^b} \\
m\frac{\mathrm{D}\boldsymbol{\lambda}_{22}^b}{\mathrm{d}t} &= -\boldsymbol{\lambda}_{12}^b - \boldsymbol{\omega}^b \times \left(m\boldsymbol{\lambda}_{22}^b\right).
\end{aligned}$$

Setting

$$\begin{aligned}
\boldsymbol{\Lambda}_1^b &= \begin{bmatrix} \boldsymbol{\Lambda}_{11}^b & \boldsymbol{\lambda}_{12}^b \\ & 0 \end{bmatrix} \\
\boldsymbol{\Lambda}_2^b &= \begin{bmatrix} \boldsymbol{\Lambda}_{21}^b & \boldsymbol{\lambda}_{22}^b \\ & 0 \end{bmatrix} \\
\mathbf{U}^b &= \begin{bmatrix} \boldsymbol{\tau}^b & \mathbf{u}^b \\ & 0 \end{bmatrix}
\end{aligned}$$

and comparing Equation (4-1.24) with Theorem (4.1.1), one deduces that

$$\tilde{\mathbf{R}}\left(\mathbf{A}, \mathbf{B}\right)\mathbf{B} = \begin{bmatrix} \mathbf{R}\left(\boldsymbol{\Omega}_a, \boldsymbol{\Omega}_b\right)\boldsymbol{\Omega}_b & 0 \\ 0 & 0 \end{bmatrix},$$

for all $\mathbf{A} = (\boldsymbol{\Omega}_a, \mathbf{v}_a), \mathbf{B} = (\boldsymbol{\Omega}_b, \mathbf{v}_b) \in \mathfrak{se}(3)$ and $\boldsymbol{\Omega}_a, \boldsymbol{\Omega}_b \in \mathfrak{so}(3)$. This is not a rigorous proof, but this result agrees with our conjecture that the curvature tensor on SE(3) agrees with the curvature tensor on the product space $\mathrm{SO}(3) \times \mathbb{R}^3$.

4.2 Constrained Optimal Trajectory Tracking on SE(3) for Imaging Applications

In this section we build on the work done in the previous sections by studying a generic constrained optimal control problem on SE(3). In this section we work in body variables and, hence, we will omit the superscript $\cdot^b$ notation throughout. We first make a few definitions.

Let $g(t) = (R(t), p(t)) \in \mathrm{SE}(3)$ denote the trajectory and $g_d(t) = (R_d(t), p_d(t)) \in \mathrm{SE}(3)$ be desired trajectory to be tracked on SE(3). Define the natural error [49] as

$$e = g_d^{-1} g = \begin{bmatrix} R_d^T R & R_d^T (p - p_d) \\ 0 & 1 \end{bmatrix} \in \mathrm{SE}(3).$$

Then the error $e = \mathrm{Id}$ whenever $g(t) = g_d(t)$, where Id is the identity element on SE(3).

While $\dot{g} = g\mathbf{V}$ satisfies a left control system differential equation, we will let the desired trajectory satisfy a right control system differential equation: $\dot{g}_d = \bar{\mathbf{V}}_d g_d$. The reason we do this is that the inverse of g_d appears in our definition for the error function. To make the error differential equation be a left control system, it is then essential, as will become more obvious below, to have $\dot{g}_d^{-1}$ be a left invariant vector field. This is done by having g_d satisfy a right control system equation. Note that if $\dot{g}_d = \bar{\mathbf{V}}_d g_d$ and since $g_d g_d^{-1} = \mathrm{Id}$, then $\dot{g}_d g_d^{-1} + g_d \dot{g}_d^{-1} = 0$ implies that $\dot{g}_d^{-1} = -g_d^{-1} \bar{\mathbf{V}}_d$. Hence, $\dot{g}_d^{-1}$ is a left-invariant vector field.

A simple calculation gives:

$$\begin{aligned} \dot{e} &= \dot{g}_d^{-1} g + g_d^{-1} \dot{g} = -g_d^{-1} \bar{\mathbf{V}}_d g + g_d^{-1} g \mathbf{V} \\ &= g_d^{-1} g \left(\mathbf{V} - g^{-1} \bar{\mathbf{V}}_d g \right) = e \left(\mathbf{V} - \mathrm{Ad}_{g^{-1}} \bar{\mathbf{V}}_d \right). \end{aligned}$$

The authors in [49] use $\mathbf{V} - \mathrm{Ad}_{g^{-1}} \bar{\mathbf{V}}_d$ to define the velocity error. In their work, it is

crucial to use this definition for velocity error in proving stability of their proposed PD control laws for stabilization and trajectory tracking. This, however, is not necessary here. As in linear feedback control, we set up our optimal control cost functional to minimize the deviation of the actual velocity from a nominal desired value. If only part of the velocity vector field is required to track a given value while others are not, then we can make use of weighting matrices to penalize some components of the velocity. These choices, as in linear feedback control theory, are independent of the error dynamics. That is to say, if we set $\mathbf{V}^e = \mathbf{V}_d - \mathbf{V} \in \mathfrak{se}(3)$, where $\mathbf{V}_d$ is the desired velocity vector field, then $\mathbf{V}^e$ does not have to satisfy $\dot{e} = e\mathbf{V}^e$; We are simply optimizing over tracking in phase space TSE(3). Hence we define the velocity error as $\mathbf{V}^e = \mathbf{V}_d - \mathbf{V}$.

Finally, note that

$$\left.\frac{\partial e_\epsilon}{\partial \epsilon}\right|_{\epsilon=0} = \left.\frac{\partial}{\partial \epsilon} g_d^{-1} g_\epsilon\right|_{\epsilon=0} = g_d^{-1} g \mathbf{W} = e\mathbf{W}. \tag{4-2.1}$$

In this section we will use weighting matrices, as opposed to weighting scalars, to penalize deviations of both position and velocity from some desired values. The use of weighting matrices as opposed to scalars allows us penalize certain components of position and velocity errors as opposed to the total position error or velocity error. We do this as follows.

Let the measure of velocity error be given by $\left\langle \mathbf{V}^e, \tilde{\mathbf{K}}_{\mathbf{v}}(\mathbf{V}^e) \right\rangle$, where $\tilde{\mathbf{K}}_{\mathbf{v}} : \mathfrak{se}(3) \to \mathfrak{se}(3)$ be a symmetric, positive semi-definite operator defined by

$$\tilde{\mathbf{K}}_{\mathbf{v}}(\mathbf{V}) = \begin{bmatrix} \mathbf{K}^r_{\mathbf{v}}(\boldsymbol{\Omega}) & \mathbf{K}^t_{\mathbf{v}}(\mathbf{v}) \\ 0 & 0 \end{bmatrix}$$

for an arbitrary $\mathbf{V} = (\boldsymbol{\Omega}, \mathbf{v}) \in \mathfrak{se}(3)$, where

$$\mathbf{K}^r_{\mathbf{v}}(\boldsymbol{\Omega}) = K^r_{\mathbf{v}}\boldsymbol{\Omega} + \boldsymbol{\Omega} K^r_{\mathbf{v}},$$

is the rotational gain operator for the error in angular velocity, $K^r_{\mathbf{v}}$ is a diagonal 3×3 positive semi-definite matrix,

$$\mathbf{K}^t_{\mathbf{v}}(\mathbf{v}) = K^t_{\mathbf{v}}\mathbf{v},$$

is the translational gain operator for the error in translational velocity, and $K^t_{\mathbf{v}}$ is a diagonal 3×3 positive definite matrix. Similar definitions apply to the control cost: $\left\langle \mathbf{U}, \tilde{\mathbf{K}}_{\mathbf{u}}(\mathbf{U}) \right\rangle$, where $\tilde{\mathbf{K}}_{\mathbf{u}} : \mathfrak{se}(3) \to \mathfrak{se}(3)$ is a symmetric, positive definite operator (positive definiteness is required for the control weighting operator).

For position error we use the logarithmic map to define the error

$$\left\langle \log(e), \tilde{\mathbf{K}}_p(\log(e)) \right\rangle,$$

where $\tilde{\mathbf{K}}_p : \mathfrak{se}(3) \to \mathfrak{se}(3)$ is a symmetric, positive semi-definite operator defined by

$$\tilde{\mathbf{K}}_p(\boldsymbol{\chi}) = \begin{bmatrix} \mathbf{K}^r_p(\boldsymbol{\psi}) & \mathbf{K}^t_p(\xi) \\ 0 & 0 \end{bmatrix}$$

for an arbitrary $\boldsymbol{\chi} = (\boldsymbol{\psi}, \xi) \in \mathfrak{se}(3)$, where

$$\mathbf{K}^r_p(\boldsymbol{\psi}) = K^r_p\boldsymbol{\psi} + \boldsymbol{\psi}K^r_p,$$

is the rotational gain operator for the error in attitude, K^r_p is a diagonal 3×3 positive semi-definite matrix,

$$\mathbf{K}^t_p(\xi) = K^t_p\xi,$$

is the translational gain operator for the error in translational position, and K^t_p is a diagonal 3×3 positive semi-definite matrix. In this case, $\boldsymbol{\chi} \in \mathfrak{se}(3)$ is viewed as the exponential coordinates of an element of the Lie group SE(3) (in fact, $\boldsymbol{\chi} = \log\left(g_d^{-1}g\right)$).

The above definitions allow us to penalize components of translational position, attitude, translational velocity and angular velocity errors independently. For example, in an imaging scenario, we may wish to minimize the magnitude of the relative

velocity in the observation plane (x-y plane) without minimizing the out of plane (z-axis) component. In this case, $K^t_{\mathbf{v}} = \mathrm{diag}(a, b, 0)$ for some $a, b > 0$. In a spin rate optimal tracking, we may desire to set $K^t_{\mathbf{v}} = 0$ and not penalize translational velocity error. If we are to minimize "jitter" as well, then both $K^r_{\mathbf{v}}$ and $K^t_{\mathbf{v}}$ will both assume nonzero values. Hence, the above formulation and the following problem statement is general enough to address many problems in spacecraft and rigid body control. Here is the problem statement.

Problem 4.2.1. *Minimize*

$$\mathcal{J} = \frac{1}{2}\int_0^T \left\langle \mathbf{U}, \tilde{\mathbf{K}}_{\mathbf{u}}(\mathbf{U}) \right\rangle + \left\langle \mathbf{V}^e, \tilde{\mathbf{K}}_{\mathbf{v}}\left(\mathbf{V}^e\right) \right\rangle + \left\langle \log\left(e\right), \tilde{\mathbf{K}}_p\left(\log\left(e\right)\right) \right\rangle \mathrm{d}t \tag{4-2.2}$$

subject to

Dynamics

$$\begin{aligned} \dot{g} &= g\mathbf{V} \\ \frac{\mathrm{D}\tilde{\mathbf{J}}\left(\mathbf{V}\right)}{\mathrm{d}t} &= \left[\tilde{\mathbf{J}}\left(\mathbf{V}\right), \mathbf{V}\right] - \left[\left[\mathbf{V}, \tilde{\mathbf{J}}\left(\mathbf{V}\right)\right]\right] + \mathbf{U} \end{aligned} \tag{4-2.3}$$

Holonomic Constraints

$$\langle \mathbf{V}, \mathbf{X}_i \rangle = 0,\ i = 1, \ldots, n,\ n < 6, \tag{4-2.4}$$

Boundary Conditions

$$g(0) = g_0,\ \mathbf{V}(0) = \mathbf{V}_0,\ g(T) = g_T,\ \mathbf{V}(T) = \mathbf{V}_T, \tag{4-2.5}$$

where $\mathbf{X}_i \in \mathfrak{se}(3)$, $i = 1, \ldots, n$, *are vector fields associated with the imposed constraints.*

Note that the constraints (4-2.6) can only be as many as five constraints on SE(3). Since SE(3) is a six dimensional manifold, having 6 constraints ($n = 6$) completely specifies the motion. Let us show how the constraint vector fields $\mathbf{X}_i$ are derived. Holonomic constraints are expressed by functions $f_i : \mathrm{SE}(3) \to \mathbb{R}^3$ as

$$f_i(g) = 0,\ i = 1, \ldots, n.$$

We derive each $\mathbf{X}_i$ as follows. Differentiate each f_i to get $\frac{\mathrm{d}f_i}{\mathrm{d}t} = 0$. Let $\mathbf{X}_i = (\mathrm{d}f_i)^\sharp \in \mathfrak{se}(3)$, where d is the exterior derivative and $\cdot^\sharp$ is the sharp operator [42]. It is easy to check that $\frac{\mathrm{d}f_i}{\mathrm{d}t} = \langle \mathbf{V}, \mathbf{X}_i \rangle = 0$.

By the independence of the vector fields $\mathbf{X}_i$ (assuming the constraints $f_i = 0$ are independent) we can combine the n constraints by introducing the lagrange multipliers ζ_i and the vector field (expressed as an element in the Lie algebra, as opposed to elements in its dual space $\mathfrak{se}^*(3)$)

$$\mathbf{Z} = \sum_{i=1}^{n} \zeta_i \mathbf{X}_i.$$

Hence, the set of n conditions (4-2.6) can alternatively be expressed as

$$\langle \mathbf{V}, \mathbf{Z} \rangle = 0. \tag{4-2.6}$$

We begin by formulating the appended (and perturbed) cost functional

$$\begin{aligned} \mathcal{J}_\epsilon \ = \ & \frac{1}{2} \int_0^T \langle \mathbf{U}_\epsilon, \mathbf{U}_\epsilon \rangle + \left\langle \mathbf{V}_\epsilon^e, \tilde{\mathbf{K}}_{\mathbf{v}} \left(\mathbf{V}_\epsilon^e \right) \right\rangle + \left\langle \log\left(e_\epsilon\right), \tilde{\mathbf{K}}_p \left(\log\left(e_\epsilon\right) \right) \right\rangle \\ & + \left\langle \mathbf{\Lambda}_1, g_\epsilon^{-1} \dot{g}_\epsilon - \mathbf{V}_\epsilon \right\rangle + \left\langle \mathbf{\Lambda}_2, \frac{\mathrm{D}\tilde{\mathbf{J}}\left(\mathbf{V}_\epsilon\right)}{\mathrm{d}t} - \left[\tilde{\mathbf{J}}\left(\mathbf{V}_\epsilon\right), \mathbf{V}_\epsilon \right] + \left[\left[\mathbf{V}_\epsilon, \tilde{\mathbf{J}}\left(\mathbf{V}_\epsilon\right) \right] \right] - \mathbf{U}_\epsilon \right\rangle \\ & + \langle \mathbf{V}_\epsilon, \mathbf{Z}_\epsilon \rangle \, \mathrm{d}t \end{aligned} \tag{4-2.7}$$

and compute $\partial \mathcal{J}_\epsilon / \partial \epsilon \big|_{\epsilon=0}$ on a term by term basis. For the first term we have

$$\frac{\partial}{\partial \epsilon} \frac{1}{2} \langle \mathbf{U}_\epsilon, \mathbf{U}_\epsilon \rangle = \left\langle \frac{\mathrm{D}\mathbf{U}_\epsilon}{\partial \epsilon} \bigg|_{\epsilon=0}, \tilde{\mathbf{K}}_{\mathbf{u}}(\mathbf{U}) \right\rangle, \tag{4-2.8}$$

where the property

$$\left\langle \mathbf{V}_1, \tilde{\mathbf{N}}\left(\mathbf{V}_2\right)\right\rangle = \left\langle \tilde{\mathbf{N}}\left(\mathbf{V}_1\right), \mathbf{V}_2\right\rangle \tag{4-2.9}$$

holds true for all symmetric, positive definite or semi-definite operators $\tilde{\mathbf{N}} : \mathfrak{se}(3) \rightarrow \mathfrak{se}(3)$ such as $\tilde{\mathbf{J}}$, $\tilde{\mathbf{K}}_p$ or $\tilde{\mathbf{K}}_p$. For the second (velocity error) term we have

$$\begin{aligned} \frac{\partial}{\partial\epsilon}\frac{1}{2}\left\langle \mathbf{V}_\epsilon^e, \tilde{\mathbf{K}}_{\mathbf{v}}\left(\mathbf{V}_\epsilon^e\right)\right\rangle &= \left\langle \left.\frac{\mathrm{D}\mathbf{V}_\epsilon^e}{\partial\epsilon}\right|_{\epsilon=0}, \tilde{\mathbf{K}}_{\mathbf{v}}\left(\mathbf{V}^e\right)\right\rangle \\ &= -\left\langle \left.\frac{\mathrm{D}\mathbf{V}_\epsilon}{\partial\epsilon}\right|_{\epsilon=0}, \tilde{\mathbf{K}}_{\mathbf{v}}\left(\mathbf{V}^e\right)\right\rangle \end{aligned} \tag{4-2.10}$$

since $\mathbf{V}_\epsilon^e = \mathbf{V}^d - \mathbf{V}_\epsilon$. For the third (configuration error) term, the computation is more involved. After a lengthy computation, which we omit here, we get

$$\begin{aligned} &\frac{\partial}{\partial\epsilon}\frac{1}{2}\left\langle \log\left(e_\epsilon\right), \tilde{\mathbf{K}}_p\left(\log\left(e_\epsilon\right)\right)\right\rangle \\ &= \left\langle \mathbf{W}_1, \mathbf{K}_p^r\left(\log\left(R_e\right)\right) + \left(p_e \times \left(R_e^T D^T(e)\mathbf{K}_p^t\left(A^{-1}\left(\boldsymbol{\psi}_e\right)p_e\right)\right)\right)^\wedge\right\rangle_{\mathrm{SO}(3)} \\ &+ \left\langle \mathbf{w}_2, A^{-T}\left(\boldsymbol{\psi}_e\right)\mathbf{K}_p^t\left(A^{-1}\left(\boldsymbol{\psi}_e\right)p_e\right)\right\rangle_{\mathbb{R}^3} =: \left\langle \mathbf{W}, B(e)\right\rangle \end{aligned} \tag{4-2.11}$$

where $(x)^\wedge = \hat{x}$, $e = (R_e, p_e)$, the function A, its inverse and its properties are given by equations (B-3.1), (B-3.2) and (B-3.3), respectively, the matrix D is given by

$$\begin{aligned} D(e) &= \frac{\mathrm{d}A^{-1}}{\mathrm{d}\boldsymbol{\psi}}\left(\boldsymbol{\psi}_e\right)\frac{\mathrm{d}}{\mathrm{d}R}\log_{\mathrm{SO}(3)} R\Big|_{R=R_e} \\ B(e) &= \begin{bmatrix} B_{11}(e) & b_{12}(e) \\ 0 & 0 \end{bmatrix} \in \mathfrak{se}(3) \\ B_{11}(e) &= \mathbf{K}_p^r\left(\log\left(R_e\right)\right) + \left(p_e \times \left(R_e^T D^T \mathbf{K}_p^t\left(A^{-1}\left(\boldsymbol{\psi}^e\right)p_e\right)\right)\right)^\wedge \in \mathfrak{so}(3) \\ b_{12}(e) &= A^{-T}\left(\boldsymbol{\psi}_e\right)\mathbf{K}_p^t\left(A^{-1}\left(\boldsymbol{\psi}_e\right)p_e\right) \in \mathbb{R}^3 \end{aligned}$$

and where $\boldsymbol{\psi}_e = \log_{\mathrm{SO}(3)} R_e \in \mathfrak{so}(3)$. Equation (4-2.11) is obtained as follows. Since

$$\log g = \begin{bmatrix} \boldsymbol{\psi} & A^{-1}(\boldsymbol{\psi})p \\ 0 & 0 \end{bmatrix}$$

then we have

$$\begin{aligned}
\frac{\partial}{\partial\epsilon}\frac{1}{2}\left\langle \log(e_\epsilon), \tilde{\mathbf{K}}_p\left(\log(e_\epsilon)\right)\right\rangle &= \frac{\partial}{\partial\epsilon}\frac{1}{2}\Big[\left\langle \log_{\mathrm{SO}(3)}\left(R_\epsilon\right), \mathbf{K}_p^r\left(\log_{\mathrm{SO}(3)}\left(R_\epsilon\right)\right)\right\rangle_{\mathrm{SO}(3)} \\
&\quad + \left\langle A^{-1}\left(\boldsymbol{\psi}_\epsilon\right)p_\epsilon, \mathbf{K}_p^t\left(A^{-1}\left(\boldsymbol{\psi}_\epsilon\right)p_\epsilon\right)\right\rangle_{\mathbf{R}^3}\Big] \\
&= \left\langle \mathbf{K}_p^r\left(\log_{\mathrm{SO}(3)} R\right), W_1\right\rangle_{\mathrm{SO}(3)} \\
&\quad + \left\langle \mathbf{K}_p^t\left(A^{-1}\left(\boldsymbol{\psi}p\right)\right), A^{-1}\left(\boldsymbol{\psi}\right)w_2\right\rangle_{\mathbb{R}^3} \\
&\quad + \left\langle \frac{\partial A^{-1}}{\partial\boldsymbol{\psi}}(\boldsymbol{\psi})\frac{\partial\boldsymbol{\psi}_\epsilon}{\partial\epsilon}\bigg|_{\epsilon=0} p, \mathbf{K}_p^t\left(A^{-1}\left(\boldsymbol{\psi}\right)p\right)\right\rangle_{\mathbb{R}^3} \\
&= \left\langle \mathbf{K}_p^r\left(\log_{\mathrm{SO}(3)} R\right), W_1\right\rangle_{\mathrm{SO}(3)} \\
&\quad + \left\langle \mathbf{K}_p^t\left(A^{-1}\left(\boldsymbol{\psi}p\right)\right), A^{-1}\left(\boldsymbol{\psi}\right)w_2\right\rangle_{\mathbb{R}^3} \\
&\quad + \left\langle \frac{\partial A^{-1}}{\partial\boldsymbol{\psi}}(\boldsymbol{\psi})\frac{\partial}{\partial R}\left(\log R\right)RW_1p, \mathbf{K}_p^t\left(A^{-1}\left(\boldsymbol{\psi}\right)p\right)\right\rangle_{\mathbb{R}^3},
\end{aligned}$$

where we used

$$\begin{aligned}
\frac{\partial\boldsymbol{\psi}_\epsilon}{\partial\epsilon}\bigg|_{\epsilon=0} = \frac{\partial}{\partial\epsilon}\log_{\mathrm{SO}(3)} R_\epsilon\bigg|_{\epsilon=0} &= \frac{\partial}{\partial R}\left(\log_{\mathrm{SO}(3)} R\right)\frac{\partial R_\epsilon}{\partial\epsilon}\bigg|_{\epsilon=0} \\
&= \frac{\partial}{\partial R}\left(\log_{\mathrm{SO}(3)} R\right)RW_1.
\end{aligned}$$

With $D(e)$ defined as above, then

$$\begin{aligned}
\left\langle \mathbf{K}_p^t\left(A^{-1}\left(\boldsymbol{\psi}\right)p\right), DRW_1p\right\rangle &= \left(DRW_1p\right)^T\mathbf{K}_p^t\left(A^{-1}\left(\boldsymbol{\psi}p\right)\right) \\
&= p^TW_1^TR^TD^T\mathbf{K}_p^t\left(A^{-1}\left(\boldsymbol{\psi}\right)p\right) \\
&= \left(W_1p\right)^T\left(R^TD^T\mathbf{K}_p^t\left(A^{-1}\left(\boldsymbol{\psi}\right)p\right)\right) \\
&= R^TD^T\mathbf{K}_p^t\left(A^{-1}\left(\boldsymbol{\psi}\right)p\right)\cdot\left(W_1p\right) \\
&= w_1\cdot\left(p\times R^TD^T\mathbf{K}_p^t\left(A^{-1}\left(\boldsymbol{\psi}\right)p\right)\right) \\
&= \left\langle W_1, \left(p\times R^TD^T\mathbf{K}_p^t\left(A^{-1}\left(\boldsymbol{\psi}\right)p\right)\right)^\wedge\right\rangle_{\mathrm{SO}(3)}
\end{aligned}$$

gives us the desired result in Equation (4-2.11). In the last equation, we used the fact that $W_1p = w_1\times p$.

For the fourth (kinematic constraint) term we have

$$\begin{aligned}\frac{\partial}{\partial\epsilon}\int_0^T \left\langle \mathbf{\Lambda}_1, g_\epsilon^{-1}\dot{g}_\epsilon - \mathbf{V}_\epsilon \right\rangle \mathrm{d}t\Big|_{\epsilon=0} &= \int_0^T \left\langle \mathbf{\Lambda}_1, [\mathbf{V},\mathbf{W}] + \frac{\mathrm{D}\mathbf{W}}{\mathrm{d}t} - \frac{\partial \mathbf{V}_\epsilon}{\partial\epsilon}\Big|_{\epsilon=0} \right\rangle \mathrm{d}t \\ &= \int_0^T -\left\langle \mathbf{W}, [\mathbf{V},\mathbf{\Lambda}_1] + [[\mathbf{V},\mathbf{\Lambda}_1]] + \frac{\mathrm{D}\mathbf{\Lambda}_1}{\mathrm{d}t} \right\rangle \\ &\quad - \left\langle \frac{\partial \mathbf{V}_\epsilon}{\partial\epsilon}\Big|_{\epsilon=0}, \mathbf{\Lambda}_1 \right\rangle \mathrm{d}t, \end{aligned} \tag{4-2.12}$$

where integration by parts has been employed. For the fifth (dynamic constraint) term, we get

$$\begin{aligned}&\frac{\partial}{\partial\epsilon}\int_0^T \left\langle \mathbf{\Lambda}_2, \frac{\mathrm{D}\tilde{\mathbf{J}}\left(\mathbf{V}_\epsilon\right)}{\mathrm{d}t} - \left[\tilde{\mathbf{J}}\left(\mathbf{V}_\epsilon\right), \mathbf{V}_\epsilon\right] + \left[[\mathbf{V}_\epsilon, \tilde{\mathbf{J}}\left(\mathbf{V}_\epsilon\right)]\right] - \mathbf{U}_\epsilon \right\rangle \mathrm{d}t\Big|_{\epsilon=0} \\ &= \int_0^T \left\langle \frac{\partial \mathbf{U}_\epsilon}{\partial\epsilon}\Big|_{\epsilon=0}, -\mathbf{\Lambda}_2 \right\rangle + \left\langle \mathbf{W}, \tilde{\mathbf{R}}\left(\tilde{\mathbf{J}}\left(\mathbf{\Lambda}_2\right), \mathbf{V}\right)\mathbf{V} \right\rangle \\ &+ \left\langle \frac{\partial \mathbf{V}_\epsilon}{\partial\epsilon}\Big|_{\epsilon=0}, -\frac{\mathrm{D}\tilde{\mathbf{J}}\left(\mathbf{\Lambda}_2\right)}{\mathrm{d}t} + \tilde{\mathbf{J}}\left([\mathbf{\Lambda}_2, \mathbf{V}]\right) - \left[\mathbf{\Lambda}_2, \tilde{\mathbf{J}}\left(\mathbf{V}\right)\right] - \left[[\mathbf{\Lambda}_2, \tilde{\mathbf{J}}\left(\mathbf{V}\right)]\right] \right\rangle \mathrm{d}t. \end{aligned} \tag{4-2.13}$$

Finally, for the sixth (and last, motion constraint) term we have

$$\begin{aligned}\frac{\partial}{\partial\epsilon}\left\langle \mathbf{V}_\epsilon, \mathbf{Z}_\epsilon \right\rangle &= \left\langle \frac{\partial \mathbf{V}_\epsilon}{\partial\epsilon}\Big|_{\epsilon=0}, \mathbf{Z} \right\rangle + \left\langle \mathbf{V}, \nabla_{\mathbf{W}}\mathbf{Z} \right\rangle \\ &= \left\langle \frac{\partial \mathbf{V}_\epsilon}{\partial\epsilon}\Big|_{\epsilon=0}, \mathbf{Z} \right\rangle - \left\langle \mathbf{W}, \nabla_{\mathbf{Z}}\mathbf{V} + [\mathbf{Z},\mathbf{V}] + [[\mathbf{Z},\mathbf{V}]] \right\rangle \end{aligned} \tag{4-2.14}$$

where we adopt the standard (geometric) notation $\nabla_{\mathbf{W}}\mathbf{Z} = \frac{\partial \mathbf{Z}_\epsilon}{\partial\epsilon}\Big|_{\epsilon=0}$ and the standard identities (which are true for any, compact or non-compact, Lie group as long as the connection is metric, affine and Levi-Civita, which, in turn, is true for the present case) $\nabla_{\mathbf{W}}\mathbf{Z} = \nabla_{\mathbf{Z}}\mathbf{W} + [\mathbf{W},\mathbf{Z}]$ and $\langle \mathbf{V}, \nabla_{\mathbf{Z}}\mathbf{W}\rangle = \mathbf{Z}\left(\langle \mathbf{V},\mathbf{W}\rangle\right) - \langle \nabla_{\mathbf{Z}}\mathbf{V}, \mathbf{W}\rangle$, and the fact that $\mathbf{Z}\left(\langle \mathbf{V},\mathbf{W}\rangle\right) = 0$ (see Lemma 3.1 in [53].)

The necessary optimality condition is determined by setting $\partial\mathcal{J}_\epsilon/\partial\epsilon\big|_{\epsilon=0} = 0$ and separating terms involving the independent vector fields $\mathbf{W}$, $\partial\mathbf{U}_\epsilon/\partial\epsilon\big|_{\epsilon=0}$ and $\partial\mathbf{V}_\epsilon/\partial\epsilon\big|_{\epsilon=0}$. Doing this we get the following theorem.

Theorem 4.2.1 (Necessary Conditions for Constrained Optimal Trajectory Tracking on SE(3)). *The necessary conditions satisfied by an optimal trajectory* $(g(t), \mathbf{V}(t), \mathbf{U}(t))$ *are given by*

$$\begin{aligned}
\dot{g} &= g\mathbf{V} \\
\frac{\mathrm{D}\tilde{\mathbf{J}}(\mathbf{V})}{\mathrm{d}t} &= -\left[\mathbf{V}, \tilde{\mathbf{J}}(\mathbf{V})\right] - \left[[\mathbf{V}, \tilde{\mathbf{J}}(\mathbf{V})]\right] + \mathbf{\Lambda}_2 \\
\mathbf{U} &= \tilde{\mathbf{K}}_{\mathbf{u}}^{-1}(\mathbf{\Lambda}_2) \\
\frac{\mathrm{D}\mathbf{\Lambda}_1}{\mathrm{d}t} &= \tilde{\mathbf{R}}\left(\tilde{\mathbf{J}}(\mathbf{\Lambda}_2), \mathbf{V}\right)\mathbf{V} - [\mathbf{V}, \mathbf{\Lambda}_1] - [[\mathbf{V}, \mathbf{\Lambda}_1]] - \nabla_{\mathbf{Z}}\mathbf{V} \\
&\quad - [\mathbf{Z}, \mathbf{V}] - [[\mathbf{Z}, \mathbf{V}]] + B(e) \\
\frac{\mathrm{D}\tilde{\mathbf{J}}(\mathbf{\Lambda}_2)}{\mathrm{d}t} &= \tilde{\mathbf{J}}([\mathbf{\Lambda}_2, \mathbf{V}]) - \left[\mathbf{\Lambda}_2, \tilde{\mathbf{J}}(\mathbf{V})\right] - \left[[\mathbf{\Lambda}_2, \tilde{\mathbf{J}}(\mathbf{V})]\right] - \mathbf{\Lambda}_1 + \mathbf{Z} - \tilde{\mathbf{K}}_{\mathbf{v}}(\mathbf{V}^e) \\
\langle \mathbf{V}, \mathbf{Z} \rangle &= 0.
\end{aligned}$$

It becomes obvious from the third equation in Theorem (4.2.1) why we require $\tilde{\mathbf{K}}_{\mathbf{u}}$ be positive definite. Also note that if we set $\tilde{\mathbf{K}}_{\mathbf{u}}$ to be the identity operator, set $\tilde{\mathbf{K}}_p$ and $\tilde{\mathbf{K}}_{\mathbf{v}}$ to be zero and $\mathbf{Z} = 0$ (i.e., no constraints), then we get back Theorem (4.1.1).

4.2.1 Example: Dual Spacecraft Interferometry on SE(2)

In this section we consider a simple example on SE(2). Let us consider the dual spacecraft interferometer studied later in Chapter 6 and the papers [36, 54, 45, 40, 38, 44, 39], but now including rigid body dynamics to the planar (two-dimensional) spacecraft model. The state $g = \in \mathrm{SE}(2)$ is the configuration of the controlled follower spacecraft, while the parent spacecraft is assumed to be fixed at the origin with $g_p(t) = (I_{2\times 2}, 0_{2\times 1})$ for all $t \in [0, T]$. Hence, g represents the relative state between

the follower and parent spacecraft. See figure (4.1). The configuration g is given by

$$g(\theta, x, y) = \begin{bmatrix} \cos\theta & -\sin\theta & x \\ \sin\theta & \cos\theta & y \\ 0 & 0 & 0 \end{bmatrix}.$$

The velocity $\mathbf{V}$ and control U are given by

$$\mathbf{V} = \begin{bmatrix} 0 & -\omega & v_x \\ \omega & 0 & v_y \\ 0 & 0 & 0 \end{bmatrix}, \; U = \begin{bmatrix} 0 & -\tau & u_x \\ \tau & 0 & u_y \\ 0 & 0 & 0 \end{bmatrix}.$$

we will evenly weigh the penalty on applying the forces u_x and u_y and torque τ with the same weight $\mathbb{R} \ni k_u > 0$. The desired trajectory is given by $g_d = (\theta_d, x_d, y_d)$, where $\theta_d = 0$ is the desired "look" angle (i.e., the desired line of sight.) It is desired to follow $\theta_d = 0$ as closely as possible. Hence, the error in angular position is $\theta_e = \theta_d - \theta = -\theta$. With $K_p^r = \begin{bmatrix} K_{p1}^r & 0 \\ 0 & K_{p2}^r \end{bmatrix}$, let $K_{p1}^r + K_{p2}^r = k_p^r$, then $\mathbf{K}_p^r(\log(R_e)) = \begin{bmatrix} 0 & -k_p^r\theta_e \\ k_p^r\theta_e & 0 \end{bmatrix} = \begin{bmatrix} 0 & k_p^r\theta \\ -k_p^r\theta & 0 \end{bmatrix}$. Instead of minimizing the deviation of the motion of the center of mass from a given desired value, we constrain the center of mass motion of the controlled spacecraft to follow a paraboloid $y_d = ax_d^2$, where $\mathbb{R} \ni a > 0$. For a motivation for the paraboloidal constraint, see [44]. Hence, we have $f(\theta, x, y) = y - ax^2$ and

$$\mathbf{X}^s = -2ax\partial_x + \partial_y = \begin{bmatrix} 0 & 0 & -2ax \\ 0 & 0 & 1 \\ 0 & 0 & 0 \end{bmatrix},$$

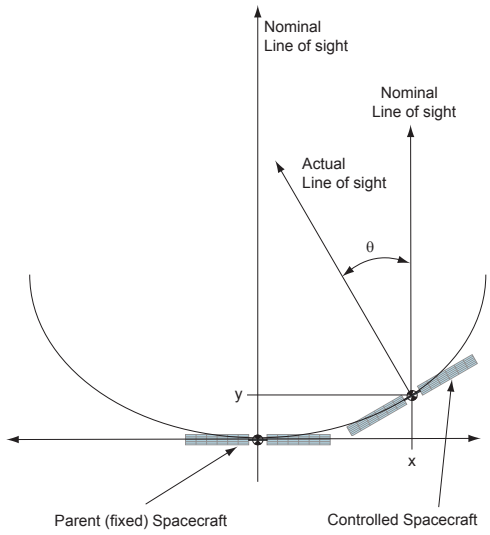

Figure 4.1: Dual spacecraft interferometry on SE(2).

which is expressed in the space fixed frame. In the body fixed frame, the corresponding constraint vector field is given by

$$\begin{aligned} Z = \zeta \mathbf{X} = \zeta \mathrm{Ad}_{g^{-1}} \mathbf{X}^s &= \zeta \left[x(-2ax\cos\theta + \sin\theta)\partial_x + y(2ax\sin\theta + \cos\theta)\partial_y \right] \\ &= \zeta \begin{bmatrix} 0 & 0 & x(-2ax\cos\theta + \sin\theta) \\ 0 & 0 & y(2ax\sin\theta + \cos\theta) \\ 0 & 0 & 0 \end{bmatrix}, \end{aligned}$$

Since we are constraining the motion of the center of mass, we may set $\mathbf{K}_p^t = 0_{2\times 2}$. Hence, we find that $B(e) = \begin{bmatrix} B_{11}(e) & b_{12}(e) \\ 0 & 0 \end{bmatrix}$ is such that $B_{11}(e) = \mathbf{K}_p^r(\log(R_e)) = \begin{bmatrix} 0 & k_p^r\theta \\ -k_p^r\theta & 0 \end{bmatrix}$ and $b_{12}(e) = 0_{2\times 1}$.

In the space-fixed frame the desired velocity is given (in space-fixed frame) by

$$\mathbf{V}_d^s = \begin{bmatrix} 0 & 0 & v_d^x \\ 0 & 0 & 0 \\ 0 & 0 & 0 \end{bmatrix}.$$

In the body-fixed frame we get:

$$\mathbf{V}_d = \mathrm{Ad}_{g^{-1}}\mathbf{V}_d^s \;=\; \begin{bmatrix} 0 & 0 & v_d^x\cos\theta \\ 0 & 0 & -v_d^x\sin\theta \\ 0 & 0 & 0 \end{bmatrix},$$

We will not penalize deviations in angular velocity from a nominal value by setting the corresponding matrix to $\mathbf{K}_v^r = 0_{2\times 2}$. We wish, however, to minimize the deviation of the space-fixed translational velocity x-component from a value of v_x while motion along the y-axis in the space-fixed frame is irrelevant. Hence, we set $\mathbf{K}_v^t = \mathrm{diag}(k_v^t, k_v^t)$, where $\mathbb{R} \ni k_v^t > 0$. Hence, with our choice of weighting velocity operator $\tilde{\mathbf{K}}_v$ we get

$$\tilde{\mathbf{K}}_v(\mathbf{V}^e) = \tilde{\mathbf{K}}_v\left(\mathbf{V} - \mathbf{V}_d\right) \;=\; \begin{bmatrix} 0 & 0 & k_v^t\left(v_d^x\cos\theta - \dot{x}\right) \\ 0 & 0 & k_v^t\left(-v_d^x\cos\theta - \dot{y}\right) \\ 0 & 0 & 0 \end{bmatrix}.$$

The Lagrange multipliers are given by

$$\mathbf{\Lambda}_i = \begin{bmatrix} 0 & -\lambda_{i1} & \lambda_{i2}^x \\ \lambda_{i1} & 0 & \lambda_{i2}^x \\ 0 & 0 & 0 \end{bmatrix},\ i = 1, 2.$$

Note that the bracket on SO(2) is identically zero: $[\cdot,\cdot]_{\mathrm{SO}(2)} = 0$. Hence, we have:

$$[\mathbf{A},\mathbf{B}] + [[\mathbf{A},\mathbf{B}]] = \begin{bmatrix} \widehat{\mathbf{v}_a \times \mathbf{v}_b} & \mathbf{\Omega}_a\mathbf{v}_b \\ 0 & 0 \end{bmatrix}$$

and $\tilde{\mathbf{R}}(\mathbf{A},\mathbf{B})\mathbf{C} \equiv 0$ for all $\mathbf{A},\mathbf{B},\mathbf{C} \in \mathfrak{se}(2)$. Moreover, since we are using the natural (flat) metric on $\mathbb{R}^3$ for $SE(2)$, then the connection $\nabla \equiv 0$. Hence, $\nabla_Z\mathbf{V} = 0$.

We can now write the necessary optimality conditions of Theorem (4.2.1) in

component form as follows:

$$
\begin{aligned}
\dot{\theta} &= \omega \\
\dot{x} &= v_x \cos\theta - v_y \sin\theta \\
\dot{y} &= v_x \sin\theta + v_y \cos\theta \\
I\dot{\omega} &= \lambda_{21} \\
m\dot{v}_x &= m\omega v_y + \lambda_{22}^x \\
m\dot{v}_y &= -m\omega v_x + \lambda_{22}^y \\
\tau &= \lambda_{21}/k_u \\
u_x &= \lambda_{22}^x/k_u \\
u_y &= \lambda_{22}^y/k_u \\
\dot{\lambda}_{11} &= (v_x\lambda_{12}^y - v_y\lambda_{12}^x) + (-2axv_y - v_x) + k_p^r\theta \\
\dot{\lambda}_{12}^x &= \omega\lambda_{12}^y \\
\dot{\lambda}_{12}^y &= -\omega\lambda_{12}^x \\
I\dot{\lambda}_{21} &= m(\lambda_{22}^x v_y - \lambda_{22}^y v_x) + \lambda_{11} \\
m\dot{\lambda}_{22}^x &= m(-\lambda_{21}v_y + \omega\lambda_{22}^y) + m\lambda_{21}v_y - \lambda_{12}^x - k_v^t(v_d^x\cos\theta - v_x) \\
m\dot{\lambda}_{22}^y &= m(-\lambda_{21}v_x - \omega\lambda_{22}^x) - m\lambda_{21}v_x - \lambda_{12}^y + k_v^t(v_d^x\sin\theta + v_y) \\
-2axv_x + v_y &= 0.
\end{aligned}
$$

where I is the moment of inertia about the out-of-plane axis and m is the mass of the spacecraft.

CHAPTER 5

Dynamic Interpolation on Riemannian Manifolds: An Application to Interferometric Imaging

In this chapter we derive necessary conditions for minimizing the cost function for a trajectory that evolves on a Riemannian manifold and satisfies a second order differential equation together with some interpolation, smoothness and motion constraints. The cost function we consider in this chapter is a weighted sum of the norm squared of the acceleration and the norm squared of the velocity and is motivated by space-based interferometric imaging applications. In this chapter, we define the dynamic interpolation problem, derive necessary conditions for an optimal solution and point out an interesting connection between the dynamic interpolation problem and imaging applications, which is the main contribution of this chapter.

5.1 Introduction

The "dynamic interpolation" problem for nonlinear control systems modeled by second-order differential equations whose configuration space is a Riemannian manifold M, was considered in the past [33, 55]. This problem is defined as follows: Given an ordered set of points in M and some smoothness constraints, generate a trajectory of the system through the application of suitable control functions such

that the resulting trajectory in configuration space (1) interpolates the given set of points, and, (2) minimizes a suitable cost function. In [33], the trajectory of interest was twice continuously differentiable and the Lagrangian in the optimization problem was given by the norm squared of the acceleration along the trajectory.

In this chapter, this still remains our interest. However, we are interested in a Lagrangian that is a weighted sum of the norm squared of the acceleration and the norm squared of the velocity. Again, not only are we interested in minimizing fuel expenditure (i.e. acceleration), but, also, in executing the maneuver with the smallest possible speed. While minimizing acceleration directly corresponds to minimal fuel expenditure, minimum speed trajectories are desired in interferometric imaging because the light collectors' speed and image quality (namely, achievable signal-to-noise ratio) are reciprocal; The larger the collectors' speeds are ("shorter exposure time"), the worse the image becomes, and vice versa [5, 6, 56, 57, 7, 45]. This is analogous to exposure time in conventional photography, where longer exposure times (without spoiling the photographic film) results in more photon arrivals and a better image.

The necessary conditions we obtain here correspond to a slight generalization of the problem as handled in [33] and is similar to that derived in [55]. The main contribution of this chapter is the interesting connection that we make between optimal path planning for imaging applications and the τ-elastic variational problem.

We note that the use of geometric control methods for spacecraft formation flying has received little attention, whereas extensive investigations have been conducted in the field of robotic path planning (see Section (IV) in [8].) This work is an attempt to use geometric optimal control theory for spacecraft formation motion planning.

We now define the dynamic interpolation τ-elastic variational problem.

The τ-Elastic Variational Problem P^τ: minimize

$$\mathcal{J}(\mathbf{q}) = \frac{1}{2}\int_{T_0}^{T_N} \left\langle \frac{\mathrm{D}^2\mathbf{q}}{\mathrm{d}t^2}, \frac{\mathrm{D}^2\mathbf{q}}{\mathrm{d}t^2} \right\rangle + \tau^2 \left\langle \frac{\mathrm{D}\mathbf{q}}{\mathrm{d}t}, \frac{\mathrm{D}\mathbf{q}}{\mathrm{d}t} \right\rangle \mathrm{d}t, \tag{5-1.1}$$

over the set Ω of $\mathcal{C}^1$-paths $\mathbf{q}$ on M, satisfying

1. the *dynamic constraint*

$$\frac{\mathrm{D}\mathbf{q}}{\mathrm{d}t}(t) = \mathbf{v}(t),\ \frac{\mathrm{D}\mathbf{v}}{\mathrm{d}t}(t) = \mathbf{u}(t), \tag{5-1.2}$$

   where $\mathbf{u}(t)$ is the control,

2. $\mathbf{q}\big|_{[T_{i-1},T_i]}$ is smooth,

3. the *interpolation constraints*

$$\mathbf{q}(T_i) = \mathbf{q}_i,\ 1 \le i \le N-1 \tag{5-1.3}$$

   for distinct set of points $\mathbf{q}_i \in M$ and fixed times T_i, where $0 = T_0 \le T_1 \le \cdots \le T_N = T$,

4. the *boundary conditions*

$$\begin{aligned} \mathbf{q}(T_0) &= \mathbf{q}_0,\ \mathbf{q}(T_N) = \mathbf{q}_N, \\ \frac{\mathrm{D}\mathbf{q}}{\mathrm{d}t}(T_0) &= \mathbf{v}_0,\ \frac{\mathrm{D}\mathbf{q}}{\mathrm{d}t}(T_N) = \mathbf{v}_N, \end{aligned} \tag{5-1.4}$$

5. and the *motion constraints*

$$\left\langle \frac{\mathrm{D}\mathbf{q}}{\mathrm{d}t}, X_i(\mathbf{q}) \right\rangle = k_i,\ i = 1, \ldots, l\ (l < n) \tag{5-1.5}$$

   for $X_i,\ i = 1, \ldots, n$, linearly independent vector fields and given constants $k_i,\ i = 1, \ldots, l$.

The chapter is organized as follows. In Section (5.2), we derive the necessary conditions an optimal solution of the τ-elastic variational problem must satisfy without the imposition of "motion" constraints. In Section (5.3), motion constraints are included in the analysis and the corresponding necessary conditions are derived. In Section (5.4), we give an idealized example motivated by interferometric imaging. Finally, in Section (5.5), we conclude with some final remarks and future work.

5.2 Dynamic Interpolation without Motion Constraints

In this section we consider the τ-elastic variational problem *without* the motion constraints (5-1.5). In [33], the authors derive necessary conditions for the dynamic interpolation, τ-elastic variational problem with $\tau = 0$. Here we slightly generalize their result to the $\tau \neq 0$ case. A similar result can be found in [55].

Theorem 5.2.1. *Let* $\mathbf{q} \in \Omega$. *If* $\boldsymbol{\alpha}$ *is an admissible variation of* $\mathbf{q}$ *with variational vector field* $\mathbf{W}_t \in \mathrm{T}_{\mathbf{q}}\Omega$, *then*

$$\begin{aligned}\frac{\mathrm{d}}{\mathrm{d}\epsilon}\mathcal{J}(\boldsymbol{\alpha}_\epsilon)\bigg|_{\epsilon=0} &= \int_{T_0}^{T_N}\left\langle \mathbf{W}_t, \frac{\mathrm{D}^4\mathbf{q}}{\mathrm{d}t^4} + R\left(\frac{\mathrm{D}^2\mathbf{q}}{\mathrm{d}t^2}, \frac{\mathrm{D}\mathbf{q}}{\mathrm{d}t}\right)\frac{\mathrm{D}\mathbf{q}}{\mathrm{d}t} - \tau^2\frac{\mathrm{D}^2\mathbf{q}}{\mathrm{d}t^2}\right\rangle \mathrm{d}t \\ &\quad + \sum_{i=1}^{N-1}\left\langle \frac{\mathrm{D}\mathbf{W}_t(T_i)}{\mathrm{d}t}, \frac{\mathrm{D}^2\mathbf{q}(T_i^-)}{\mathrm{d}t^2} - \frac{\mathrm{D}^2\mathbf{q}(T_i^+)}{\mathrm{d}t^2}\right\rangle. \end{aligned} \tag{5-2.1}$$

Proof Let $\boldsymbol{\alpha}$ be an admissible variation of $\mathbf{q} \in \Omega$. Then

$$\mathcal{J}(\boldsymbol{\alpha}_\epsilon) = \frac{1}{2}\int_{T_0}^{T_N}\left\langle \frac{\mathrm{D}^2\boldsymbol{\alpha}_\epsilon}{\partial t^2}, \frac{\mathrm{D}^2\boldsymbol{\alpha}_\epsilon}{\partial t^2}\right\rangle + \tau^2\left\langle \frac{\mathrm{D}\boldsymbol{\alpha}_\epsilon}{\partial t}, \frac{\mathrm{D}\boldsymbol{\alpha}_\epsilon}{\partial t}\right\rangle \mathrm{d}t.$$

Taking variations with respect to ϵ, one obtains

$$\frac{\mathrm{D}\mathcal{J}}{\mathrm{d}\epsilon} = \int_{T_0}^{T_N}\left\langle \frac{\mathrm{D}}{\partial\epsilon}\frac{\mathrm{D}^2\boldsymbol{\alpha}_\epsilon}{\partial t^2}, \frac{\mathrm{D}^2\boldsymbol{\alpha}_\epsilon}{\partial t^2}\right\rangle + \tau^2\left\langle \frac{\mathrm{D}^2\boldsymbol{\alpha}_\epsilon}{\partial\epsilon\partial t}, \frac{\mathrm{D}\boldsymbol{\alpha}_\epsilon}{\partial t}\right\rangle \mathrm{d}t.$$

From Facts (A.4.1) and (A.4.2), we have

$$\frac{\mathrm{D}}{\partial\epsilon}\frac{\mathrm{D}^2\boldsymbol{\alpha}}{\partial t^2} = \frac{\mathrm{D}^2}{\partial t^2}\frac{\mathrm{D}\boldsymbol{\alpha}}{\partial\epsilon} + R\left(\frac{\mathrm{D}\boldsymbol{\alpha}}{\partial\epsilon}, \frac{\mathrm{D}\boldsymbol{\alpha}}{\partial t}\right)\frac{\mathrm{D}\boldsymbol{\alpha}}{\partial t}.$$

Thus,

$$\begin{aligned}\frac{\mathrm{d}}{\mathrm{d}\epsilon}\mathcal{J}(\boldsymbol{\alpha}_\epsilon) &= \int_{T_0}^{T_N}\Bigg[\left\langle\frac{\mathrm{D}^2}{\partial t^2}\frac{\mathrm{D}\boldsymbol{\alpha}_\epsilon}{\partial\epsilon},\frac{\mathrm{D}^2\boldsymbol{\alpha}_\epsilon}{\partial t^2}\right\rangle \\ &\quad+\left\langle R\left(\frac{\mathrm{D}\boldsymbol{\alpha}}{\partial\epsilon},\frac{\mathrm{D}\boldsymbol{\alpha}}{\partial t}\right)\frac{\mathrm{D}\boldsymbol{\alpha}}{\partial t},\frac{\mathrm{D}^2\boldsymbol{\alpha}_\epsilon}{\partial t^2}\right\rangle+\tau^2\left\langle\frac{\mathrm{D}^2\boldsymbol{\alpha}_\epsilon}{\partial t\partial\epsilon},\frac{\mathrm{D}\boldsymbol{\alpha}_\epsilon}{\partial t}\right\rangle\Bigg]\mathrm{d}t.\end{aligned}$$

For the first term, integrate by parts twice to obtain

$$\begin{aligned}\int_{T_0}^{T_N}\left\langle\frac{\mathrm{D}^2}{\partial t^2}\frac{\mathrm{D}\boldsymbol{\alpha}}{\partial\epsilon},\frac{\mathrm{D}^2\boldsymbol{\alpha}}{\partial t^2}\right\rangle\mathrm{d}t &= \left[\left\langle\frac{\mathrm{D}}{\partial t}\frac{\mathrm{D}\boldsymbol{\alpha}}{\partial\epsilon},\frac{\mathrm{D}^2\boldsymbol{\alpha}}{\partial t^2}\right\rangle-\left\langle\frac{\mathrm{D}\boldsymbol{\alpha}}{\partial\epsilon},\frac{\mathrm{D}^3\boldsymbol{\alpha}}{\partial t^3}\right\rangle\right]_{T_0}^{T_N} \\ &\quad+\int_{T_0}^{T_N}\left\langle\frac{\mathrm{D}\boldsymbol{\alpha}}{\partial\epsilon},\frac{\mathrm{D}^4\boldsymbol{\alpha}}{\partial t^4}\right\rangle\mathrm{d}t.\end{aligned}$$

For the second term, apply Fact (A.2.3) to obtain

$$\int_{T_0}^{T_N}\left\langle R\left(\frac{\mathrm{D}\boldsymbol{\alpha}}{\partial\epsilon},\frac{\mathrm{D}\boldsymbol{\alpha}}{\partial t}\right)\frac{\mathrm{D}\boldsymbol{\alpha}}{\partial t},\frac{\mathrm{D}^2\boldsymbol{\alpha}}{\partial t^2}\right\rangle\mathrm{d}t=\int_{T_0}^{T_N}\left\langle R\left(\frac{\mathrm{D}^2\boldsymbol{\alpha}}{\partial t^2},\frac{\mathrm{D}\boldsymbol{\alpha}}{\partial t}\right)\frac{\mathrm{D}\boldsymbol{\alpha}}{\partial t},\frac{\mathrm{D}\boldsymbol{\alpha}}{\partial\epsilon}\right\rangle\mathrm{d}t.$$

Finally, integrate the third term once by parts to get

$$\int_{T_0}^{T_N}\tau^2\left\langle\frac{\mathrm{D}^2\boldsymbol{\alpha}}{\partial t\partial\epsilon},\frac{\mathrm{D}\boldsymbol{\alpha}}{\partial t}\right\rangle\mathrm{d}t=\left[\tau^2\left\langle\frac{\mathrm{D}\boldsymbol{\alpha}}{\partial\epsilon},\frac{\mathrm{D}\boldsymbol{\alpha}}{\partial t}\right\rangle\right]_{T_0}^{T_N}-\int_{T_0}^{T_N}\tau^2\left\langle\frac{\mathrm{D}\boldsymbol{\alpha}}{\partial\epsilon},\frac{\mathrm{D}^2\boldsymbol{\alpha}}{\partial t^2}\right\rangle\mathrm{d}t.$$

Thus, we have

$$\begin{aligned}\frac{\mathrm{d}}{\mathrm{d}\epsilon}\mathcal{J}(\boldsymbol{\alpha}) &= \int_{T_0}^{T_N}\left\langle\frac{\mathrm{D}\boldsymbol{\alpha}}{\partial\epsilon},\frac{\mathrm{D}^4\boldsymbol{\alpha}}{\partial t^4}+R\left(\frac{\mathrm{D}^2\boldsymbol{\alpha}}{\partial t^2},\frac{\mathrm{D}\boldsymbol{\alpha}}{\partial t}\right)\frac{\mathrm{D}\boldsymbol{\alpha}}{\partial t}-\tau^2\frac{\mathrm{D}^2\boldsymbol{\alpha}}{\partial t^2}\right\rangle\mathrm{d}t \\ &\quad+\left[\left\langle\frac{\mathrm{D}}{\partial t}\frac{\mathrm{D}\boldsymbol{\alpha}}{\partial\epsilon},\frac{\mathrm{D}^2\boldsymbol{\alpha}}{\partial t^2}\right\rangle-\left\langle\frac{\mathrm{D}\boldsymbol{\alpha}}{\partial\epsilon},\frac{\mathrm{D}^3\boldsymbol{\alpha}}{\partial t^3}\right\rangle+\tau^2\left\langle\frac{\mathrm{D}\boldsymbol{\alpha}}{\partial\epsilon},\frac{\mathrm{D}\boldsymbol{\alpha}}{\partial t}\right\rangle\right]_{T_0}^{T_N}.\end{aligned}$$

Setting $\epsilon=0$ results in Equation (5-2.1) by virtue of the third and fourth properties in equations (A-4.1).

■

Then, as in [55], one can define the *first variation* of $\mathcal{J}$ at $\mathbf{q}$, which is a linear transformation on $\mathrm{T}_{\mathbf{q}}\Omega$: $E(\mathbf{W}_t)=\frac{\mathrm{d}}{\mathrm{d}\epsilon}\mathcal{J}\left(\boldsymbol{\alpha}_\epsilon\right)\big|_{\epsilon=0}$. For a local minimizer $\mathbf{q}\in\Omega$, all admissible variations $\boldsymbol{\alpha}_\epsilon$ of $\mathbf{q}$ with associated vector field $\mathbf{W}_t$, we have $\mathcal{J}(\mathbf{q})=\mathcal{J}(\boldsymbol{\alpha}_0)\leq\mathcal{J}(\boldsymbol{\alpha}_\epsilon)$, $\boldsymbol{\alpha}\in(-\epsilon,\epsilon)$ and, consequently, $E(\mathbf{W}_t)=\frac{\mathrm{d}}{\mathrm{d}\epsilon}\mathcal{J}\left(\boldsymbol{\alpha}_\epsilon\right)\big|_{\epsilon=0}=0$. Any curve $\mathbf{q}\in\Omega$ for which $E(\mathbf{W}_t)=0$, for all $\mathbf{W}_t\in\mathrm{T}_{\mathbf{q}}\Omega$, is called a *critical curve* of $\mathcal{J}$.

Theorem 5.2.2. *If $\mathbf{q} \in \Omega$ is a local minimizer of $\mathcal{J}$, then $\mathbf{q}(t)$ is $\mathcal{C}^2$ and satisfies*

$$\frac{\mathrm{D}^4\mathbf{q}}{\mathrm{d}t^4} + R\left(\frac{\mathrm{D}^2\mathbf{q}}{\mathrm{d}t^2}, \frac{\mathrm{D}\mathbf{q}}{\mathrm{d}t}\right)\frac{\mathrm{D}\mathbf{q}}{\mathrm{d}t} - \tau^2\frac{\mathrm{D}^2\mathbf{q}}{\mathrm{d}t^2} \equiv 0, \tag{5-2.2}$$

$t \in [T_{i-1}, T_i]\,,\ i = 1, \ldots, N.$

Proof Suppose $\mathbf{q} \in \Omega$ is a local minimizer of $\mathcal{J}$ over Ω. Define a smooth real-valued function $f(t)$ on $[T_0, T_N]$ such that $f(T_i) = f'(T_i) = 0$ for $i = 0, \ldots, N$ and $f(t) > 0$ on (T_{i-1}, T_i) for $i = 1, \ldots, N$. Let $\mathbf{W}_t = f(t)\left[\frac{\mathrm{D}^4\mathbf{q}(t)}{\mathrm{d}t^4} + R\left(\frac{\mathrm{D}^2\mathbf{q}(t)}{\mathrm{d}t^2}, \frac{\mathrm{D}\mathbf{q}(t)}{\mathrm{d}t}\right)\frac{\mathrm{D}\mathbf{q}(t)}{\mathrm{d}t} - \tau^2\frac{\mathrm{D}^2\mathbf{q}(t)}{\mathrm{d}t^2}\right]$. By our choice of the function $f(t)$ each term under the summation sign in equation (5-2.1) is zero and we have

$$E(\mathbf{W}_t) = \int_{T_0}^{T_N} f\left\|\frac{\mathrm{D}^4\mathbf{q}}{\mathrm{d}t^4} + R\left(\frac{\mathrm{D}^2\mathbf{q}}{\mathrm{d}t^2}, \frac{\mathrm{D}\mathbf{q}}{\mathrm{d}t}\right)\frac{\mathrm{D}\mathbf{q}}{\mathrm{d}t} - \tau^2\frac{\mathrm{D}^2\mathbf{q}}{\mathrm{d}t^2}\right\|^2 \mathrm{d}t.$$

Since $f(t) > 0$ for almost every $t \in\ [T_0, T_N]$ and by virtue of the smoothness of the integrand we then have

$$\left\|\frac{\mathrm{D}^4\mathbf{q}(t)}{\mathrm{d}t^4} + R\left(\frac{\mathrm{D}^2\mathbf{q}(t)}{\mathrm{d}t^2}, \frac{\mathrm{D}\mathbf{q}(t)}{\mathrm{d}t}\right)\frac{\mathrm{D}\mathbf{q}(t)}{\mathrm{d}t} - \tau^2\frac{\mathrm{D}^2\mathbf{q}(t)}{\mathrm{d}t^2}\right\| = 0.$$

In other words, we have shown that a necessary condition for a curve $\mathbf{q} \in \Omega$ to be a minimizer of $\mathcal{J}$ is that

$$\frac{\mathrm{D}^4\mathbf{q}(t)}{\mathrm{d}t^4} + R\left(\frac{\mathrm{D}^2\mathbf{q}(t)}{\mathrm{d}t^2}, \frac{\mathrm{D}\mathbf{q}(t)}{\mathrm{d}t}\right)\frac{\mathrm{D}\mathbf{q}(t)}{\mathrm{d}t} - \tau^2\frac{\mathrm{D}^2\mathbf{q}(t)}{\mathrm{d}t^2} \equiv 0,$$

$t \in [T_{i-1}, T_i]\,,\ i = 1, \ldots, N$. We are left to show that $\mathbf{q}$ is $\mathcal{C}^2$ on $[T_0, T_N]$. To do that, let $\mathbf{W}_t \in \mathrm{T}_{\mathbf{q}}\Omega$ be a vector field that satisfies

$$\frac{\mathrm{D}}{\mathrm{d}t}\mathbf{W}_t = \frac{\mathrm{D}^2\mathbf{q}}{\mathrm{d}t^2}\left(T_i^+\right) - \frac{\mathrm{D}^2\mathbf{q}}{\mathrm{d}t^2}\left(T_i^-\right),$$

for $i = 1, \ldots, N-1$. This and equation (5-2.2) imply that

$$E\left(\mathbf{W}_t\right) = \sum_{i=1}^{N-1}\left\|\frac{\mathrm{D}^2\mathbf{q}}{\mathrm{d}t^2}\left(T_i^+\right) - \frac{\mathrm{D}^2\mathbf{q}}{\mathrm{d}t^2}\left(T_i^-\right)\right\|^2 = 0,$$

which implies that $\frac{\mathrm{D}^2\mathbf{q}}{\mathrm{d}t^2}\left(T_i^+\right) = \frac{\mathrm{D}^2\mathbf{q}}{\mathrm{d}t^2}\left(T_i^-\right)$. Hence, $\mathbf{q}$ is shown to be $\mathcal{C}^2$. Since $\mathbf{q}$ satisfies a fourth order differential equation, it must also be smooth on $[T_0, T_N]$.

■

5.3 Dynamic Interpolation with Motion Constraints

Here we consider the dynamic interpolation, τ-elastic variational problem with the motion constraints (5-1.5). The result is known for $\tau = 0$ [33] and similar problems have been dealt with extensively by many authors in relation to nonholonomic mechanics and control (see [58].) Here we re-derive the necessary conditions for an arbitrary value of τ (i.e., the problem P^τ.)

As in [33], define the one forms $\boldsymbol{\omega}_i(X) = \langle X_i, X\rangle$ and the two forms $\mathrm{d}\boldsymbol{\omega}_i$, $i = 1, \ldots, l$, where d is the exterior derivative. Defining $\lrcorner$ as the contraction operator, the 1-form $X \lrcorner \mathrm{d}\boldsymbol{\omega}_i$ satisfies: $X \lrcorner \mathrm{d}\boldsymbol{\omega}_i(Y) = \boldsymbol{\omega}_i(X, Y)$. One may define tensors S_i such that $S_{i_{\mathbf{q}}} : \mathrm{T}_{\mathbf{q}}M \to \mathrm{T}_{\mathbf{q}}M$, by setting $\mathrm{d}\boldsymbol{\omega}_i(X, Y) = \langle S_i(X), Y\rangle = -\langle S_i(Y), X\rangle$. We now have a theorem for normal extremals of problem P^τ. The following theorem is a generalization of results found in [55, 30].

Theorem 5.3.1. *A necessary condition for $\mathbf{q} \in \Omega$ to be a normal extremal for problem P^τ is that $\mathbf{q}$ is $\mathcal{C}^2$ and there exist smooth functions $\boldsymbol{\lambda}_i(t)$ such that*

$$\begin{aligned}\frac{\mathrm{D}^4\mathbf{q}(t)}{\mathrm{d}t^4} \quad + \quad & R\left(\frac{\mathrm{D}^2\mathbf{q}(t)}{\mathrm{d}t^2}, \frac{\mathrm{D}\mathbf{q}(t)}{\mathrm{d}t}\right)\frac{\mathrm{D}\mathbf{q}(t)}{\mathrm{d}t} - \tau^2\frac{\mathrm{D}^2\mathbf{q}(t)}{\mathrm{d}t^2} \\ & - \sum_{i=1}^{l}\frac{\mathrm{d}\boldsymbol{\lambda}_i}{\mathrm{d}t}X_i - \sum_{i=1}^{l}\boldsymbol{\lambda}_i S_i\left(\frac{\mathrm{D}\mathbf{q}}{\mathrm{d}t}\right) \equiv 0 \end{aligned} \tag{5-3.1}$$

and

$$\left\langle \frac{\mathrm{D}\mathbf{q}}{\mathrm{d}t}, X_i(\mathbf{q})\right\rangle = k_i,\ i = 1, \ldots, l\ (l < n) \tag{5-3.2}$$

for $t \in [T_{i-1}, T_i]$, $i = 1, \ldots, N$.

Proof First, augment the Lagrangian by terms

$$\sum_{i=1}^{l}\boldsymbol{\lambda}_i\left\langle \frac{\mathrm{D}\mathbf{q}}{\mathrm{d}t}, X_i(\mathbf{q})\right\rangle = \sum_{i=1}^{l}\boldsymbol{\lambda}_i\boldsymbol{\omega}_i\left(\frac{\mathrm{D}\mathbf{q}}{\mathrm{d}t}\right).$$

The counterpart of Equation (5-2.1) for the problem P^τ is

$$\begin{aligned}\left.\frac{\mathrm{d}}{\mathrm{d}\epsilon}\mathcal{J}(\boldsymbol{\alpha}_\epsilon)\right|_{\epsilon=0} &= \int_{T_0}^{T_N}\left[\left\langle \mathbf{W}_t, \frac{\mathrm{D}^4\mathbf{q}}{\mathrm{d}t^4} + R\left(\frac{\mathrm{D}^2\mathbf{q}}{\mathrm{d}t^2}, \frac{\mathrm{D}\mathbf{q}}{\mathrm{d}t}\right)\frac{\mathrm{D}\mathbf{q}}{\mathrm{d}t} - \tau^2\frac{\mathrm{D}^2\mathbf{q}}{\mathrm{d}t^2}\right\rangle\right.\\ &\quad + \sum_{i=1}^{l}\boldsymbol{\lambda}_i\left\langle\frac{\mathrm{D}}{\partial t}\frac{\mathrm{D}\boldsymbol{\alpha}}{\partial\epsilon}, X_i(\boldsymbol{\alpha})\right\rangle\Big|_{\epsilon=0} + \sum_{i=1}^{l}\boldsymbol{\lambda}_i\left\langle\frac{\mathrm{D}\boldsymbol{\alpha}}{\partial t}, \frac{\mathrm{D}}{\partial\epsilon}X_i(\boldsymbol{\alpha})\right\rangle\Big|_{\epsilon=0}\Bigg]\mathrm{d}t\\ &\quad + \sum_{i=1}^{N-1}\left\langle\frac{\mathrm{D}\mathbf{W}_t(T_i)}{\mathrm{d}t}, \frac{\mathrm{D}^2\mathbf{q}(T_i^-)}{\mathrm{d}t^2} - \frac{\mathrm{D}^2\mathbf{q}(T_i^+)}{\mathrm{d}t^2}\right\rangle.\end{aligned}$$

The last term in the integrand is simply

$$\sum_{i=1}^{l}\boldsymbol{\lambda}_i\left\langle\frac{\mathrm{D}\boldsymbol{\alpha}}{\partial t}, \frac{\mathrm{D}}{\partial\epsilon}X_i(\boldsymbol{\alpha})\right\rangle\Big|_{\epsilon=0} = \sum_{i=1}^{l}\boldsymbol{\lambda}_i\left\langle\frac{\mathrm{D}\mathbf{q}}{\mathrm{d}t}, \nabla_{\mathbf{W}_t}X_i\right\rangle,$$

where $\nabla_{\mathbf{W}_t}X_i$ is the covariant differentiation of X_i, $i = 1, \ldots, l$, with respect to $\mathbf{W}_t$. As for the second term in the integrand, integrate by parts to obtain

$$\begin{aligned}&\int_{T_0}^{T_N}\sum_{i=1}^{l}\boldsymbol{\lambda}_i\left\langle\frac{\mathrm{D}}{\partial t}\frac{\mathrm{D}\boldsymbol{\alpha}}{\partial\epsilon}, X_i(\boldsymbol{\alpha})\right\rangle\Big|_{\epsilon=0}\mathrm{d}t\\ &= -\int_{T_0}^{T_N}\sum_{i=1}^{l}\left[\frac{\mathrm{d}\boldsymbol{\lambda}_i}{\mathrm{d}t}\langle\mathbf{W}_t, X_i(\mathbf{q})\rangle + \boldsymbol{\lambda}_i\left\langle\mathbf{W}_t, \frac{\mathrm{D}X_i(\mathbf{q})}{\mathrm{d}t}\right\rangle\right]\mathrm{d}t,\end{aligned}$$

where the third property in equations (A-4.1) has been used. Making use of some of the properties of the Riemannian connection and recalling the definition of the exterior derivative of a one form $\boldsymbol{\omega}$:

$$\mathrm{d}\boldsymbol{\omega}(X, Y) = X\boldsymbol{\omega}(Y) - Y\boldsymbol{\omega}(X) - \boldsymbol{\omega}([X, Y])$$

for all vector fields X and Y on M, then, for the one forms $\boldsymbol{\omega}_i$ such that $\boldsymbol{\omega}_i(\mathbf{W}_t) = \langle\mathbf{W}_t, X_i\rangle$, one has

$$\mathrm{d}\boldsymbol{\omega}_i(X, Y) = \langle\nabla_X X_i, Y\rangle - \langle\nabla_Y X_i, X\rangle.$$

Setting $X = \frac{\mathrm{D}\mathbf{q}}{\mathrm{d}t}$ and $Y = \mathbf{W}_t$, we thus have

$$\begin{aligned}-\sum_{i=1}^{l}\boldsymbol{\lambda}_i\left\langle\mathbf{W}_t, \frac{\mathrm{D}X_i(\mathbf{q})}{\mathrm{d}t}\right\rangle + \sum_{i=1}^{l}\boldsymbol{\lambda}_i\left\langle\frac{\mathrm{D}\mathbf{q}}{\mathrm{d}t}, \nabla_{\mathbf{W}_t}X_i\right\rangle &= -\sum_{i=1}^{l}\boldsymbol{\lambda}_i\mathrm{d}\boldsymbol{\omega}_i\left(\frac{\mathrm{D}\mathbf{q}}{\mathrm{d}t}, \mathbf{W}_t\right)\\ &= -\left\langle\sum_{i=1}^{l}\boldsymbol{\lambda}_i S_i\left(\frac{\mathrm{D}\mathbf{q}}{\mathrm{d}t}\right), \mathbf{W}_t\right\rangle.\end{aligned}$$

From the above, $\frac{\mathrm{d}}{\mathrm{d}\epsilon}\mathcal{J}(\boldsymbol{\alpha}_\epsilon)\big|_{\epsilon=0}$ reduces to

$$\begin{aligned}\frac{\mathrm{d}}{\mathrm{d}\epsilon}\mathcal{J}(\boldsymbol{\alpha}_\epsilon)\bigg|_{\epsilon=0} &= \int_{T_0}^{T_N}\Bigg[\left\langle \mathbf{W}_t, \frac{\mathrm{D}^4\mathbf{q}}{\mathrm{d}t^4} + R\left(\frac{\mathrm{D}^2\mathbf{q}}{\mathrm{d}t^2}, \frac{\mathrm{D}\mathbf{q}}{\mathrm{d}t}\right)\frac{\mathrm{D}\mathbf{q}}{\mathrm{d}t}\right.\\ &\quad \left. -\tau^2\frac{\mathrm{D}^2\mathbf{q}}{\mathrm{d}t^2} - \sum_{i=1}^{l}\frac{\mathrm{d}\boldsymbol{\lambda}_i}{\mathrm{d}t}X_i - \sum_{i=1}^{l}\boldsymbol{\lambda}_i S_i\left(\frac{\mathrm{D}\mathbf{q}}{\mathrm{d}t}\right)\right\rangle \mathrm{d}t\\ &\quad + \sum_{i=1}^{N-1}\left\langle \frac{\mathrm{D}\mathbf{W}_t(T_i)}{\mathrm{d}t}, \frac{\mathrm{D}^2\mathbf{q}(T_i^-)}{\mathrm{d}t^2} - \frac{\mathrm{D}^2\mathbf{q}(T_i^+)}{\mathrm{d}t^2}\right\rangle \equiv 0.\end{aligned}$$

Next, define a smooth real-valued function $f(t)$ on $[T_0, T_N]$ such that $f(T_i) = f'(T_i) = 0$ for $i = 0, \ldots, N$ and $f(t) > 0$ on (T_{i-1}, T_i) for $i = 1, \ldots, N$. One can set $\mathbf{W}_t := f(t)\tilde{\mathbf{W}}_t$, where $\tilde{\mathbf{W}}(t)$ is arbitrary and such that $\mathbf{W}_t$ still satisfies the properties (A-4.1). This sets the term outside the integral to zero. Moreover, since $\mathbf{W}_t$ is an arbitrary tangent vector field, this immediately results in the necessary conditions for the trajectory $\mathbf{q}$ to be an extremal of the variational problem P^τ. These are

$$\frac{\mathrm{D}^4\mathbf{q}}{\mathrm{d}t^4} + R\left(\frac{\mathrm{D}^2\mathbf{q}}{\mathrm{d}t^2}, \frac{\mathrm{D}\mathbf{q}}{\mathrm{d}t}\right)\frac{\mathrm{D}\mathbf{q}}{\mathrm{d}t} - \tau^2\frac{\mathrm{D}^2\mathbf{q}}{\mathrm{d}t^2} - \sum_{i=1}^{l}\frac{\mathrm{d}\boldsymbol{\lambda}_i}{\mathrm{d}t}X_i - \sum_{i=1}^{l}\boldsymbol{\lambda}_i S_i\left(\frac{\mathrm{D}\mathbf{q}}{\mathrm{d}t}\right) \equiv 0$$

and the constraints

$$\left\langle \frac{\mathrm{D}\mathbf{q}}{\mathrm{d}t}, X_i(\mathbf{q})\right\rangle = k_i,\ i = 1, \ldots, l\ (l < n)$$

and, therefore, proving the theorem.

■

5.4 An Application to Interferometric Imaging

As an illustration for the above notions, we consider the execution of a two-spacecraft spiral maneuver as will be discussed in Chapter 6 and as in [45]. Though this problem may be physically achievable, it is very inefficient fuel-wise. We study this example for its simplicity. More practical and interesting examples include spiraling about a libration point in a Halo orbit. In the current problem, however,

spacecraft # 1 is fixed in space while spacecraft # 2 is made to move along a linear spiral, as defined below. The intuition behind this type of maneuver for interferometric imaging applications can be found in Chapter 6 and in [45], which we summarize as follows. As spacecraft # 2 executes the linear spiral motion and recedes away from the fixed spacecraft # 1, the baseline between the two spacecraft increases linearly from a minimum value to a maximum value. Mapping this motion to the two-dimensional spatial frequency domain (also known in the literature as the u-v plane) of the two-dimensional (optical) signal, the optical system samples all frequencies inside a desired "coverage" area. The size of this coverage area is inversely proportional to the system's achievable angular resolution; The larger the coverage area is the smaller the angular resolution becomes. This two-spacecraft spiral maneuver is one simple way to achieving frequency domain plane coverage. Other constellation designs that achieve this goal also exist (see Chapter 7 and [18, 19, 20].)

We study two versions of the problem. First, we take the manifold M to be $\mathbb{R}^2$ and impose a constraint that forces the motion of the second spacecraft to follow a linear spiral (Case A.) We also study the problem in $\mathbb{R}^3$, where we desire to execute the spiral motion on a sphere (Case B.) Here, we may treat the spiral as a motion constraint and set M to be the sphere. One may think of this as a tentative precursor to dealing with a formation restricted to moving on a spherical manifold about a central body (e.g. an asteroid.) Eventually, the goal is to add a central gravitational field. This problem will be dealt with in a future chapter.

Case A Here we treat the manifold M as $\mathbb{R}^2$ and impose a constraint that forces the motion of the second spacecraft to follow a linear spiral. The equations of motion, in Cartesian coordinates, of spacecraft # 2 (with spacecraft # 1 fixed at the origin)

are given by

$$\ddot{x} = u_x \text{ and } \ddot{y} = u_y, \tag{5-4.1}$$

where u_x and u_y are the control variables. The spiral constraint, in polar coordinates, is given by

$$r = \varsigma\left(\pi + \theta\right), \tag{5-4.2}$$

where $r = \sqrt{x^2 + y^2}$, $\tan\theta = \frac{y}{x}$, $\varsigma = \frac{\lambda}{\pi\theta_p}$, and λ and θ_p are constant parameters defined in Chapter 6. This is a holonomic constraint that can be expressed in (cartesian coordinates) differential form by

$$\left(x\sqrt{x^2+y^2} + ky\right)\mathrm{d}x + \left(y\sqrt{x^2+y^2} - kx\right)\mathrm{d}y = 0. \tag{5-4.3}$$

Let $\mathbf{q}(t) = [x(t)\ y(t)]^T$. It is desired to solve the τ-elastic variational problem, where we aim at minimizing

$$\frac{1}{2}\int_0^T \left[\left\langle \frac{\mathrm{D}^2\mathbf{q}(t)}{\mathrm{d}t^2}, \frac{\mathrm{D}^2\mathbf{q}(t)}{\mathrm{d}t^2}\right\rangle + \tau^2\left\langle \frac{\mathrm{D}\mathbf{q}(t)}{\mathrm{d}t}, \frac{\mathrm{D}\mathbf{q}(t)}{\mathrm{d}t}\right\rangle\right]\mathrm{d}t, \tag{5-4.4}$$

subject to the *motion* constraint:

$$\left\langle \frac{\mathrm{D}\mathbf{q}}{\mathrm{d}t}, X_1(\mathbf{q})\right\rangle = 0, \tag{5-4.5}$$

the boundary conditions:

$$x(0) = x_0,\ y(0) = y_0,\ x(T) = x_T, \text{ and } y(T) = y_T \tag{5-4.6}$$

and the dynamics (5-4.1), where the vector field $X_1(\mathbf{q})$ is given by

$$X_1 = \begin{bmatrix} x\sqrt{x^2+y^2} + ky \\ y\sqrt{x^2+y^2} - kx \end{bmatrix}$$

and the values of $x_0,\ y_0,\ x_T$ and y_T are defined to satisfy the motion constraint at $t = 0,\ T$ –to be found in Chapter 6.

First, note that since $M = \mathbb{R}^2$ we have $\mathrm{D}/\mathrm{d}t = \mathrm{d}/\mathrm{d}t$ and the curvature tensor, R, is identically equal to zero. The corresponding differential form for the constraint (5-4.3) is given by $\boldsymbol{\omega}_1 = \left(x\sqrt{x^2+y^2} + ky\right)\mathrm{d}x + \left(y\sqrt{x^2+y^2} - kx\right)\mathrm{d}y$. The two form $\mathrm{d}\boldsymbol{\omega}_1$ is therefore $\mathrm{d}\boldsymbol{\omega}_1 = -2\varsigma \mathrm{d}x \wedge \mathrm{d}y$, where $\wedge$ denotes the wedge product. Next, the one form $\frac{\mathrm{d}\mathbf{q}}{\mathrm{d}t} \lrcorner \mathrm{d}\boldsymbol{\omega}_1$ is found to be

$$\frac{\mathrm{d}\mathbf{q}}{\mathrm{d}t} \lrcorner \mathrm{d}\boldsymbol{\omega}_1 = 2\varsigma\left(\dot{y}\mathrm{d}x - \dot{x}\mathrm{d}y\right)$$

and therefore we have

$$S_1\left(\frac{\mathrm{d}\mathbf{q}}{\mathrm{d}t}\right) = 2\varsigma\left(\dot{y}\frac{\partial}{\partial x} - \dot{x}\frac{\partial}{\partial y}\right).$$

Since $l = 1$, then set $\boldsymbol{\lambda}_1 = \boldsymbol{\lambda}$. Theorem (5.3.1) then implies that an optimal solution to this version of the problem should satisfy the differential equations

$$\begin{aligned}
\frac{\mathrm{d}^4x}{\mathrm{d}t^4} - \tau^2\frac{\mathrm{d}^2x}{\mathrm{d}t^2} - \frac{\mathrm{d}\boldsymbol{\lambda}}{\mathrm{d}t}\left(x\sqrt{x^2+y^2} + ky\right) - 2\varsigma\boldsymbol{\lambda}\dot{y} &= 0, \\
\frac{\mathrm{d}^4y}{\mathrm{d}t^4} - \tau^2\frac{\mathrm{d}^2y}{\mathrm{d}t^2} - \frac{\mathrm{d}\boldsymbol{\lambda}}{\mathrm{d}t}\left(y\sqrt{x^2+y^2} - kx\right) + 2\varsigma\boldsymbol{\lambda}\dot{x} &= 0,
\end{aligned}$$

the constraints (5-4.5) and the boundary conditions (5-4.6).

Case B Here we study the problem in $\mathbb{R}^3$ and treat the spiral as a motion constraint and set M to be a sphere of constant radius ρ. M has dimension equal to 2. Thus, we choose to work with the spherical coordinates θ and ϕ (see Figure (5.1).) We may now consider the following equations of motion for spacecraft # 2:

$$\ddot{\theta} = u_\theta, \text{ and } \ddot{\phi} = u_\phi, \tag{5-4.7}$$

where u_θ and u_ϕ are the control variables. We then impose the spiral constraint (5-4.2) in terms of the coordinates θ and ϕ as follows. Since r is the projection of

ρ onto the x-y plane, then $r = \rho \sin\phi$. The spiral constraint can be expressed in (spherical coordinate) differential form as

$$-\varsigma \mathrm{d}\theta + \rho\cos\phi \mathrm{d}\phi = 0. \tag{5-4.8}$$

Let $\mathbf{q}(t) = [\theta(t)\ \phi(t)]^T$. It is desired to solve the τ-elastic variational problem, where we aim at minimizing (5-4.4) subject to the *motion* constraint:

$$\left\langle \frac{\mathrm{D}\mathbf{q}}{\mathrm{d}t}, X_1(\mathbf{q}) \right\rangle = 0, \tag{5-4.9}$$

the boundary conditions:

$$\theta(0) = \theta_0,\ \phi(0) = \phi_0,\ \theta(T) = \theta_T,\ \text{and}\ \phi(T) = \phi_T \tag{5-4.10}$$

and the dynamics (5-4.7), where the vector field $X_1(\mathbf{q})$ is given by

$$X_1 = \begin{bmatrix} -\varsigma \\ \\ \rho\cos\phi \end{bmatrix}$$

and the values of $\theta(0) = \theta_0,\ \phi(0) = \phi_0,\ \theta(T) = \theta_T$, and $\phi(T) = \phi_T$ are defined to satisfy the motion constraint *and* lie on M at times 0 and T. Note that we are only interested in the projection of the motion onto a plane parallel to the $x-y$ plane, where $x = r\cos\theta$ and $y = r\sin\theta$. With spacecraft # 2 moving on only a hemisphere, spacecraft # 1 will be fixed at $(0, 0, +\rho)$ or $(0, 0, -\rho)$ if $\dot{\theta}(0) > 0$ or $\dot{\theta}(0) < 0$, respectively.

First, we need to compute the curvature vector field $R\left(\frac{\mathrm{D}^2\mathbf{q}}{\mathrm{d}t^2}, \frac{\mathrm{D}\mathbf{q}}{\mathrm{d}t}\right)\frac{\mathrm{D}\mathbf{q}}{\mathrm{d}t}$ for this problem. Following standard methods for computing the curvature tensor (see, for instance, [59, 60]), one finds that

$$\begin{aligned} R\left(\frac{\mathrm{D}^2\mathbf{q}}{\mathrm{d}t^2}, \frac{\mathrm{D}\mathbf{q}}{\mathrm{d}t}\right)\frac{\mathrm{D}\mathbf{q}}{\mathrm{d}t} \;=\; & \left[\frac{\mathrm{D}^2\phi}{\mathrm{d}t^2}\frac{\mathrm{D}\phi}{\mathrm{d}t}\frac{\mathrm{D}\theta}{\mathrm{d}t} - \frac{\mathrm{D}^2\theta}{\mathrm{d}t^2}\left(\frac{\mathrm{D}\phi}{\mathrm{d}t}\right)^2\right]\frac{\partial}{\partial\theta} \\ & + \left[\frac{\mathrm{D}^2\theta}{\mathrm{d}t^2}\frac{\mathrm{D}\theta}{\mathrm{d}t}\frac{\mathrm{D}\phi}{\mathrm{d}t} - \frac{\mathrm{D}^2\phi}{\mathrm{d}t^2}\left(\frac{\mathrm{D}\theta}{\mathrm{d}t}\right)^2\right]\sin^2\phi\frac{\partial}{\partial\phi}. \end{aligned}$$

The corresponding differential form for the constraint (5-4.8) is given by $\boldsymbol{\omega}_1 = -\varsigma \mathrm{d}\theta + \rho\cos\phi \mathrm{d}\phi$. The two form $\mathrm{d}\boldsymbol{\omega}_1$ turns out to be $\mathrm{d}\boldsymbol{\omega}_1 = 0$ and, therefore, $\frac{\mathrm{D}\mathbf{q}}{\mathrm{d}t} \lrcorner \mathrm{d}\boldsymbol{\omega}_1 = 0$ and $S_i\left(\frac{\mathrm{D}\mathbf{q}}{\mathrm{d}t}\right) = 0$. Since $l = 1$, then set $\boldsymbol{\lambda}_1 = \boldsymbol{\lambda}$. Theorem (5.3.1) implies that an optimal solution to this version of the problem should satisfy the differential equations

$$\begin{aligned} \frac{\mathrm{D}^4\theta}{\mathrm{d}t^4} + \frac{\mathrm{D}^2\phi}{\mathrm{d}t^2}\frac{\mathrm{D}\phi}{\mathrm{d}t}\frac{\mathrm{D}\theta}{\mathrm{d}t} - \frac{\mathrm{D}^2\theta}{\mathrm{d}t^2}\left(\frac{\mathrm{D}\phi}{\mathrm{d}t}\right)^2 - \tau^2\frac{\mathrm{D}^2\theta}{\mathrm{d}t^2} + \varsigma\frac{\mathrm{d}\boldsymbol{\lambda}}{\mathrm{d}t} &= 0, \\ \frac{\mathrm{D}^4\phi}{\mathrm{d}t^4} + \left[\frac{\mathrm{D}^2\theta}{\mathrm{d}t^2}\frac{\mathrm{D}\theta}{\mathrm{d}t}\frac{\mathrm{D}\phi}{\mathrm{d}t} - \frac{\mathrm{D}^2\phi}{\mathrm{d}t^2}\left(\frac{\mathrm{D}\theta}{\mathrm{d}t}\right)^2\right]\sin^2\phi - \tau^2\frac{\mathrm{D}^2\phi}{\mathrm{d}t^2} + \rho\cos\phi\frac{\mathrm{d}\boldsymbol{\lambda}}{\mathrm{d}t} &= 0, \end{aligned}$$

the constraints (5-4.9) and the boundary conditions (5-4.10).

Remarks

1. To obtain differential equations for the lagrange multipliers $\boldsymbol{\lambda}_i$, $i = 1, \ldots, l$, one differentiates the motion constraints (5-3.2) three times, which are sufficient as long as the assumption that the vector fields X_i, $i = 1, \ldots, l$, are independent.

2. The first term in the cost function $\mathcal{J}$ of Equation (5-4.4) penalizes fuel expenditure. The second term is included because in applications such as the two-spacecraft imaging constellation it is desired to execute the maneuver at the slowest possible speed within a certain time period, T, in order to improve image quality (i.e., maximize the number of collected photons.)

3. In Case A, one may treat the manifold M as the linear spiral and imbed it in $\mathbb{R}^2$. The equations of motion of spacecraft # 2 are still given by Equations (5-4.1). Letting $\mathbf{q}(t) = [x(t)\ y(t)]^T$, it is desired to solve the τ-elastic variational problem, where we aim at minimizing (5-4.4) subject to the dynamics (5-4.1) without the imposition of any further motion constraints. Thus, the last two terms in Equation (5-3.1) are now eliminated at the expense of computing the curvature tensor, R.

4. For Case B, an alternative approach could have been followed. We may study the problem in $\mathbb{R}^3$ and treat the spiral as a motion constraint and set M to be a sphere of radius ρ. The equations of motion, in Cartesian coordinates, of spacecraft # 2 are given by

$$\ddot{x} = u_x,\ \ddot{y} = u_y,\ \ddot{z} = u_z. \tag{5-4.11}$$

We set M to be the sphere of radius ρ, and impose the spiral constraint (5-4.3) on $\mathbb{R}^3$.

Let $\mathbf{q}(t) = [x(t)\ y(t)\ z(t)]^T$. It is desired to solve the τ-elastic variational problem, where we aim at minimizing (5-4.4) subject to the *motion* constraint:

$$\left\langle \frac{\mathrm{D}\mathbf{q}}{\mathrm{d}t}, X_1(\mathbf{q}) \right\rangle = 0, \tag{5-4.12}$$

the boundary conditions:

$$\begin{aligned} &x(0) = x_0,\ y(0) = y_0,\ z(0) = z_0, \\ &x(T) = x_T, y(T) = y_T,\ z(T) = z_T \end{aligned} \tag{5-4.13}$$

and the dynamics (5-4.11), where $X_1(\mathbf{q})$ is given by

$$X_1 = \begin{bmatrix} x\sqrt{x^2+y^2} + ky \\ y\sqrt{x^2+y^2} - kx \\ 0 \end{bmatrix}$$

and the values of $x_0,\ y_0,\ z_0,\ x_T,\ y_T$ and z_T are defined to satisfy the motion constraint *and* lie on M at $t = 0,\ T$. The resulting trajectory is different from that obtained in Case B. The reason is that we have chosen a different set of control signals to be minimized.

5. Similarly to Remark 2, one may treat M in Remark 3 as $\mathbb{R}^3$ and impose two motion constraints:

$$\left\langle \frac{\mathrm{D}\mathbf{q}}{\mathrm{d}t}, X_i(\mathbf{q}) \right\rangle = 0, \ i = 1, 2$$

corresponding to the sphere ($i = 1$) and the spiral ($i = 2$), where the vector fields $X_i(\mathbf{q})$, $i = 1, 2$, are given by

$$X_1 = \begin{bmatrix} x \\ y \\ z \end{bmatrix}, \text{ and}$$

$$X_2 = \begin{bmatrix} x\sqrt{x^2+y^2} + ky \\ y\sqrt{x^2+y^2} - kx \\ 0 \end{bmatrix}.$$

Here we avoid computing the curvature R (which is zero everywhere) at the expense of having an additional lagrange multiplier that would need to be computed when integrating the differential equations that an optimal trajectory must satisfy.

6. The imaging problem as stated above does not involve interpolation constraints. The only constraints are the boundary conditions, the dynamics, and some geometric or motion constraints. Thus, the results obtained in Section (5.3) are generalized versions of the problem (with interpolation constraints on $\mathbf{q}$.) One may easily think of extensions to the above example were interpolation constraints to be imposed.

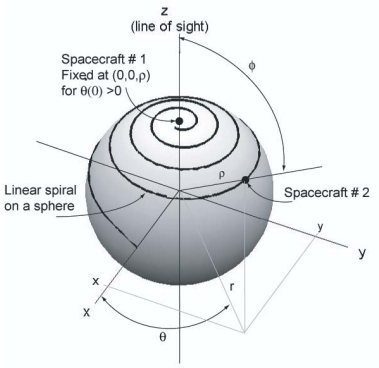

Figure 5.1: Variable definition for Case B.

5.5 Conclusion

In this chapter we derived necessary conditions for minimizing the cost function for a trajectory that evolves on a Riemannian manifold and satisfies a second order differential equation together with some interpolation, smoothness and motion constraints. The cost function we consider in this chapter is a weighted sum of the norm squared of the acceleration and the norm squared of the velocity and is motivated by multi-spacecraft interferometric imaging applications. We defined the dynamic interpolation problem, derived the necessary conditions for an optimal solution and gave examples motivated by an imaging application.

CHAPTER 6

Optimal Fuel-Image Motion Planning for a Class of Dual Spacecraft Formations

In this chapter we first introduce a class of spiral motions that satisfies imaging objectives and seek simple solutions to the problem of motion design and control of a formation for imaging applications. Based on the observations drawn from these simple controls, an optimal control problem is formulated for the proposed class of spiral motions to achieve minimum fuel consumption, while satisfying imaging constraints. The first main contribution made in this chapter is that we combine two ideas introduced separately in the literature and propose a maneuver that offers improved imaging performance. We then formulate an optimal control problem to minimize fuel consumption and further maximize image quality by minimizing the relative speed, which is proportional to the signal-to-noise ratio of the reconstructed image. We use the maximum principle to derive the necessary optimality conditions and show that they are also sufficient and that the resulting control law is unique. Finally, we apply a continuation method to solve for the unique optimal trajectory.

6.1 Motion Design for Wave Number Plane Coverage

In this chapter we address the issue of motion design and control for an interferometric observatory composed of two satellites that ensures a non-zero value of the MTF within a desired region in the wave number plane. We assume that the system is in free space; the only forces acting on the system are the spacecraft thrusters. Note that this is a reasonable analogue for a spacecraft at the libration point L_2. For example, in [61], the authors discuss the feasibility of nulling natural forces and replacing them with "new" dynamics. In this and sections (6.2) and (6.3), we motivate the coplanar dual spacecraft spiraling maneuver and give simple examples. In Sections (6.5), (6.6) and (6.7), we generalize the formation to dual spacecraft spirals on a paraboloid and formulate an optimal control problem which we solve numerically in Section (6.8).

In the coplanar problem, one of the spacecraft is stationary and located at the origin of an inertial reference frame. Let $\mathbf{q}_1 \equiv \mathbf{0}$ and $\mathbf{q}_2$ be the position vectors of the first and second satellites, respectively. Thus $\mathbf{q}_2$ also describes the relative position vector between the two satellites. Since we only consider the motion in a plane perpendicular to the line of sight of the observatory, let $\mathbf{q} = (r, \theta)$ in polar coordinates be the projection of $\mathbf{q}_2$ onto such plane. Here we only consider the motion of the second spacecraft (the first is fixed at the origin) and only one of the picture frame discs (while the second will have an identical motion that is symmetric about the origin.) Thus, by $(\tilde{r}, \theta)$ we imply the polar coordinates of one picture frame disc center. One way to ensure full coverage of the resolution disc is to initialize the second spacecraft such that at $t = 0$ we have $(\tilde{r} = \frac{1}{\theta_p}, \theta = 0)$, make it follow a linear spiral as a function of θ, and to impose the terminal condition that at $t = T$ we

have ($\tilde{r} = \frac{(m+1)}{2\theta_p}, \theta = \frac{(m-1)\pi}{2}$), where T is the terminal time. This motion implies that the two picture frame discs are initialized such that they lie outside the picture frame disc whose center is fixed at the origin, and moves spirally outwards till they lie outside resolution disc.

Note that $\tilde{r} = 0$ is a singularity, which produces poor numerical results for the motion near the origin, and thus we do not initialize the system at this value. However, the discussion at the end of Section (2.1) implies that initializing the system with $\tilde{r} = 1/\theta_p$ results in some regions close to the origin of the wave number plane that will not be covered (the shaded region in Figure (6.1).) It will be shown in simulation that this is not necessarily true, and that the initial condition we impose suffices for full coverage, especially near the origin. Thus $\tilde{r}$ and θ are constrained to satisfy

$$\tilde{r}(\theta(t)) = \frac{1}{\pi\theta_p}(\pi + \theta), \ \theta \in \left[0, \frac{(m-1)\pi}{2}\right]. \tag{6-1.1}$$

This implies that

$$r(\theta(t)) = \frac{\lambda}{\pi\theta_p}(\pi + \theta), \ \theta \in \left[0, \frac{(m-1)\pi}{2}\right]. \tag{6-1.2}$$

The first and second time derivatives of the constraint (6-1.2) also need to be satisfied:

$$\dot{r} = \frac{\lambda}{\pi\theta_p}\dot{\theta}, \ \forall t \in [0, T], \tag{6-1.3}$$

and

$$\ddot{r} = \frac{\lambda}{\pi\theta_p}\ddot{\theta}, \ \forall t \in [0, T], \tag{6-1.4}$$

where $\dot{r}$ and $\ddot{r}$ are the first and second time derivatives of r with respect to time.

Figure (6.1) shows an example of the trajectory in the physical and wave number planes for an object that is located at $\bar{z} = 15$pc (1pc$= 3.085 \times 10^{13}$km), with a picture frame that is $\bar{L} = 12,760$km wide, with $m = 17$ pixels and, thus, a pixel size

of $L = 750.6$km (i.e. this constellation maneuver is capable of detecting any object whose size is greater than L.) These are the values that are used throughout this chapter. These values correspond to applications such as JPL's Terrestrial Planet Finder (TPF) and they could also be adjusted for Earth imaging applications. In the latter case, the maneuver spans a few meters only, as opposed to few thousands of kilometers as in the example we treat in this chapter.

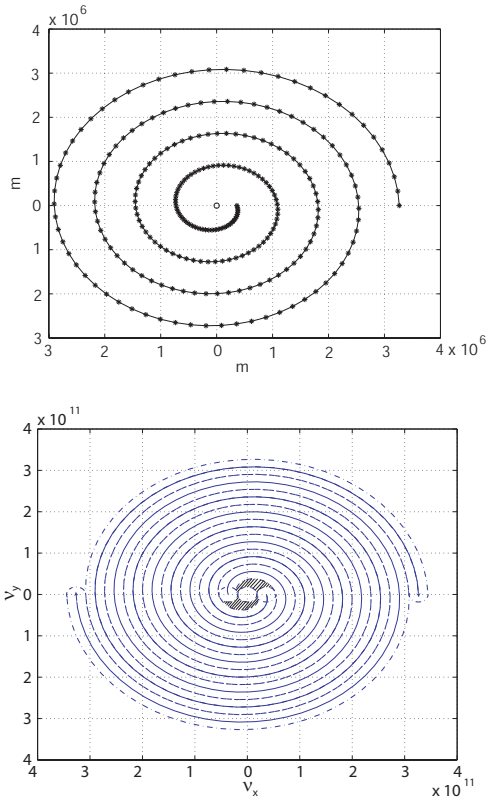

Figure 6.1: Motion in the physical (in meters, top) and wave number (dimensionless, bottom) planes.

6.2 Equations of Motion with a Spiral Constraint

In this section we derive the constrained equations of motion of the second spacecraft relative to the origin. After dividing throughout by the mass of the second spacecraft, the two degree of freedom equations of motion for the system are de-

scribed in polar coordinates by

$$\ddot{r} - r\dot{\theta}^2 = u_n, \tag{6-2.1}$$

and

$$r\ddot{\theta} + 2\dot{r}\dot{\theta} = u_t, \tag{6-2.2}$$

where u_n is the radial component of the thrust vector and u_t is the tangential component of the thrust vector, both divided by the mass of the spacecraft. Applying the configuration constraint in (6-1.2) to the system of equations (6-2.1)-(6-2.2) results in the following two *dependent* equations that describe the motion

$$\ddot{\theta} - f(\theta)\dot{\theta}^2 = \tilde{u}_n, \tag{6-2.3}$$

and

$$f(\theta)\ddot{\theta} + 2\dot{\theta}^2 = \tilde{u}_t, \tag{6-2.4}$$

where $f(\theta) = \pi + \theta$, $\tilde{u}_n = \frac{\pi\theta_p}{\lambda}u_n$ and $\tilde{u}_t = \frac{\pi\theta_p}{\lambda}u_t$. Note that these two equations are equivalent. By solving for $\ddot{\theta}$ in (6-2.3) and (6-2.4) and equating the resulting expressions, one finds that the tangential and radial components of the force-per-mass vector are related such that

$$\tilde{u}_n = -\left[f(\theta) + \frac{2}{f(\theta)}\right]\dot{\theta}^2 + \frac{1}{f(\theta)}\tilde{u}_t. \tag{6-2.5}$$

By solving either (6-2.3) or (6-2.4) such that θ goes from 0 to $\frac{(m-1)\pi}{2}$ we are guaranteed that the spacecraft will have gone through one entire "image" maneuver and covered the wave number plane.

6.3 Simple Controllers to Achieve Imaging Objectives

In this section we investigate the performance of five controllers that are designed to satisfy the spiral motion constraint. The two main performance considerations are image quality and fuel consumption. Image quality requires full coverage of the resolution disc and the attainment of a desired signal-to-noise ratio. An image quality performance measure was stated in Section (2.2), which we advise the reader to review. We re-write the main equations here again. First, the image quality performance measure can be expressed as:

$$\mathcal{I} = \int_0^T dt \int d\boldsymbol{\nu} \left(1 - \Gamma^R(\boldsymbol{\nu}, t)\right), \tag{6-3.1}$$

where R is a "risk factor" and $\Gamma(\boldsymbol{\nu}, t)$ is the estimated signal-to-noise ratio of the interferometric measurement divided by the desired signal-to-noise ratio. Using Poisson statistics in a semi-classical photon arrival fluctuation calculation (Section 4.4.3 in [62]), this can be shown to be proportional to the square root of the MTF magnitude. Hence, Γ is given by:

$$\Gamma(\boldsymbol{\nu}, t) = \begin{cases} 1 & \text{if } \alpha \hat{M}^{1/2} \geq 1 \\ \alpha \hat{M}^{1/2} & \text{otherwise} \end{cases}, \tag{6-3.2}$$

where α is inversely proportional to the desired signal-to-noise ratio and $\hat{M}$ is computed from Equation (2-1.21). The larger the risk factor R the more conservative the imaging performance measure becomes. Regions in the wave number plane where Γ is less than unity correspond to spatial frequencies of the signal that do not satisfy the desired signal-to-noise ratio, while $\Gamma = 1$ implies both coverage and achievement of the desired signal-to-noise ratio at the corresponding spatial frequency.

Recall also that since the $\hat{A}_p$ functions are evaluated at points corresponding to the trajectories of the relative position vectors, note that the rate at which the

$\hat{A}_p(\boldsymbol{\nu} - \frac{\mathbf{q}}{\lambda \bar{z}})$ function moves in the frequency domain is proportional to the relative velocity between the spacecraft pair. Hence, if the relative velocity has a large magnitude, $\hat{A}_p$ moves too fast in the frequency domain. This, in turn, may not allow for the MTF to accumulate to a satisfactory level to achieve the desired SNR (as reflected in the Γ function) and, hence, results in reduced signal strength allowing for the noise signal to overwhelm the measured signal. This results, by definition, to $\Gamma < 1$. This implies that the value of Γ and, hence,the SNR, function is inversely proportional to the square root of the relative speed between the spacecraft in the constellation. Therefore, there is a critical relative speed v^* such that the picture frame discs achieve $\Gamma = 1$ at the frequencies they visit and such that $\Gamma < 1$ if the relative speed $v < v^*$.

In Section (2.1), the model for the picture frame disc given by Equation (2-1.23), we have assumed that the area covered by the picture frame disc is being covered in a uniform fashion. However, the coverage it achieves has a nonuniform distribution that resembles a Gaussian. It can be shown that the width of this distribution is determined by the relative speed between the spacecraft. For low speeds the picture frame disc could even have a diameter that is slightly larger than $1/\theta_p$. For large speeds the picture frame disc will have a distribution with an effective width that is smaller than $1/\theta_p$. Thus, speed primarily affects signal-to-noise ratio and the distribution of the signal within the picture frame disc as it moves in the wave number plane.

The performance measure used for fuel consumption is

$$\mathcal{U} = \int_0^T \left(u_n^2(t) + u_t^2(t) \right) dt. \tag{6-3.3}$$

The two cost functions in (6-3.1) and (6-3.3) are the basis for evaluating the imaging

performance and fuel consumption. The sum $\mathcal{J} = w_1\mathcal{I} + w_2\mathcal{U}$, where w_i $(i = 1, 2)$ are weighting coefficients, could be used as the objective function for a nonlinear optimal controller that optimizes both fuel consumption and image quality. Next we consider benchmark problems for controller design.

Maneuver 1: Constant Speed Motion As mentioned above, it is desirable to have a uniform signal-to-noise ratio over the entire resolution disc region in the wave number plane. This can be achieved by setting the magnitude of the velocity to be:

$$V = \sqrt{\left(r\dot{\theta}\right)^2 + \dot{r}^2} = v^*, \tag{6-3.4}$$

which is constant. Taking the derivative of this condition,

$$r\dot{\theta}\left(\dot{r}\dot{\theta} + r\ddot{\theta}\right) + \dot{r}\ddot{r} = 0, \tag{6-3.5}$$

substituting r, $\dot{r}$ and $\ddot{r}$ using (6-1.2)-(6-1.4) and rearranging one gets the closed loop differential equation

$$\ddot{\theta} = -\frac{f(\theta)}{1 + f^2(\theta)}\dot{\theta}^2, \tag{6-3.6}$$

which will achieve full coverage of the wave number plane if it satisfies the correct boundary conditions. From Equation (6-2.3), the radial component of the control thrust is given by

$$\tilde{u}_n = -f(\theta)\dot{\theta}^2\left[1 + \frac{1}{1 + f^2(\theta)}\right]. \tag{6-3.7}$$

Using this and Equation (6-2.5), the tangential component, $\tilde{u}_t$ is thus

$$\tilde{u}_t = \dot{\theta}^2\left(2 - \frac{f^2(\theta)}{1 + f^2(\theta)}\right). \tag{6-3.8}$$

Maneuver 2: Constant Tangential Velocity A simplified version of the situation considered in the previous paragraph is to assume that only the tangential

component of the velocity vector is constant; $V_t = r\dot{\theta}$ is constant. Taking the the derivative of this condition,

$$\dot{r}\dot{\theta} + r\ddot{\theta} = 0, \tag{6-3.9}$$

substituting r, $\dot{r}$ and $\ddot{r}$ using (6-1.2)-(6-1.4) and rearranging one gets the closed loop differential equation

$$\ddot{\theta} = -\frac{1}{f(\theta)}\dot{\theta}^2. \tag{6-3.10}$$

From Equation (6-2.3), the radial component of the control thrust is given by

$$\tilde{u}_n = -\dot{\theta}^2 \left[f(\theta) + \frac{1}{f(\theta)} \right]. \tag{6-3.11}$$

Using this and Equation (6-2.5), the tangential component, $\tilde{u}_t$, is thus

$$\tilde{u}_t = \dot{\theta}^2. \tag{6-3.12}$$

Maneuver 3: Constant Angular Rate Next, consider the situation where $\dot{\theta}$ is a constant. Thus $\ddot{\theta} = 0$, which implies that θ is a linear function of time. After applying the boundary conditions, one obtains an explicit solution for θ

$$\theta(t) = \frac{(m-1)\pi}{2T}t. \tag{6-3.13}$$

Since $\dot{r} = \frac{\lambda}{\pi\theta_p}\dot{\theta}$, it is also constant and $\ddot{r} = 0$. From Equation (6-2.3), the radial component of the thrust vector is given by

$$\tilde{u}_n = -f(\theta)\dot{\theta}^2. \tag{6-3.14}$$

And from Equation (6-2.4), the tangential component of the thrust vector is given by

$$\tilde{u}_t = 2\dot{\theta}^2. \tag{6-3.15}$$

Maneuver 4: Zero Tangential Acceleration Consider not applying any tangential thrust; then $\tilde{u}_t = 0$ and Equation (6-2.5) implies that

$$\tilde{u}_n = -\left[f(\theta) + \frac{2}{f(\theta)}\right]\dot{\theta}^2. \tag{6-3.16}$$

Finally, the closed loop differential equation is

$$\ddot{\theta} = -\frac{2}{f(\theta)}\dot{\theta}^2. \tag{6-3.17}$$

6.3.1 Results

In the results we present here, Maneuver (1) represents the benchmark solution to the problem. It is the solution that achieves the two imaging objectives since (1) it follows a linear spiral that completely covers the desired resolution disc and (2) it moves at a constant speed that is sufficient to attain the desired signal-to-noise ratio. First we determined the value of v^* and set the initial condition for Maneuver (1) such that the spacecraft has an initial speed equal to v^*. This speed is guaranteed to be maintained by the additional speed constraint (6-3.4). We simulated the system and determined the terminal time T. Thus, for all other cases, we set the initial conditions such that each individual maneuver is completed at $t = T$. Finally, we use Eqs. (6-3.1) and (6-3.3) to evaluate the performance of all four motions. A reference speed, v^*, that achieves the desired signal-to-noise ratio is assumed to be 30m/s and T was found to be 17 days and 17 hours.

Figures (6.2)-(6.6) show the time evolution of r, θ, V, u_n and u_t for all four maneuvers. Figures (6.7) and (6.8) show how the Γ function accumulates and how the image forms with time for Maneuvers (1) and (4). These represent the two interesting cases: Maneuver (1) is the benchmark solution and Maneuver (4) shows that Γ by itself evaluated at the end of the maneuver is not sufficient to judge

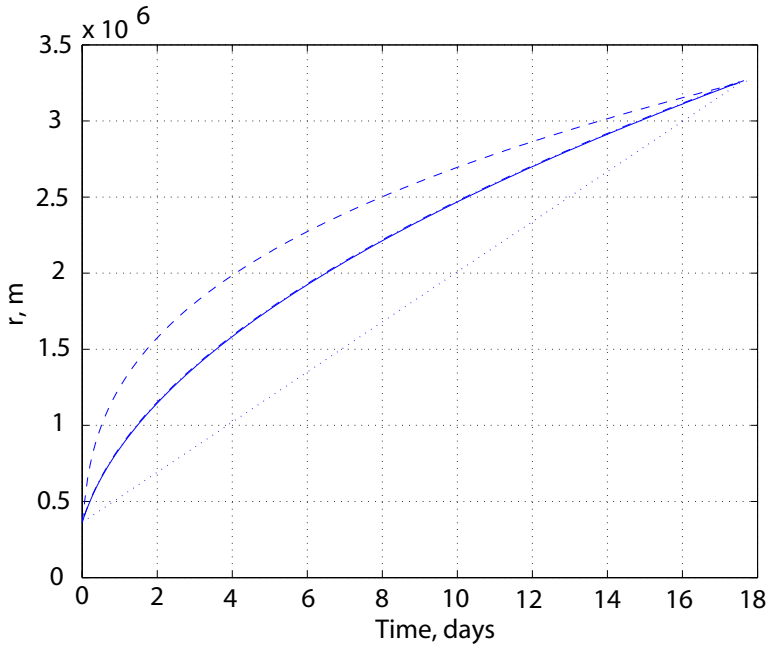

Figure 6.2: $r(t)$ for Maneuver (1) (solid), Maneuver (2) (dash-dotted), Maneuver (3) (dotted) and Maneuver (4) (dashed.)

the quality of the final image. Maneuver (2) produces results almost identical to Maneuver (1) and we will only comment on the results for Maneuver (3).

The image formation algorithm was developed by our group at the University of Michigan and has been used in this section to demonstrate the concepts presented in this chapter. The algorithm assumes a given target planet, which includes planet surface details. It also assumes a statistical model for noise. It simulates the motion of the spacecraft, computes the resulting Γ function, and estimates the image.

For Maneuver (1), note that the speed is constant throughout the maneuver (upper left chart in Figure (6.4).) Consequently, we expect a uniform Γ function throughout the wave number plane (Figure (6.7)); the desired signal-to-noise ratio is attained everywhere in the plane. However, for Maneuver (4), we note that we start off with a speed of 110m/s, which is larger than v^*. That is why near the center of the resolution disc (i.e. by the fifth day) we can see some partial coverage, resulting

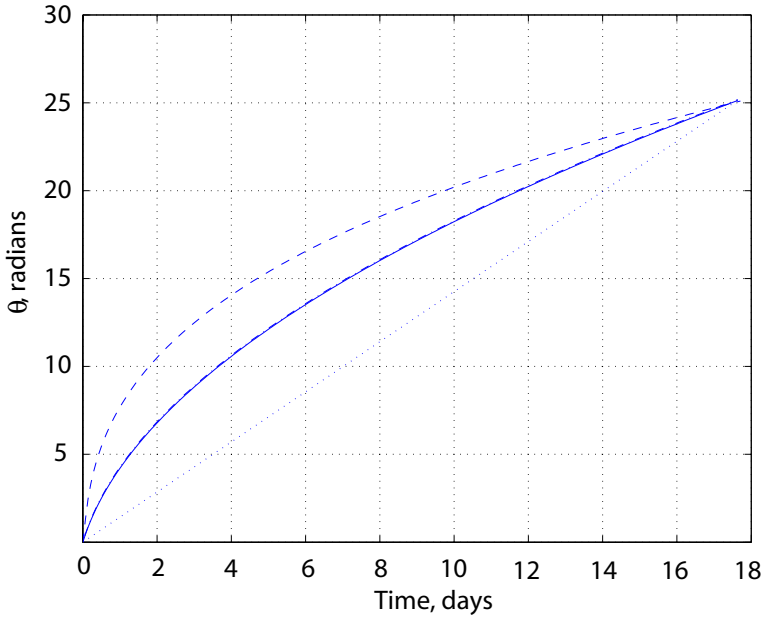

Figure 6.3: $\theta(t)$ for Maneuver (1) (solid), Maneuver (2) (dash-dotted), Maneuver (3) (dotted) and Maneuver (4) (dashed.)

in a signal-to-noise ratio that is lower than the desired. We also expect that for Maneuver (4), the picture frame disc to be significantly narrower than the nominal value, $1/\theta_p$. Thus, at low frequencies the formation in Maneuver (1) performs better than the formation in Maneuver (4).

On the other hand, as the the spacecraft in Maneuver (4) proceeds beyond the fifth day, its speed drops below v^*, thus, achieving the desired signal-to-noise ratio. Moreover, one should expect a wider picture frame disc signal distribution. Beyond the fifth day of the maneuvers, both cases will achieve equal imaging performance for all but the last 2π radians of the maneuvers. During the last spiral revolution, the spacecraft in Maneuver (4) will have a wider picture frame disc than that of Maneuver (1) and will, thus, furnish bonus high frequency coverage in the wave number plane.

Therefore, during one phase of the maneuvers the formation in Maneuver (1)

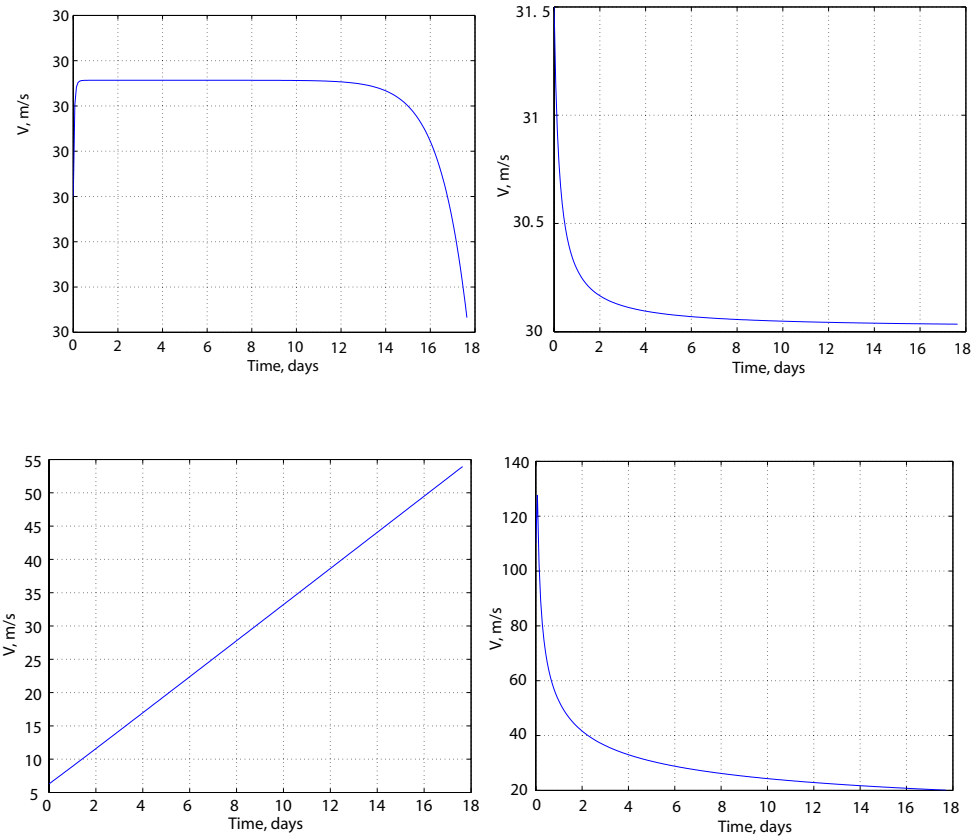

Figure 6.4: The total speed for Maneuver (1) (upper left), Maneuver (2) (upper right), Maneuver (3) (lower left) and Maneuver (4) (lower right.)

has superior performance than the formation in Maneuver (4). During the second phase the reverse is true. Figure (6.9) is a surface plot of the difference between the Γ functions of Maneuvers (1) and (4). Computing the imaging performance measure (6-3.1) one finds that Maneuver (4) has an overall smaller imaging performance measure than Maneuver (1) (Table (1).) This implies that the bonus coverage the formation in Maneuver (4) achieves at high frequencies outweighs the deficient coverage at low frequencies. If the imaging performance is restricted to the resolution disc only, then Maneuver (1) will achieve better imaging performance than Maneuver (4) because the latter leaves gaps at low frequencies.

On the other hand, because the spacecraft in Maneuver (4) is forced to move at

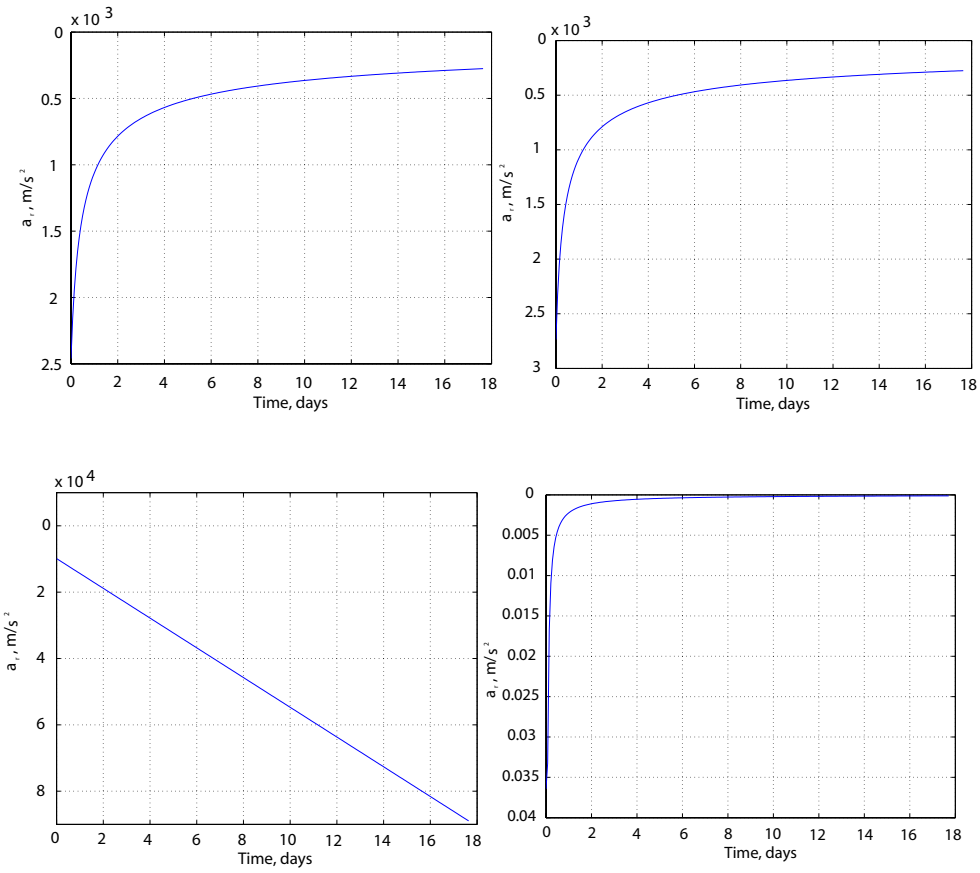

Figure 6.5: Radial acceleration, u_n, for maneuver (1) (upper left), Maneuver (2) (upper right), Maneuver (3) (lower left) and Maneuver (4) (lower right.)

a speed lower than that in Maneuver (1), more fuel is required to slow it down than that in Maneuver (1). Indeed, Maneuver (4) results in the least efficient maneuver as far as fuel consumption is concerned but it is the most efficient in terms of image quality.

Table (1) shows a summary of the performance of all four maneuvers. We note that, as one might expect, Maneuvers (1) and (2) perform almost equally. Both result in intermediate image quality and fuel expenditure. Maneuver (3) requires the least amount of fuel but with the poorest performance. The reverse statement is true for Maneuver (4). Therefore, this result suggests that there exists a tradeoff between image quality and fuel expenditure.

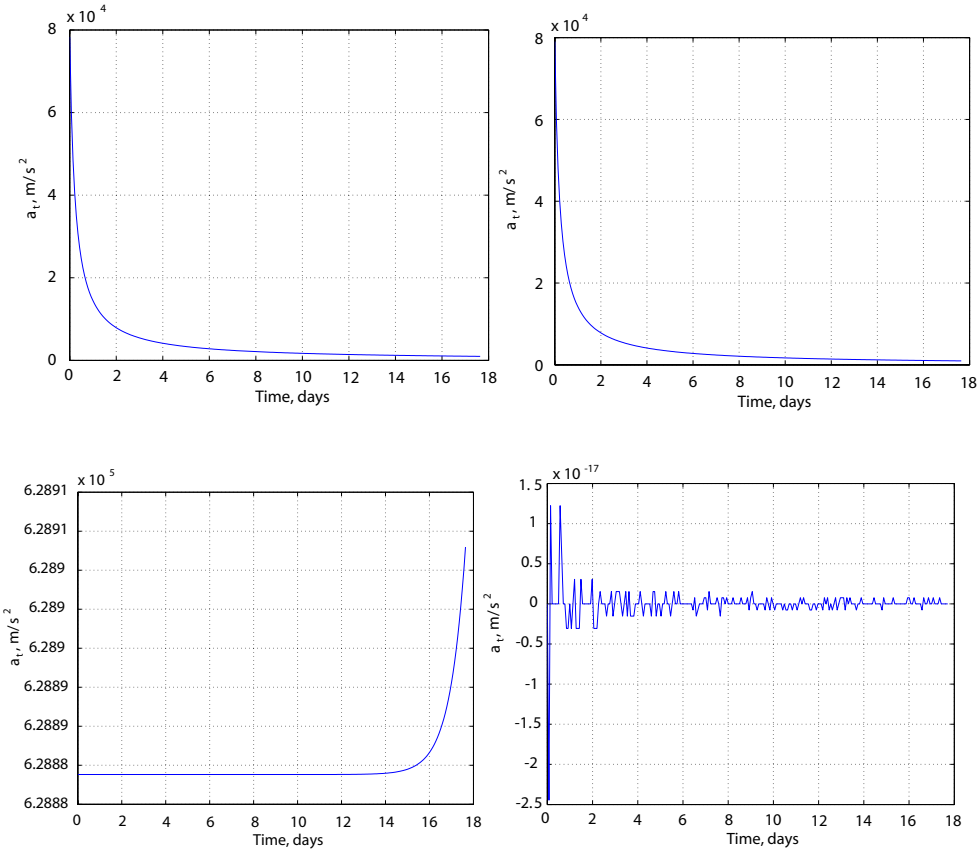

Figure 6.6: Tangential acceleration, u_t, for Maneuver (1) (upper left), Maneuver (2) (upper right), Maneuver (3) (lower left) and Maneuver (4) (lower right.)

	$\mathcal{I}$, $\times 10^9$	$\mathcal{U}$, m/s
Maneuver (1)	5.14	0.53
Maneuver (2)	5.13	0.55
Maneuver (3)	6.27	0.46
Maneuver (4)	4.62	15.02

Table 6.1: Performance measures for Maneuvers (1)-(4).

Note that the imaging performance index (6-3.1) is a function of the final time, T. As T is increased sufficiently the above result will change. For instance, in the limit as T approaches infinity, the partial coverage ($\Gamma < 1$) that Maneuver (4) leaves behind at low frequencies represents a nonzero constant quantity which is being integrated over an infinite time horizon. Thus, the resulting performance index will

be infinite, which means that Maneuver (4) is infeasible in the limit. For Maneuver (1), on the other hand, satisfying the critical speed threshold, v^*, ensures that for all past coverage we have $\Gamma = 1$. However, note that the integral computed up to any finite point in time will be nonzero due to the remaining uncovered region of the resolution disc. Moreover, any maneuver that results in $\Gamma = 1$ everywhere in the resolution disc with a finite imaging performance index in finite time, such as Maneuver (1), is also expected to do so in the limit as T approaches infinity. Thus we see that in the limit as T approaches infinity Maneuver (1) will be feasible whereas maneuver (4) will be considered infeasible.

6.4 Dual Spiraling on a Paraboloid

Let us now consider having the collector spacecraft evolve on a virtual paraboloid, whose axis of symmetry coincides with the common formation line of sight, in three dimensional space as shown in Figure (6.10). The paraboloid results in improved focusing properties for the constellation [36]. Combining this new constraint with spiral such that the collector spacecraft evolves on a spiral embedded on the paraboloid should result in both improved focusing properties as well as improved signal content (the effect of covering the frequency plane using a spiral maneuver.)

A third important consideration to take into account is signal-to-noise ratio (SNR) of the reconstructed image. It is desired that all frequencies in $\mathcal{D}_R$ be sampled while maximizing SNR. Recalling the discussion at the end of Section (2.2), SNR can be controlled by controlling the relative speed (projected on the observation plane, which is perpendicular to the line of sight) between the spacecraft in the formation (see Chapter 2 and [5, 40].) As the projected relative speed between the spacecraft pair is minimized, the achievable SNR is maximized. Intuitively, as a spacecraft

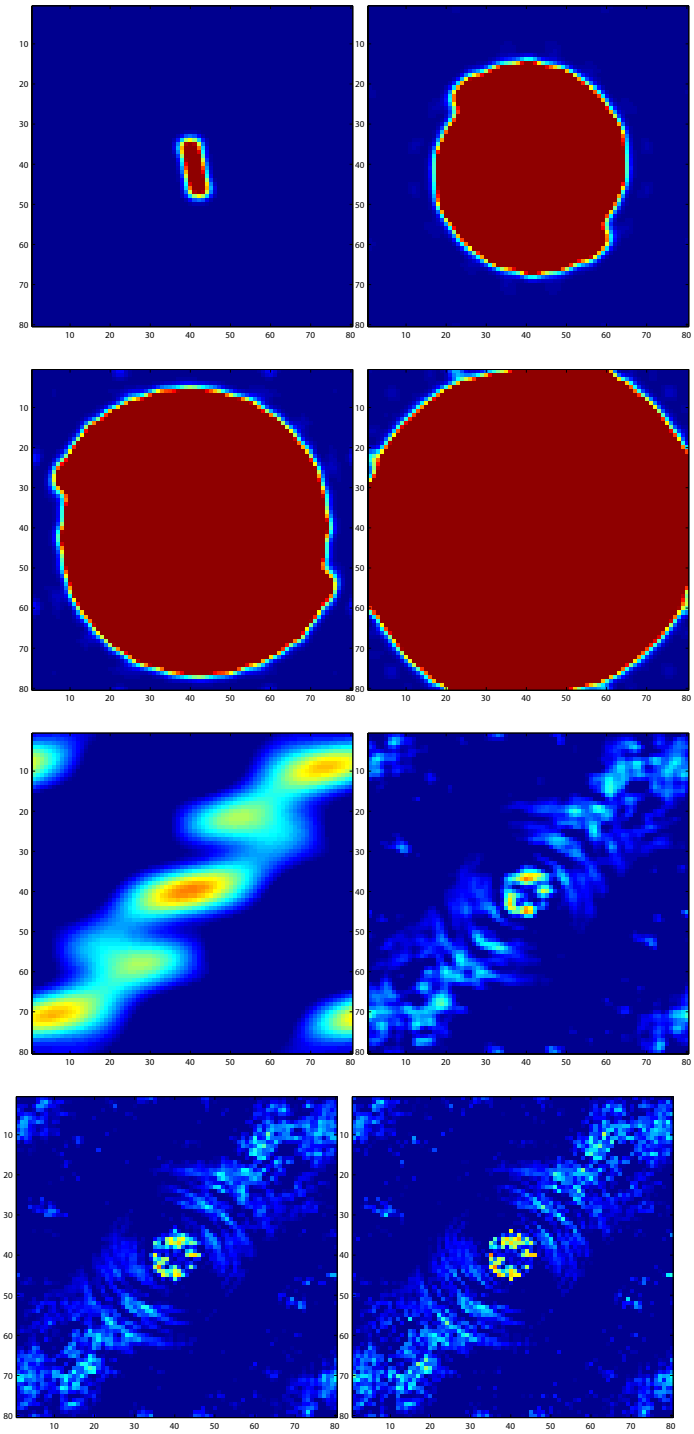

Figure 6.7: Γ (top four figures) and estimated image (bottom four figures) at $t = 0$, at $t = 5.9$ days, at $t = 11.8$ days and at $t = 17.7$ days for Maneuver (1).

moves slower, it spends more time in the neighborhood of a relative position state in space. This leads to more photon (that is, image information) collection from

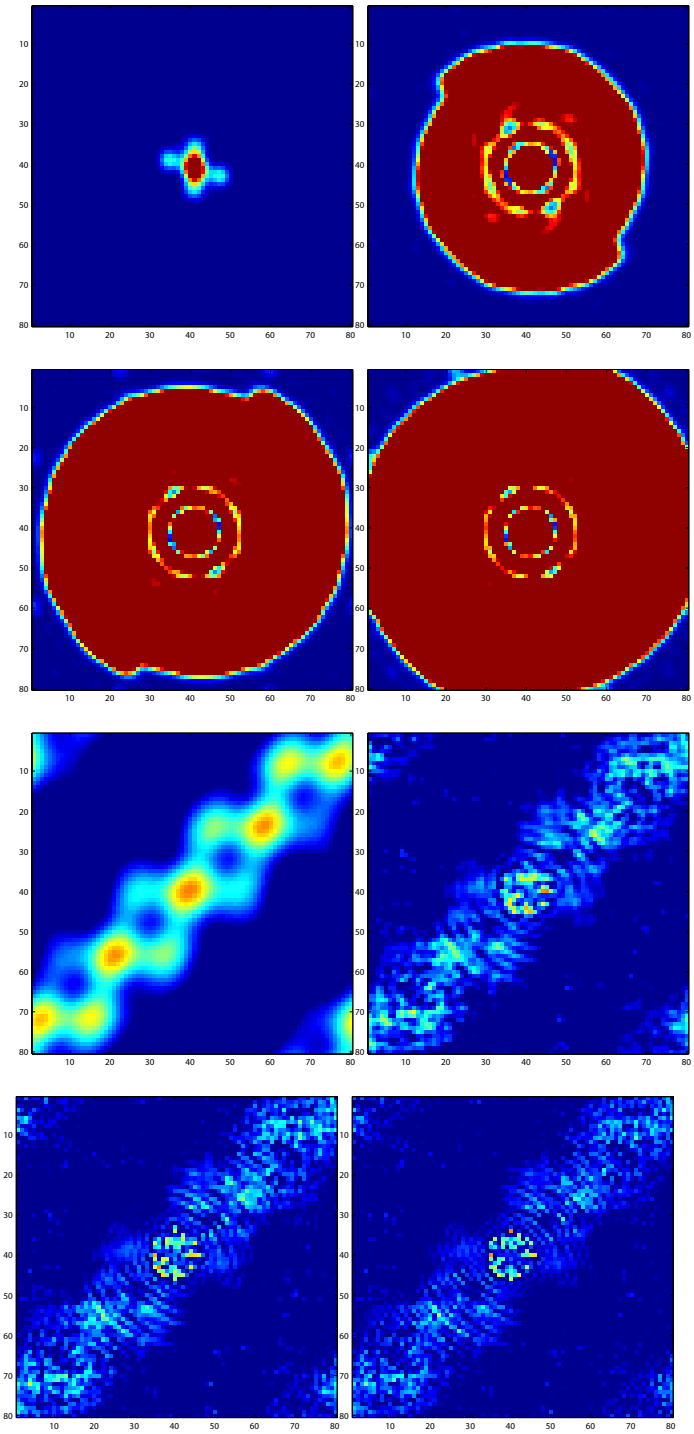

Figure 6.8: Γ (top four figures) and estimated image (bottom four figures) at $t = 0$, at $t = 5.9$ days, at $t = 11.8$ days and at $t = 17.7$ days for Maneuver (4).

that neighborhood, resulting in a stronger signal. This is analogous to the notion of exposure time in photography, where the longer the shutter time, the more photons

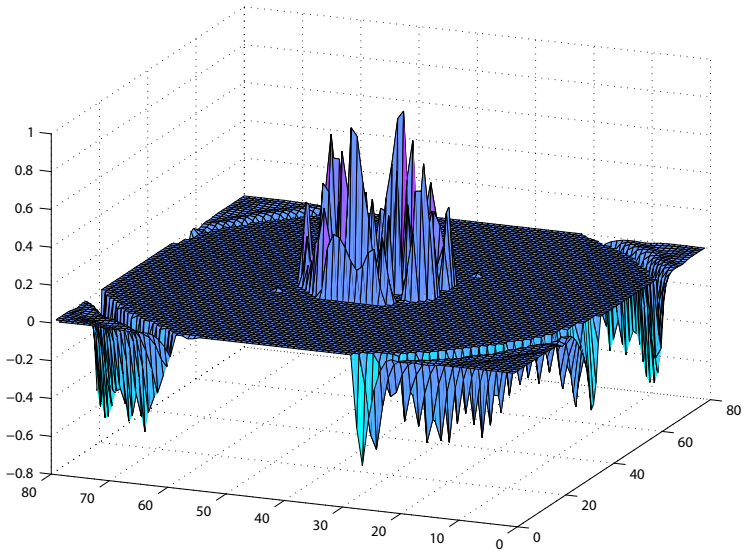

Figure 6.9: $\Gamma_1 - \Gamma_4$.

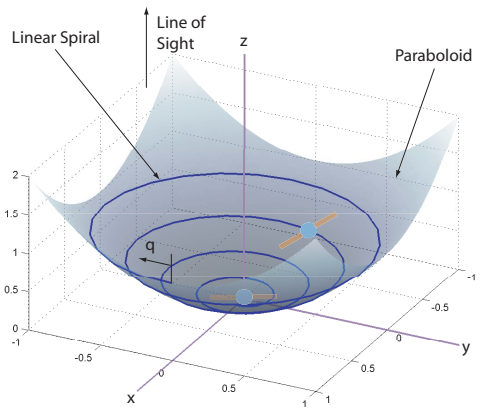

Figure 6.10: The basic interferometer.

get deposited on the photographic film and the better is the image.

The above provides a guideline for the formulation of an optimal control problem. The problem we consider is slightly different than the τ-elastic variational or the dynamic coverage problems considered in Chapter 5 and in [40, 38, 43] in that it is a restricted version of these problems to handle the dual-spacecraft formation described

above. The spacecraft are modeled as point particles. With the combiner spacecraft fixed at the focus of the paraboloid, the collector is constrained to move along a spiral embedded on a paraboloid, which is a one dimensional manifold. Hence, the system possesses only a single degree of freedom, which is the motion on the one dimensional manifold. SNR is taken into account by attempting to minimize a cost functional that is a weighted sum of the projected relative speed and fuel. The goal is to solve for the time parametrization of the control vector that minimizes the cost functional and reconstruct the time history of the collector spacecraft's traversal of the spiral curve embedded on the manifold.

Here is how the rest of the chapter is organized. In Section (6.5), we briefly review the various aspects of image reconstruction. In Section (6.6), we give a general description of the model in three dimensions and define the various variables involved in the three-dimensional situation. With this done, we are in a position to define the optimal control problem and derive the necessary optimality conditions. These necessary conditions are shown to also be sufficient by proving that the optimal control problem is strictly convex. Strict convexity also guarantees that a solution of the optimality conditions is in fact unique. This is done in Section (6.7). In Section (6.8), we apply a continuation method to solve the necessary and sufficient conditions and verify that, indeed, they are solutions by showing that the Hamiltonian is constant along the trajectory. This furnishes the unique optimal trajectory. We conclude with some final remarks on future work in Section (6.9).

6.5 Imaging and the Coverage Problem

In this section we briefly review the various aspects of multi-spacecraft interferometric imaging given in Section (3.2). The discussion is for a generic formation

of any number of spacecraft. In later sections, we specialize the discussion to dual spacecraft interferometry. Consider a formation of N spacecraft. Let $\mathbf{q}_i$ denote the coordinates of the i^{th} spacecraft, $i \in \mathcal{I} = \{1, \ldots, N\}$. For later development, consider $\mathbf{q}_i$ to belong to some one- or two-dimensional continuously differentiable manifold M embedded in $\mathbb{R}^3$. Also let $\mathbf{q}_i = (x_i, y_i, z_i)$ denote the position of the i^{th} spacecraft in $\mathbb{R}^3$. In general, we have

$$\mathbf{q}_i = (x_i, y_i, z_i) \quad = \quad \mathbf{f}(\mathbf{q}_i), \tag{6-5.1}$$

where $\mathbf{f} : M \to \mathbb{R}^3$ is a continuously differentiable mapping on M.

Let $O = \mathbb{R}^2$ be the observation plane (see Figure (6.10.) The observation plane is a plane perpendicular to the line of sight (which we assume to be along the z-direction in $\mathbb{R}^3$) and whose origin coincides with the point $(0, 0, 0)$ (that is, the origin of $\mathbb{R}^3$.) Assume that the maximum displacement along the line of sight of any spacecraft in the formation is bounded above by ε. That is to say $z_i < \varepsilon$. Let $\bar{z}$ denote the range from the observation plane to the target to be imaged. As shown in Chapter 2, if $\varepsilon \ll \bar{z}$, then any inter-spacecraft off-set along the line of sight between the spacecraft in the formation does not affect the quality of the reconstructed image [5]. Since the goal in the Origins program is to reconstruct images of extra-solar objects, the assumption that $\varepsilon \ll \bar{z}$ is valid.

Hence, in extra-solar interferometric imaging, we are interested in the relative position dynamics as projected onto the observation plane O. We are therefore interested in the projected relative trajectories:

$$\tilde{\mathbf{q}}_{ij}(t) \quad = \quad \mathbb{P}\left(\mathbf{q}_j(t) - \mathbf{q}_i(t)\right), \tag{6-5.2}$$

where $\tilde{\mathbf{q}}_{ij} : [0, T] \to O$ are curves on O and $\mathbb{P}$ is the mapping that projects relative trajectories in M onto the observation plane O. Note that $\mathbb{P} = \mathbb{P}_{xy} \circ \mathbf{f}$, where

$\mathbb{P}_{xy} : \mathbb{R}^3 \to \mathbb{R}^2$ is a linear projection mapping having the matrix representation

$$\begin{bmatrix} 1 & 0 & 0 \\ 0 & 1 & 0 \end{bmatrix}. \tag{6-5.3}$$

In multi-aperture interferometry, there are two main imaging goals. The first is simply referred to as frequency domain coverage. Here, we only state the coverage goal and refer the reader to [5] for a more detailed discussion. We are interested in having the resolution disc as defined by the set $\mathcal{D}_R = \left\{ (\nu_x, \nu_y) : \sqrt{u^2 + v^2} \leq 1/\theta_r \right\}$ be completely covered by some ball of radius r_p centered at $\lambda\tilde{\mathbf{q}}_{ij}(t)$, for some $t \in [0, T]$, i and j, where θ_r is the angular resolution and λ is the wavelength of the electromagnetic signal of interest. An image is said to be successfully completed if a maneuver $\mathcal{M}$ satisfies the following condition.

Definition 6.5.1. (**Successful Imaging Maneuver**) An imaging maneuver $\mathcal{M}$ is said to be successful if, for each $(\nu_x, \nu_y) \in \mathcal{D}_R$, there exists a time $t \in [0, T]$ and some $i, j = 1, \ldots, N$ such that $(\nu_x, \nu_y) \in \bar{B}_{r_p}\left(\lambda\tilde{\mathbf{q}}_{ij}(t)\right)$, where $\bar{B}_x(\mathbf{y})$ is a *closed* ball in $\mathbb{R}^2$ of radius x centered at $\mathbf{y}$. r_p is proportional to the size of the telescope's airy disc.

The second objective is that all frequencies in $\mathcal{D}_R$ must be sampled while maximizing the signal-to-noise ratio (SNR.) SNR can be controlled by controlling the relative speeds between the spacecraft in the formation [5]. As the projected relative speed, denoted by $\|\dot{\tilde{\mathbf{q}}}_{ij}\|$, between a spacecraft pair is minimized, so is the achievable SNR. Intuitively, as a spacecraft moves more slowly, it has more time spent in the neighborhood of a relative position state in space. This leads to more photon (that is, image information) collection from that neighborhood, resulting in a stronger signal. This is analogous to the notion of exposure time in photography, where the longer the shutter time is, the more photons get deposited on the photographic film and the better the image gets.

6.6 A Class of Dual-Spacecraft Interferometers

In this section we state the two geometric constraints imposed on the position of the collector spacecraft. We also derive the equations of motion of the collector spacecraft in terms of a single coordinate, which we choose to be the arc length traversed by the collector along the spiral.

6.6.1 The Paraboloid Virtual Surface

The combiner spacecraft carries the ability to delay any wavefront it receives in its own aperture by an amount equal to twice the distance to the center of the paraboloid, thus simulating the delay for a ray that passes through the focus and reflects back to it. The collector spacecraft flies anywhere along the paraboloidal surface, carrying a mirror that reflects a second segment of the wavefront to the combiner at the focus, which then interferometrically combines the light from the two received apertures to synthesize a baseline equal to the perpendicular separation of the two spacecraft. Because optical delay lines are difficult to build with large delays, one can then chose to use a very deep virtual paraboloid, and fly the collector spacecraft far up "above" the focal-point spacecraft, allowing for a much longer baseline than the focal spacecraft's length of delay for its local wavefront might indicate. However, the main reason for a paraboloid surface choice for the collector spacecraft is that a plane wavefront reflecting off a paraboloidal surface will come to a common focus.

In cartesian coordinates a generic paraboloidal surface is described by:

$$z = \frac{1}{2}\left(\frac{\rho^2}{\beta^2} - \beta^2\right), \tag{6-6.1}$$

where

$$\rho = \sqrt{x^2 + y^2}$$

and β is a parameter that controls the depth of the paraboloid. Note that vertex of the paraboloid is located at the point $(0, 0, -\beta^2/2)$.

6.6.2 The Spiral Maneuver

In the x-y plane, the projected position may be given in terms of polar coordinates (ρ, θ). One way to ensure full coverage of the resolution disc $\mathcal{D}_R$ is to initialize the second spacecraft such that at $t = 0$ we have $(\rho = \frac{1}{\theta_p}, \theta = 0)$, make it follow a linear spiral as a function of θ, and to impose the terminal condition that at $t = T$ we have $\rho = \frac{(m+1)}{2\theta_p}, \theta = \frac{(m-1)\pi}{2})$, where T is the terminal maneuver time. The number m is an integer that is equal to the number of pixels in the reconstructed image and θ_p is a parameter such that $\theta_p = m\theta_r$. This motion implies that the two coverage balls $\bar{B}_{r_p}(\tilde{\mathbf{q}}_{12})$ and $\bar{B}_{r_p}(\tilde{\mathbf{q}}_{21})$ are initialized such that they lie outside the central (fixed) ball $\bar{B}_{r_p}(\tilde{\mathbf{q}}_{00}) = \bar{B}_{r_p}(0, 0)$ and move spirally outwards till they lie outside the resolution disc $\mathcal{D}_R$. Thus ρ and θ are constrained to satisfy

$$\rho(\theta) = k(\pi + \theta), \ \theta \in \left[0, \frac{(m-1)\pi}{2}\right], \tag{6-6.2}$$

where $k = \frac{\lambda}{\pi\theta_p}$. Note that in general we take $\theta \in [0, \infty)$ and not restrict it to the set $[0, 2\pi)$.

Figure (6.1) shows an example of a trajectory in the physical and frequency planes for an object that is located at $\bar{z} = 15$pc (1pc$= 3.085 \times 10^{13}$km), with a field of view that is $\bar{L} = 12,760$km wide, with $m = 17$ pixels and, thus, a pixel size of $L = 750.6$km (i.e. this constellation maneuver is capable of detecting any object whose size is greater than L.) These values correspond to applications such as JPL's Terrestrial Planet Finder (TPF) and they could also be adjusted for Earth imaging applications [3]. In the latter case, the maneuver spans a few meters only, as opposed to few thousands of kilometers.

As shown by the illustration in Figure (6.1), the spiral maneuver is capable of entirely ensuring the coverage of the resolution disc $\mathcal{D}_R$. Hence, it ensures attaining a successful maneuver.

6.6.3 Equations of Motion

Since we have a single spacecraft to control, then the number of spacecraft $N = 1$. Enforcing the constraints (6-6.1) and (6-6.2) one finds that the position of the collector spacecraft in terms of the angular position θ is given by:

$$\mathbf{q}(\theta) = (x, y, z) \quad = \quad \left((k(\pi + \theta)\cos\theta, k(\pi + \theta)\sin\theta, \frac{1}{2}\left(\frac{k^2}{\beta^2}(\pi + \theta)^2 - \beta^2\right)\right). \tag{6-6.3}$$

We will use the arc length q traversed along the spiral as the single global coordinate on the one-dimensional manifold M. The arc length q is obtained as a function of θ using the definition of the arc length of a curve in space:

$$q(\theta) = h(\theta) = \int_0^\theta \left\| \frac{\partial \mathbf{q}(\theta')}{\partial \theta'} \right\| \mathrm{d}\theta',$$

where

$$\frac{\partial \mathbf{q}}{\partial \theta} \quad = \quad [k\cos\theta - k\,(\pi + \theta)\sin\theta]\,\mathbf{e}_x + [k\sin\theta + k\,(\pi + \theta)\cos\theta]\,\mathbf{e}_y + \left[\frac{k^2\,(\pi + \theta)}{\beta^2}\right]\mathbf{e}_z, \tag{6-6.4}$$

where $\mathbf{e}_x$, $\mathbf{e}_y$ and $\mathbf{e}_z$ denote unit vectors in the x, y and z directions, respectively. By the geometry of the problem described in previous paragraphs, it is easy to see that the function h is both one-to-one and onto. Hence, given a value for q, one can uniquely solve for θ using

$$\theta = h^{-1}(q). \tag{6-6.5}$$

Though, one can obtain $h(\theta)$ explicitly in terms of θ (we omit it here due to space restrictions), there does not seem to an analytic expression for h^{-1}.

Let $\mathbf{e}_t$ and $\mathbf{e}_n$ denote the unit vectors tangent and normal unit vectors at a point $q(t) \in M$, respectively. If we $\mathbf{v} = v\mathbf{e}_t = \dot{q}\mathbf{e}_t$ denote the velocity of the collector spacecraft, $\mathbf{a} = u_t\mathbf{e}_t + a_n\mathbf{e}_n$ its acceleration and $\mathbf{u} = u_t\mathbf{e}_t + u_n\mathbf{e}_n$ the thrust vector applied to the collector, then the equations of motion are written in path-variable form as [63]:

$$\begin{aligned} \dot{q} &= v \\ \dot{v} &= u_t, \end{aligned} \tag{6-6.6}$$

where we assume a unit mass for the collector spacecraft. Note that the normal component of the control vector is constrained to satisfy:

$$u_n = a_n = \frac{v^2}{R(\theta)}, \tag{6-6.7}$$

where $R(\theta)$ is the radius of curvature of the curve M expressed in terms of the polar angle location θ. R is given by $\frac{1}{R} = \left\| \frac{\mathrm{d}\mathbf{e}_t}{\mathrm{d}q} \right\| = \|(\mathrm{d}\mathbf{e}_t/\mathrm{d}\theta) \cdot (\mathrm{d}\theta/\mathrm{d}q)\|$. In terms of θ, we find that[1]

$$\frac{1}{R(\theta)} = \frac{r(\theta)\left[k^2(\pi+\theta)^2 + \beta^4\left(1+(\pi+\theta)^2\right)\right]}{\sqrt{\beta^4\left(2+(\pi+\theta)^2\right)^2 + k^2\left(1+(\pi+\theta)^2\left(3+(\pi+\theta)^2\right)\right)}}.$$

In computing the curvature, we have used:

$$\mathrm{d}q = r(\theta)\mathrm{d}\theta = \left\| \frac{\partial h}{\partial \theta} \right\| \mathrm{d}\theta, \tag{6-6.8}$$

where

$$r(\theta) = k\sqrt{1 + \left(1 + \frac{k^2}{\beta^4}\right)(\pi+\theta)^2}. \tag{6-6.9}$$

---

[1] All symbolic computations were verified in Mathematica®.

6.7 Necessary and Sufficient Optimality Conditions

In this section we first formulate an optimal control problem and use the maximum principle to derive the necessary conditions. We then show that the problem is convex and, hence, that the necessary optimality conditions are also sufficient.

With the two geometric constraints imposed on the collector spacecraft, we have achieved a successful maneuver (by virtue of the paraboloid constraint) and achieved improved focusing properties (by virtue of the paraboloid constraint.) We are then left with only one degree of freedom, namely the time parametrization of the arc length $q(t)$. This may finally be determined by formulating an optimal control problem that aims at choosing the time parametrization that minimizes the speed and fuel expenditure of the collector spacecraft, which are the last two criteria to be considered in the motion path planning problem for the dual-spacecraft interferometer.

The goal is to minimize the cost functional:

$$\mathcal{J} = \int_0^T \frac{1}{2} \langle \mathbf{u}, \mathbf{u} \rangle + \frac{\tau^2}{2} \langle \tilde{\mathbf{v}}, \tilde{\mathbf{v}} \rangle \, \mathrm{d}t \tag{6-7.1}$$

subject to the dynamic constraints (6-6.6) and the boundary conditions:

$$q(0) = 0, \ v(0) = v_0, \ q(T) = q_T, \ v(T) = v_T, \tag{6-7.2}$$

where $q_T = h\left(\theta = \frac{(m-1)\pi}{2}\right)$. In Equation (6-7.1), $\tilde{\mathbf{v}} = \dot{\tilde{q}}$ is the projected velocity of the collector on the x-y plane and $\mathbf{u} = u_t \mathbf{e}_t + u_n \mathbf{e}_n$ is the total thrust vector. $\langle \cdot, \cdot \rangle$ denotes the Euclidean inner product defined on $\mathbb{R}^3$.

To compute $\tilde{\mathbf{v}}$ in terms of q and $\dot{q}$, we first need to obtain an expression for $\dot{\theta}$ in terms of q and $\dot{q}$. Differentiating Equation (6-6.4), we obtain

$$\dot{q} = r(\theta)\dot{\theta}, \tag{6-7.3}$$

where $r(\theta)$ is given by Equation (6-6.9). Using this and Equations (6-6.3) and (6-6.5), we have:

$$\tilde{\mathbf{v}} = \dot{x}\mathbf{e}_x + \dot{y}\mathbf{e}_y = P_x(\theta, v)\mathbf{e}_x + P_y(\theta, v)\mathbf{e}_y, \tag{6-7.4}$$

where

$$\begin{aligned} P_x(\theta, v) &= \frac{v}{r(\theta)}\Big[k\cos(\theta) - k(\pi+\theta)\sin(\theta)\Big] \\ P_y(\theta, v) &= \frac{v}{r(\theta)}\Big[k\sin(\theta) + k(\pi+\theta)\cos(\theta)\Big]. \end{aligned}$$

In fact, one can show that

$$\langle \tilde{\mathbf{v}}, \tilde{\mathbf{v}} \rangle = \frac{k^2 v^2}{r^2(\theta)}\left[1 + (\pi+\theta)^2\right]. \tag{6-7.5}$$

Hence the cost is given by:

$$\frac{1}{2}u_t^2 + \frac{v^4}{2R^2(\theta)} + \frac{\tau^2}{2}\frac{k^2 v^2}{r^2(\theta)}\left(1 + (\pi+\theta)^2\right). \tag{6-7.6}$$

Note that any variable that is an explicit function of θ is also a function, implicitly, of q via the relation (6-6.5).

We now apply the maximum principle to derive the necessary optimality conditions. First define the pre-Hamiltonian:

$$\hat{H}(\theta, v, u_t, p_1, p_2) = -\frac{1}{2}u_t^2 - \frac{v^4}{2R^2(\theta)} - \frac{\tau^2}{2}\frac{k^2 v^2}{r^2(\theta)}\left(1 + (\pi+\theta)^2\right) + p_1 v + p_2 u_t, \tag{6-7.7}$$

where p_1 and p_2 are the momenta variables. From the necessary optimality condition $\frac{\partial \hat{H}}{\partial u_t} = 0$, we find that $u_t = p_2$. Substituting this into Equation (6-7.7), we get the Hamiltonian function:

$$H(\theta, v, p_1, p_2) = p_1 v + \frac{1}{2}p_2^2 - \frac{v^4}{2R^2(\theta)} - \frac{\tau^2}{2}\frac{k^2 v^2}{r^2(\theta)}\left(1 + (\pi+\theta)^2\right). \tag{6-7.8}$$

The necessary conditions are given by:

$$\begin{aligned}
\dot{q} &= \frac{\partial H}{\partial p_1} = v \\
\dot{v} &= \frac{\partial H}{\partial p_2} = p_2 \\
\dot{p}_1 &= -\frac{\partial H}{\partial q} = -\frac{1}{r(\theta)}\left[\frac{v^4}{R^3(\theta)}\frac{\partial R}{\partial \theta}\right. \\
&\quad \left. -\frac{\tau^2 k^2 v^2}{r^2(\theta)}(\pi+\theta) + \frac{\tau^2 k^2 v^2}{r^3(\theta)}\frac{\partial r}{\partial \theta}\left[1+(\pi+\theta)^2\right]\right] \\
\dot{p}_2 &= -\frac{\partial H}{\partial v} = -p_1 + \frac{2v^3}{R^2(\theta)} + \frac{\tau^2 k^2 v}{r^2(\theta)}\left[1+(\pi+\theta)^2\right].
\end{aligned} \tag{6-7.9}$$

We have used the fact that $\partial q/\partial\theta = r(\theta)$ and used the chain rule in computing the derivative of $r(\theta)$ and $R(\theta)$ with respect to q. Since we have $\dot{q} = v = r(\theta)\dot{\theta}$, the necessary conditions may also be expressed in terms of (θ, v, p_1, p_2) as:

$$\begin{aligned}
\dot{\theta} &= \frac{v}{r(\theta)} \\
\dot{v} &= \frac{\partial H}{\partial p_2} = p_2 \\
\dot{p}_1 &= -\frac{\partial H}{\partial q} = -\frac{1}{r(\theta)}\left[\frac{v^4}{R^3(\theta)}\frac{\partial R}{\partial \theta}\right. \\
&\quad \left. -\frac{\tau^2 k^2 v^2}{r^2(\theta)}(\pi+\theta) + \frac{\tau^2 k^2 v^2}{r^3(\theta)}\frac{\partial r}{\partial \theta}\left[1+(\pi+\theta)^2\right]\right] \\
\dot{p}_2 &= -\frac{\partial H}{\partial v} = -p_1 + \frac{2v^3}{R^2(\theta)} + \frac{\tau^2 k^2 v}{r^2(\theta)}\left[1+(\pi+\theta)^2\right].
\end{aligned} \tag{6-7.10}$$

Since the equations are all stated explicitly in terms of θ and not q, the necessary conditions in the form (6-7.10) are more convenient to use in the computations in the next section.

We now show that the necessary conditions (6-7.9) (equivalently, (6-7.10)) are also sufficient and that there exists a unique solution to the problem. This is done by showing that we have a strictly convex optimal control problem. First, we need the following standard result.

Lemma 6.7.1. *Let $f(x) = h(g(x)) : \mathbb{R} \to \mathbb{R}$, where $g : \mathbb{R} \to \mathbb{R}$ is concave and $h : \mathbb{R} \to \mathbb{R}$ is convex and non-increasing. Then $f(x)$ is convex.*

Proof This is a standard result which is easily proven as follows. Note that $f''(x) = h''(g')^2 + h'g''$, where the prime indicates the derivative with respect to the argument. Since, g is concave, then $g'' \leq 0$ for all x in $\mathbb{R}$. Since h is convex, then $h'' \geq 0$ and since it is non-increasing, then $h' \leq 0$ for all $x \in \mathbb{R}$. This shows that $f''(x) \geq 0$ for all $x \in \mathbb{R}$. Hence, $f(x)$ is convex for all $x \in \mathbb{R}$.

■

Strict convexity is obtained if h were strictly convex and strictly decreasing (that is, $h''(x) > 0$ and $h'(x) < 0$ for all $x \in \mathbb{R}$) and $g(x)$ were strictly concave (that is, $g''(x) < 0$ for all $x \in \mathbb{R}$.)

Since the dynamics (6-6.6) are linear and the variables q, v and u_t are all unconstrained (that is, $q, v, u_t \in \mathbb{R}$) and, hence, belong to trivially convex sets, we only need to show that the cost function in Equation (6-7.1) is strictly convex in q, v and u_t to guarantee sufficiency of the necessary conditions and uniqueness of the solution (see Corollary on page 214 and Theorem 10 on page 216 in [64].) Since the cost (6-7.6) is quadratic in u_t, then it is strictly convex in u_t. It is also strictly convex in v since it is a sum of a quadratic and a fourth power of v (both are strictly convex and the sum of two strictly convex functions is also strictly convex.)

What remains to show is that the cost (6-7.6) is convex in q. This is done by showing that $h_1(\theta) = 1/R^2(\theta)$ and $h_2(\theta) = (1 + (\pi + \theta)^2)/r^2(\theta)$ are convex and non-increasing in θ and that $\theta = h^{-1}(q)$ is concave in q. Since the sum of two convex functions is also convex, then the q-dependent terms of the cost (6-7.6) is convex.

First, note that:

$$h_1'(\theta) = -\frac{\chi_1(\theta)}{k^2\left[k^2(\pi+\theta)^2+\beta^4(1+(\pi+\theta)^2)\right]^4} < 0 \tag{6-7.11}$$

and

$$h_1''(\theta) = \frac{\chi_2(\theta)}{k^2\left[k^2(\pi+\theta)^2+\beta^4(1+(\pi+\theta)^2)\right]^5} > 0 \tag{6-7.12}$$

for all $\theta \in [0,(m-1)\pi/2]$ where

$$\begin{aligned}\chi_1(\theta) &= 2\beta^8(\pi+\theta)\Big[\beta^8(2+(\pi+\theta)^2)(4+(\pi+\theta)^2)\\ &\quad +k^4(3+(\pi+\theta)^2(6+(\pi+\theta)^2))\\ &\quad +2\beta^4k^2(6+(\pi+\theta)^2(6+(\pi+\theta)^2))\Big] > 0\end{aligned}$$

and

$$\begin{aligned}\chi_2(\theta) &= 2\beta^8\Big[3k^6(\pi+\theta)^2(7+(\pi+\theta)^2(10+(\pi+\theta)^2))\\ &\quad +\beta^{12}(-8+(\pi+\theta)^2(2+(\pi+\theta)^2)(19+3(\pi+\theta)^2))\\ &\quad +\beta^8k^2(-12+(\pi+\theta)^2(104+(\pi+\theta)^2(80+9(\pi+\theta)^2)))\\ &\quad +\beta^4k^4(-3+(\pi+\theta)^2(87+(\pi+\theta)^2(85+9(\pi+\theta)^2)))\Big] > 0\end{aligned}$$

for all $\theta \in [0,(m-1)\pi/2]$. Hence, $h_1(\theta)$ is strictly convex and is strictly decreasing for all $\theta \in [0,(m-1)\pi/2]$. For h_1, first write it explicitly in θ:

$$h_2(\theta) = \frac{1+(\pi+\theta)^2}{k^2\left[1+\left(1+\frac{k^2}{\beta^4}\right)(\pi+\theta)^2\right]}.$$

The derivatives of h_2 are given by:

$$h_2'(\theta) = -\frac{2\beta^4(\pi+\theta)}{\left[k^2(\pi+\theta)^2+\beta^4(1+(\pi+\theta)^2)\right]^2} < 0$$

and

$$h_2''(\theta) = \frac{2\beta^4\left[3k^2(\pi+\theta)^2+\beta^4(-1+3(\pi+\theta)^2)\right]}{\left[k^2(\pi+\theta)^2+\beta^4(1+(\pi+\theta)^2)\right]^3} > 0$$

for all $\theta \in [0, (m-1)\pi/2]$. Hence, $h_2(\theta)$ is strictly convex and is strictly decreasing for all $\theta \in [0, (m-1)\pi/2]$. Finally, we need to show that $\theta = h^{-1}(q)$ is strictly concave. Using Equation (6-6.8), we have

$$\frac{\mathrm{d}\theta}{\mathrm{d}q} = \frac{1}{r(\theta)}$$

and

$$\frac{\mathrm{d}^2\theta}{\mathrm{d}q^2} = -\frac{1}{r^2(\theta)}\frac{\mathrm{d}r}{\mathrm{d}\theta}\frac{\mathrm{d}\theta}{\mathrm{d}q}.$$

Since, $\mathrm{d}\theta/\mathrm{d}q = 1/r$ and

$$\frac{\mathrm{d}r}{\mathrm{d}\theta} = \frac{k^2}{r(\theta)}\left(1 + \frac{k^2}{\beta^4}\right)(\pi + \theta)$$

then we have

$$\frac{\mathrm{d}^2\theta}{\mathrm{d}q^2} = -\frac{k^2}{r^4(\theta)}\left(1 + \frac{k^2}{\beta^4}\right)(\pi + \theta),$$

which is strictly negative for all $\theta \in [0, (m-1)\pi/2]$. This shows that $\theta = h^{-1}(q)$ is a strictly concave function of q for all value of θ in the desired range.

The above arguments show that we have a strictly convex problem since we have a strictly convex cost function, linear dynamics and since the space of candidate trajectories $(q(t), v(t), u_t(t)) \in \mathbb{R}^3$, which is trivially convex, for all $t \in [0, T]$. Based on the Corollary on page 214 and Theorem 10 on page 216 in [64], this gives the following result.

Theorem 6.7.1. *The necessary conditions (6-7.9) (or, equivalently, (6-7.10)) are also sufficient. A solution to these necessary and sufficient conditions is the unique optimal solution to the optimal control problem.*

6.8 Numerical Solution

In this section we numerically obtain the unique solution to the necessary and sufficient conditions given by Equations (6-7.9) or (6-7.10). We use Matlab®'s bvp4c.m function, the two-point boundary value problem solver. This uses a simple shooting method that requires an initial guess for the time parameterized states: $q(t)$ (or $\theta(t)$), $v(t)$, $p_1(t)$ and $p_2(t)$. Since an initial guess is hard to obtain, we use continuation method (homotopy) to solve the problem (a general discussion of the method applied to two point boundary value problems can be found in Chapter 7 in [65].) This is done as follows.

First let us re-derive the necessary conditions for the modified cost functional. The goal is to minimize the cost functional:

$$\mathcal{J}_\varepsilon = \int_0^T \frac{1}{2}u_t^2 + \frac{\varepsilon}{2}\left[\frac{v^4}{R^2(\theta)} + \frac{\tau^2 k^2 v^2}{r^2(\theta)}\left(1+(\pi+\theta)^2\right)\right]\mathrm{d}t. \tag{6-8.1}$$

For this cost function, one can show that the Hamiltonian and the necessary and sufficient optimality conditions are given by:

$$H_\varepsilon(\theta, v, p_1, p_2, \varepsilon) = p_1 v + \frac{1}{2}p_2^2 - \frac{\varepsilon}{2}\left[\frac{v^4}{R^2(\theta)}\frac{\tau^2 k^2 v^2}{r^2(\theta)}\left(1+(\pi+\theta)^2\right)\right]. \tag{6-8.2}$$

The necessary conditions are given by:

$$\begin{aligned}
\dot{q} &= v \\
\dot{v} &= p_2 \\
\dot{p}_1 &= -\frac{\varepsilon}{r(\theta)}\left[\frac{v^4}{R^3(\theta)}\frac{\partial R}{\partial \theta}\right. \\
&\quad \left. -\frac{\tau^2 k^2 v^2}{r^2(\theta)}(\pi+\theta) + \frac{\tau^2 k^2 v^2}{r^3(\theta)}\frac{\partial r}{\partial \theta}\left[1+(\pi+\theta)^2\right]\right] \\
\dot{p}_2 &= -p_1 + \varepsilon\left[\frac{2v^3}{R^2(\theta)} + \frac{\tau^2 k^2 v}{r^2(\theta)}\left(1+(\pi+\theta)^2\right)\right].
\end{aligned} \tag{6-8.3}$$

Note that these are still sufficient and that the solution is unique for each $\varepsilon \in [0,1]$. If we set $\varepsilon = 0$, then the necessary and sufficient conditions become:

$$\begin{aligned} \dot{q} &= v \\ \dot{v} &= p_2 \\ \dot{p}_1 &= 0 \\ \dot{p}_2 &= -p_1, \end{aligned}$$

which now form a set of linear differential equations. One can easily solve these differential equations to obtain:

$$\begin{aligned} q(t) &= v_0 t - \frac{t^3}{6} p_1^0 + \frac{t^2}{2} p_2^0 \\ v(t) &= v_0 - \frac{t^2}{2} p_1^0 + t p_2^0 \\ p_1(t) &= p_1^0 \\ p_2(t) &= -t p_1^0 + p_2^0, \end{aligned} \tag{6-8.4}$$

where p_1^0 and p_2^0 are constants given by:

$$\begin{aligned} p_1^0 &= -\frac{6}{T^2}(v_T + v_0) + \frac{12}{T^3} q_T \\ p_2^0 &= \frac{6}{T^2} q_T - \frac{2}{T} v_T - \frac{4}{T} v_0 \end{aligned}$$

and where q_T, v_0 and v_T are the boundary conditions.

In a continuation method, one uses the solution to the problem with $\varepsilon = \varepsilon_0 = 0$ (that is, Equations (6-8.4)) as the initial guess for $\varepsilon_1 = \delta$, where δ is a sufficiently small parameter. Assuming that the problem with $\varepsilon = \varepsilon_1 = \delta$ has been successfully solved, one then uses this solution as the initial guess for the next step with, say, $\varepsilon = \varepsilon_2 = 2\delta$. This is repeated until $\varepsilon = \varepsilon_j = j\delta$ is sufficiently close to $\varepsilon = 1$. At this point, we are able to solve the two point boundary value problem (6-8.3) with $\varepsilon = 1$, which corresponds to the original problem (6-7.9) we are seeking to solve.

Consider the optimal control problem with $\tau = 10$, $\beta = 10$, $T = 1000$ seconds, $q_0 = 0$, $q_T = 5.26 \times 10^5$ km, $v_T = v_0 = 0$ m/s and using the same values used to generate Figure (6.1) which give $k = 1.154 \times 10^4$. The continuation method is applied starting with the explicit solution (6-8.4) (corresponding to $\varepsilon = 0$) with a step size of $\delta = 0.01$. The result is shown in Figure (6.11). In the figure, we plot the solution with $\varepsilon = 0$, $\varepsilon = 0.33$, $\varepsilon = 0.50$, $\varepsilon = 0.67$ and $\varepsilon = 1.0$, which corresponds to the desired solution to our problem. To show that, indeed, the solution is continuous in $q(t)$ and $v(t)$ (which is not clear in Figure (6.11) since solutions roughly overlap), $q(t)$ and $v(t)$ are plotted in Figure (6.12) for $t \leq 100.01$ seconds. One can now see that the solution varies smoothly as a function of ε.

As a final check on the numerical solutions shown in Figure (6.11), the Hamiltonian H_ε must be constant along the motion for every value of ε. Evaluating H_ε for the different values of ε, we get $H_{\varepsilon=0}(t) = 4.982 \times 10^6$ (with 0% deviation from the mean value since this is the exact solution), $H_{\varepsilon=0.33}(t) = 3.74 \times 10^8$ (0.22% deviation), $H_{\varepsilon=0.5}(t) = 5.57 \times 10^8$ (0.23% deviation), $H_{\varepsilon=0.67}(t) = 7.40 \times 10^8$ (0.25% deviation) and $H_{\varepsilon=1}(t) = 1.09 \times 10^9$ (0.26% deviation) on average for all values of time $t \in [0, 1000]$. The small perturbations in the values of the Hamiltonian is attributed to numerical errors involved in the computation, where we note that as ε is increased, the % error increases. The Hamiltonian is plotted in Figure (6.13).

6.9 Conclusion

In this chapter, we reviewed the main elements of formation flying for imaging applications, including the coverage problem. We specialized the discussion to a class of two spacecraft spiraling formations on a paraboloidal surface. The geometry of the problem was described and the governing dynamic equations derived. We

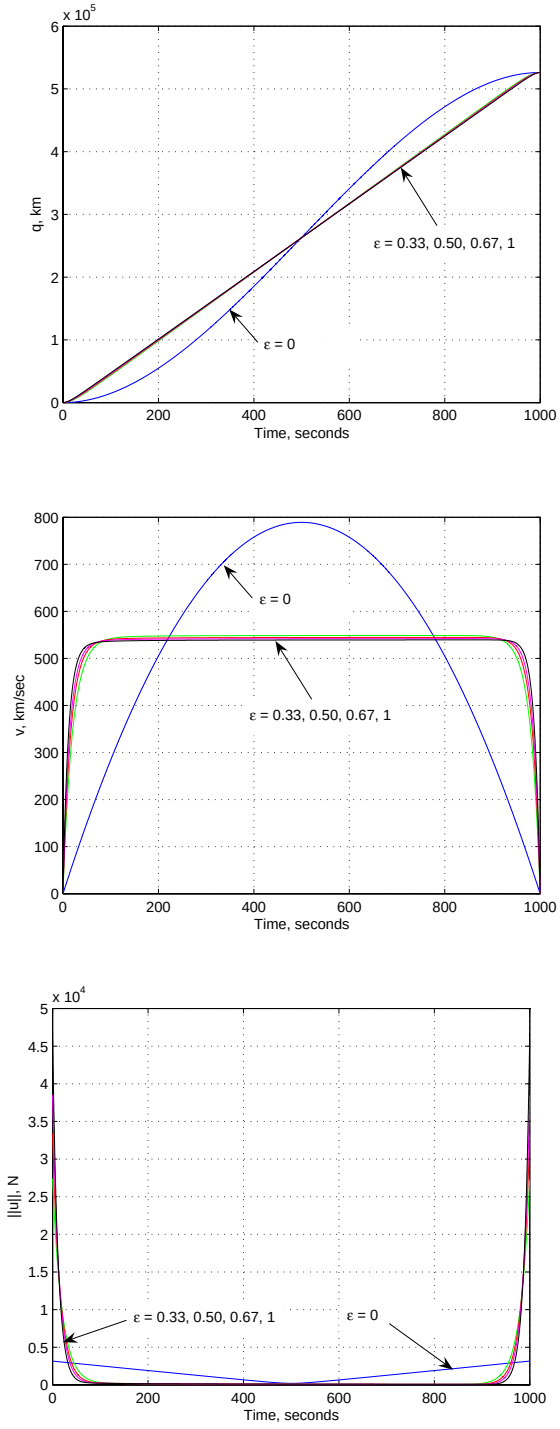

Figure 6.11: $q(t)$, $v(t)$ and $\|u(t)\|$ for $\varepsilon = 0$ (exact solution), $\varepsilon = 0.33$, $\varepsilon = 0.50$, $\varepsilon = 0.67$ and $\varepsilon = 1.00$, which is the desired solution for the optimal control problem.

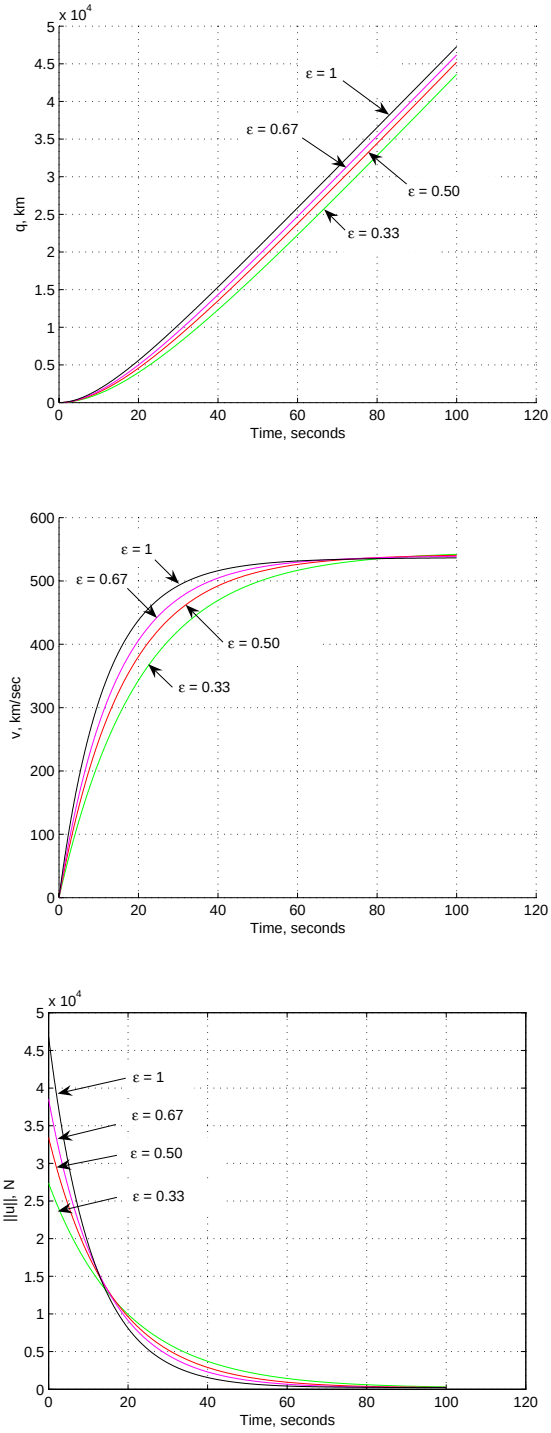

Figure 6.12: $q(t)$, $v(t)$ and $\|u(t)\|$ for $t \leq 1.401$ seconds.

then formulated an optimal control problem that aims to minimize a cost functional composed of a weighted sum of fuel expenditure and the projected relative speed.

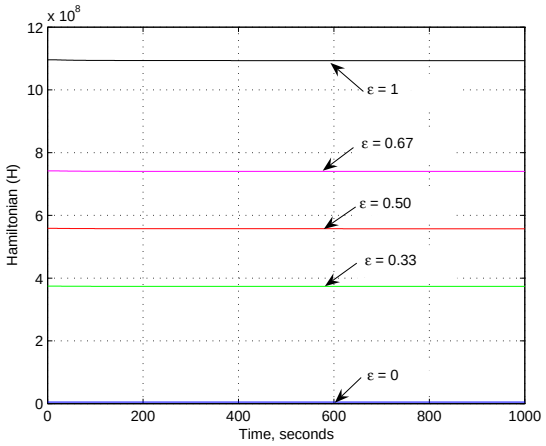

Figure 6.13: Hamiltonian for the cases $\varepsilon = 0$, $\varepsilon = 0.33$, $\varepsilon = 0.50$, $\varepsilon = 0.67$ and $\varepsilon = 1.00$.

This cost function is chosen to both reduce mission fuel costs and improve image quality by increasing SNR. The necessary conditions were derived and were shown to be sufficient. We also showed that the solution is unique. We used a continuation procedure to solve the resulting two point boundary value problem and numerically find the optimal trajectory. Results show evidence of a tradeoff between image quality and fuel expenditure. A parametric study will also be conducted to study the effects of the various model parameters on image quality.

CHAPTER 7

Interferometric Observatories in Earth Orbit

In this chapter we propose a class of satellite constellations that can act as interferometric observatories in Low Earth Orbit (LEO), capable of forming high angular resolution images in time scales of a few hours without the need for active control. First we review the requirements to achieve these imaging goals in Section (7.1). In Section (7.2) we define a class of constellations that can achieve these goals in LEO. An optimization procedure is also defined that supplies m pixels of resolution with a minimum number of satellites. For the example considered, this procedure results in an observatory that is within 0-2 satellites from a lower bound of $\sqrt{m}$ satellites. We introduce a linear imaging constellation and formulate a concise 0-1 mathematical program, the solution of which is the solution to optimal aperture configuration for full coverage of the wave number plane. This is done in Sections (7.3) and (7.4).

The effect of eccentric spacecraft trajectories and gravity field J_2 perturbations on wave number plane coverage are considered in Sections (7.5) and (7.6). Conditions for complete wave number plane coverage are found for certain classes of orbit perturbations. This analysis leads to design criteria for interferometric observatories that ensure wave number plane coverage as a function of perturbation strength. In Section (7.5.1), we show that any perturbation in orbit eccentricity induces lack of

u-v plane coverage. Hence, under J_2 short-period perturbations, the u-v plane is not completely covered since J_2 is sufficient to cause perturbations in eccentricity. In Section (7.5.2), we address short-period J_2 perturbations and derive expressions for in-plane perturbations in position as a function of the orbital elements and obtain an upper bound for the magnitude of the perturbed in-plane position vector. In Section (7.6), we adjust the nominal observatory design in such a way as to guarantee full coverage of the u-v plane under general eccentricity perturbations and short-period J_2 effects.

Finally, in Section (7.8) we discuss some practical implementation issues and the use of the zonal J_2 effect to scan the observatory across the celestial sphere. We conclude the chapter with some final remarks in Section (7.9).

7.1 Review

In this section we summarize the discussion in Section (2.1). Let $\mathbf{q}_{ij}$ be the projected relative position between spacecraft i and j, where $i, j = 0, 1, \ldots, N-1$ and N is the number of satellites, onto the observation plane O. Let $\bar{z}$ be the distance from the image plane to the observation plane. Denote by the term "picture frame" the angular extent of the intended image on the image plane. The picture frame has a diameter of length $\bar{L}$. Pixelating the image plane into an $m \times m$ grid, the size of each pixel is $L = \bar{L}/m$, and the resulting angular resolution is $\theta_r = L/\bar{z}$. Additionally, the angular extent of the desired picture frame is given by $\theta_p = \bar{L}/\bar{z}$, leading to $\theta_p = m\theta_r$.

Recall Figure (7.1). Dimensions of features in the wave number plane are the reciprocals of the corresponding dimensions in the physical plane. Thus the resolution disc is a disc of diameter $1/\theta_r$ and is the region where we desire the MTF to have

nonzero values (henceforth, simply denoted by wave number plane coverage.) The picture frame region is a circular disc of diameter $1/\theta_p$. Therefore, the diameter of the resolution disc is m times the diameter of the picture frame disc in the wave number plane. As the relative position vector of two spacecraft varies in the physical plane, the picture frame disc moves in the wave number plane, where its center follows the trajectory of the vector given by $\pm\mathbf{q}_{ij}/\lambda$, where λ is the imaging wavelength of interest. Each satellite, by itself, will contribute a disc that is centered at the origin with a diameter of $1/\theta_p$, and each pair of satellites will contribute two discs of diameter $1/\theta_p$ located 180 degrees apart with a radius of $\frac{q_{ij}}{\lambda}$ from the center, where $q_{ij} = |\mathbf{q}_{ij}|$. Define the minimum relative distance between satellites to be $d_{\min} = \lambda/\theta_p$. To completely cover the resolution disc in the wave number plane it is sufficient to have satellites distributed such that there exist pairs with relative distances $d_{\min}$, $2d_{\min}$, $\cdots$, $\frac{1}{2}(m-1)d_{\min}$. Let $d_{\max} = \frac{1}{2}(m-1)d_{\min}$.

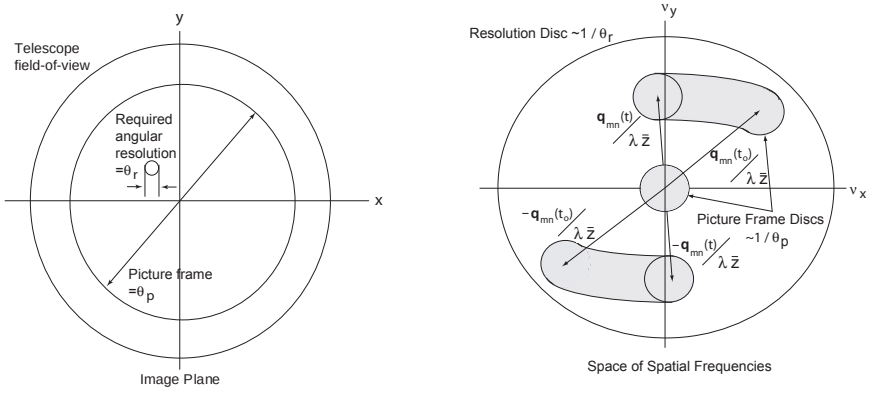

Figure 7.1: Physical and wave number plane variables. To indicate time progress, we show the trajectory on an interval $[t_0, t]$.

7.2 Circular Orbit Constellations

We propose a class of very long baseline constellations that achieves the requirement that the wave number plane be completely covered. The satellite constellation is placed on a circular arc that is a segment of a low Earth orbit and whose center is located at the center of the Earth (see Figure (7.2).) The satellites are distributed such that the second satellite is located at a distance of $d_{\min}$ from the first satellite, the third at $2d_{\min}$ from the first, the fourth at $3d_{\min}$ from the first, and so on. Thus, a constellation of N_f satellites will have the N^{th} satellite located at a distance of $(N-1)d_{\min}$ from the first. This distribution, defined as the "fundamental" constellation, implies that there are $m = 2N_f - 1$ pixels and ensures the complete coverage of the wave number plane, once the constellation is rotated 180$^{\text{o}}$ (i.e. after half an orbit period.) Figure (7.2) shows the geometry of this configuration for $N_f = 3$ satellites ($m = 5$ pixels.) We nominally assume that the orbit plane is perpendicular to the line of sight to the target.

To compute the precise locations of the satellites in the constellation, specify wavelength of interest, λ, and the desired angular extent of the picture frame $\theta_p = \bar{L}/\bar{z}$. Given a number of satellites N_f, or the number of pixels m, one then obtains the corresponding angular resolution, θ_r, and knowledge of θ_p enables us to compute $d_{\min}$ and $d_{\max}$. Throughout this note we use the following values: $\lambda = 10 \times 10^{-6}$m, $\bar{z} = 7.408 \times 10^{14}$km ($\sim$ 24 parsec from the Earth), $\bar{L} = 13 \times 10^{3}$km $r_{\text{o}} = 7,200$km and $d_{\min} = 569.52$km.

Let $\boldsymbol{\imath}$ and $\boldsymbol{\jmath}$ be two orthogonal unit vectors in the orbit plane, the position vector

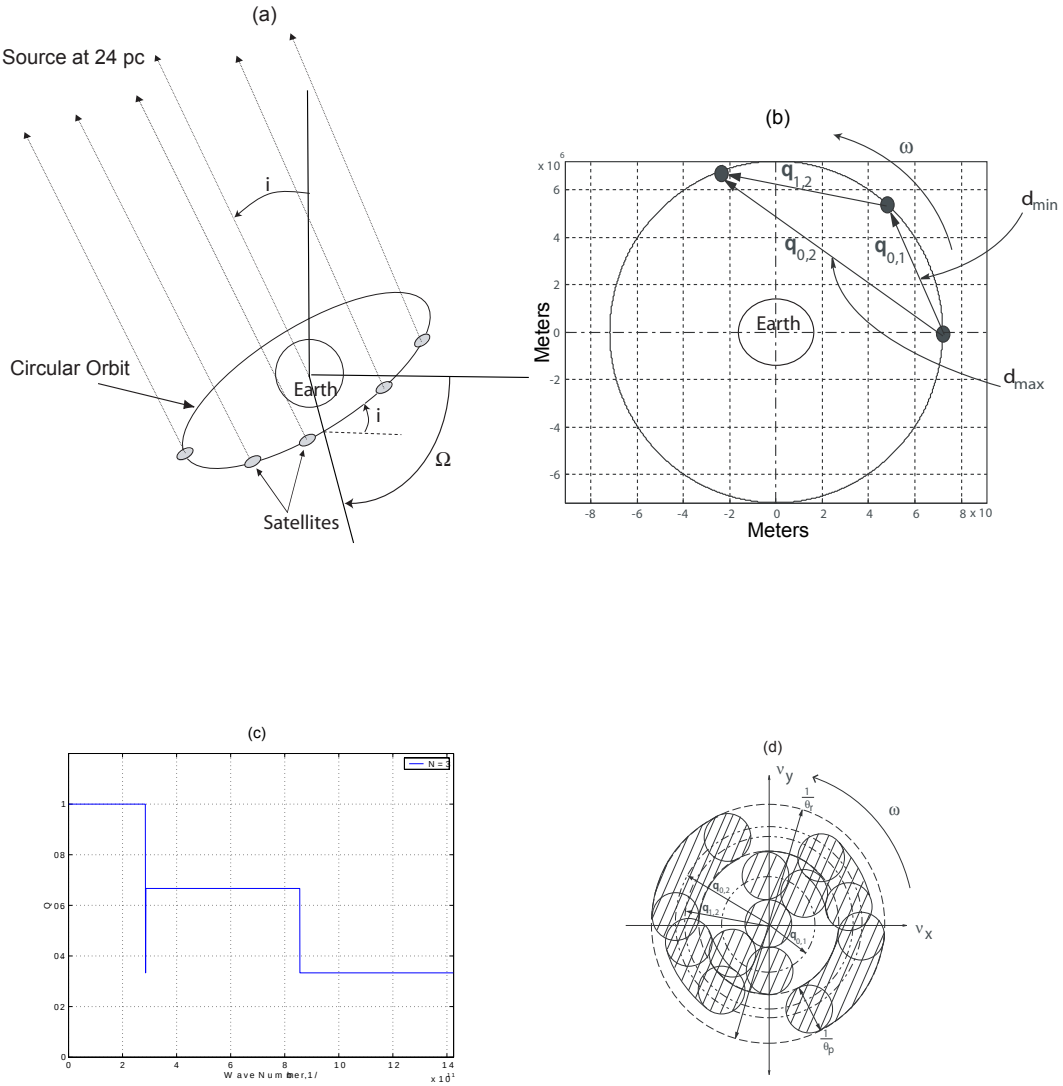

Figure 7.2: (a) A three dimensional sketch of the imaging observatory (not to scale.) (b) Physical distribution in the orbit for $N_f = 3$ (not to scale.) (c) Q curve for $N_f = 3$ in the fundamental constellation. (d) Physical distribution in the wave number plane for $N_f = 3$, $m = 5$ (not to scale.)

of the nth satellite, $n = 0, \cdots, N_f - 1$, is

$$\begin{aligned}\mathbf{q}_n(t) &= r_o\Bigg\{\left[\cos(\omega t)\left(1-\frac{n^2}{2}\left(\frac{d_{\min}}{r_o}\right)^2\right)-\sin(\omega t)n\frac{d_{\min}}{r_o}\sqrt{1-\left(\frac{n}{2}\right)^2\left(\frac{d_{\min}}{r_o}\right)^2}\right]\boldsymbol{\imath}\\ &\quad+\left[\sin(\omega t)\left(1-\frac{n^2}{2}\left(\frac{d_{\min}}{r_o}\right)^2\right)+\cos(\omega t)n\frac{d_{\min}}{r_o}\sqrt{1-\left(\frac{n}{2}\right)^2\left(\frac{d_{\min}}{r_o}\right)^2}\right]\boldsymbol{\jmath}\Bigg\},\end{aligned} \tag{7-2.1}$$

where ω is the orbit angular velocity of the nominal circular orbit

$$\omega = \sqrt{\frac{\mu}{r_o^3}}, \tag{7-2.2}$$

and r_o is the orbit radius. The relative position vector from satellite l to satellite n is given by

$$\begin{aligned}\mathbf{q}_{lk}(t) = d_{\min}\Bigg\{\Bigg[&\cos(\omega t)(l^2-n^2)\frac{d_{\min}}{2r_o} \\ &+\sin(\omega t)\left(-n\sqrt{1-n^2\left(\frac{d_{\min}}{2r_o}\right)^2}+l\sqrt{1-l^2\left(\frac{d_{\min}}{2r_o}\right)^2}\right)\Bigg]\boldsymbol{\imath} \\ &+\Bigg[\sin(\omega t)(l^2-n^2)\frac{d_{\min}}{2r_o}+\cos(\omega t)\left(n\sqrt{1-n^2\left(\frac{d_{\min}}{2r_o}\right)^2}-l\sqrt{1-l^2\left(\frac{d_{\min}}{2r_o}\right)^2}\right)\Bigg]\boldsymbol{\jmath}\Bigg\}.\end{aligned} \tag{7-2.3}$$

In the wave number plane the relative position vector is $\tilde{\mathbf{q}}_{lk} = \mathbf{q}_{lk}/\lambda$, a vector emanating from the origin with its tip at the center of the picture frame disc. Ignoring orbit perturbations, the above satellite arrangement guarantees that each $\mathbf{q}_{lk}$ has a constant magnitude (since they are distributed along the same circular orbit), which is given by

$$\begin{aligned}\tilde{q}_{lk} &= \frac{2r_o\kappa}{\lambda(N_f-1)} \\ &\quad\times\sqrt{\left((l^2-n^2)\frac{\kappa}{N_f-1}\right)^2+\left(n\sqrt{1-\left(\frac{n\kappa}{N_f-1}\right)^2}-l\sqrt{1-\left(\frac{l\kappa}{N_f-1}\right)^2}\right)^2},\end{aligned} \tag{7-2.4}$$

where $\kappa = \frac{d_{\max}}{2r_o}$. Note that $0 < \kappa \leq 1$, where $\kappa \to 0$ as either $d_{\max} \to 0$ or $r_o \to \infty$. The latter case arises if the constellation is placed on an orbit with small curvature. As $\kappa \to 0$ we have $\tilde{q}_{lk} \to d_{\min}/\lambda$. $\kappa = 1$ only when $d_{\max} = 2r_o$ (i.e. when the constellation spans 180°.)

Note that all $\mathbf{q}_{lk}$'s rotate at the same (constant) rate, ω and that this constellation will sweep out the resolution disc in the wave number plane over half an orbit. If the line of sight is tilted away from the orbit normal by an angle ϵ, coverage of the wave number plane will range from full angular resolution θ_r to a minimum angular resolution of $\theta_r \cdot \cos\epsilon$. Figure (7.2) shows the wave number plane coverage for $N_f = 3$. Note that imaging in the opposite direction is possible by rotating the spacecraft 180^o about the radius vector.

For the above parameters, the observatory is performing 1.9461×10^{-6} milli-arcsec imaging at 10μm. Formation keeping and spacecraft pointing of a formation having a maximum baseline of about 14,000km, with a 24pc target and under the influence of J_2, drag and other perturbations is expected to be a difficult control problem. This may require much tighter pointing requirements than the Hubble Space Telescope. However, note that each aperture in our constellation will probably not be as large as and will not involve as many flexible structures as the Hubble Space Telescope. Moreover, note that since all the spacecraft lie on the same circular orbit, they will all be subject to the same differential perturbations, whose short-term effects are small. Still, these short-term effects can be accounted for by performing accurate relative position measurements between the spacecraft -an issue that is not specific to our observatory, but that is common to a typical interferometric formation.

7.3 Minimizing the number of satellites for a given resolution

In the fundamental constellation, we define the "fundamental" baselines by $\mathbf{q}_{0,n}$ ($n = 0, \ldots, N-1$) and the "bonus" baselines by $\mathbf{q}_{l,n}$, $l \neq 0$. By themselves, the fundamental baselines guarantee complete coverage of the wave number plane over

half an orbit period, and the bonus baselines provide redundant coverage. For large N_f, there will be an excessive number of multiple coverage areas, implying that the number of satellites can be reduced with the resolution disc still being completely covered.

To carry out this minimization it is not necessary to consider the two dimensional wave number plane, and is sufficient to consider the one dimensional wave number space. Define a ray in the wave number plane parameterized by the radius $\nu \in [0, \nu_{\max}]$, where $\nu_{\max} = 1/(2\theta_r)$. Let the contribution of each pair of satellites (l, n) to the image coverage be given by

$$f_{ln}(\nu) = \begin{cases} 1 & \text{if } \nu \in [\tilde{q}_{ln} - \frac{\bar{d}_{\min}}{2}, \tilde{q}_{ln} + \frac{\bar{d}_{\min}}{2}] \\ 0 & \text{otherwise} \end{cases}, \tag{7-3.1}$$

for $l = 0, \ldots, N-1$ and $n = l, \ldots, N-1$, where $\bar{d}_{\min} = d_{\min}/\lambda$. Next, define the function $Q(\nu) = \frac{1}{N} \sum_{l=0}^{N-1} \sum_{n=l}^{N-1} f_{ln}(\nu)$ which is the superposition of all contributions. Figure (7.2) shows Q for $N = N_f = 3$ ($m = 5$ pixels) and Figure (7.3) shows Q for $N_f = 16$ ($m = 31$.) For the $N_f = 1$, 2, 3 and 4 cases removing any satellite will immediately cause a portion of the resolution disc to not be covered, thus the minimum number of satellites for these cases is $N_{\min}(m) = \frac{1}{2}(m+1)$. For larger numbers of satellites (i.e., larger number of pixels, m) this is not true.

Our current minimization problem is stated as: "Starting from a fundamental constellation, with a corresponding fixed number of pixels m, maximize the number of satellites that can be removed from the constellation under the constraint that $Q(\nu) > 0$ on the interval $\nu \in [0, \nu_{\max}]$." The constraint ensures complete coverage of the wave number line, meaning that each point on the line is covered by at least one satellite pair. Satellite arrangements that violate the lower bound are immediately discarded as they will have "gaps" in the wave number line, which lead to spatial

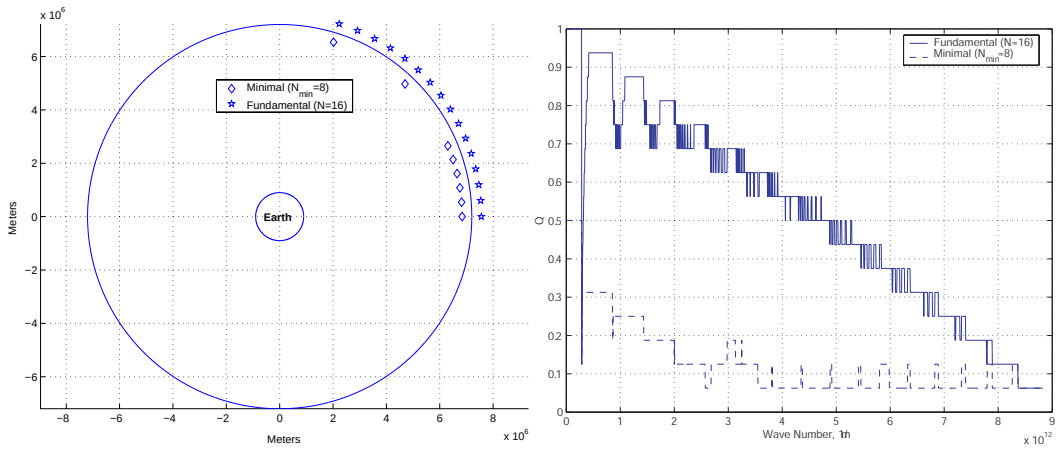

Figure 7.3: Fundamental and minimal distributions (not to scale) and Q curves for $m = 31$.

frequencies that will not be covered.

To solve this problem, an algorithm was implemented that computes the Q function for the fundamental constellation and all its subsets, found by removing one satellite at a time, two at a time, and so forth. Satellite combinations that violate the lower threshold are discarded and the remaining solutions with a minimum number of satellites, $N_{\min}(m)$, constitute the minimal set. Note that for a given m there may be several different constellations with the same, minimum, number of satellites.

In a fundamental constellation of N_f satellites, there are up to

$$\sum_{n=1}^{N_f} \left(\begin{array}{c} N_f \\ \\ n \end{array} \right) = 2^{N_f} - 1 \qquad \text{(7-3.2)}$$

trials that this algorithm may need to make, for large N_f this is unreasonably large. There are, however, numerous ways to speed up the computation by restricting the space of trials considered, some of which have been used in our computations. This algorithm has been implemented for $m = 3, 5, 7, \ldots, 39$, the results summarized in Table (1). Figure (7.3) shows Q for a fundamental constellation of $N_f = 16$ satellites ($m = 31$ pixels) and a minimum of $N_{\min}(31) = 8$ satellites. The $N_{\min}$ curve

shown is the one that maximizes the area under the Q curve over all the 28 possible constellations with 8 satellites, and is comprised of satellites $0, 1, 2, 3, 4, 5, 10$ and 15. It is important to note that the minimal sets may change with the factor $\frac{d_{\min}}{r_o}$ in Equation (7-2.4).

A lower bound on the size of a constellation can be determined as follows. For a constellation of N satellites, there are exactly

$$\begin{pmatrix} N \\ 2 \end{pmatrix} = \frac{1}{2} N (N-1)$$

baselines. Each baseline provides 2 pixels, plus one for the self pixels giving a total of $m = N(N-1) + 1$. Thus a lower bound on the number of satellites to cover m pixels is given by:

$$N_{lb} = \text{int}^+ \left[\frac{1}{2} \left(1 + \sqrt{4m - 3} \right) \right],$$

where $\text{int}^+ [x]$ is the smallest integer larger than or equal to x. A solution can have no fewer than this number of satellites in the constellation without having gaps in the wave number plane. Moreover, there may not exist solutions with $N_{\min} = N_{lb}$. For example, for $m = 15$ the minimal solution has $N_{\min} = 5$, which is equal to the lower bound. For $m = 29$ the minimal solution has $N_{\min} = 7$, which has one more satellite than the lower bound of 6 (see Table (1).) For large m, the lower bound is approximately $\text{int}^+ [\sqrt{m}]$.

7.4 The Linear Array and its Relation to the LEO constellation

Assume now that we distribute the spacecraft on a linear segment instead of a circular arc (see Figure (7.4).) There are two ways in which such a situation may rise. The first situation is exemplified by a multi-aperture single spacecraft mission.

Fundamental number of satellites (N_f)	Number of Pixels $m = 2N_f - 1$	Minimum Number of Satellites $N_{\min}$	Number of Solutions	Lower Bound N_{lb}
1	1	1	1	1
2	3	2	1	2
3	5	3	1	3
4	7	4	1	3
5	9	4	2	4
6	11	5	3	4
7	13	5	3	4
8	15	5	1	5
9	17	6	10	5
10	19	6	3	5
11	21	6	2	5
12	23	7	18	6
13	25	7	12	6
14	27	7	4	6
15	29	7	1	6
16	31	8	28	6
17	33	8	19	7
18	35	8	3	7
19	37	9	142	7
20	39	9	91	7

Table 7.1: Summary of results for a 7200 km orbit, with $\frac{d_{\min}}{r_o} = 0.0791$ and $\theta_p = 1.75 \times 10^{-11}$.

With the apertures arranged on a line, as opposed to a circular arc, we could still achieve full wave number coverage by a simple 180° rotation of the spacecraft about an axis that is along the line of sight. Since the solution we propose for the LEO observatory hinges on the assumption that the apertures are rigidly connected and the whole constellation performs a simple rotation about an axis passing through the Earth center, then the concept design proposed above should apply for the linear aperture spacecraft as well in a space-based short baseline interferometric mission. We may then want to address the same question posed above: how to achieve maximum angular resolution with the minimum number of satellites and without gaps

on the wave number line? For example, University of Michigan's proposed EV3M [66] imaging spacecraft is one where all apertures are positioned linearly to maximize the achievable angular resolution of the spacecraft with three apertures only ($N_f = 4$ s/c, $N_{\min} = 3$ s/c, $m = 7$ pixels), while fully covering the wave number plane.

Second, note that in the limit as $\kappa \to 0$, an Earth-orbiting constellation may be approximated, to first order, as a linear array constellation. Thus a solution of the linear constellation will be the same as that for the Earth-orbiting constellation for κ sufficiently small (i.e. either $d_{\max}$ or r_o sufficiently small.) As will be shown below, the optimization problem for the linear array can be expressed as a 0-1 mathematical program that can be solved using existing techniques. Techniques, such as evolutionary programming, furnish solutions for high dimensional problems with small computational time, as opposed to exhaustive search algorithms as the one discussed above. This is an advantage in constellation design especially in the case where the constellation contains a very large number of small-sized satellites, where an exhaustive algorithm may take weeks of computation time even on the fastest computers available nowadays. Below, the linear array constellation problem will be formulated, solution techniques will be discussed and, in the next section, how this solution can be used as one for the Earth-orbiting array will be discussed.

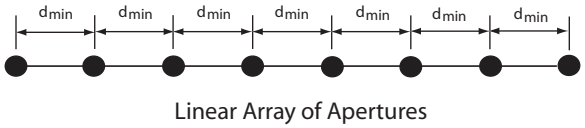

Figure 7.4: Linear Array Layout

In the "fundamental" arrangement of a linear array of apertures, the relative

distance between satellites l and n on the wave number line is given by:

$$\tilde{q}_{lk} = |n - l| \, \frac{d_{\min}}{\lambda}. \tag{7-4.1}$$

In Section (2), we parameterized the wave number line by the actual wave number, ν. Instead, suppose we parameterize it by $\frac{\nu\lambda}{d_{\min}}$. Thus, for the linear constellation, each satellite pair will contribute to a "wave number bin" $[\bar{\chi} - 0.5, \bar{\chi} + 0.5]$ centered at $\bar{\chi}$, where $\bar{\chi} = \frac{\tilde{q}_{lk}\lambda}{d_{\min}}$.

Let x_i denote the state of each aperture: x_i is 1 if it is selected as a member of the constellation or 0 if not. So, $x \in \mathbb{B}^{N_f}$, where $\mathbb{B} = \{0, 1\}$ and N_f is the number of satellites in the fundamental set. Note that for a particular choice of apertures, $c^T x$ represents the total number of satellites for that particular choice of apertures, where c is an N_f vector of 1's.

Next, it can be shown that $b_n(x) = x^T \mathbb{I}_k x$, $n = 1, \ldots, N_f$, is equal to the number of contributions to interval number n, where the first interval is centered at the origin and the N_fth interval is the outermost one and where $\mathbb{I}_n$ is a matrix of zeros except for the $(n-1)$st super diagonal. For example, if $N_f = 5$ and satellites $1, 2, 4$ are only selected, then the total number of satellites is equal to $[1\ 1\ 1\ 1\ 1] \cdot [1\ 1\ 0\ 1\ 0]^T = 3$ satellites. Also, for this case $b_1 = 3$ contributions due to satellites 1, 2 and 4 each paired with itself,

$$b_2 = [1\ 1\ 0\ 1\ 0] \begin{bmatrix} 0 & 1 & 0 & 0 & 0 \\ 0 & 0 & 1 & 0 & 0 \\ 0 & 0 & 0 & 1 & 0 \\ 0 & 0 & 0 & 0 & 1 \\ 0 & 0 & 0 & 0 & 0 \end{bmatrix} \begin{bmatrix} 1 \\ 1 \\ 0 \\ 1 \\ 0 \end{bmatrix} = 1,$$

contributions due to the pairing of satellites 1 and 2, $b_3 = 1$ contributions due to pairing of satellites 2 and 4, $b_4 = 1$ contributions due to pairing of satellites 1 and

4 and finally $b_5 = 0$ due to no pairing of satellites which are $5d_{\min}$ apart from each other.

Thus the set of designs with the minimum number of satellites that completely cover the wave number line are all *global* solutions to the following minimization problem:

$$\begin{aligned} &\min_x \ c^T x \\ &\text{s.t. } b_n(x) \geq 1, \ n = 1, \ldots, N_f \\ &x \in \mathbb{B}^{N_f}. \end{aligned} \tag{7-4.2}$$

This problem is generally known in the literature as a combinatoric/integer 0-1 programme, mostly with linear cost function and linear constraints [67]. The solution of this problem requires the minimization of a linear cost function subject to a quadratic constraint. Still, general 0-1 programming techniques exist to solve the program in Equation (7-4.2).

7.4.1 Numerical Results

We first attempt to solve this problem by applying a thorough search algorithm as discussed in the previous section. Figure (7.5) shows the number of feasible solutions (top left), the number of minimal solutions (top right), $N_{\min}$ (bottom left) and the CPU time (using a a.5GHz IBM platform) in seconds (bottom right.) The advantage of this algorithm is that it gives complete information on all possible minimal solutions (e.g. they configuration of spacecraft in each solution.) The main drawback is the computational time involved to obtain the results. For example, for $N_f = 21$ spacecraft there are 2.5×10^5 feasible solutions that all require evaluation of their Q functions consuming about 7 hours using the exact search algorithm.

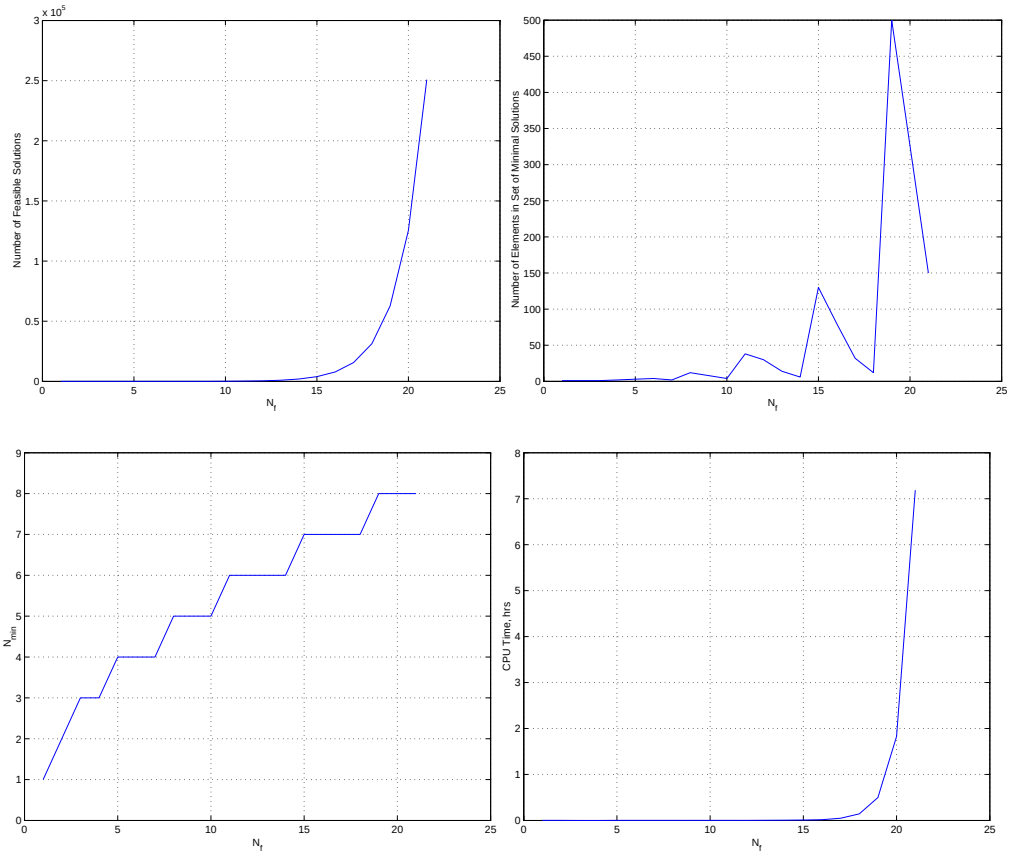

Figure 7.5: Exact Search Algorithm Results

To decrease the amount of CPU time, a statistical approach to solving the above 0-1 program is to utilize an evolutionary programming (EP) method. This is schematically summarized in Figure (7.6). The results of applying this algorithm are shown in Figure (7.7). We notice a tremendous amount of computation time savings. Using this algorithm we can arrive at solutions in about 18 seconds for $N_f = 21$ spacecraft. Due to the random nature of the search algorithm of the EP method, we note that we do not have full information regarding the total number of solutions available, the size of the feasible set or the exact design of the constellation (i.e. we may only know what $N_{\min}$ is, but not the exact spacecraft chosen for the design.)

A closer look at the right hand plot in Figure (7.6) shows that we seem to be able to get the correct solution up to $N_f = 32$. However, for $N_f = 37$ we notice a drop

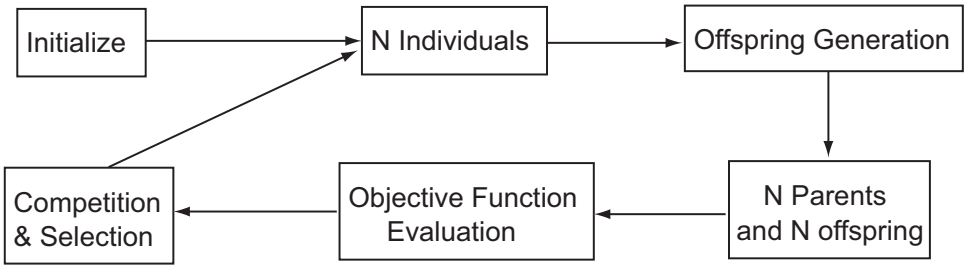

Figure 7.6: An Evolutionary Programming Method

in $N_{\min}$. Since it is not possible for a larger fundamental constellation (that achieves higher angular resolution) to achieve a smaller $N_{\min}$ than a smaller fundamental constellation, then we know that the $N_{\min}$ obtained using the EP algorithm is for $N_f = 37$ is not correct. This result casts larger doubt that the results obtained for $N_f > 37$ will be correct either, though we could be confident that results for values of $N_f \leq 36$ seem to be plausible.

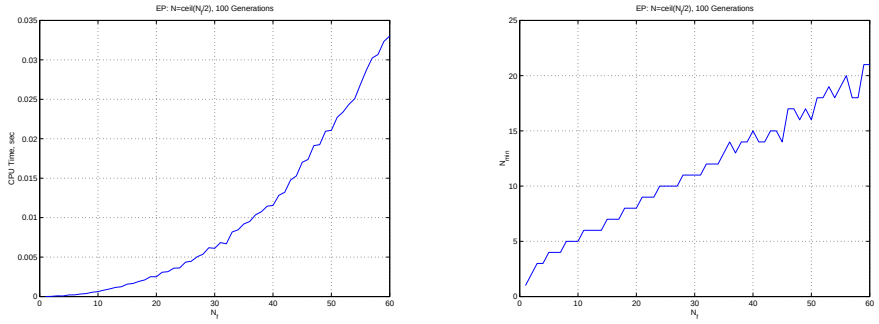

Figure 7.7: EP Algorithm Results

We observe that the algorithm performs poorly for higher values of N_f though much more faster than the exact search algorithm. In general one would trade off accuracy of solutions for speed in an EP algorithm. One may wish to improve

the results, though at the expense of longer computational time, by constricting the offspring generated to be ones that are visible in the first place. The results are shown in Figure (7.8), where we observe that consistent results are obtained for values of $N_f \leq 23$. For $N_f = 23$, the computation time is 1.8 hours versus 18 seconds for the general EP algorithm and more than 7 hours for the thorough search algorithm.

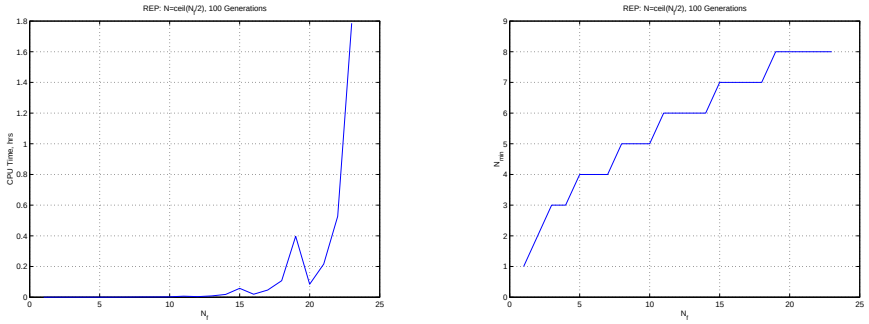

Figure 7.8: Restricted EP Algorithm Results

7.4.2 The Linear Array and the Earth-Orbiting Observatory

Assume that we can find a distance preserving isometry, ϕ, between the (curved) Earth-orbiting and the linear array geometries discussed above. As mentioned above, the significance of the linear problem is that we can readily solve this problem (as stated in Equation (7-4.2)) and then compute the corresponding solution on the curved one-dimensional space through the inverse mapping ϕ^{-1} (see Figure (7.9).) The main benefit is that we can utilize techniques available in the literature for solving the 0-1 program in Equation (7-4.2) to compute the solution to an Earth-orbiting configuration. First, recall the definition for an isometry and isometric

spaces [68]:

Definition 7.4.1 (Isometry and Isometric Spaces). Let M_1 and M_2 be two topological spaces. An isometry $\phi : M_1 \to M_2$ is a one-to-one correspondence such that $d_2(\phi(x), \phi(y)) = d_1(x, y)$ for all $x, y \in M_1$, where $d_1(\cdot, \cdot)$ and $d_2(\cdot, \cdot)$ are distance functions on M_1 and M_2, respectively. If there exists an isometry $\phi : M_1 \to M_2$, then M_1 and M_2 are called isometric.

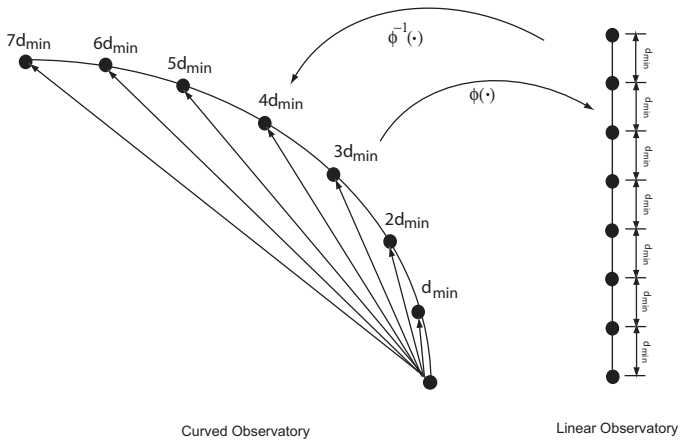

Figure 7.9: Relation between the Linear And Earth-Orbiting Constellations

S^1 being the circle in $\mathbb{R}^2$ with radius r_o, let $M_C \subset S^1$ denote the one-dimensional space for a curved Earth-orbiting constellation and $M_L \subset \mathbb{R}^1$ be the one-dimensional space, which is simply a line segment on $\mathbb{R}^1$, for the linear aperture constellation.

Let $d_C(s_l, s_n)$ be the Euclidean distance in $\mathbb{R}^2$ between satellites n and l on M_C and let $d_L(s_l, s_n)$ be the Euclidean distance in $\mathbb{R}^1$ between satellites n and l on M_L. d_C and d_L are given by

$$d_C(s_l, s_n) = \frac{2r_o\kappa}{\lambda(N_f - 1)} \times \sqrt{\left((l^2 - n^2)\frac{\kappa}{N_f - 1}\right)^2 + \left(n\sqrt{1 - \left(\frac{n\kappa}{N_f - 1}\right)^2} - l\sqrt{1 - \left(\frac{l\kappa}{N_f - 1}\right)^2}\right)^2} \tag{7-4.3}$$

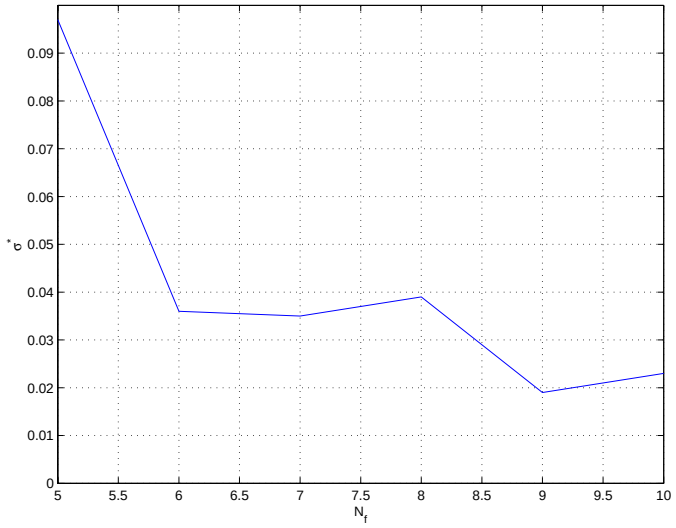

Figure 7.10: Critical value of κ, κ^*, for $5 \leq N_f \leq 10$.

and

$$d_L(s_l, s_n) = |n - l|\, d_{\min}/\lambda \tag{7-4.4}$$

Due to the way spacecraft are arranged in the fundamental configuration, M_C and M_L may not have an isometry. That is because if M_C is simply unfolded onto M_L, spacecraft nodes on M_C do not map onto spacecraft nodes on M_L. Though it is true that the real line $\mathbb{R}^1$ and the circle S^1 have the isometry $\phi(t) = (r_o \sin t, r_o \cos t) : \mathbb{R}^1 \to S^1 \subset \mathbb{R}^2$ using a metric that measures distance *along* the curves, this is not true in our case because the metric we use is the direct shortest distance between points in $\mathbb{R}^2$ as opposed to a metric along S^1.

For $\kappa \neq 0$, points on $M_C \subset S^1$ are shifted when M_C is unfolded onto M_L. Despite the fact that the total distance from the zeroth spacecraft to the $(N_f - 1)^{\text{st}}$ spacecraft is preserved and is equal to $d_{\max}$, distances between intermediate spacecraft are not.

However, note that:

$$\lim_{\kappa \to 0} d_C(s_l, s_n) = d_L(s_l, s_n). \tag{7-4.5}$$

In other words, $d_C(s_l, s_n) \to d_L(s_l, s_n)$ as the curvature of M_C or $d_{\max}$ approach zero.

Thus, for sufficiently small κ, the solution to the linear array should be identical to that of the curved array to first order. In the next section we show results that indicate that for sufficiently small κ, the solution to the mathematical program in Equation (7-4.2) is also a solution to the Earth-orbiting constellation configuration.

7.5 Effects of Orbit Perturbations on the Constellation

In this and the next section we discuss the effect of J_2 orbit perturbations on image quality and propose a procedure to modify the constellation design to abate the effects of these perturbations.

7.5.1 Eccentricity Effects on Wave Number Plane Coverage

In this section we study the effects that small orbital perturbations have on the constellation trajectories in orbit, and, in turn, on wave number plane coverage. The main objective is to show that any general eccentricity perturbation immediately leads to gaps in the frequency domain. This implies that for a J_2-perturbed orbit, frequency domain gaps are expected to occur, which is addressed in the next section. Below, we denote by N the number of spacecraft in the constellation (either minimal or fundamental, but not otherwise[1].) Let the set $\mathcal{I}$ be the set of spacecraft indexes in the set of chosen spacecraft. Here we assume that κ is sufficiently small for the linear array assumption to hold. With this assumption, solutions to (7-4.2) will also be solutions to the curved constellation (that is, $\kappa \neq 0$.)

Let x and y be the axes of a fixed frame of reference whose origin O is located at the center of the Earth (see Figure (7.11).) In the x-y frame, the spacecraft locations

[1]This assumption is made in order to facilitate the proofs of Theorem 3.1 below.

are approximated by

$$
\begin{aligned}
x_i &= r_0 \cos(nt) + A_i \sin(nt + \phi_i) \cos(nt) - \left[y_i^0 - 2A_i \cos(nt + \phi_i) \right] \sin(nt), \\
y_i &= r_0 \sin(nt) + A_i \sin(nt + \phi_i) \sin(nt) + \left[y_i^0 - 2A_i \cos(nt + \phi_i) \right] \cos(nt).
\end{aligned}
$$

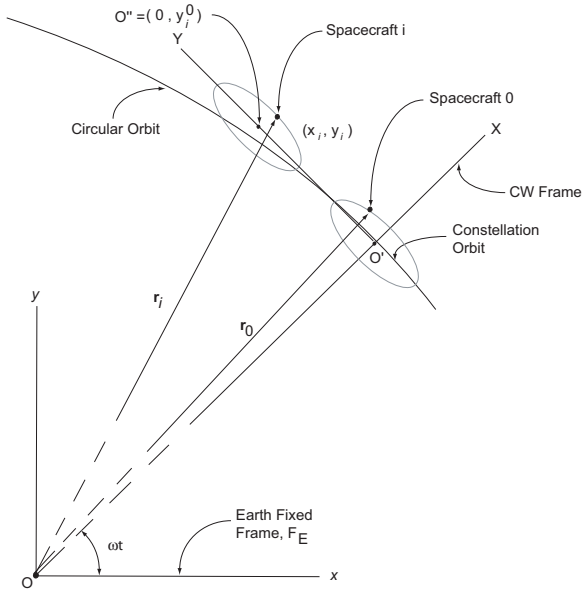

Figure 7.11: The problem geometry.

Recall that $\mathbf{q}_i$ is the position vector of the i^{th} spacecraft in the x-y reference frame. In the wave number plane, the coordinate of the ij^{th} picture frame disc is, thus, given by

$$
\begin{aligned}
\tilde{x}_{ij}(t) &:= \frac{x_j(t) - x_i(t)}{\lambda} \\
&= \frac{1}{\lambda} \Bigg\{ \left[A_j \sin(nt + \phi_j) - A_i \sin(nt + \phi_i) \right] \cos(nt) \\
&\quad - \left[\left(y_j^0 - y_i^0 \right) - 2 \left(A_j \cos(nt + \phi_j) - A_i \cos(nt + \phi_i) \right) \right] \sin(nt) \Bigg\}, \\
\tilde{y}_{ij}(t) &:= \frac{y_j(t) - y_i(t)}{\lambda} \\
&= \frac{1}{\lambda} \Bigg\{ \left[A_j \sin(nt + \phi_j) - A_i \sin(nt + \phi_i) \right] \sin(nt) \\
&\quad + \left[\left(y_j^0 - y_i^0 \right) - 2 \left(A_j \cos(nt + \phi_j) - A_i \cos(nt + \phi_i) \right) \right] \cos(nt) \Bigg\}.
\end{aligned}
$$

Note that $\tilde{\mathbf{q}}_{ij}(t) = (1/\lambda)\mathbf{q}_{ij}(t) = \mathbf{q}_j - \mathbf{q}_i$, $i, j \in \mathcal{I}$ is simply equal to the vector $(\tilde{x}_{ij}(t), \tilde{y}_{ij}(t))$ in the wave number plane.

Now, for this general setting of the problem, we consider the following question: Let $\|\cdot\|_2$ denote the 2-norm on $\mathbb{R}^2$. Fix a wave number vector $\mathbf{v} = (v_x, v_y) \in \mathbb{R}^2$ such that $\|\mathbf{v}\|_2 \leq 1/(2\theta_r)$. For any $i, j \in \mathcal{I}$, does there exist a set of time intervals $\mathcal{T} \in [0, 2\pi/n]$ (possibly just singleton sets) such that the inequality

$$\|\tilde{\mathbf{q}}_{ij}(t) - \mathbf{v}\|_2 \leq \frac{1}{2\theta_p} \tag{7-5.1}$$

holds? In other words, are points in the wave number plane of magnitude $v = \sqrt{v_x^2 + v_y^2}$, $v \leq 1/(2\theta_r)$, covered for some time during a single orbit period? Bsy construction one answer is that if $A_i = 0$ for all $i \in \mathcal{I}$, then for each $v \leq 1/(2\theta_r)$ there exists an i and j such that the inequality holds, and, thus, coverage of the resolution disc is achieved. This can be proven as follows.

Assumption 7.5.1. Note that due to the symmetry of the trajectories in the wave number plane, one can assume that $j \geq i$, $i, j \in \mathcal{I}$, and study the trajectories $\tilde{\mathbf{q}}_{ij}(t)$. The trajectories of $\tilde{\mathbf{q}}_{ij}(t)$ with $i \geq j$ will follow a path symmetric to those with $j \geq i$. Henceforth, we assume that $j \geq i$.

Theorem 7.5.1. *If $A_i = 0$ for all $i \in \mathcal{I}$, then the inequality (7-5.1) is satisfied for all $v \leq 1/(2\theta_r)$.*

Proof If $A_i = 0$ for all $i \in \mathcal{I}$, we have

$$\begin{aligned} \tilde{x}_{ij} &= -\frac{1}{\lambda}\left(y_j^0 - y_i^0\right)\sin(nt), \text{ and} \\ \tilde{y}_{ij} &= \frac{1}{\lambda}\left(y_j^0 - y_i^0\right)\cos(nt). \end{aligned}$$

Let $\mathbf{v} = (v_x, v_y)$ have polar coordinates (v, θ_v). Then, $v_x = v\cos\theta_v$ and $v_y = v\sin\theta_v$.

Thus,

$$\begin{aligned}\|\tilde{\mathbf{q}}_{ij}(t)-\mathbf{v}\|_2^2 &= \left\|\left(-\frac{1}{\lambda}\left(y_j^0-y_i^0\right)\sin(nt)-v_x,\frac{1}{\lambda}\left(y_j^0-y_i^0\right)\cos(nt)-v_y\right)\right\|_2^2\\ &= \frac{1}{\lambda^2}(j-i)^2d_{\min}^2+v^2+\frac{2}{\lambda}(j-i)d_{\min}\left(\sin(nt)v_x-\cos(nt)v_y\right).\end{aligned}$$

First, if $v<1/(2\theta_p)$, let $j=i$, for any $j,i\in\mathcal{I}$, and therefore we have

$$\|\tilde{\mathbf{q}}_{ij}(t)-\mathbf{v}\|_2^2=v^2<\frac{1}{2\theta_p},$$

which proves the theorem for $v<1/(2\theta_p)$. On the other hand, if $1/(2\theta_p)\leq v\leq 1/(2\theta_r)$, then there exists $n=1,\ldots,N_f-1$ such that $[1/(2\theta_p)]\,[n-(1/2)]\leq v\leq [1/(2\theta_p)]\,[n+(1/2)]$. In either a minimal or the fundamental constellation, by design there exist spacecraft i and j such that $j-i=n$ for all $n=1,\ldots,N_f-1$. Let $j-i=n$. Therefore, we have

$$\begin{aligned}\|\tilde{\mathbf{q}}_{ij}(t)-\mathbf{v}\|_2^2 &= n^2\frac{d_{\min}^2}{\lambda^2}+v^2+\frac{2kv}{\theta_p}\left(\cos\theta_v\sin(nt)-\sin\theta_v\cos(nt)\right)\\ &\leq \left(\frac{2n^2}{\theta_p^2}+\frac{n}{\theta_p^2}\right)\left(1+\cos\theta_v\sin(nt)-\sin\theta_v\cos(nt)\right)+\frac{1}{4\theta_p^2},\end{aligned}$$

where the inequality $v\leq[1/(2\theta_p)]\,[n+(1/2)]$ and the fact that $d_{\min}/\lambda=1/\theta_p$ have been used. If we set $nt=\theta_v-(\pi/2)$, then $1+\cos\theta_v\sin(nt)-\sin\theta_v\cos(nt)=0$. This results in

$$\|\tilde{\mathbf{q}}_{ij}(t)-\mathbf{v}\|_2^2\leq\frac{1}{4\theta_p^2},$$

which proves the theorem for $1/(2\theta_p)\leq v\leq 1/(2\theta_r)$.

■

Remark 7.5.1. Note that the phase angles ϕ_i, $i\in\mathcal{I}$, are not defined when $A_i=0$, $i=0,\ldots,N-1$.

Corollary 7.5.1. *If $A_i=A$ and $\phi_i=\phi$ for all $i\in\mathcal{I}$ then the inequality (7-5.1) is satisfied for all $v\leq 1/(2\theta_r)$.*

Proof If $A_i = A$ and $\phi_i = \phi$ for all $i \in \mathcal{I}$, then we have

$$\begin{aligned} \tilde{x}_{ij} &= -\frac{1}{\lambda}\left(y_j^0 - y_i^0\right)\sin(nt), \text{ and} \\ \tilde{y}_{ij} &= \frac{1}{\lambda}\left(y_j^0 - y_i^0\right)\cos(nt) \end{aligned}$$

and the proof follows as in Theorem (7.5.1).

■

Next, we assume that all $A_i = A,\ i \in \mathcal{I}$, are the same but the phase angles may be arbitrary. This case is of special interest. Assume we have knowledge of the upper bound on orbit eccentricity, denoted $e_{\max}$, for all spacecraft orbits. Thus, the maximum amplitude any one of the spacecraft ellipses in the CW frame achieves is given by $A_i = A = e_{\max} r_o$, for all $i \in \mathcal{I}$. By studying this version of the problem, we can make some useful conclusions regarding wave number plane coverage and, possibly, ideas for how to take these perturbations into account in the design of interferometric observatories so that they attain complete coverage of the wave number plane.

From Corollary (7.5.1), if all spacecraft were in phase then the wave number plane is completely covered. This represents one extreme. The other extreme is when any two neighboring spacecraft[2] are 180 degrees out of phase with each other. Since distance is an invariant under any frame of reference, the center of the ij^{th} picture frame can be expressed as

$$\|\tilde{\mathbf{q}}_{ij}(t)\|_2^2 = \left(\tilde{x}_{ij}^2 + \tilde{y}_{ij}^2\right) = \tilde{x}_{ij}^2 + \tilde{y}_{ij}^2,$$

where $\tilde{x}_{ij} = (1/\lambda)\,(x_j - x_i)$ and $\tilde{y}_{ij} = (1/\lambda)\,(y_j - y_i)$:

$$\tilde{x}_{ij}(t) = \frac{1}{\lambda}\left[A_j \sin(nt + \phi_j) - A_i \sin(nt + \phi_i)\right], \tag{7-5.2}$$

$$\tilde{y}_{ij}(t) = \frac{1}{\lambda}\left\{\left(y_j^0 - y_i^0\right) - 2\left[A_j \cos(nt + \phi_j) - A_i \cos(nt + \phi_i)\right]\right\} \tag{7-5.3}$$

---

[2]In a minimal solution, recall that neighboring satellites are not necessarily such that $j = i \pm 1$.

Furthermore, let

$$\tilde{\mathbf{q}}_{ij}^{*} = \left(0, (j-i)\frac{d_{\min}}{\lambda}\right)$$

be the nominal (zero eccentricity) relative position vector, where the components are given in the CW frame. Thus, for $A_i = A,\ i \in \mathcal{I}$, and assuming that j and i correspond to neighboring spacecraft with say, $\phi_i = 0$ and $\phi_j = \pi$, we then have

$$f_{ij} = \left\|\tilde{\mathbf{q}}_{ij} - \tilde{\mathbf{q}}_{ij}^{*}\right\|_2^2 = \frac{4A^2}{\lambda^2}\left[1 + 3\cos^2(nt)\right],$$

which represents the magnitude square of the position deviation. The deviation f_{ij} attains a maximum value of $16A^2/\lambda^2$ at $nt = 0,\ \pi$ and a minimum value of $4A^2/\lambda^2$ at $\pi/2,\ nt = 3\pi/2$. This implies that portions of the resolution disc will not be covered if the existing spacing is chosen with no overlap. An example is given in Figure 7.12 for $N_f = 2$. In the figure, the dotted circle represents the wave number disc, the solid line represents $\tilde{\mathbf{q}}_{ij}$ and the dashed lines are the boundaries of the picture frame disc. Shaded regions represent those parts of the resolution disc that are not covered. Indeed the minimum and maximum values of $\|\tilde{\mathbf{q}}_{ij}\|_2$ take place along the ν_x axis and ν_y-axis, respectively. Note that the x-y axes are out of phase from the ν_x-ν_y axes by $\pi/2$ due to the fact that the spacecraft are initialized in an upward position. This upward configuration corresponds to points on the ν_y axis in the frequency domain as opposed to the ν_x axis.

Further, assume eccentricity perturbations such that $A_i = A,\ i \in \mathcal{I}$, and that each neighboring spacecraft are 180° out of phase from each other, the minimum possible distance between any neighboring spacecraft is given by $d_{\min} - 4A$. In order that no two neighboring spacecraft trajectories cross each other we must constrain $A < d_{\min}/4$, which corresponds to a bound on eccentricity $e \leq d_{\min}/(4r_o)$. Figure (7.13) shows the trajectory in the wave number plane for a two spacecraft system

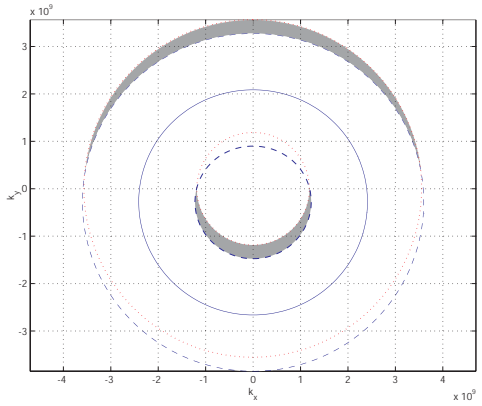

Figure 7.12: Wave number plane trajectory for a 180° out-of-phase two spacecraft system with equivalent eccentricity ($A = e_{\max} r_o$, $e_{\max} = 1 \times 10^{-4}$, $r_o = 7.2 \times 10^3$km.)

with path crossing ($A = e_{\max} r_o = 14.4$ km $> d_{\min}/4 = 5.93$ km and $e_{\max} = 0.002$, whereas the upper bound on e is 8.24×10^{-4}.) Note here that when the spacecraft are closest to each other, higher portions of the wave number plane are not covered. Hence, if the perturbation in the eccentricity is such that

$$A < \frac{d_{\min}}{4} \tag{7-5.4}$$

then the potential for spacecraft crossing each others' paths, and, consequently, the potential for collisions, is diminished.

The above discussion implies that for equal A_i, $i \in \mathcal{I}$, we must have equal phases for complete coverage. In practice, however, trajectory initialization errors will always exist. We next assume that such errors do exist. In other words we assume that $\phi_j - \phi_i$ is sufficiently small. First note that with $A_i = A$, $i \in \mathcal{I}$, equations (7-5.2) can be re-written as

$$\begin{aligned}
\tilde{x}_{ij}(t) &= \frac{A}{\lambda} \left\{ \sin(nt) \left[\cos(\phi_j) - \cos(\phi_i) \right] + \cos(nt) \left[\sin(\phi_j) - \sin(\phi_i) \right] \right\}, \\
\tilde{y}_{ij}(t) &= (j-i) \frac{d_{\min}}{\lambda} + \frac{2A}{\lambda} \left\{ \sin(nt) \left[\sin(\phi_j) - \sin(\phi_i) \right] - \cos(nt) \left[\cos(\phi_j) - \cos(\phi_i) \right] \right\}.
\end{aligned}$$

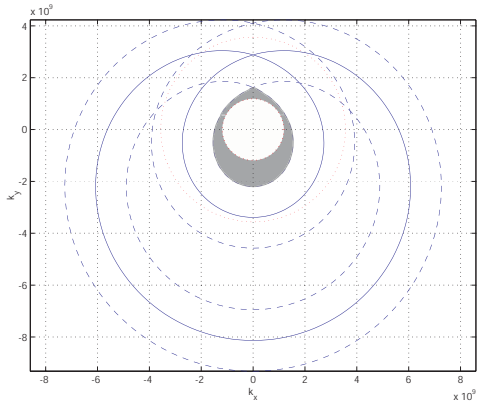

Figure 7.13: Trajectory crossing in the wave number plane for a two spacecraft constellation with equivalent eccentricity ($A = e_{\max} r_o$, $e = 0.002$, $r_o = 7.2 \times 10^3$km.)

With $\phi_j,\ \phi_i \approx 0$, linearize $\tilde{x}_{ij}$ and $\tilde{y}_{ij}$ with respect to ϕ_i and ϕ_j to obtain

$$\begin{aligned} \tilde{x}_{ij}(t) &\approx \frac{A}{\lambda}\cos(nt)\left(\phi_j - \phi_i\right), \\ \tilde{y}_{ij}(t) &\approx (j-i)\frac{d_{\min}}{\lambda} + \frac{2A}{\lambda}\sin(nt)\left(\phi_j - \phi_i\right). \end{aligned}$$

Thus, we have

$$f_{ij} = \left\|\tilde{\mathbf{q}}_{ij} - \tilde{\mathbf{q}}^*_{ij}\right\|_2^2 = \frac{A^2}{\lambda^2}\phi_{ij}^2\left[1 + 3\sin^2(nt)\right],$$

where $\phi_{ij} = \phi_j - \phi_i$ is the difference in initial values of the phase angles. This shows that perturbations due to small errors in phase have a second order effect on the ensuing trajectory. The deviation f_{ij} attains a maximum value of $4A^2\phi_{ij}^2/\lambda^2$ at $nt = \pi/2,\ 3\pi/2$ and a minimum value of $A^2\phi_{ij}^2/\lambda^2$ at $nt = 0,\ \pi$.

Assume now that all spacecraft are in phase with arbitrary A_i and $\phi_i = 0$, $i \in \mathcal{I}$. Then one finds that the deviation f_{ij} is given by $f_{ij} = (A_{ij}^2/\lambda^2)\left[1 + 3\cos^2(nt)\right]$, where $A_{ij} = A_j - A_i$. First, note that the perturbation is second order in the difference in amplitudes. Hence, initializing the spacecraft with a sufficiently small error leads to second order effects on the relative trajectories. Therefore, f_{ij} attains a maximum

value of $4A_{ij}^2/\lambda^2$ at $nt = 0,\ \pi$ and a minimum value of A_{ij}^2/λ^2 at $nt = \pi/2,\ 3\pi/2$. An example is shown in Figure (7.14). Note that some higher frequency components are not covered.

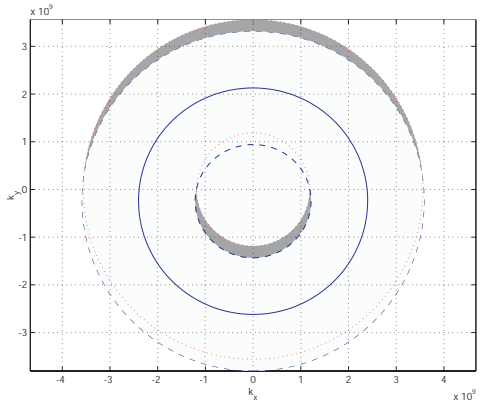

Figure 7.14: Wave number plane trajectory for an in-phase two spacecraft system with different eccentricities ($A_1 = 2.569$km, $A_2 = 1.341$km.)

To illustrate the complexity of the problem in the general case, Figure (7.15) shows the trajectories in the wave number plane and their lack of coverage regions (the shaded areas) for the cases when $N_f = 2$ and $N_f = 5$, for which the nominal minimal solutions contain $N_o = 2$ and $N_o = 4$ spacecraft, respectively, with randomly chosen eccentricities and phases. For the former case, we have $A_0 = 4.65$ km ($e_0 = 6.46 \times 10^{-4}$) and $A_1 = 4.04$ km ($e_1 = 5.61 \times 10^{-4}$) and $\phi_0 = 165.99°$ and $\phi_1 = 204.42°$. For the latter case, we have a maximum eccentricity of 4.97×10^{-4} and a minimum eccentricity of 4.86×10^{-5} and a maximum phase of 356.43° and a minimum phase of 5.40°, where the spacecraft with index $i = 2 \notin \mathcal{I}$.

Finally, Figure (7.16) shows the result for $N_f = 5$ with a maximum eccentricity of 1.5×10^{-3} and a minimum value of 3.20×10^{-4} and a maximum phase of 335.37° and a minimum phase of 197.56°. These values result in path crossing since $A_1,\ A_4 > d_{\min}/4 = 5.93$ km. Note the complexity of the wave number plane coverage

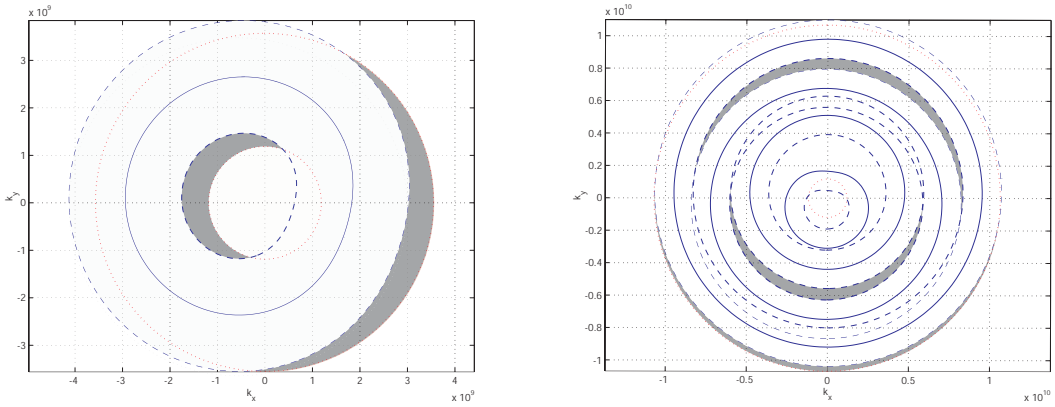

Figure 7.15: Wave number plane trajectory for (a) $N_f = 2$ and (b) $N_f = 5$.

trajectories as well as the lack of coverage area.

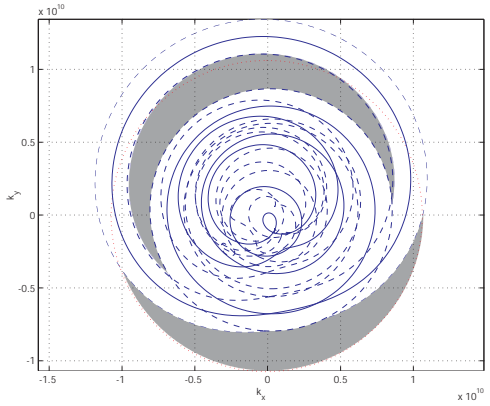

Figure 7.16: Wave number plane trajectory for $N_f = 5$ with path crossing.

7.5.2 J_2 Effects on Imaging

In this section we study short-period perturbation effects of the second zonal harmonic, J_2, on frequency domain coverage. In [23], the authors derive necessary conditions to establish J_2 invariant relative orbits using mean orbital elements, working with the first order secular J_2 effects. The resulting conditions guarantee that the drift rate of the ascending node and the mean argument of latitude is the same for all spacecraft in the formation. The gravity coefficient J_2 also induces short-period

perturbations within a single orbit period. These perturbations will in general result in a lack of frequency domain coverage.

As discussed earlier in the Chapter and as in [19], secular drift in the longitude of the ascending node allows the observatory to scan the entire celestial sphere within one nodal period. Reference [23] derives the conditions necessary for formation keeping by controlling inter-spacecraft distances. This is because nominal trajectories in [23] are allowed to be different. We, on the other hand, will use their conditions to ensure that each spacecraft does not drift from its nominal circular path as opposed to maintaining formation directly. This is by virtue of the fact that all spacecraft in our observatory have identical nominal trajectories.

In our work we address short-period J_2 effects as follows. Let $\mathbf{E} = (a, e, \chi, \Omega, \omega, \imath)$, where a is the semi-major axis, e is the eccentricity, $\imath$ is the inclination, Ω is the longitude of the ascending node, ω is the argument of perigee and $M = nt - n\tau = nt + \chi$ is the mean anomaly with τ being the time at epoch. First, we have the following relationship between the perturbations in the position vector $\mathbf{q}$ in a frame we denote by F_E, which is fixed at the center of the Earth (hence, the subscript E in F_E), and perturbations in the orbital elements:

$$\Delta\mathbf{q} = \frac{\partial\mathbf{q}}{\partial\mathbf{E}}\Delta\mathbf{E}, \tag{7-5.5}$$

where Δ denotes a perturbation in the variable under consideration. Since, x, y and z can be expressed in terms of $\mathbf{E}$ as

$$\begin{aligned} x &= r\left[\cos\Omega\cos\left(f+\omega\right) - \sin\Omega\sin\left(f+\omega\right)\cos\imath\right] \\ y &= r\left[\sin\Omega\cos\left(f+\omega\right) + \cos\Omega\sin\left(f+\omega\right)\cos\imath\right] \\ z &= r\sin\left(f+\omega\right)\sin\imath. \end{aligned} \tag{7-5.6}$$

where

$$r = \frac{a(1-e^2)}{1+e\cos f} \tag{7-5.7}$$

and f is the true anomaly, then we have

$$\frac{\partial \mathbf{q}}{\partial \mathbf{E}} = \begin{bmatrix} \frac{\partial x}{\partial a} & \frac{\partial x}{\partial e} & \frac{\partial x}{\partial f}\frac{\mathrm{d}f}{\mathrm{d}M}\frac{\mathrm{d}M}{\mathrm{d}\chi} & \frac{\partial x}{\partial \Omega} & \frac{\partial x}{\partial \omega} & \frac{\partial x}{\partial \imath} \\ \frac{\partial y}{\partial a} & \frac{\partial y}{\partial e} & \frac{\partial y}{\partial f}\frac{\mathrm{d}f}{\mathrm{d}M}\frac{\mathrm{d}M}{\mathrm{d}\chi} & \frac{\partial y}{\partial \Omega} & \frac{\partial y}{\partial \omega} & \frac{\partial y}{\partial \imath} \\ \frac{\partial z}{\partial a} & \frac{\partial z}{\partial e} & \frac{\partial z}{\partial f}\frac{\mathrm{d}f}{\mathrm{d}M}\frac{\mathrm{d}M}{\mathrm{d}\chi} & \frac{\partial z}{\partial \Omega} & \frac{\partial z}{\partial \omega} & \frac{\partial z}{\partial \imath} \end{bmatrix}, \tag{7-5.8}$$

where $\mathrm{d}M/\mathrm{d}\chi = 1$ and

$$\frac{\mathrm{d}f}{\mathrm{d}M} = \left(\frac{a}{r}\right)^2 \left(1-e^2\right)^{\frac{1}{2}}. \tag{7-5.9}$$

Note, however, that the choice of elements $\mathbf{E}$ is singular for an orbit whose eccentricity is nominally zero. Hence, we use the set of orbital elements $\mathbf{E}' = (a, \imath, \epsilon, \Omega, h, k)$, where $\epsilon = \Omega + \omega + \chi$ is the mean longitude of the epoch, $h = e\sin\omega$ and $k = e\cos\omega$. In what follows we refrain from taking the limit as $e \to 0$ until later in the analysis in order to fully cancel out any tentative singularities in the derivation. If we write $\Delta\mathbf{E}' = T^{-1}\Delta\mathbf{E}$ with

$$T^{-1} = \begin{bmatrix} 1 & 0 & 0 & 0 & 0 & 0 \\ 0 & 0 & 0 & 0 & 0 & 1 \\ 0 & 0 & 1 & 1 & 1 & 0 \\ 0 & 0 & 0 & 1 & 0 & 0 \\ 0 & \sin\omega & 0 & 0 & e\cos\omega & 0 \\ 0 & \cos\omega & 0 & 0 & -e\cos\omega & 0 \end{bmatrix} \tag{7-5.10}$$

then we have

$$\Delta\mathbf{q} = \frac{\partial \mathbf{q}}{\partial \mathbf{E}} T \Delta\mathbf{E}'. \tag{7-5.11}$$

Let $G = \lim_{e\to 0} \frac{\partial \mathbf{q}}{\partial \mathbf{E}} T$. Then G is given by

$$
\begin{aligned}
G \;=\; & \left[\begin{array}{cccc}
\mathrm{c}_\Omega \mathrm{c}_{\omega+f} - \mathrm{s}_\Omega \mathrm{c}_\imath \mathrm{s}_{\omega+f} & a\mathrm{s}_\Omega \mathrm{s}_\imath \mathrm{s}_{\omega+f} & -a\left(\mathrm{c}_\Omega \mathrm{s}_{\omega+f} + \mathrm{s}_\Omega \mathrm{c}_\imath \mathrm{c}_{\omega+f}\right) & a\left(1-\mathrm{c}_\imath\right)\mathrm{s}_{\Omega-(\omega+f)} \\
\mathrm{s}_\Omega \mathrm{c}_{\omega+f} + \mathrm{c}_\Omega \mathrm{c}_\imath \mathrm{s}_{\omega+f} & -a\mathrm{c}_\Omega \mathrm{s}_\imath \mathrm{s}_{\omega+f} & a\left(-\mathrm{s}_\Omega \mathrm{s}_{\omega+f} + \mathrm{c}_\Omega \mathrm{c}_\imath \mathrm{c}_{\omega+f}\right) & a\left(1-\mathrm{c}_\imath\right)\mathrm{c}_{\Omega-(\omega+f)} \\
\mathrm{s}_\imath \mathrm{s}_{\omega+f} & a\mathrm{c}_\imath \mathrm{s}_{\omega+f} & a\mathrm{s}_\imath \mathrm{c}_{\omega+f} & -a\mathrm{s}_\imath \mathrm{c}_{\omega+f} \\
\frac{a}{2}\left[\mathrm{s}_\Omega \mathrm{c}_\imath\left(2+\mathrm{c}_{2\omega}+\mathrm{c}_{2f}\right) + \mathrm{c}_\Omega\left(\mathrm{s}_{2f}+\mathrm{s}_{2\omega}\right)\right] & -\frac{a}{2}\left[\mathrm{c}_\Omega\left(2+\mathrm{c}_{2f}-\mathrm{c}_{2\omega}\right) - \mathrm{s}_\Omega \mathrm{c}_\imath\left(\mathrm{s}_{2f}-\mathrm{c}_{2\omega}\right)\right] \\
\frac{a}{2}\left[\mathrm{s}_\Omega\left(\mathrm{s}_{2f}+\mathrm{s}_{2\omega}\right) - \mathrm{c}_\Omega \mathrm{c}_\imath\left(2+\mathrm{c}_{2\omega}+\mathrm{c}_{2f}\right)\right] & -\frac{a}{2}\left[\mathrm{s}_\Omega\left(2+\mathrm{c}_{2f}-\mathrm{c}_{2\omega}\right) + \mathrm{c}_\Omega \mathrm{c}_\imath\left(\mathrm{s}_{2f}-\mathrm{c}_{2\omega}\right)\right] \\
-\frac{a\mathrm{s}_\imath}{2}\left(2+\mathrm{c}_{2f}+\mathrm{c}_{2\omega}\right) & -\frac{a\mathrm{s}_\imath}{2}\left(\mathrm{s}_{2f}-\mathrm{s}_{2\omega}\right)
\end{array}\right], \\
\end{aligned}
$$

where we use the notation $\mathrm{s}_u = \sin u$ and $\mathrm{c}_u = \cos u$. With $\Delta\mathbf{E}' = \{\Delta a_p,\ \Delta\imath_p,\ \Delta\epsilon_p,\ \Delta\Omega_p,\ \Delta h_p,\ \Delta k_p\}$, note that the elements of $\Delta\mathbf{E}'$ are dimensionless except for Δa_p. Hence, we normalize Δa_p by its mean value a for dimensional consistency. By defining $\Delta\mathbf{E}'' = \{\Delta a_p/a, \Delta\imath_p, \Delta\epsilon_p, \Delta\Omega_p, \Delta h_p, \Delta k_p\}$, one can rewrite the relation in equation (7-5.11) as $\Delta\mathbf{q} = G_0 \Delta\mathbf{E}''$, where

$$
\begin{aligned}
G_0 \;=\; a & \left[\begin{array}{cccc}
\mathrm{c}_\Omega \mathrm{c}_{\omega+f} - \mathrm{s}_\Omega \mathrm{c}_\imath \mathrm{s}_{\omega+f} & \mathrm{s}_\Omega \mathrm{s}_\imath \mathrm{s}_{\omega+f} & -\mathrm{c}_\Omega \mathrm{s}_{\omega+f} - \mathrm{s}_\Omega \mathrm{c}_\imath \mathrm{c}_{\omega+f} & \left(1-\mathrm{c}_\imath\right)\mathrm{s}_{\Omega-(\omega+f)} \\
\mathrm{s}_\Omega \mathrm{c}_{\omega+f} + \mathrm{c}_\Omega \mathrm{c}_\imath \mathrm{s}_{\omega+f} & -\mathrm{c}_\Omega \mathrm{s}_\imath \mathrm{s}_{\omega+f} & -\mathrm{s}_\Omega \mathrm{s}_{\omega+f} + \mathrm{c}_\Omega \mathrm{c}_\imath \mathrm{c}_{\omega+f} & \left(1-\mathrm{c}_\imath\right)\mathrm{c}_{\Omega-(\omega+f)} \\
\mathrm{s}_\imath \mathrm{s}_{\omega+f} & \mathrm{c}_\imath \mathrm{s}_{\omega+f} & \mathrm{s}_\imath \mathrm{c}_{\omega+f} & -\mathrm{s}_\imath \mathrm{c}_{\omega+f} \\
\frac{1}{2}\left[\mathrm{s}_\Omega \mathrm{c}_\imath\left(2+\mathrm{c}_{2\omega}+\mathrm{c}_{2f}\right) + \mathrm{c}_\Omega\left(\mathrm{s}_{2f}+\mathrm{s}_{2\omega}\right)\right] & -\frac{1}{2}\left[\mathrm{c}_\Omega\left(2+\mathrm{c}_{2f}-\mathrm{c}_{2\omega}\right) - \mathrm{s}_\Omega \mathrm{c}_\imath\left(\mathrm{s}_{2f}-\mathrm{c}_{2\omega}\right)\right] \\
\frac{1}{2}\left[\mathrm{s}_\Omega\left(\mathrm{s}_{2f}+\mathrm{s}_{2\omega}\right) - \mathrm{c}_\Omega \mathrm{c}_\imath\left(2+\mathrm{c}_{2\omega}+\mathrm{c}_{2f}\right)\right] & -\frac{1}{2}\left[\mathrm{s}_\Omega\left(2+\mathrm{c}_{2f}-\mathrm{c}_{2\omega}\right) + \mathrm{c}_\Omega \mathrm{c}_\imath\left(\mathrm{s}_{2f}-\mathrm{c}_{2\omega}\right)\right] \\
-\frac{\mathrm{s}_\imath}{2}\left(2+\mathrm{c}_{2f}+\mathrm{c}_{2\omega}\right) & -\frac{\mathrm{s}_\imath}{2}\left(\mathrm{s}_{2f}-\mathrm{s}_{2\omega}\right)
\end{array}\right].
\end{aligned}
$$

The basic equations to be used to obtain $\Delta\mathbf{E}''$ are Lagrange's planetary equations, which express the rate of change of the orbit elements as a function of the perturbing function and the mean orbit elements. The perturbing function that expresses the short-period J_2 perturbations is given by [69]

$$
\begin{aligned}
F \;=\; & \frac{3}{2}\frac{\mu J_2 R^2}{a^3}\left(\frac{a}{r}\right)^3 \left\{ \left(\frac{1}{3} - \frac{1}{2}\sin^2\imath\right)\left[1 - \left(\frac{r}{a}\right)^3\left(1-e^2\right)^{-3/2}\right] \right. \\
& \left. + \frac{1}{2}\sin^2\imath\cos 2\left(f+\omega\right) \right\}. \qquad \text{(7-5.12)}
\end{aligned}
$$

The Lagrange planetary equations can be found in equation (6.29) in [69] for the set $\mathbf{E}$. One may proceed as in [69] (Section (10.4.1)) to obtain closed form solutions for the non-singular set of orbital elements $\mathbf{E}''$ with f being the independent variable.

However, given the complexity of the equations under consideration, this tends to be a tedious computation. An alternative method is to use the relation $\Delta\mathbf{E}' = T^{-1}\Delta\mathbf{E}$ to compute the osculating orbital element deviations $\Delta\mathbf{E}'$ from ΔE that can be found in [69] (pages 317-318.) Note again that we let e be arbitrary to obtain $\Delta\mathbf{E}'$ and *then* take the limit as $e \to 0$. Extracting the periodic part of the motion only (since secular terms cancel out in a relative motion study), the resulting equations are

$$\begin{aligned}
\frac{\Delta a_p}{a} &= \frac{3}{2}\frac{J_2R^2}{a^2}\sin^2\imath\cos 2(f+\omega) \\
\Delta\imath_p &= \frac{3}{8}\frac{J_2R^2}{a^2}\sin 2\imath\cos 2(f+\omega) \\
\Delta\epsilon_p &= \frac{3}{4}\frac{J_2R^2}{a^2}\Big[-2+5\sin^2\imath+2\cos\imath\big(-\sin\omega\cos\omega \\
&\quad +2\sin\omega\cos\omega\cos^2 f-\sin f\cos f+2\cos^2\omega\sin f\cos f\big)\Big] \qquad \text{(7-5.13)} \\
\Delta\Omega_p &= \frac{3}{4}\frac{J_2R^2}{a^2}\cos\imath\sin 2(f+w) \\
\Delta h_p &= \frac{1}{16}\frac{J_2R^2}{a^2}\left[3\sin(\omega+f)\left(1+7\cos 2\imath\right)+7\sin 3(\omega+f)\left(1-\cos 2\imath\right)\right] \\
\Delta k_p &= \frac{1}{16}\frac{J_2R^2}{a^2}\left[3\cos(\omega+f)\left(3+5\cos 2\imath\right)+7\cos 3(\omega+f)\left(1-\cos 2\imath\right)\right],
\end{aligned}$$

where the independent variable is the true anomaly f as opposed to time t. These equations will become singular for small inclinations. However, we are interested in orbits with an inclination $\imath = 45^\circ$ to be able to scan the entire celestial sphere within one nodal period. We do not make the substitution $\imath = 45^\circ$ here to allow for other applications for which $\imath = 45^\circ$ is not the case.

Therefore, we have $\Delta\mathbf{q} = G_0\Delta\mathbf{E}''$, where $\Delta\mathbf{E}''$ is computed from equation (7-5.13). Note that the perturbations $\Delta\mathbf{q}$ are expressed in the Earth-fixed frame F_E. However, we are interested in in-orbital plane perturbations in spacecraft positions –assuming that the line of sight is perpendicular to the orbit plane[3]. Perturbations

[3]If we are imaging in a direction not perpendicular to the orbit plane (say in the polar direction

of the position vector in a direction normal to the orbit plane do not affect the image quality. This is due to the fact that the range to the target, $\bar{z}$, is too large to have J_2-induced perturbations in the normal direction affect image quality[4].

Let $\mathbf{I}, \mathbf{J}, \mathbf{K}$ be a dextral set of orthonormal unit vectors, where $\mathbf{I}$ points towards the ascending node, $\mathbf{K}$ is perpendicular to the orbit plane and $\mathbf{J}$ is such that $\mathbf{J} = \mathbf{K} \times \mathbf{I}$. Denote this moving frame by F_O. For this choice of frame, the coordinates, x, y, Z, in the F_O frame are related to the coordinates, x, y, z, in the F_E frame by

$$\begin{bmatrix} x \\ y \\ Z \end{bmatrix} = R \begin{bmatrix} x \\ y \\ z \end{bmatrix},$$

where the rotation matrix R is given by

$$R = \begin{bmatrix} \mathrm{c}_\Omega & \mathrm{s}_\Omega & 0 \\ -\mathrm{s}_\Omega \mathrm{c}_\imath & \mathrm{c}_\Omega \mathrm{c}_\imath & \mathrm{s}_\imath \\ \mathrm{s}_\Omega \mathrm{s}_\imath & -\mathrm{c}_\Omega \mathrm{s}_\imath & \mathrm{c}_\imath \end{bmatrix}.$$

Let $P_O = [\, x \; y \; Z]^T$ and $P_E = [\, x \; y \; z]^T$. The perturbed coordinates are therefore related by[5]

$$\Delta P_O = R \Delta P_E.$$

Hence we have

$$\Delta P_O = R G_0 \Delta \mathbf{E}''. \tag{7-5.14}$$

---

for a 45° inclination orbit), then perturbations normal to the orbit plane will affect frequency domain coverage. This, however, is a more complex problem (as picture frame discs become elliptic) and we restrict our attention to the case when the line of sight is perpendicular to the orbit plane.

[4]In fact, one can show that even significant deviations along the line of sight, which is normal to the observation plane (that is, in our case, the orbit plane) do not affect image quality.

[5]The matrix R is a function of mean orbit elements and, hence, $\Delta R = 0$.

Next, we derive a conservative upper bound for perturbations in the x and y coordinates of P_O. First let $P_O^{XY} = [x\ y]^T = I_{XY} P_O$, where the projection matrix I_{XY} is given by

$$I_{XY} = \begin{bmatrix} 1 & 0 & 0 \\ 0 & 1 & 0 \end{bmatrix},$$

and let $\left\|\Delta P_O^{XY}\right\| = \sqrt{\Delta x^2 + \Delta y^2}$ denote the magnitude of the total in-plane perturbation of the position vector. Therefore, we have

$$\left\|\Delta P_O^{XY}\right\| \;=\; \left\|I_{XY} R G_0 \Delta \mathbf{E}''\right\|. \tag{7-5.15}$$

If we let $H = I_{XY} R G_0$, then by the Schwartz and triangular inequalities we have

$$\begin{aligned} \left\|\Delta P_O^{XY}(f)\right\| &\le \|H\| \cdot \|\Delta \mathbf{E}''\| \\ &\le \|H\| \left(\left| \frac{\Delta a}{a}(f) \right| + |\Delta \imath(f)| + |\Delta \epsilon(f)| + |\Delta \Omega(f)| + |\Delta h(f)| + |\Delta k(f)| \right) \\ &= \|H\|\, \Delta(f), \end{aligned}$$

where $\Delta(f)$ denotes the second term (in brackets) after the second inequality. Finally, one now simply computes the maximum in-plane deflection in the magnitude of the position vector as

$$\Delta_{\max}^{OP}\mathbf{q} = \max_{0 \le f \le 2\pi} \|H\|\, \Delta(f). \tag{7-5.16}$$

Equation (7-5.15) or (7-5.16) can now be used to obtain a conservative estimate of deflection of a spacecraft from its nominal circular trajectory due to short-period J_2 effects. With this, one may further assume the linear array design, in which the slightest perturbation from the nominal trajectory will immediately induce gaps in the frequency domain, is used. Note that this assumption is also conservative because, in a curved constellation, redundant multiple coverage exists between the different picture frame circular trajectories (that is to say, the frequency "bins" blend

into each other.) Therefore, if the nominal design is modified such that with the J_2 perturbations in any of the spacecraft's position is given given by $\Delta^{OP}_{\max}\mathbf{q}$, we can then guarantee complete coverage of the frequency domain. This we investigate in Section (7.6).

Note that there are several definitions for a matrix norm. With each choice of norm a different upper bound is obtained. The most widely used matrix norms are the 1, 2, infinity and Frobenius norms. For more on matrix norms, consult any reference on linear algebra such as [70].) It was generally found that these approximations were too conservative and the least conservative was the two-norm.

On the other hand, one may also compute the exact expression for $\left\|\Delta P_O^{XY}\right\|$ from equation (7-5.15). If we set $\Omega = \omega = 0$ and $\imath = 45^\circ$, $\left\|\Delta P_O^{XY}\right\|$ is computed as

$$\left\|\Delta P_O^{XY}\right\| = \frac{\sqrt{512}}{512}\frac{J_2R^2}{a}\left(126 - 34\cos 2f + 3\cos 4f - 14\cos 6f - 49\cos 8f\right)^{\frac{1}{2}} \quad (7\text{-}5.17)$$

Figure 7.17 shows a comparison between the exact value for $\left\|\Delta P_O^{XY}\right\|$ and the conservative upper bound on $\left\|\Delta P_O^{XY}\right\|$ using the two-norm for $0 \leq f \leq 2\pi$ with $a = 7,200$km. Even though the two-norm definition is the least conservative, we observe in Figure (7.17) that this approximation is an order of magnitude higher than the exact maximum value. One may also compute the maxima and minima of $\left\|\Delta P_O^{XY}\right\|$ from equation (7-5.17). $\left\|\Delta P_O^{XY}\right\|$ was computed numerically and was found to have a maximum value of

$$0.6116\frac{J_2R^2}{a} = 3.73 \text{ km}$$

at $f = 0.39\pi,\ 0.61\pi,\ 1.39\pi,\ 1.61\pi$ and a minimum value of

$$\frac{1}{4}\frac{J_2R^2}{a} = 1.53 \text{ km}$$

at $f = 0,\ \pi$.

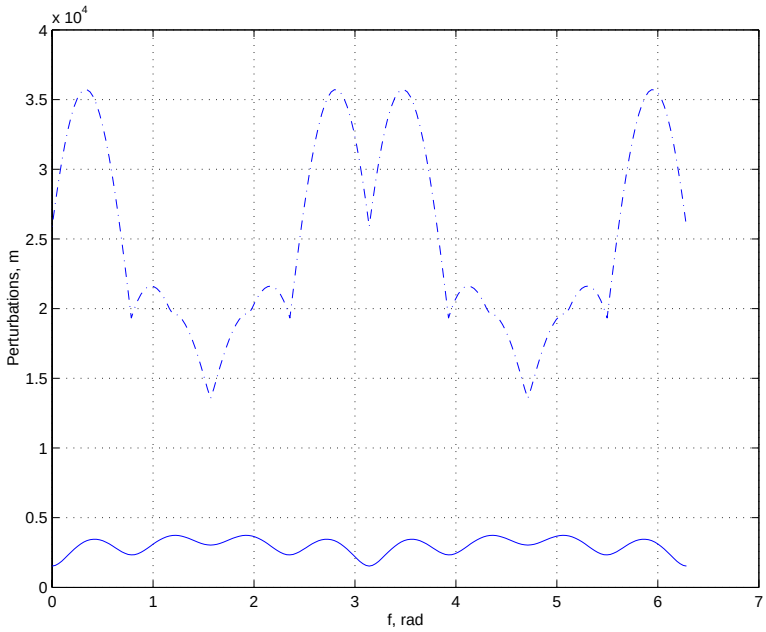

Figure 7.17: Exact $\left\|\Delta P_O^{XY}\right\|$ (solid) and the conservative upper bound $\Delta_{\max}^{OP}\mathbf{q}$ using the two-norm (dash-dotted.)

7.6 Design for Complete Wave Number Plane Coverage Under Perturbations

7.6.1 Eccentricity Corrections

In this section we modify the design procedure to account for perturbations due to orbit eccentricities and J_2. First, note that perturbations in relative position vectors result in gaps in the frequency domain at high and low frequencies, where high frequency components correspond to the finer details of an image and low frequency components correspond to the coarser details. Hence, since it is meaningless to attempt to reconstruct an image with fine details while ignoring the main, coarser details, low frequency components are more crucial to be able to reconstruct than higher frequency components. Based on this observation, and since we will not be able to account for both low and high frequency gaps within a single orbit period, the nominal configuration design is modified to ensure coverage of the low frequency

components at the cost of leaving out the highest spatial frequencies. This is done as follows.

Let $\Delta_{\max}$ denote the maximum perturbation in the frequency domain. $\Delta_{\max}$ may correspond to either perturbations in orbit eccentricity or, more generally, to J_2. For simplicity, we will use perturbations in orbit eccentricity to illustrate how the design is modified to ensure low frequency coverage. At the end of this section, we also comment on how this is done to counterbalance J_2 effects. Simply shifting the centers of the picture frame discs by an amount of $\Delta_{\max}$ corresponds to decreasing the inter-spacecraft distances by an amount of $\lambda\Delta_{\max}$ in the physical domain. Therefore, if $d_{\min} = \lambda/\theta_p$ is the nominal distance between a pair of spacecraft in the *fundamental* set, then let

$$d^*_{\min} = d_{\min} - \lambda\Delta_{\max} = \lambda\left(\frac{1}{\theta_p} - \Delta_{\max}\right) \tag{7-6.1}$$

be the new inter-spacecraft distance in the fundamental set. This also leads to a total contraction of the constellation. Consequently, this leads to shifting the centers of the picture frame discs in the frequency domain by $\Delta_{\max}$. While under perturbations, this design modification ensures "closing up" all low frequency gaps at the cost of decreasing the overall effective system resolving power. To regain coverage of the higher frequencies, we may append the constellation by an additional spacecraft to increase the maximum constellation baseline as well as improve the effective angular resolution of the observatory.

Note that the minimal design that follows from the modified configuration of the fundamental set may be different from that derived from the nominal fundamental set. However, since the modified fundamental configuration ensures coverage of low frequencies, the minimal configuration, by definition, will also retain the same property.

We now give some examples. In Section (7.5.1), the first scenario we considered was that of having two spacecraft which are 180° out of phase but with the same eccentricity. The maximum perturbation in the frequency domain was computed as $\sqrt{f_{ij}} = 4A/\lambda$. Hence, we set $\Delta_{\max} = 4A/\lambda$. The top left plot in Figure (7.18) shows the frequency domain coverage for the modified design corresponding to the nominal trajectory used in Figure (7.12). Note that all low frequency content is recovered at the expense of additional lack of high frequency coverage.

The top right plot in Figure (7.18) shows frequency domain coverage using the modified design corresponding to two in-phase spacecraft with different eccentricities. This plot is the modified version of the one that appears in Figure (7.14). Here we set $\Delta_{\max} = \sqrt{f_{ij}} = 2\left|A_1 - A_0\right|/\lambda$ as discussed in Section (7.5.1). Again, we achieve complete coverage of the lower frequency components at the cost of additional lack of high frequency coverage.

If $\delta^i_{\max}$ is the maximum perturbation in the position of spacecraft $i \in \mathcal{I}$, then note that whenever the inter-spacecraft spacing is decreased we must ensure not to violate the inequality

$$\delta^i_{\max} + \delta^j_{\max} < d^*_{\min},\ i,\ j \in \mathcal{I} \tag{7-6.2}$$

for any two neighboring spacecraft i and j, otherwise the spacecraft may cross paths, which, in turn, may lead to collisions. To give an example where this may happen, consider again the problem where $N_f = 2$, $A_0 = 4.65$ km and $A_1 = 4.04$ km and phases $\phi_0 = 165.99°$ and $\phi_1 = 204.42°$. The unmodified frequency coverage is shown in Figure (7.15) (left.) As a conservative estimate, we may set $\lambda\Delta_{\max} = 4\max\{A_0, A_1\} = 18.6$ km. However, as shown in Figure (7.18) (bottom left), this leads to trajectory crossing since $d^*_{\min}/4 = 1.29\text{km} < A_0,\ A_1$. One may obtain expressions for f_{ij}, from which one can compute the maximum deviation in

the frequency domain for the ij^{th} picture frame disc. This is then used to compute $\Delta_{\max}$. By iteration, it was found that setting $\lambda\Delta_{\max} = 1.25\lambda \max\{A_0, A_1\} = 5.81$ km indeed ensures coverage of low frequency content as shown in the bottom right plot in Figure (7.18). We note here that $d^*_{\min} = 17.93$ km $> 2A_0 + 2A_1 = 17.38$ km and the condition (7-6.2) is met. Hence path crossing does not take place.

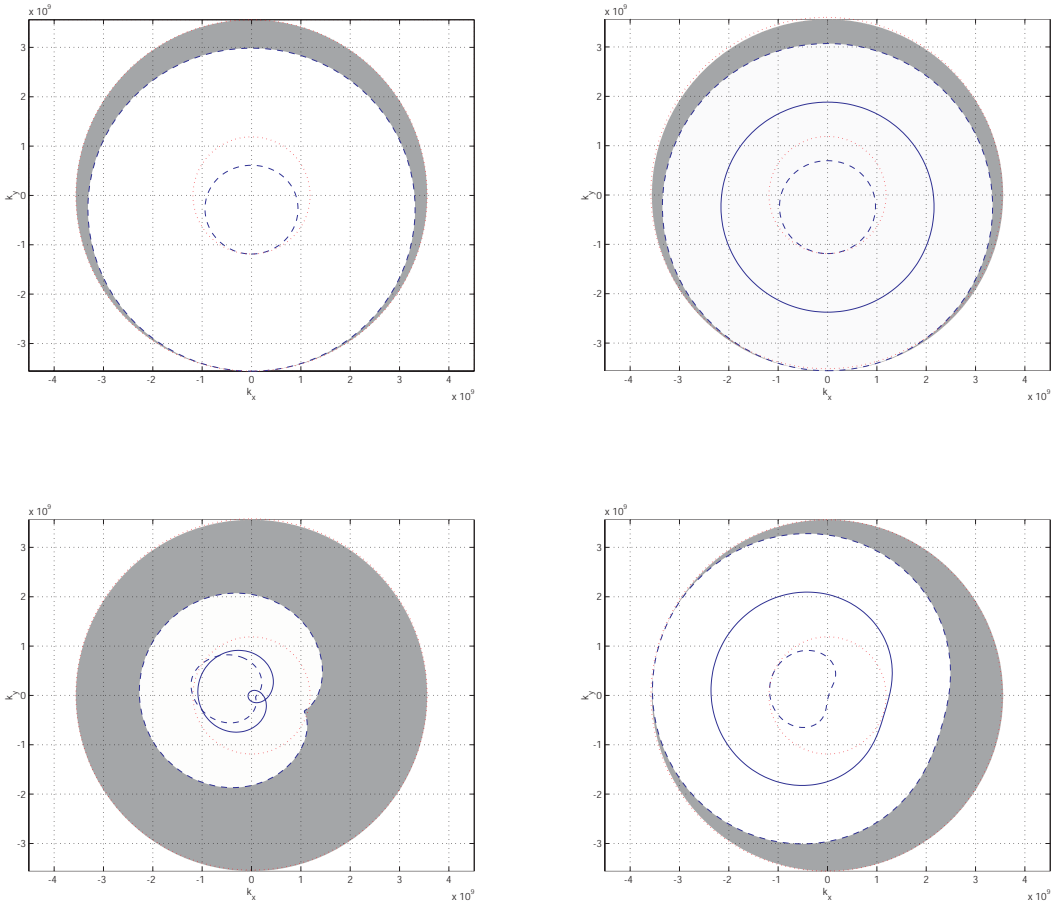

Figure 7.18: Modified wave number plane coverage corresponding to Figures 7.12, 7.14 and the left plot of Figure (7.15).

7.6.2 J_2 Corrections

Finally, for J_2, the inter-spacecraft distance may be set at

$$d^*_{\min} = d_{\min} - 2 \max_{i \in \mathcal{I}} \max_{0 \le f \le 2\pi} \left\| P^{XY}_{O_i} \right\|$$

assuming that the maximum perturbation of a pair of spacecraft from their nominal path occur at different points in time. Analogous to the eccentric orbit case, this choice for $d^*_{\min}$ will ensure complete coverage of the frequency domain despite the short-period J_2 perturbations. Using the same numerical values for Ω, ω and a as in Section (7.5.2), we find that the maximum perturbation of each spacecraft from its nominal value is 3.73km. Hence, we have $d^*_{\min} = d_{\min} - 2 \times 3.73 = d_{\min} - 7.46$ in kilometers. Note that in the frequency domain $\Delta_{\max} = 7.46 \times 10^3/\lambda = 7.46 \times 10^8$ for a signal with a wavelength $\lambda = 10\mu$m.

7.7 On the Optimality of a Class of Circular Earth-Orbiting Observatories

In this section we show that the circular Earth-orbiting observatory is optimal in the sense of Chapter 2. Hence, Chapter 2 is a prerequisite to this section.

We choose the terminal time T such that T spans an integer multiple, say l, of the orbit period $T_{\rm o}$: $T = lT_{\rm o}$. The reason for having to wait for multiple orbits before capturing an image is due to the fact that coverage in the frequency domain is radially uneven. That is to say, for each $\nu^* \in \mathbb{R}$, we have even coverage for all $\boldsymbol{\nu}$ satisfying $\|\boldsymbol{\nu}\| = \nu^*$ after each half orbit period. However, as ν^* changes, the value of z changes (in fact decreases as shown above.) Hence, we choose l such that after $l/2$ orbit periods the value of the normalized MTF $z(\boldsymbol{\nu}, t)$ is at least unity everywhere inside the resolution disc D_v. If we let h denote the saturation function:

$$h(x) = \begin{cases} x & 0 \le x < 1 \\ 1 & x \ge 1 \end{cases}$$

then we require to have the terminal condition on z be given by

$$h(z(\boldsymbol{\nu}, T)) = 1 \tag{7-7.1}$$

for all $\boldsymbol{\nu} \in D_v$. Specifying T automatically specifies the orbit size.

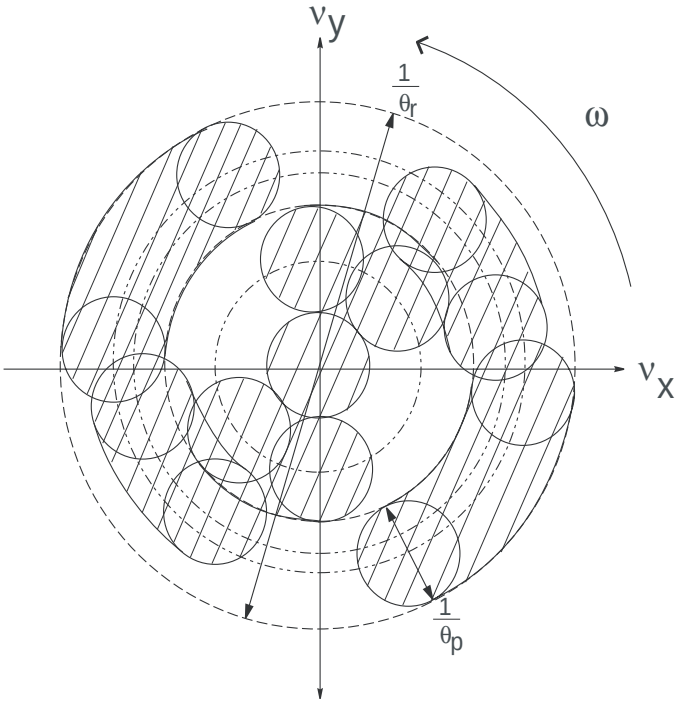

Figure 7.19: Physical distribution in the wave number plane for a three-spacecraft formation.

Since we are now dealing with a system of particles under the influence of gravity, let us now re-derive the necessary conditions with a gravitational field modeled in the system dynamics. Hence, the dynamics are now given by:

$$\begin{aligned} \dot{\mathbf{q}}_i(t) &= \mathbf{v}_i(t) \\ \dot{\mathbf{v}}_i(t) &= \mathbf{u}_i + \mathbf{g}(\mathbf{q}_i) \end{aligned} \tag{7-7.2}$$

for all spacecraft $i = 1, \ldots, N$. The cost function and initial conditions are as before.

The function $\hat{H}$ is now given by:

$$\begin{aligned}\hat{H}(t) &= \sum_{i=1}^{N}\left[\mathbf{p}_{\mathbf{q}_i}\cdot\mathbf{v}_i+\mathbf{p}_{\mathbf{v}_i}\cdot(\mathbf{u}_i+\mathbf{g}(\mathbf{q}_i))\right]\\ &\quad+\mu p_y\left(\sum_{i=1}^{N}\|\mathbf{u}_i\|^2\right)+\left\langle p_z(\boldsymbol{\nu},t),\sum_{l,n=1,n\neq l}^{N}\hat{A}_p\left(\boldsymbol{\nu}-\mathbf{q}_{mn}\right)\right\rangle. \quad (7\text{-}7.3)\end{aligned}$$

The necessary condition for optimality still implies that

$$\mathbf{u}_i = -\frac{1}{2\mu p_y}\mathbf{p}_{\mathbf{v}_i}$$

and, hence, the Hamiltonian is given by:

$$H(t) = \sum_{i=1}^{N}\left[\mathbf{p}_{\mathbf{q}_i}\cdot\mathbf{v}_i-\frac{\|\mathbf{p}_{\mathbf{v}_i}\|^2}{4\mu p_y}+\mathbf{p}_{\mathbf{v}_i}\cdot\mathbf{g}(\mathbf{q}_i)\right]+\left\langle p_z(\boldsymbol{\nu},t),\sum_{l,n=1,n\neq l}^{N}\hat{A}_p\left(\boldsymbol{\nu}-\mathbf{q}_{mn}\right)\right\rangle, \quad (7\text{-}7.4)$$

Transversality conditions are the same as before:

$$\begin{aligned}\mathbf{p}_{\mathbf{q}_i}(T) &= \mathbf{p}_{\mathbf{v}_i}(T)=0\\ p_z(\boldsymbol{\nu},T) &= p_z^f(\boldsymbol{\nu}) \quad (7\text{-}7.5)\\ p_y(T) &= 1.\end{aligned}$$

The necessary optimality conditions are now given by:

$$\begin{aligned}\dot{\mathbf{q}}_i(t) &= \mathbf{v}_i(t)\\ \dot{\mathbf{v}}_i(t) &= -\frac{\mathbf{p}_{\mathbf{v}_i}(t)}{2\mu}+\mathbf{g}(\mathbf{q}_i)\\ \dot{y}(t) &= \sum_{i=1}^{N}\frac{\|\mathbf{p}_{\mathbf{v}_i}(t)\|^2}{4\mu} \quad (7\text{-}7.6)\\ \dot{z}(\boldsymbol{\nu},t) &= \sum_{l,n=1,n\neq l}^{N}\hat{A}_p\left(\boldsymbol{\nu}-\mathbf{q}_{mn}(t)\right)\\ \dot{\mathbf{p}}_{\mathbf{q}_i}(t) &= -\nabla_{\mathbf{q}_i}\mathbf{g}(\mathbf{q}_i)\cdot\mathbf{p}_{\mathbf{v}_i}\\ &\quad+\frac{1}{\lambda\bar{z}}\left\langle p_z^f(\boldsymbol{\nu}),\sum_{n=1,\neq i}^{N}\left(-\nabla\hat{A}_p(\boldsymbol{\nu}-\mathbf{q}_{in}(t))+\nabla\hat{A}_p(\boldsymbol{\nu}+\mathbf{q}_{in}(t))\right)\right\rangle\\ \dot{\mathbf{p}}_{\mathbf{v}_i}(t) &= -\mathbf{p}_{\mathbf{q}_i}(t)\end{aligned}$$

Nominally for the circular orbit observatory, fuel is not required to keep formation (ignoring J_2 and, possibly, drag for LEO and other perturbations.) Hence we have $\mathbf{u}_i(t) = 0$ for all $t \in [0, T]$. Hence we have the following results: $\mathbf{p}_{\mathbf{v}_i}(t) = \mathbf{p}_{\mathbf{q}_i} = 0$. Hence, the corresponding transversality conditions (namely, $\mathbf{p}_{\mathbf{v}_i}(T) = \mathbf{p}_{\mathbf{q}_i}(T) = 0$) are immediately satisfied. The necessary conditions then become:

$$\begin{aligned}
\dot{\mathbf{q}}_i(t) &= \mathbf{v}_i(t) \\
\dot{\mathbf{v}}_i(t) &= \mathbf{g}(\mathbf{q}_i) \\
\dot{y}(t) &= 0 \\
\dot{z}(\boldsymbol{\nu}, t) &= \sum_{l,n=1,n\neq l}^{N} \hat{A}_p \left(\boldsymbol{\nu} - \mathbf{q}_{mn}(t)\right) \\
0 &= \left\langle p_z^f\left(\boldsymbol{\nu}\right), \sum_{n=1,\neq i}^{N} \left(-\nabla \hat{A}_p(\boldsymbol{\nu} - \mathbf{q}_{in}(t)) + \nabla \hat{A}_p(\boldsymbol{\nu} + \mathbf{q}_{in}(t))\right) \right\rangle .
\end{aligned} \tag{7-7.7}$$

Note that the first two equations in the equations (7-7.7) simply express the Keplarian motion in differential equation form, which is necessary by design. Secondly, the initial condition $y(0) = 0$ and the third equation gives $y(t) = 0$ for all $t \in [0, T]$. In particular the total cost is $y(T) = 0$. Since the cost functional is positive definite, then if the formation satisfies the terminal necessary conditions, then the Earth-orbiting observatory is optimal. To check for this we need to verify that the terminal condition (7-7.1) and that the last condition in Equation (7-7.7) are satisfied. By construction, the formation makes enough orbits l such that at terminal time T we have $h(z(\boldsymbol{\nu}, T)) = 1$ and, hence, satisfying the terminal condition. As for the last condition in Equation (7-7.7), Similar to the discussion made in the last paragraph of Section (2.6), any symmetric function $p_z^f(\boldsymbol{\nu})$ (such as $p_z^f(\boldsymbol{\nu}) \equiv 0$) will satisfy this condition by symmetry of the the second term in the inner product. This shows that the Earth-orbiting formation is an optimal solution to the problem.

A final remark is in order. The basic assumption above is that the formation

maintains its rigidity. The Earth-orbiting observatory will maintain formation even when in eccentric orbits as long as the spacecraft elliptic motions are in phase and have the same value for the semi-major axis. Once rigidity is not maintained, gaps emerge and symmetries will be broken in the frequency domain. This will immediately violate the necessary conditions and the formation does not satisfy the necessary conditions, in the strict mathematical sense discussed in this chapter, and is thus sub-optimal.

7.8 The Interferometric Observatory

The Earth-orbiting constellation configurations proposed above will completely cover the wave number plane in half an orbit period, while imaging for several orbital periods will result in improved image quality. Thus, over a short period (days at most) an image can be formed. If we place the constellation in an inclined orbit, the orbit plane will precess relative to inertial space and the constellation will scan across the celestial sphere at a constant rate, effectively repeating its coverage after half a nodal period. The precession rate of the orbit plane is given by [69]

$$\dot{\Omega} = -\frac{3}{2}\sqrt{\frac{\mu}{r_o^3}}\frac{R_o^2 J_2}{r_o^2}\cos(\imath),$$

where $R_o = 6378.14$km is the Earth's radius, $J_2 = 0.00108263$ is the second zonal harmonic of the Earth, $\mu = 3.986005 \times 10^5 \text{km}^3/\text{s}^2$ is the Earth's gravitational constant, $\imath$ is the inclination, r_o is the orbital radius, and the precession period of the node is $T = \frac{2\pi}{\dot{\Omega}}$. For an 800km altitude orbit inclined at 45^o to the equator, the precession period is 77 days. For a constellation in a 45^o or 135^o inclination orbit, every point on the celestial sphere can be imaged with an angular resolution ranging from θ_r to $\theta_r/\sqrt{2}$ within half a nodal period.

An important design consideration is the speed at which the picture frame disc moves in the wave number plane, as this affects the image quality. The larger this speed is, the poorer the image quality becomes. Given an upper bound on the wave plane velocity, v^*, and a desired angular resolution, θ_r, this constrains the angular rate at which the picture frame disc moves in the wave number plane, equal to the mean motion of the orbit, $\omega \leq \frac{1}{2}v^*\theta_r$. This bounds the desired orbit radius, $r_o \geq \sqrt[3]{\frac{4\mu}{(v^*\theta_r)^2}}$. Thus, the choice of orbit radius does not depend only on the desired baselines (determined from the desired angular resolution), but also on the desired image quality. Note that it is possible to trade a higher speed in the wave number plane (shorter period) with additional observations, striking a balance between the two.

Other issues of concern are the signal detection, transmission and interference. There are certain optical technologies that are assumed to exist for the proposed very long baseline LEO observatory to be feasible. We assume that either a heterodyne or a direct detection method is used. Heterodyne detection has the advantage of selecting and detecting only the components of the wavefront of the source that are in phase with the wavefront of a local laser oscillator [71]. Thus, heterodyne detection furnishes phase information. On the other hand, direct detection, though less efficient as far as signal to noise is concerned, is still feasible via spatial filtering with a glass fiber to obtain a single geometric mode [72]. Local heterodyne detection, however, has a major advantage over direct detection Michelson interferometry. Direct detection requires that the detected signal be divided into $N-1$ equal parts, where N is the number of satellites in the constellation, corresponding to $N-1$ baselines. This results in the reduction of the signal by a factor of $N-1$. Each of the $N-1$ signals will possess a reduced SNR. This is exacerbated due to the presence of large

background noise and the long distances over which the signals are transmitted from each spacecraft to a combiner spacecraft. For wavelengths above $\sim 4\mu$m, heterodyne detection is likely to be superior because of these problems with direct detection. It could be shown, however, that below $\sim 4\mu$m, direct detection will have better SNR properties than heterodyne detection. For a 10μm mission, such as the one proposed in this chapter, heterodyne detection is advantageous.

A technique different from heterodyne detection is also under investigation by our group at the University of Michigan. This is Fourier Transform Spectral Interferometry for electric field reconstruction in a separated spacecraft interferometric mission. Novel optical techniques exist, such as Dual-Quadtrature Spectral Interferometry (DQSI) and Spectral Phase Interferometry for Direct Electric Field Reconstruction (SPIDER), that aim at the full characterization of an electric field, both temporally and spatially [73, 74]. The goal of such research, which has so far been developed for highly coherent sources and is currently being developed for non-coherent sources, is to extract necessary information in digital form that allow for performing the interference process digitally on a microchip. Once such digital information is available, these can be sent via communication links such as radio frequency signals to a central processing unit located on one of the spacecraft for the mutual intensity computations and metrology measurements. In light of technologies such as heterodyne detection or electric field reconstruction, a very long baseline mission such as the one we propose in this chapter should be feasible as far as the optics are concerned.

A final remark is that JPL's Terrestrial Planet Finder (TPF) technology is an IR interferometer that currently does not involve baselines longer than 100m between apertures. TPF may provide an angular resolution that is as small as 0.75 milliarcsec at 3μm and 1000m baseline. This corresponds to single pixel detection of a

planet located 0.5AU from a sun-like star [3]. The main aim of TPF is to detect an earth-like planet by separating the planet from its parent star and capturing its light on a single pixel. In contrast, the underlying aim of the proposed observatory is to form a multi-pixel image of the disk of the planet. In consequence, the very long baseline constellation, such as the example we use here, offers 1.9461×10^{-6} milli-arcsec resolution at 10μm and a longest baseline of over 14,000km.

7.9 Conclusion

In this chapter, the imaging objectives are stated and a class of constellations that can achieve high angular resolution images in LEO was discussed. An optimization procedure is also defined that supplies m pixels of resolution with a minimum number of satellites. We introduced a linear imaging constellation and formulated a 0-1 mathematical programme, the solution of which is the solution to the optimal aperture configuration for full coverage of the wave number plane. This in turn, helps to numerically solve the constellation design problem for a general Earth-orbiting constellation.

A sufficient condition for complete u-v plane coverage when under eccentric orbits was stated and proven. We also addressed short period effects of J_2 on imaging. First, we derived analytical expressions for the maximum perturbations in the position of the constellation spacecraft as a function of the osculating orbit elements. These studies lead to design criteria that ensure wave number plane coverage as a function of perturbation size for both eccentricity and J_2 perturbations. The modified design, however, leads to additional lack of coverage of higher frequencies and reduces the overall resolving power of the constellation.

Finally, we discussed how the zonal J_2 effect can be utilized to scan the observa-

tory across the celestial sphere and, finally, we discuss some practical implementation issues. Future research will study the behavior of similar constellations subject to more general gravitational fields.

CHAPTER 8

Conclusion and Future Work

This dissertation aims at using the relationship between the motion of an interferometric imaging formation and the quality of the reconstructed image –via the notion of the Modulation Transfer Function– for the motion design and guidance of the formation. The MTF was introduced in Chapter 2 and was used to formulate an optimal control law that seeks to improve the quality of the image while minimizing fuel expenditure. This problem has close connections to problems in optimal control of infinite dimensional systems since there are two independent variables (time t and frequency $\boldsymbol{\nu}$) appearing in the dynamics. The main difference between the imaging problem and other problems involving wave propagation is that the former has no transport properties, that is, the constraints are only finite dimensional differential equations as opposed to partial differential equations. Optimal control of infinite dimensional systems, in general, has not reached its maturity and is subject to open research. For more on optimal control of infinite dimensional systems, see for example [75]. In particular, future research will focus on optimal control of infinite dimensional systems and the multi-spacecraft imaging problem.

Using tools from geometric mechanics and differential geometry, in Chapter 3 we introduce the dynamic coverage optimal control problem. Instead of deriving

an optimal control law that is explicitly a function of image quality as was done in Chapter 2, in the dynamic coverage problem the resulting control law is only a function of the relative position and velocity vectors between all spacecraft in the formation. Such a control is shown to result in the same optimal behavior as obtained in Chapter 2. Though the problem is formulated assuming a point particle model for each spacecraft, since the problem statement is given on generic manifolds, the model may be extended to formations of rigid bodies, where spacecraft attitude is also taken into account.

The modeling of each spacecraft as a rigid body was studied in Chapter 4. The problem statement as formulated in Chapter 4 (as well as the dynamic interpolation problem of Chapter 5) is appropriate only for dual spacecraft formations, assuming one spacecraft is fixed in space and the second free to evolve in $\mathbb{R}^3$. In particular, the main contribution of Chapter 4 is the introduction and analysis of the optimal trajectory tracking problem on SE(3). Future work will focus on extending this problem to formations of three or more spacecraft. Some related open problems include the use of Poisson reduction theory to reduce the complexity of the system by utilizing the presence of conserved quantities (such as energy or momentum) plus any symmetric properties of the system. For more on the history of reduction theory, see Chapter 1 in [76] and [89] and references therein. Another related open problem is that of applying geometry-preserving numerical integrators to formations of spacecraft. The development of numerical integrators that preserve the structure (such as the Lie algebra properties of a Lie group) or conserved quantities (such as energy and momentum) have received special attention in recent years. See for example [77] and [78] and references therein. On the other hand, the development of geometry preserving numerical schemes for solving two point boundary value problems still

remains an open problem, see [79] for example.

In Chapter 6, the dual spacecraft spiraling (on the paraboloid) formation was introduced. An optimal control problem was formulated that aims at meeting the imaging constraints while minimizing fuel consumption and improving the signal-to-noise ratio. It was shown that the problem is convex and that a unique and global optimal solution exists. The method of continuation was used to solve for the unique global optimal trajectory. Open problems include the extension of this class of spiraling maneuvers to three or more spacecraft formations, analogous to the four spacecraft time-optimal spiraling maneuver introduced in [5].

Finally, an Earth-orbiting observatory that satisfies the necessary conditions for optimality, with the potential to be implemented in a future Origins mission, was proposed and studied in Chapter 7. Future research will study the behavior of these constellations when subject to other types of perturbations such as drag and the influence of a third body. Practical implementation issues, such as signal synchronization, transmission, digitization, storage and processing are also of significant concern and must also be the subject of future research.

APPENDICES

APPENDIX A

Mathematical Background to Geometric Mechanics and Optimal Control

In this appendix we give a very brief introduction to basic notions from differential geometry and geometric mechanics. It is not intended by any means to be comprehensive. We include material in this appendix based on three reasons. Firstly, we may include material in this appendix that is implicitly at the heart of the geometric tools used in the main body of the dissertation. For example, Lagrange multipliers appearing in many chapters are objects that belong to the cotangent space. The cotangent space itself is not explicitly discussed in the body of the dissertation but we do so in this appendix. Secondly, we will also make definitions and include results that are needed, not in the main body of the dissertation, but to make other definitions and derive other results included in and are central to the dissertation. Finally, often we include material that will not be used anywhere in this dissertation. The goal is to make this appendix a bit more comprehensive in nature. The interested reader should thus consult the following references on the theory and applications of geometric mechanics (not in any specific order) for a full and comprehensive understanding of this beautiful subject matter.

Differential Geometry: The books by Abraham, Marsden and Ratiu [80], Boothby

[60], Burke [81], Crampin and Pirani [82], do Carmo [83] and [84], Kobayashi and Nomizu [85], Milnor [41], Onishchik and Vinberg [50], the comprehensive multi-volume book by Spivak [59], Warner [52] and references therein.

Geometric Mechanics: The books by Abraham and Marsden [86], Abraham, Marsden and Ratiu [80], Arnold [87], Bloch [42], Burke [81], Monforte [88], Marsden [89] and references therein.

Geometric Control Theory: The books by Bloch [42], Bullo and Lewis [51], Agrachev and Sachkov [90], Jurdevic [91], Monforte [88], Marsden [89], Marsden and Ratiu [92], Murray, Li and Sastry [93] and references therein.

Geometric Optimal Control Theory: The book by Agrachev and Sachkov [90], the thesis by Camarinha [55] and the papers by Noakes, Heinzinger and Paden [30], Crouch and Jackson [35], Crouch and Jackson [31], Crouch and Silva-Leite [32] and [33], Crouch, Silva-Leite and Camarinha [34], Silva-Leite, Camarinha and Crouch [94] and references therein.

Geometry and Space Time Physics: The beautiful book by Misner, Thorne and Wheeler [95].

A.1 Basics of Differential Geometry

A.1.1 Fundamentals

Definition A.1.1 (Diffeomorphism). Let M and N be two sets. A map $\phi : M \to N$ is a *diffeomorphism* if the inverse map $\phi^{-1} : N \to M$ exists and is $\mathcal{C}^\infty$.

Definition A.1.2 (Homeomorphism and Homeomorphic Sets). A continuous map $f : A \subset \mathbb{R}^n \to \mathbb{R}^n$ is a *homeomorphism* onto $f(A)$ if f is one-to-one and the

inverse $f^{-1} : f(A) \subset \mathbb{R}^n \to \mathbb{R}^n$ is continuous. In this case A and $f(A)$ are called *homeomorphic sets* [84].

Definition A.1.3 (Local Chart). Let S be a set. A *local chart* on S is a bijection, ϕ, from a set $U \subset S$ to an open subset of some finite dimensional vector space F.

Definition A.1.4 (Compatibility of Local Charts). Two local charts (U_i, ϕ_i) and (U_j, ϕ_j), with $U_i,\ U_j \subset S$ and $U_i \bigcap U_j = 0$, are *compatible* if the overlap maps (for example $\phi_{ji} = \phi_j \cdot \phi_i^{-1} | \phi_i \left(U_i \bigcap U_j\right)$) are $\mathcal{C}^\infty$ diffeomorphic.

Definition A.1.5 (Atlas). An *atlas* $\mathcal{A}$ on S is a family of charts $\{(U_i, \phi_i) : i \in I\}$ such that

1. $S = \bigcup \{U_i | i \in I\}$.

2. Any two charts in $\mathcal{A}$ are compatible.

Definition A.1.6 (Equivalence of Atlases). Two atlases $\mathcal{A}_1$ and $\mathcal{A}_2$ are *equivalent* if $\mathcal{A}_1 \bigcap \mathcal{A}_2$ is an atlas.

Definition A.1.7 (Differentiable Structure). A *differentiable structure* $\mathcal{I}$ on S is an equivalence class of atlases on S.

Definition A.1.8 (Maximal Atlas). The union of atlases in $\mathcal{I}$, $\mathcal{A}_\mathcal{I} = \bigcup \{\mathcal{A} | \mathcal{A} \in \mathcal{I}\}$ defines the *maximal atlas* of $\mathcal{I}$.

Definition A.1.9 (Differentiable Manifold). A *differentiable manifold* is the pair $(S, \mathcal{I})$, where S is a set and $\mathcal{I}$ is a differentiable structure (often taken as the maximal atlas.)

Example The n-sphere, S^n, is a manifold. To see this, in $\mathbb{R}^{n+1}$, S^n is the set of all $\mathbf{q} \in \mathbb{R}^{n+1}$ such that $||\mathbf{q}|| = 1$. One can locally construct bijections from S^n to $\mathbb{R}^n$, say, stereographically from the south or north pole onto a hyperplane tangent to the north or south pole, respectively. These are two bijections with the south or north pole, respectively, removed, onto $\mathbb{R}^n$. In a region covered by both coordinate systems, we are able to change coordinates smoothly and, thus, any two such bijective maps are compatible. The resulting topology on $\mathbb{R}^n$ is the same as that induced on S^n in $\mathbb{R}^{n+1}$. Thus, S^n is a manifold in $\mathbb{R}^{n+1}$[86].

Definition A.1.10 (Submanifold). $N \subset M$ is a p-dimensional *submanifold* if and only if $\forall \mathbf{q} \in N$, $\exists\,(U, \phi)$ a chart, where $\mathbf{q} \in U$ and $\phi : U \to (q_1, \ldots, q_n)$, such that $\phi | U \bigcap N \to (q_1, \ldots, q_p, 0, \ldots, 0)$, where $(q_1, \ldots, q_n)$ are some coordinates on F (F as defined in definition (A.1.3).

Definition A.1.11 (Embedded Submanifold). M is said to be an *embedded k-dimensional submanifold* of Euclidean space $\mathbb{R}^n$ if in a neighborhood U of every $\mathbf{q} \in M$ there exists $n-k$ functions $f_1 : U \to \mathbb{R}, \ldots, f_{n-k} : U \to \mathbb{R}$ such that the intersection of U with M is given by $f_1 = 0, \ldots, f_{n-k} = 0$ and vectors $\mathrm{grad} f_1, \ldots, \mathrm{grad} f_{n-k}$ are linearly independent.

Definition A.1.12 (Tangent Space and Tangent Vectors). If M is a manifold k-dimensional manifold in $\mathbb{E}^n$ (i.e. $\mathbb{R}^n$ with an Euclidean norm) then every point $\mathbf{q}$ has a k-dimensional *tangent space* $\mathrm{T}_{\mathbf{q}} M$; the orthogonal compliment to $\{\mathrm{grad} f_1, \ldots, \mathrm{grad} f_{n-k}\}$. Vectors in $\mathrm{T}_{\mathbf{q}} M$ are called *tangent vectors* to M at $\mathbf{q}$.

Definition A.1.13 (Tangent Maps on $\mathbb{R}^n$). Let E and F be vector spaces and let $f : U \subset E \to V \subset F$, where U and V are open sets and f is class $mathcal C^{r+1}$.

Define the *tangent map* of f, $\mathrm{T}f$ (or, f_*), by $\mathrm{T}f : \mathrm{T}U = U \times E \to \mathrm{T}V = V \times F$, where $\mathrm{T}f(u, \mathbf{e}) = (f(u), \mathrm{D}f(u) \cdot \mathbf{e})$, $\mathbf{e} \in E$ and $u \in U$. $\mathrm{T}f$ is of class $mathcalC^r$.

The tangent space to M at $\mathbf{q}$ is the set of all tangent vectors to curves in M passing through $\mathbf{q}$. In other words, if $\mathbf{c}(t)$ is an arbitrary curve in M, with $\mathbf{c}(0) = \mathbf{q}$, the tangent space is the set of all vectors $\mathbf{v} = \dot{\mathbf{q}} = \frac{\mathrm{d}}{\mathrm{d}t}\big|_{t=0}\mathbf{c}(t)$.

Definition A.1.14 (Equivalence of Curves). Two curves $\mathbf{c}_1(t)$ and $\mathbf{c}_2(t)$ are said to be *equivalent* at $\mathbf{q}$ if $\mathbf{c}_1(0) = \mathbf{c}_2(0) = \mathbf{q}$ and $\lim_{t\to 0} \frac{\mathbf{c}_1(t) - \mathbf{c}_2(t)}{t} = \mathbf{0}$ in some chart.

A tangent vector to M at $\mathbf{q}$ is an *equivalence class* of curves $\mathbf{c}(t)$ with $\mathbf{c}(0) = \mathbf{q}$. The set of all tangent vectors at M is the tangent space at $\mathbf{q} \in M$, $\mathrm{T}_{\mathbf{q}}M$.

Definition A.1.15 (Tangent Bundle). The *tangent bundle* of M is the set $\mathrm{T}M = \bigcup_{\mathbf{q}\in M} \mathrm{T}_{\mathbf{q}}M$.

Definition A.1.16 (Tangent Bundle Projection). Let $(q^1, \ldots, q^n)$ be local coordinates on $M(q)$ and denote by $\dot{q}_1, \ldots, \dot{q}_n$ the components of a tangent vector in this coordinate system. $(q, \dot{q})$ give local coordinates on $\mathrm{T}M$. The mapping $\tau : \mathrm{T}M \to M$ maps a tangent vector $\dot{\mathbf{q}}$ at the point $\mathbf{q} \in M$. τ is called the *tangent bundle projection.*

Remark A.1.1. Note that $\tau : (\mathbf{q}, \dot{\mathbf{q}}) \to \mathbf{q}$ is not a one-to-one mapping. Moreover, the mapping $\tau^{-1}(\mathbf{q}) = \mathrm{T}_{\mathbf{q}}M$ is called the *fiber* over $\mathbf{q}$.

Definition A.1.17 (Tangent Maps on Manifolds). Let M and N be two differentiable manifolds and let $\mathbf{q} \in M$. A *tangent map* is a $mathcalC^1$ map $f : M \to N$ given by $\mathrm{T}f_{\mathbf{q}} = f_{*\mathbf{q}} : \mathrm{T}_{\mathbf{q}}M \to \mathrm{T}_{f(\mathbf{q})}N$. More precisely, let $\mathbf{v} \in \mathrm{T}_{\mathbf{q}}M$ and consider any curve $\mathbf{c}(t)$ with $\mathbf{c}(0) = \mathbf{q}$ and $\frac{\mathrm{d}\mathbf{c}(t)}{\mathrm{d}t}\big|_{t=0} = \mathbf{v}$. Then, $\mathrm{T}f_{\mathbf{q}}(\mathbf{v}) = \frac{\mathrm{d}}{\mathrm{d}t}\big|_{t=0} f(\mathbf{c}(t))$. The union of all such mappings gives the *tangent map* $\mathrm{T}f = f_* : \mathrm{T}M \to \mathrm{T}N$.

Remark A.1.2. $\mathrm{T}f_{\mathbf{q}}(\mathbf{v})$ does not depend on the chosen curve $\mathbf{c}(t)$.

Definition A.1.18 (Vector Fields). A *vector field* on a manifold M is a section of the tangent bundle $\mathrm{T}M$ of M. In other words, it is a map $\mathbf{X} : M \to \mathrm{T}M$ such that $\mathbf{X}(\mathbf{q}) \in \mathrm{T}_{\mathbf{q}}M$, $\forall \mathbf{q} \in M$.

Let (U, ϕ) be a coordinate chart around $\mathbf{q} \in M$ and let λ be a smooth function on M. With this coordinate chart associate n tangent vectors at $\mathbf{q}$: $\left(\frac{\partial}{\partial \phi_1}\right)_{\mathbf{q}}, \ldots, \left(\frac{\partial}{\partial \phi_n}\right)_{\mathbf{q}}$, which are defined as:

$$\left(\frac{\partial}{\partial \phi_i}\right)_{\mathbf{q}} (\lambda) = \left[\frac{\partial \left(\lambda \cdot \phi^{-1}\right)}{\partial q_i}\right]_{\mathbf{X}=\phi(\mathbf{q})}$$

These vectors form a basis for the tangent space at $\mathbf{q}$. In other words, any vector $\mathbf{v} \in \mathrm{T}_{\mathbf{q}}M$ can be written as $\mathbf{v} = \sum_{i=1}^{n} v_i \left(\frac{\partial}{\partial \phi_i}\right)_{\mathbf{q}}$. A nice way to put it is that a vector field is a rule for picking a tangent vector at every point in the manifold.

The set of all vector fields on M is denoted by $\mathcal{X}(M)$.

Definition A.1.19 (Integral Curve). Let $U \subset \mathbb{R}^n$ be an open set and let $\mathbf{X} \in \mathcal{X}(M)$ be a vector field on U. An *integral curve* of $\mathbf{X}$ with initial condition $\mathbf{q}_0$ is differentiable curve $\mathbf{c}$ defined on some open interval $I \subset \mathbb{R}$ containing 0 such that $\mathbf{c}(0) = \mathbf{q}_0$ and $\mathbf{c}'(t) = \mathbf{X}(c(t))$ for all $t \in I$.

Locally, if $\mathbf{X}$ is given by $(q^1, \ldots, q^n)$, i.e. $\mathbf{X} = q^1 \frac{\partial}{\partial q_1} + \ldots + q^n \frac{\partial}{\partial q_n}$, and $\mathbf{c}(t) = (c^1(t), \ldots, c^n(t))$ the above definition implies that $\dot{c}_i = q^i(c^1(t), \ldots, c^n(t))$, $i = 1, \ldots, n$.

A.1.2 Exterior Forms and Tensors

Definition A.1.20 (Exterior One-Forms). An *exterior form of degree one* on a vector space $\mathbb{R}^n$ is a linear function mapping $\mathbb{R}^n$ to $\mathbb{R}$. Under vector addition and scalar multiplication, the set of all such forms is itself a vector space called the dual space of $\mathbb{R}^n$, denoted by $(\mathbb{R}^n)^*$.

If $\phi_1, \ldots, \phi_n$ is a basis for $(\mathbb{R}^n)^*$ and $\boldsymbol{\omega} = \sum_{i=1}^n a_i \phi_i$ is an arbitrary one-form, then $\boldsymbol{\omega}(\mathbf{v}) = \sum_{i=1}^n a_i \phi_i(\mathbf{v})$, where $\mathbf{v}$ is a vector in $\mathbb{R}^n$.

The dual basis is defined by $\phi_j(\mathbf{e}_i) = \delta_{ij}$, where $\mathbf{e}_i$, $i = 1, \ldots, n$, form a basis for $\mathbb{R}^n$.

Example A simple one-form is the work done by a force field $\mathbf{F} \in \mathbb{R}^3$ on the displacement $\mathbf{d}$. The one-form is expressed by $\boldsymbol{\omega}(\mathbf{d}) = \langle \mathbf{F}, \mathbf{d} \rangle$, where $\langle \cdot, \cdot \rangle$ is the inner product in Euclidean space [87].

Definition A.1.21 (Exterior Two-Forms). An *exterior form of degree two*, $\boldsymbol{\omega}^2 : \mathbb{R}^n \times \mathbb{R}^n \to \mathbb{R}$, is a function on pairs of vectors, which is *bilinear* and *skew symmetric*. In other words,

$$\begin{aligned} \boldsymbol{\omega}^2(\lambda_1 \mathbf{v}_1 + \lambda_2 \mathbf{v}_2, \mathbf{v}_3) &= \lambda_1 \boldsymbol{\omega}^2(\mathbf{v}_1, \mathbf{v}_3) + \lambda_2 \boldsymbol{\omega}^2(\mathbf{v}_2, \mathbf{v}_3), \ \forall \mathbf{v}_1, \ \mathbf{v}_2, \ \mathbf{v}_3 \in \mathbb{R}^n, \ \lambda_1, \ \lambda_2 \in \mathbb{R} \\ \boldsymbol{\omega}^2(\mathbf{v}_1, \mathbf{v}_2) &= -\boldsymbol{\omega}^2(\mathbf{v}_2, \mathbf{v}_1), \ \forall \mathbf{v}_1, \ \mathbf{v}_2 \in \mathbb{R}^n. \end{aligned}$$

The set of all two-forms on $\mathbb{R}^n$ forms a vector space.

Example The oriented area of the parallelogram constructed on the vectors $\mathbf{v}_1$ and $\mathbf{v}_2$ in $\mathbb{R}^2$ is a two-form given by

$$\boldsymbol{\omega}(\mathbf{v}_1, \mathbf{v}_2) = \begin{vmatrix} v_{11} & v_{12} \\ v_{21} & v_{22} \end{vmatrix},$$

where $\mathbf{v}_1 = v_{11}\mathbf{e}_1 + v_{12}\mathbf{e}_2$ and $\mathbf{v}_2 = v_{21}\mathbf{e}_1 + v_{22}\mathbf{e}_2$ [87].

Exercise For every two-form $\boldsymbol{\omega}$ in $\mathbb{R}^n$, $\boldsymbol{\omega}(\mathbf{v}, \mathbf{v}) = 0$ for all $\mathbf{v} \in \mathbb{R}^n$. This is obvious from the second property of two-forms given in the above definition; $\boldsymbol{\omega}(\mathbf{v}, \mathbf{v}) = -\boldsymbol{\omega}(\mathbf{v}, \mathbf{v})$ and, thus $\boldsymbol{\omega}(\mathbf{v}, \mathbf{v}) = 0$ [87].

Definition A.1.22 (Exterior k-Forms). An *exterior form of degree* k, $\boldsymbol{\omega} : \mathbb{R}^n \times \mathbb{R}^n \ldots \times \mathbb{R}^n \to \mathbb{R}$, is a function on k vectors, which is *k-linear* and *antisymmetric*. In other words,

$$\begin{aligned}
\boldsymbol{\omega}(\lambda_1 \mathbf{v}_1 + \lambda_2 \mathbf{v}_1', \mathbf{v}_2, \ldots, \mathbf{v}_k) &= \lambda_1 \boldsymbol{\omega}(\mathbf{v}_1, \mathbf{v}_2, \ldots, \mathbf{v}_3) + \lambda_2 \boldsymbol{\omega}(\mathbf{v}_1', \mathbf{v}_2, \ldots, \mathbf{v}_k), \\
&\qquad \forall\ \mathbf{v}_1',\ \mathbf{v}_k \in \mathbb{R}^n,\ \lambda_1,\ \lambda_2 \in \mathbb{R} \\
\boldsymbol{\omega}(\mathbf{v}_{i_1}, \ldots, \mathbf{v}_{i_k}) &= (-1)^{\nu} \boldsymbol{\omega}(\mathbf{v}_1, \ldots, \mathbf{v}_k),\ \forall \mathbf{v}_1,\ \ldots,\ \mathbf{v}_k \in \mathbb{R}^n,
\end{aligned}$$

where

$$\nu = \begin{cases} 0 & \text{if the permutation } \mathrm{i}_1, \ldots, \mathrm{i}_\mathrm{k} \text{ is even} \\ 1 & \text{if the permutation } \mathrm{i}_1, \ldots, \mathrm{i}_\mathrm{k} \text{ is odd} \end{cases}.$$

Example The oriented volume of a parallelepiped with edges $\mathbf{v}_1$, ..., $\mathbf{v}_n$ in Euclidean space $\mathbb{R}^n$ is an n-form. The volume is given by

$$\boldsymbol{\omega}(\mathbf{v}_1, \ldots, \mathbf{v}_1) = \begin{vmatrix} v_{11} & \cdots & v_{1n} \\ \vdots & & \vdots \\ v_{n1} & \cdots & v_{nn} \end{vmatrix},$$

where $\mathbf{v}_i = \sum_{j=1}^{n} v_{ij} \mathbf{e}_j$. This is an n-form because the determinant operation satisfies the two properties of a general n-form that are stated in definition (A.1.22) [87].

Remark A.1.3. Defining the addition and scalar multiplication operations for k-forms by

$$(\boldsymbol{\omega}_1 + \boldsymbol{\omega}_2)(\mathbf{v}_1, \mathbf{v}_2) = \boldsymbol{\omega}_1(\mathbf{v}_1, \mathbf{v}_2) + \boldsymbol{\omega}_2(\mathbf{v}_1, \mathbf{v}_2)$$

and

$$(\lambda \boldsymbol{\omega})(\mathbf{v}_1, \mathbf{v}_2) = \lambda \boldsymbol{\omega}(\mathbf{v}_1, \mathbf{v}_2),$$

respectively, one has a real vector space for the set of all k-forms on $\mathbb{R}^n$.

Fact A.1.1. *The vector space of k-forms on $\mathbb{R}^n$ is a finite-dimensional vector space with dimension C_n^k. For example, the vector space of two-forms on $\mathbb{R}^n$ is a finite-dimensional space with dimension $C_n^1 = n(n-1)/2$ [87].*

Definition A.1.23 (Exterior Product of Two One-Forms). The *exterior product* of two one-forms $\boldsymbol{\omega}_1$ and $\boldsymbol{\omega}_2$ is the two-form defined by

$$\boldsymbol{\omega}_1 \wedge \boldsymbol{\omega}_2(\mathbf{v}_1, \mathbf{v}_2) = \begin{vmatrix} \boldsymbol{\omega}_1(\mathbf{v}_1) & \boldsymbol{\omega}_2(\mathbf{v}_1) \\ \boldsymbol{\omega}_1(\mathbf{v}_2) & \boldsymbol{\omega}_2(\mathbf{v}_2) \end{vmatrix}.$$

Exercise To show that the above definition for the exterior product is indeed a two-form note that first we have

$$\begin{aligned} \boldsymbol{\omega}_1 \wedge \boldsymbol{\omega}_2(\mathbf{v}_2, \mathbf{v}_1) &= \begin{vmatrix} \boldsymbol{\omega}_1(\mathbf{v}_2) & \boldsymbol{\omega}_2(\mathbf{v}_2) \\ \boldsymbol{\omega}_1(\mathbf{v}_1) & \boldsymbol{\omega}_2(\mathbf{v}_1) \end{vmatrix} \\ &= \boldsymbol{\omega}_1(\mathbf{v}_2)\boldsymbol{\omega}_2(\mathbf{v}_1) - \boldsymbol{\omega}_2(\mathbf{v}_2)\boldsymbol{\omega}_1(\mathbf{v}_1) \\ &= -\left[\boldsymbol{\omega}_1(\mathbf{v}_1)\boldsymbol{\omega}_2(\mathbf{v}_2) - \boldsymbol{\omega}_2(\mathbf{v}_1)\boldsymbol{\omega}_1(\mathbf{v}_2)\right] \\ &= -\begin{vmatrix} \boldsymbol{\omega}_1(\mathbf{v}_1) & \boldsymbol{\omega}_2(\mathbf{v}_1) \\ \boldsymbol{\omega}_1(\mathbf{v}_1) & \boldsymbol{\omega}_2(\mathbf{v}_1) \end{vmatrix} \\ &= -\boldsymbol{\omega}_1 \wedge \boldsymbol{\omega}_2(\mathbf{v}_1, \mathbf{v}_2), \end{aligned}$$

which is the second property in definition (A.1.21). As for the first property in the definition, note that

$$\begin{aligned}
\boldsymbol{\omega}_1 \wedge \boldsymbol{\omega}_2(\lambda_1\mathbf{v}_1 + \lambda_2\mathbf{v}_1', \mathbf{v}_2) &= \begin{vmatrix} \boldsymbol{\omega}_1(\lambda_1\mathbf{v}_1 + \lambda_2\mathbf{v}_1') & \boldsymbol{\omega}_2(\lambda_1\mathbf{v}_1 + \lambda_2\mathbf{v}_1') \\ \boldsymbol{\omega}_1(\mathbf{v}_2) & \boldsymbol{\omega}_2(\mathbf{v}_2) \end{vmatrix} \\
&= \begin{vmatrix} \lambda_1\boldsymbol{\omega}_1(\mathbf{v}_1) + \lambda_2\boldsymbol{\omega}_1(\mathbf{v}_1') & \lambda_1\boldsymbol{\omega}_2(\mathbf{v}_1) + \lambda_2\boldsymbol{\omega}_2(\mathbf{v}_1') \\ \boldsymbol{\omega}_1(\mathbf{v}_2) & \boldsymbol{\omega}_2(\mathbf{v}_2) \end{vmatrix} \\
&= (\lambda_1\boldsymbol{\omega}_1(\mathbf{v}_1) + \lambda_2\boldsymbol{\omega}_1(\mathbf{v}_1'))\,\boldsymbol{\omega}_2(\mathbf{v}_2) \\
&\quad - (\lambda_1\boldsymbol{\omega}_2(\mathbf{v}_1) + \lambda_2\boldsymbol{\omega}_2(\mathbf{v}_1'))\,\boldsymbol{\omega}_1(\mathbf{v}_2) \\
&= \lambda_1 \begin{vmatrix} \boldsymbol{\omega}_1(\mathbf{v}_1) & \boldsymbol{\omega}_2(\mathbf{v}_1) \\ \boldsymbol{\omega}_1(\mathbf{v}_2) & \boldsymbol{\omega}_2(\mathbf{v}_2) \end{vmatrix} + \lambda_2 \begin{vmatrix} \boldsymbol{\omega}_1(\mathbf{v}_1') & \boldsymbol{\omega}_2(\mathbf{v}_1') \\ \boldsymbol{\omega}_1(\mathbf{v}_2) & \boldsymbol{\omega}_2(\mathbf{v}_2) \end{vmatrix} \\
&= \lambda_1\boldsymbol{\omega}_1 \wedge \boldsymbol{\omega}_2(\mathbf{v}_1, \mathbf{v}_2) + \lambda_2\boldsymbol{\omega}_1 \wedge \boldsymbol{\omega}_2(\mathbf{v}_1', \mathbf{v}_2).
\end{aligned}$$

Thus the first property is also satisfied. Therefore, the exterior product of two one-forms as defined in definition (A.1.23) is indeed a two-form.

Definition A.1.24 (Exterior Product of k One-Forms). More generally, suppose that we are given k one-forms $\boldsymbol{\omega}_1, \ldots, \boldsymbol{\omega}_k$. The exterior product is defined as

$$(\boldsymbol{\omega}_1 \wedge \ldots \wedge \boldsymbol{\omega}_k)(\mathbf{v}_1, \ldots, \mathbf{v}_k) = \begin{vmatrix} \boldsymbol{\omega}_1(\mathbf{v}_1) & \cdots & \boldsymbol{\omega}_k(\mathbf{v}_1) \\ \vdots & & \vdots \\ \boldsymbol{\omega}_1(\mathbf{v}_k) & \cdots & \boldsymbol{\omega}_k(\mathbf{v}_k) \end{vmatrix}.$$

Exercise One can show that the exterior product of k one-forms is itself a k-form. Let $\Omega = (\boldsymbol{\omega}_1 \wedge \ldots \wedge \boldsymbol{\omega}_k)$. Thus we need to show that Ω is a k-form. To do this we need to show that $\Omega(\lambda_1\mathbf{v}_1 + \lambda_2\mathbf{v}_1', \ldots, \mathbf{v}_k) = \lambda_1\Omega(\mathbf{v}_1, \ldots, \mathbf{v}_k) + \lambda_2\Omega(\mathbf{v}_1', \ldots, \mathbf{v}_k)$, which

is true because

$$
\begin{aligned}
\Omega(\lambda_1\mathbf{v}_1+\lambda_2\mathbf{v}_1',\ldots,\mathbf{v}_k) &= \begin{vmatrix} \boldsymbol{\omega}_1(\lambda_1\mathbf{v}_1+\lambda_2\mathbf{v}_1') & \cdots & \boldsymbol{\omega}_k(\lambda_1\mathbf{v}_1+\lambda_2\mathbf{v}_1') \\ \boldsymbol{\omega}_1(\mathbf{v}_2) & \cdots & \boldsymbol{\omega}_k(\mathbf{v}_2) \\ \vdots & & \vdots \\ \boldsymbol{\omega}_1(\mathbf{v}_k) & \cdots & \boldsymbol{\omega}_k(\mathbf{v}_k) \end{vmatrix} \\
&= \begin{vmatrix} \lambda_1\boldsymbol{\omega}_1(\mathbf{v}_1)+\lambda_2\boldsymbol{\omega}_1(\mathbf{v}_1') & \cdots & \lambda_1\boldsymbol{\omega}_k(\mathbf{v}_1)+\lambda_2\boldsymbol{\omega}_k(\mathbf{v}_1') \\ \boldsymbol{\omega}_1(\mathbf{v}_2) & \cdots & \boldsymbol{\omega}_k(\mathbf{v}_2) \\ \vdots & & \vdots \\ \boldsymbol{\omega}_1(\mathbf{v}_k) & \cdots & \boldsymbol{\omega}_k(\mathbf{v}_k) \end{vmatrix} \\
&= \sum_{i=1}^{k}(-1)^{i+1}\left(\lambda_1\boldsymbol{\omega}_i(\mathbf{v}_1)+\lambda_2\boldsymbol{\omega}_i(\mathbf{v}_1')\right)\left|\begin{matrix} \boldsymbol{\omega}_1(\mathbf{v}_2) & \cdots & \boldsymbol{\omega}_k(\mathbf{v}_2) \\ \vdots & & \vdots \\ \boldsymbol{\omega}_1(\mathbf{v}_k) & \cdots & \boldsymbol{\omega}_k(\mathbf{v}_k) \end{matrix}\right|_i \\
&= \lambda_1\begin{vmatrix} \boldsymbol{\omega}_1(\mathbf{v}_1) & \cdots & \boldsymbol{\omega}_k(\mathbf{v}_1) \\ \vdots & & \vdots \\ \boldsymbol{\omega}_1(\mathbf{v}_k) & \cdots & \boldsymbol{\omega}_k(\mathbf{v}_k) \end{vmatrix} + \lambda_2\begin{vmatrix} \boldsymbol{\omega}_1(\mathbf{v}_1') & \cdots & \boldsymbol{\omega}_k(\mathbf{v}_1') \\ \vdots & & \vdots \\ \boldsymbol{\omega}_1(\mathbf{v}_k) & \cdots & \boldsymbol{\omega}_k(\mathbf{v}_k) \end{vmatrix} \\
&= \lambda_1\Omega(\mathbf{v}_1,\ldots,\mathbf{v}_k)+\lambda_2\Omega(\mathbf{v}_1',\ldots,\mathbf{v}_k),
\end{aligned}
$$

where we have used the definition of a matrix determinant and the fact that $\boldsymbol{\omega}_1,\ldots,\boldsymbol{\omega}_k$ are one-forms. If we let A be a $(k-1)\times k$ matrix, $|A|_i$ is defined here as the determinant of the matrix A with the i^{th} column and i^{th} row removed. The second property that we need to show is that $\Omega(\mathbf{v}_{i_1},\ldots,\mathbf{v}_{i_k}) = (-1)^{\nu}\boldsymbol{\omega}(\mathbf{v}_1,\ldots,\mathbf{v}_k)$, $\forall\mathbf{v}_1,\ \ldots,\ \mathbf{v}_k\in\mathbb{R}^n$. This can be shown in a fashion similar two that used in the above example for the exterior product of two one-forms using some properties of the determinant.

Definition A.1.25 (Tensors). Let E be a vector space. A a multi-linear map of

the form

$$\mathrm{T}^r_s(E) = L^{(r+s)}(\underbrace{E^*,\ldots,E^*}_{\text{r copies}},\underbrace{E,\ldots,E}_{\text{s copies}}) : \underbrace{E^*\times\ldots\times E^*}_{\text{r copies}}\times\underbrace{E\times\ldots\times E}_{\text{s copies}}\to\mathbb{R}$$

is called a *tensor* on E. It is said to be *contravariant* of order r and *covariant* of order s. It is also said to be of type $\begin{pmatrix} r \\ s \end{pmatrix}$.

Definition A.1.26 (Tensor Product). Let $t_1 \in \mathrm{T}^{r_1}_{s_1}(E)$ and $t_2 \in \mathrm{T}^{r_1}_{s_1}(E)$. The *tensor product* $t_1 \otimes t_2 \in \mathrm{T}^{r_1+r_2}_{s_1+s_2}(E)$ is given by

$$\begin{aligned} &t_1\otimes t_2(\beta^1,\ldots,\beta^{r_1},\gamma^1,\ldots,\gamma^{r_2},f_1,\ldots,f_{s_1},g_1,\ldots,g_{s_2}) \\ &= t_1(\beta^1,\ldots,\beta^{r_1},f_1,\ldots,f_{s_1})t_2(\gamma^1,\ldots,\gamma^{r_2},g_1,\ldots,g_{s_2}), \end{aligned}$$

where $\beta^i,\ \gamma^i \in E^*$ and $f_i,\ g_i \in E$.

Remark A.1.4. Let $t \in \mathrm{T}^0_k(E,\mathbb{R})$. t is called *skew symmetric* if

$$t(e_1,\ldots,e_k) = \mathrm{sign}(\sigma)\ t(e_{\sigma(1)},\ldots,e_{\sigma(k)}),$$

where $\sigma(\cdot)$ is a permutation. in other words, t changes sign whenever two entries are interchanged.

Remark A.1.5. One can *skewify* an element t of $\mathrm{T}^0_k(E)$ by using the alternating map:

$$A\ t(e_1,\ldots,e_k) = \frac{1}{k!}\sum_{\sigma\in S_k}\mathrm{sign}(\sigma)\ t(e_{\sigma(1)},\ldots,e_{\sigma(k)}),$$

where S_k is the set of all possible permutations.

Example If α and β are two one-forms, then

$$\begin{aligned} A\ (\alpha\otimes\beta)(\mathbf{v}_1,\mathbf{v}_2) &= \frac{1}{2!}(\alpha(\mathbf{v}_1)\beta(\mathbf{v}_2)+(-1)\alpha(\mathbf{v}_2)\beta(\mathbf{v}_1)) \\ &= \frac{1}{2}(\alpha(\mathbf{v}_1)\beta(\mathbf{v}_2)-\alpha(\mathbf{v}_2)\beta(\mathbf{v}_1)) \\ &= \frac{1}{2!}\alpha\wedge\beta((v)_1,(v)_2). \end{aligned}$$

Definition A.1.27 (Exterior Product). Let $\alpha \in \mathrm{T}^0_k(E)$ and $B \in \mathrm{T}^0_l(E)$. The *exterior (wedge) product*, $\alpha \wedge \beta \in \Lambda^{k+l}(E)$ is defined by

$$\alpha \wedge \beta = \frac{(k+l)!}{k!l!} A(\alpha \otimes \beta),$$

where $\Lambda^{k+l}(E)$ is the set of $(k+l)$-forms on E.

A.1.3 Differential Forms

One can now extend the notions introduced in the previous section to *tensor fields* and *differential forms* on a manifold M. First, lets consider the *differential one- and two-forms*.

Definition A.1.28 (Differential One-Form). Let M be a manifold and $f : M \to \mathbb{R}$ be a $\mathcal{C}^1$ function. Let $\mathbf{q} \in M$ and $\mathbf{c}(t)$ be a smooth curve in M with $\mathbf{c}(0) = \mathbf{q}$. The *differential one-form* of f at $\mathbf{q}$, $\mathrm{d}f_{\mathbf{q}}$, is the linear map $\mathrm{d}f_{\mathbf{q}} : \mathrm{T}_{\mathbf{q}}M \to \mathbb{R}$ defined as follows. Let $\mathbf{v} = \frac{\mathrm{d}}{\mathrm{d}t}\mathbf{c}(t)\Big|_{t=0}$, then $\mathrm{d}f_{\mathbf{q}}(\mathbf{v}) = \frac{\mathrm{d}}{\mathrm{d}t}\Big|_{t=0} f(\mathbf{c}(t))$. $\mathrm{d}f_{\mathbf{q}}$ is a one-form on $\mathrm{T}_{\mathbf{q}}M$. Denote by $\mathrm{d}f$ the smooth map that maps the tangent bundle, $\mathrm{T}M$, to the real line; $\mathrm{d}f : \mathrm{T}M \to \mathbb{R}$.

Fact A.1.2. *Every differential one-form on the space $\mathbb{R}^n$ with a given coordinate system $q_1, q_2, \ldots, q_n$ can be written uniquely in the form*

$$\boldsymbol{\omega} = a_1(\mathbf{q})\mathrm{d}q_1 + a_2(\mathbf{q})\mathrm{d}q_2 + \cdots + a_n(\mathbf{q})\mathrm{d}q_n,$$

where the coefficients $a_i(\mathbf{q}$, $i = 1, \ldots, n$, are smooth functions [87].

Definition A.1.29 (Tensor Field k-form). Denote by $\Gamma^r_s(M)$ the rth-order contravariant and sth-order covariant tensor field. $t \in \Gamma^r_s(M)$ has the local form

$$t(u) = t^{i_1,i_2,\ldots,i_r}_{j_1,j_2,\ldots,j_s}(u) \frac{\partial}{\partial q^{i_1}} \otimes \ldots \otimes \frac{\partial}{\partial q^{i_r}} \otimes \mathrm{d}q^{j_1} \otimes \ldots \otimes \mathrm{d}q^{j_s},$$

where $u \in U$ and U is a local chart.

Definition A.1.30 (Differential k-Form). A differential k-form $\boldsymbol{\omega}^k\big|_{\mathbf{q}}$ at a point $\mathbf{q}$ of a manifold M is an exterior k-form on the tangent space $\mathrm{T}_{\mathbf{q}}M$ to M at $\mathbf{q}$.

Fact A.1.3. *Denote by $\Omega^k(M)$ the set of differential k-forms on M. The differential form $\boldsymbol{\omega} \in \Omega^k(M)$ on M, has the local form*

$$\boldsymbol{\omega}(\mathbf{q}) = \sum_{i_1<\cdots<i_k} a_{i_1,\ldots,i_k}(\mathbf{q}) \mathrm{d}q_{i_1} \wedge \ldots \wedge \mathrm{d}q_{i_k},$$

with $i_1 < \cdots < i_k$.

Definition A.1.31 (Cotangent Vectors, Cotangent Spaces and the Cotangent Bundle). Let M be an n-dimensional differentiable manifold. A *cotangent vector* is a one-form on the tangent space to M at $\mathbf{q} \in M$. The *dual* or *cotangent space*, denoted $\mathrm{T}^*_{\mathbf{q}}M$, to the tangent space $\mathrm{T}_{\mathbf{q}}M$ is the set of all cotangent vectors to M at $\mathbf{q}$ and is an n-dimensional space. The union of the cotangent spaces to M at all points $\mathbf{q} \in M$ is called the *cotangent bundle*, denoted T^*M.

Definition A.1.32 (Exterior Derivative). Let $\alpha = \alpha_{i_1,\ldots,i_k} \mathrm{d}q^{i_1} \wedge \ldots \wedge \mathrm{d}q^{i_k}$ be a differential k-form. Define the *exterior derivative*, $\mathrm{d}(\cdot)$, as $\mathrm{d}\alpha = \frac{\partial \alpha_{i_1,\ldots,i_k}}{\mathrm{d}q^i} \mathrm{d}q^i \wedge \mathrm{d}q^{i_1} \wedge \ldots \wedge \mathrm{d}q^{i_k}$, where $i_1 < \ldots < i_k$. In particular, note that $\mathrm{d}(q^i) = \frac{\partial q^i}{\partial q^i}\mathrm{d}q^i = \mathrm{d}q^i$ and that $\mathrm{d}(\mathrm{d}q^i) = \frac{\partial (1)}{\partial q^i}\mathrm{d}q^i \wedge \mathrm{d}q^i = 0$.

Definition A.1.33 (Interior Product). Let M be a manifold, $\mathbf{X}$ be a vector field on M and $\boldsymbol{\omega} \in \Omega^{k+1}(M)$ a $(k+1)$-form. The *interior product*, $i_{\mathbf{X}}\boldsymbol{\omega}(\cdot)$, is defined by

$$i_{\mathbf{X}}\boldsymbol{\omega}(q_1, q_2, \ldots, q_k) = \boldsymbol{\omega}(\mathbf{X}, q_1, q_2, \ldots, q_k) \in \Omega^k(M).$$

$i_{\mathbf{X}}\boldsymbol{\omega}(\cdot)$ is sometimes denoted $\mathbf{X} \lrcorner\, \boldsymbol{\omega}$.

Example Let α and β be two one-forms. Then $\{i_{\mathbf{X}}(\alpha \wedge \beta)\}(\mathbf{Y}) = \alpha \wedge \beta(\mathbf{X}, \mathbf{Y}) = \alpha(\mathbf{X})\beta(\mathbf{Y}) - \alpha(\mathbf{Y})\alpha(\mathbf{X})$. More generally, if α is a k-form and β is a l-form, then $i_{\mathbf{X}}(\alpha \wedge \beta) = ((i_{\mathbf{X}}\alpha \wedge \beta) + (-1)^{kl}\alpha \wedge (i_{\mathbf{X}}\beta)$.

Definition A.1.34 (Pull-Back and Push-Forward). Let α be a k-form on a smooth manifold N and let $\phi : M \to N$, where M is also a smooth manifold. Define the *pull-back* operation on α by ϕ, denoted $\phi^*\alpha$, by $(\phi^*\alpha)(\mathbf{v}_1, \ldots, \mathbf{v}_k) = \alpha(\phi(\mathbf{q}))(\mathrm{T}_\mathbf{q}\phi \cdot \mathbf{v}_1, \ldots, \mathrm{T}_\mathbf{q}\phi \cdot \mathbf{v}_k)$, for some $\mathbf{q} \in M$, and where $\mathbf{v}_i \in \mathrm{T}_\mathbf{q}M$, $i = 1, \ldots, k$. The *push-forward* operation on α by ϕ^{-1}, denoted $\phi_*\alpha$, is defined as $(\phi_*\alpha)(\mathbf{v}_1, \ldots, \mathbf{v}_k) = \left((\phi^{-1})^* \alpha\right)(\mathbf{v}_1, \ldots, \mathbf{v}_k)$.

Definition A.1.35 (Exterior Derivative). The *exterior derivative* of a k-form α on a manifold M is a $(k+1)$-form, denoted $d\alpha$, defined by the following proposition.

Proposition A.1.1. *There exists a unique mapping* d *from k-forms to $(k+1)$-forms on M such that*

1. *If $f \in mathcalC^\infty(M)$, then* df *is the differential of f.*
2. dα *is linear in α;* $\mathrm{d}(c_1\alpha_1 + c_2\alpha_2) = c_1\mathrm{d}(\alpha_1) + c_2\mathrm{d}(\alpha_2)$.
3. *Product rule: if α is a k-form and β a l-form, then* $\mathrm{d}(\alpha \wedge \beta) = \mathrm{d}\alpha \wedge \beta + (-1)^k \alpha \wedge \mathrm{d}\beta$.
4. $\mathrm{d}(\mathrm{d}\alpha) = 0$.
5. d *is local:* $\mathrm{d}(\alpha|U) = \mathrm{d}\alpha\big|_U$.

In local coordinates, if $\alpha = \alpha_{i_1,\ldots,i_k}\mathrm{d}q^{i_1} \wedge \ldots \wedge \mathrm{d}q^{i_k}$, then d$\alpha$ is given by

$$\mathrm{d}\alpha = \sum_j \frac{\mathrm{d}\alpha_{i_1,\ldots,i_k}}{\mathrm{d}q^j}\mathrm{d}q^j \wedge \mathrm{d}q^{i_1} \wedge \ldots \wedge \mathrm{d}q^{i_k}.$$

Lemma A.1.1. *The* d *operator commutes with pull-back:* $\mathrm{d}(\phi^*\alpha) = \phi^*(\mathrm{d}\alpha)$.

Definition A.1.36 (Lie Derivative). Let α be a k-form and $\mathbf{X}$ be a vector field on M with flow $\Phi_t : M \to M; q \to q_t$. The *Lie derivative* of α along $\mathbf{X}$ is defined as

$$\mathcal{L}_\mathbf{X}\alpha = \lim_{t\to 0}\frac{1}{t}\left[\Phi_t^* \cdot \alpha(q_t) - \alpha(q)\right] = \frac{\mathrm{d}}{\mathrm{d}t}\Phi_t^*\alpha\big|_{t=0}.$$

Theorem A.1.1 (Lie Derivative Theorem).

$$\frac{\mathrm{d}}{\mathrm{d}t}\Phi_t^*\alpha = \Phi_t^*\mathcal{L}_{\mathbf{X}}\alpha.$$

Example Given a vector field $\mathbf{X}$ on M and a function $f : M \to \mathbb{R}$, then the Lie derivative of f along $\mathbf{X}$ is given by

$$\mathcal{L}_{\mathbf{X}} f = \lim_{t\to 0} \frac{1}{t}\left[f(\mathbf{q} + t\mathbf{v}) - f(\mathbf{q})\right] = \nabla f \cdot \mathbf{v},$$

which the directional derivative of f along $\mathbf{v}$, where $\mathbf{q} \in M$ and $\mathbf{v} \in \mathrm{T}_{\mathbf{q}}M$ (i.e. $\mathbf{X} = \sum_i^n v^i \frac{\partial}{\partial q^i}$ and $\mathbf{v} = [v^1 \ v^2 \ \cdots \ v^n]$).

If $\mathbf{Y}$ is a vector field on N and $\phi : M \to N$, then the pull-back $\phi^*\mathbf{Y}$ is a vector field on M, given by: $\left(\phi^*\mathbf{Y}\right)(\mathbf{q}) = \mathrm{T}_{\mathbf{q}}\phi^{-1} \cdot \mathbf{Y} \cdot \phi$, which is the tangent map inverse of ϕ.

Definition A.1.37 (Differential Operators and Derivations). A *differential operator* is one that measures some of the terms in the Taylor Series expansion of a map. A first order differential operator that is sensitive to the linear terms is called a *derivation*. In other words, an operator $\mathbf{X}$ (such as a vector field) is called a derivation if it obeys the Leibniz rule for derivatives

$$\mathbf{X}(fg) = f\mathbf{X}(g) + g\mathbf{X}(f),$$

where f and g are two functions [81].

The following paragraphs are essential for subsequent developments.

Definition A.1.38 (The Lie Bracket). Let $\mathbf{X}$ and $\mathbf{Y}$ be two vector fields and $f : M \to \mathbb{R}$. One can then operate on f with $\mathbf{X}$ to find at every point the derivative of f in the direction of $\mathbf{X}$, $\mathbf{X}(f)$. The outcome of this operation, $\mathbf{X}(f)$, is another function, which can be operated on by $\mathbf{Y}$, $\mathbf{Y}[\mathbf{X}(f)]$. The *Lie bracket* of $\mathbf{X}$ and $\mathbf{Y}$, $[\mathbf{X}, \mathbf{Y}]$, defines a unique vector field: $[\mathbf{X}, \mathbf{Y}] : f \to \mathbf{X}[\mathbf{Y}(f)] - \mathbf{Y}[\mathbf{X}(f)]$.

Example The derivative of $f = x^2 + y^2$ in the direction $(\partial/\partial x + \partial/\partial y)$ is given by $(\partial/\partial x + \partial/\partial y)(x^2 + y^2) = 2(x + y)$.

Theorem A.1.2. *The Lie bracket of two vector fields* $\mathbf{X}$ *and* $\mathbf{Y}$ *is a derivation.*

Proof

$$\begin{aligned}
[\mathbf{X}, \mathbf{Y}](fg) &= \mathbf{X}[\mathbf{Y}(fg)] - \mathbf{Y}[\mathbf{X}(fg)] \\
&= \mathbf{X}[f\mathbf{Y}(g) + g\mathbf{Y}(f)] - \mathbf{Y}[f\mathbf{X}(g) + g\mathbf{X}(f)] \\
&= f\mathbf{X}[\mathbf{Y}(g)] + g\mathbf{X}[\mathbf{Y}(f)] - f\mathbf{Y}[\mathbf{X}(g)] - g\mathbf{X}[\mathbf{Y}(f)] \\
&= f\left\{\mathbf{X}[\mathbf{Y}(g)] - \mathbf{Y}[\mathbf{X}(g)]\right\} + g\left\{\mathbf{X}[\mathbf{Y}(f)] - \mathbf{Y}[\mathbf{X}(f)]\right\} \\
&= f[\mathbf{X}, \mathbf{Y}](g) + g[\mathbf{X}, \mathbf{Y}](f),
\end{aligned}$$

where the fact that $\mathbf{X}$ and $\mathbf{Y}$ are both (linear) vector fields, then each is a derivation.

■

Theorem A.1.3. *The Lie bracket satisfies the Jacobi identity; if* $\mathbf{X}$*,* $\mathbf{Y}$ *and* $\mathbf{Z}$ *are vector fields, then:*

$$[\mathbf{X}, [\mathbf{Y}, \mathbf{Z}]] + [\mathbf{Y}, [\mathbf{Z}, \mathbf{X}]] + [\mathbf{Z}, [\mathbf{X}, \mathbf{Y}]] = 0.$$

Proof Let f be a smooth function on M. First, compute $[\mathbf{X}, [\mathbf{Y}, \mathbf{Z}]]$:

$$\begin{aligned}
[\mathbf{X}, [\mathbf{Y}, \mathbf{Z}]](f) &= \mathbf{X}\left\{\mathbf{Y}[\mathbf{Z}(f)] - \mathbf{Z}[\mathbf{Y}(f)]\right\} - [\mathbf{Y}, \mathbf{Z}]\left\{\mathbf{X}(f)\right\} \\
&= \mathbf{X}\left\{\mathbf{Y}[\mathbf{Z}(f)]\right\} - \mathbf{X}\left\{\mathbf{Z}[\mathbf{Y}(f)]\right\} - \mathbf{Y}\left\{\mathbf{Z}[\mathbf{X}(f)]\right\} + \mathbf{Z}\left\{\mathbf{Y}[\mathbf{X}(f)]\right\}.
\end{aligned}$$

Likewise, we have

$$[\mathbf{Y}, [\mathbf{Z}, \mathbf{X}]](f) = \mathbf{Y}\left\{\mathbf{Z}[\mathbf{X}(f)]\right\} - \mathbf{Y}\left\{\mathbf{X}[\mathbf{Z}(f)]\right\} - \mathbf{Z}\left\{\mathbf{X}[\mathbf{Y}(f)]\right\} + \mathbf{X}\left\{\mathbf{Z}[\mathbf{Y}(f)]\right\}$$

and

$$[\mathbf{Z}, [\mathbf{X}, \mathbf{Y}]](f) = \mathbf{Z}\left\{\mathbf{X}[\mathbf{Y}(f)]\right\} - \mathbf{Z}\left\{\mathbf{Y}[\mathbf{X}(f)]\right\} - \mathbf{X}\left\{\mathbf{Y}[\mathbf{Z}(f)]\right\} + \mathbf{Y}\left\{\mathbf{X}[\mathbf{Z}(f)]\right\}.$$

Summing the above three expressions one obtains Jacobi's identity.

■

Remark A.1.6. The Lie bracket $[\mathbf{X}, \mathbf{Y}]$ is sometimes denoted $\mathcal{L}_{\mathbf{X}}\mathbf{Y}$. So, if Φ_t is the flow of $\mathbf{X}$, then the dynamic definition of the Lie derivative applies: $\mathcal{L}_{\mathbf{X}}\mathbf{Y} = \frac{\mathrm{d}}{\mathrm{d}t}\big|_{t=0}\phi_t^*\mathbf{Y}$.

A.2 Fiber Bundles

Definition A.2.1 (The Fiber Bundle). A *fiber bundle* is a space M for which the following are given: a space B called the *base space*, a *projection* $\phi : M \to B$ with fibers $\phi^{-1}(\mathbf{r})$, $\mathbf{r} \in B$, homeomorphic to a space F, a *structure group* G of homeomorphisms of F into itself, and a *covering* of B by open sets U_j, satisfying

1. the bundle is locally trivial; that is $\phi^{-1}(U_j)$ is homeomorphic to the product space $U_j \times F$ and

2. if h_j is the map giving the homeomorphism on the fibers above the set U_j, for any $\mathbf{q} \in U_j \bigcap U_k$, then $h_j\left(h_k^{-1}\right)$ is an element of the structure group G.

The bundle is called a *principal bundle* if the fibers of the bundle are homeomorphic to the structure group and it is called a *vector bundle* if it is homeomorphic to a vector space.

In simple terms, the fiber bundle is a pair of manifolds M and B and a projection $\pi : M \to B$. The base space B is the space on which the field is defined, M is the space where the field is graphed, while π is the map that assigns to each point on the graph a point in B where the field variable is defined. For $\mathbf{r} \in B$, $\pi^{-1}(\mathbf{r})$ is called the fiber over $\mathbf{r}$ and is the space of field variables (the fiber.) These fibers usually

have a geometric structure, but, in case they are all vector spaces, then the bundle is referred to as a vector bundle [81].

Example The simplest example for a fiber bundle is that of the graph of a real-valued function $f : \mathbb{R}^n \to \mathbb{R}$. The graph of f lies in a space that has one additional dimension, $\mathbb{R}^{n+1}$. f is now a hypersurface in the larger $(n+1)$-dimensional space. The original space, $\mathbb{R}^n$, is the base space B, whereas the larger $(n+1)$-dimensional space is the fiber bundle M. For $n = 2$, a point in the base B is (x, y), where x and y are the coordinates. The corresponding point in the bundle M is $(x, y, f(x, y))$ and $\pi[(x, y, f(x, y))] = (x, y)$, while $\pi^{-1}(x, y) = (x, y, f(x, y))$.

Example $\mathrm{T}S^1$ is a vector bundle, the tangent bundle to the circle. The base is S^1 and the fibers are homeomorphic to $\mathbb{R}$.

Definition A.2.2 (Section). A *section* is a map $\Gamma : B \to M$ such that $\pi \cdot \Gamma(\mathbf{r}) = \mathbf{r}$. Γ assigns to each point a field quantity at that point.

Example An important bundle is the cotangent bundle defined above. This is the field of one-forms on a manifold M, T^*M. Let $\mathbf{q}$ be the coordinates for points in M, $\boldsymbol{\omega}$ be a one-form on M, whose coordinates are $\mathbf{p}$. Thus, $\omega = \mathbf{p}\mathrm{d}\mathbf{q} = \sum_{i=1}^{n} p_i \mathrm{d}q^i$. Reasonable coordinates for a point in the cotangent bundle T^*M is $(q^1, \ldots, q^n, p_1, \ldots, p_n)$. The base space here would be M, the fiber bundle is T^*M and the projection $\pi : \mathrm{T}^*M \to M : \pi(q^1, \ldots, q^n, p_1, \ldots, p_n) = (q^1, \ldots, q^n)$.

Example The tangent bundle, $\mathrm{T}M$, is another fiber bundle. The base space is the manifold M. The tangent space together with M constitute the fiber $\mathrm{T}M$. Reasonable coordinates for a point in the cotangent bundle $\mathrm{T}M$ is $(q^1, \ldots, q^n, v_1, \ldots, v_n)$,

where $(v_1, \ldots, v_n)$ is the coordinate of a tangent vector. The projection $\pi : \mathrm{T}M \rightarrow M : \pi(q^1, \ldots, q^n, v_1, \ldots, v_n) = (q^1, \ldots, q^n)$.

For the case of real-valued functions, the values of f at different points on B can be directly compared and the gradient of the function (its local rate of change) furnishes the geometric structure. However, for bundles where the fibers are fields (such as a vector field) as opposed to function values, field values are not directly comparable. To be able to compare field-values at different points on the manifold, additional structure is added to the manifold so that the field values all lie in spaces of similar structure (but not necessarily in the same space.)

For vector fields on a planar manifold one can directly compare the field values and come up with constant fields (that do not vary from one point on the manifold to another.) For an arbitrary manifold. A *connection* is a tool that is used to single out fields that are "constant" (at least in some sense) across the base space M. These fields are called *horizontal* fields. First, the notion of a *vertical space* will be defined.

Definition A.2.3 (Vertical Space). Given a fiber bundle M with a projection map π, let $\mathrm{T}_{\mathbf{q}}\pi$ denote the tangent map at any point. The kernel of $\mathrm{T}_{\mathbf{q}}\pi$ at any point $\mathbf{q}$ is called the *vertical space* and is denoted by $\mathcal{V}_{\mathbf{q}}$: $\mathcal{V}_{\mathbf{q}} = \mathrm{Ker}(\mathrm{T}_{\mathbf{q}}\pi) = \left\{\mathbf{v_q} \in T_{\mathbf{q}}M : \mathrm{T}_{\mathbf{q}}\pi\left(\mathbf{v_q}\right) = 0 \in \mathrm{T}_{\pi(\mathbf{q})}B\right\}$.

Definition A.2.4 (Ehresmann Connection). An *Ehresmann connection* A is a vertical vector-valued one-form on M that satisfies:

1. $A_{\mathbf{q}} : \mathrm{T}_{\mathbf{q}}M \rightarrow \mathcal{V}_{\mathbf{q}}$ is a linear map for each point $\mathbf{q} \in M$.

2. A is a projection: $A(\mathbf{v_q}) = \mathbf{v_q},\ \forall \mathbf{v_q} \in \mathcal{V}_{\mathbf{q}}$.

Definition A.2.5 (Horizontal Space). The *horizontal space* $\mathcal{H}_{\mathbf{q}}$ is the kernel of $A_{\mathbf{q}}$: $\mathcal{H}_{\mathbf{q}} = \mathrm{Ker}\left(A_{\mathbf{q}}\right) = \{\mathbf{v_q} \in \mathrm{T}_{\mathbf{q}}M : A_{\mathbf{q}}\left(\mathbf{v_q}\right) = 0 \in \mathcal{V}_{\mathbf{q}}\}$.

Fact A.2.1. $\mathrm{T}_{\mathbf{q}}M = \mathcal{H}_{\mathbf{q}} \oplus \mathcal{V}_{\mathbf{q}}$; $\mathrm{T}_{\mathbf{q}}M$ *is the direct sum of* $\mathcal{H}_{\mathbf{q}}$ *and* $\mathcal{V}_{\mathbf{q}}$.

Lemma A.2.1. *Let the bundle coordinates be defined by* (r^α, s^a) *for the base and fiber. Thus,* $\pi(r^\alpha, s^a) = r^\alpha$. *Then the connection* A *can be represented locally by a vector-valued differential form* ω^a*:* $A = \omega^a \frac{\partial}{\partial s^a}$, *where* $\omega^a(\mathbf{v_q}) = \mathrm{d}s^a + A^a_\alpha(\mathbf{v_q})\mathrm{d}r^\alpha$.

Proof Let $\mathbf{v_q}$ be an element of $\mathrm{T}_{\mathbf{q}}M$: $\mathbf{v_q} = \sum_\beta \dot{r}^\beta \frac{\partial}{\partial r^\beta} + \sum_b \dot{s}^b \frac{\partial}{\partial s^b}$. Then $\omega^a(\mathbf{v_q}) = \dot{s}^a + A^a_\alpha \dot{r}^\alpha$ and $A(\mathbf{v_q}) = (\dot{s}^a + A^a_\alpha \dot{r}^\alpha)\frac{\partial}{\partial s^a}$. Thus, $A(A(\mathbf{v_q})) = \omega^a \frac{\partial}{\partial s^a}\left[(\dot{s}^a + A^a_\alpha \dot{r}^\alpha)\frac{\partial}{\partial s^a}\right] = (\mathrm{d}s^a + A^a_\alpha(r,s)\mathrm{d}r^\alpha)(\dot{s}^a + A^a_\alpha \dot{r}^a)\frac{\partial^2}{(\partial s^a)^2} = (\dot{s}^a + A^a_\alpha \dot{r}^a)\frac{\partial}{\partial s^a} = A(\mathbf{v_q})$. This shows that $A = \omega^a \frac{\partial}{\partial s^a}$ is a projection. As for linearity, $A = \omega^a \frac{\partial}{\partial s^a}$ is evidently linear as the vector-valued differential one-form ω^a is linear by definition.

■

Definition A.2.6 (Horizontal Lift). Given an Ehresmann connection A, a point $\mathbf{q} \in M$ and a vector $\mathbf{v_r} \in \mathrm{T}_{\mathbf{r}}B$ tangent to the base at a point $\mathbf{r} = \pi(\mathbf{q}) \in B$, define the *horizontal lift* of $\mathbf{v_r}$ to be the unique vector $\mathbf{v}^h_{\mathbf{r}}$ in $\mathcal{H}_{\mathbf{q}}$ that projects to $\mathbf{v_q}$ under $\mathrm{T}_{\mathbf{q}}\pi$: $\mathrm{T}_{\mathbf{q}}\pi(\mathbf{v}^h_{\mathbf{q}}) = \mathbf{v_q}$.

Definition A.2.7. The *horizontal part* of a vector $\mathbf{X_q} \in \mathrm{T}_{\mathbf{q}}M$ is defined as: $\mathrm{hor}\,\mathbf{X_q} = \mathbf{X_q} - A(\mathbf{q}) \cdot \mathbf{X_q}$.

Fact A.2.2. *From the above one concludes that the vertical projection is a map given by:* $(\dot{r}^\alpha, \dot{s}^\alpha) \to (0, \dot{s}^a + A^a_\alpha \dot{r}^\alpha)$ *and the horizontal projection is a map given by:* $(\dot{r}^\alpha, \dot{s}^\alpha) \to (\dot{r}^\alpha, -A^a_\alpha \dot{r}^\alpha)$.

Definition A.2.8 (Curvature of a Connection). The *curvature* of a connection A is the vertical-vector-valued two-form B on M defined by its action on two vector fields $\mathbf{X}$ and $\mathbf{Y}$ on M by: $B(\mathbf{X}, \mathbf{Y}) = -A([\mathrm{hor}\,\mathbf{X}, \mathrm{hor}\,\mathbf{Y}])$, where the bracket $[\cdot,\cdot]$ denotes the Jacobi-Lie bracket of vector fields obtained by extending the stated vectors to vector fields.

Definition A.2.9 (Linear Connections). A *linear connection* is one where the sum of two horizontal sections be horizontal; if $(\dot{r}^\alpha, \dot{s}^a)$ and $\left(\dot{q}^\alpha, \dot{\hat{s}}^a\right)$ are horizontal, then so should be $\left(\dot{r}^\alpha, \dot{s}^a + \dot{\hat{s}}^a\right)$. In other words, if $\dot{s}^a + A^a_\alpha(\mathbf{r}, \mathbf{s})\dot{q}^\alpha = \dot{\hat{s}}^a + A^a_\alpha(\mathbf{r}, \hat{\mathbf{s}})\dot{q}^\alpha = 0$, then it is required that $\dot{s}^a + \dot{\hat{s}}^a + A^a_\alpha(\mathbf{r}, \mathbf{s} + \hat{\mathbf{s}})\dot{q}^\alpha = 0$. In this case, the connection coefficients take the form: $A^a_\alpha = \sum_b \Gamma^a_{\alpha b}(\mathbf{q}) s^b$.

Definition A.2.10 (Affine Connections). If the bundle is the tangent bundle, the connection is called *affine* and the coefficients given in definition (A.2.9) are called the components of the affine connection in the tangent bundle.

Definition A.2.11 (Parallel Transport). A tangent vector $\mathbf{v_q}$ is said to be *parallel transported* along a curve $\mathbf{q}(t)$ if $\mathbf{v_q}$ is always horizontal along the curve. In other words, $A(\mathbf{v_q}) \equiv 0$ along $\mathbf{q}(t)$.

Definition A.2.12 (Geodesic Motion and its Equation). In the tangent bundle $s^a = \dot{r}^a$. The *geodesic motion* along a curve $\mathbf{q}(t)$ is defined as the motion for which the tangent vector is parallel transported along the curve. From lemma (A.2.1) and definition (A.2.9), we have the *equation of geodesic motion*: $A(\mathbf{v_q}) = \ddot{r}^a + \Gamma^a_{bc}\dot{r}^b\dot{r}^b = 0$.

Definition A.2.13 (The Covariant Derivative). A linear connection in the tangent bundle can be defined as a map from two vector fields $(\mathbf{X}, \mathbf{Y}) \to \nabla_{\mathbf{X}}\mathbf{Y}$ that satisfies the following properties:

1. $\nabla_{f\mathbf{X}+g\mathbf{Y}}\mathbf{X} = f\nabla_{\mathbf{X}}\mathbf{Z} + g\nabla_{\mathbf{Y}}\mathbf{Z}$,
2. $\nabla_{\mathbf{X}}(\mathbf{Y} + \mathbf{Z}) = \nabla_{\mathbf{X}}\mathbf{Y} + \nabla_{\mathbf{X}}\mathbf{Z}$, and
3. $\nabla_{\mathbf{X}}(f\mathbf{Y}) = f\nabla_{\mathbf{X}}\mathbf{Y} + (\mathrm{d}f \cdot \mathbf{X})\,\mathbf{Y}$,

where f and g are two smooth functions, $\mathbf{X}$, $\mathbf{Y}$ and $\mathbf{Z}$ are vector fields and $\mathrm{d}f \cdot \mathbf{X}$ is the Lie derivative, or the directional derivative of f along $\mathbf{X}$ (see example after

Theorem (A.1.1).) ∇ can be represented as an expansion of its basis vectors, $\nabla_{\partial/\partial q_i}$, and each can be expanded in terms of a set of basis vectors for the vector field $\partial/\partial q_j$: $\nabla_{\partial/\partial q_k}\partial/\partial q_i = \sum_j \Gamma^j_{ki}\frac{\partial}{\partial q_j}$. If $\mathbf{X}$ and $\mathbf{Y}$ are two vector fields given locally by $\mathbf{X} = X^k\left(\partial/\partial q_k\right)$ and $\mathbf{Y} = Y^j\left(\partial/\partial q_j\right)$, respectively, then properties (1) and (3) above imply:

$$\begin{aligned}
\nabla_{\mathbf{X}}\mathbf{Y} &= \sum_k\sum_j \nabla_{X^k\frac{\partial}{\partial q_k}}Y^j\frac{\partial}{\partial q_j} \\
&= \sum_k\sum_j\left(X^kY^j\nabla_{\frac{\partial}{\partial q_k}}\frac{\partial}{\partial q_j} + X^k\mathrm{d}Y^j\cdot\frac{\partial}{\partial q_k}\frac{\partial}{\partial q_j}\right) \\
&= \sum_i\sum_k\sum_j\left[X^kY^j\Gamma^i_{kj} + X^j\frac{\partial Y^i}{\partial q_j}\right]\frac{\partial}{\partial q_i}
\end{aligned}$$

Next, let us revisit the geodesic equations. Note that the i^{th} component of $\dot{\mathbf{q}}$ is given by $\dot{q}^i\partial/\partial q_i$. One can now compute $\nabla_{\dot{\mathbf{q}}}\dot{\mathbf{q}}$ using the above properties:

$$\begin{aligned}
\nabla_{\dot{\mathbf{q}}}\dot{\mathbf{q}} &= \sum_i\sum_j \nabla_{\dot{q}^i\partial/\partial q_i}\dot{q}^j\partial/\partial q_j \\
&= \dot{q}^i\nabla_{\partial/\partial q_i}\dot{q}^j\frac{\partial}{\partial q_j} \\
&= \dot{q}^i\frac{\partial}{\partial q_i}\dot{q}^j\frac{\partial}{\partial q_j} + \dot{q}^i\dot{q}^j\Gamma^k_{ij}\frac{\partial}{\partial q_k} \\
&= \left(\ddot{q}^j + \Gamma^j_{ik}\dot{q}^i\dot{q}^k\right)\frac{\partial}{\partial q_j} = 0,
\end{aligned}$$

where the chain rule has been used for the fourth equality and the last equality is true by virtue of the geodesic equations introduced in definition (A.2.12). Thus, the geodesic equations can be written as $\nabla_{\dot{\mathbf{q}}}\dot{\mathbf{q}} = 0$. $\nabla_{\dot{\mathbf{q}}}\dot{\mathbf{q}}$ is sometimes denoted by $\frac{\mathrm{D}^2\mathbf{q}}{\mathrm{d}t^2}$. Finally, the *covariant derivative*, denoted $\frac{\mathrm{D}\mathbf{X}}{\mathrm{d}t}$, is defined as $\frac{\mathrm{D}\mathbf{X}}{\mathrm{d}t} = \nabla_{\dot{\mathbf{q}}(t)}\mathbf{X}$. In local coordinates the covariant derivative is given by: $\frac{\mathrm{D}\mathbf{X}}{\mathrm{d}t} = \nabla_{\dot{\mathbf{q}}(t)}\mathbf{X} = \nabla_{\dot{q}^i\partial/\partial q_i}X^j\partial/\partial q_j = \left(\dot{q}^j\frac{\partial X^i}{\partial q^j} + \Gamma^i_{kj}X^k\dot{q}^j\right)\frac{\partial}{\partial q^i} = \left(\dot{X}^i + \Gamma^i_{kj}X^k\dot{q}^j\right)\frac{\partial}{\partial q^i}$. Finally, note that if we set $\mathbf{X} = \dot{\mathbf{q}}$, we recover the geodesic equations.

One should think of $\frac{\mathrm{D}\mathbf{X}}{\mathrm{d}t}$ as the time derivative of the field $\mathbf{X}$ on $\mathrm{T}_{\mathbf{q}(t)}M$ as the

systems evolves on M with time. When M is flat space $\mathbb{R}^n$, then $\frac{\mathrm{D}\mathbf{X}}{\mathrm{d}t}$ is simply the time derivative of the filed in $\mathbb{R}^n$. And since it is flat space, we have $\mathrm{T}_{\mathbf{q}(t)}M = M$ and thus the operation $\frac{\mathrm{D}}{\mathrm{d}t}$ is simply $\frac{\mathrm{d}}{\mathrm{d}t}$. In other words, $\frac{\mathrm{D}\mathbf{X}}{\mathrm{d}t} = \frac{\mathrm{d}\mathbf{q}}{\mathrm{d}t}$.

Definition A.2.14 (Curvature and Torsion Tensors). Let $\mathbf{X}$, $\mathbf{Y}$ and $\mathbf{Z}$ be arbitrary vector fields on M. The *curvature tensor* R and the *torsion tensor* T are defined by

$$R(\mathbf{X},\mathbf{Y})(\mathbf{Z}) = \nabla_{\mathbf{X}}(\nabla_{\mathbf{Y}}\mathbf{Z}) - \nabla_{\mathbf{Y}}(\nabla_{\mathbf{X}}\mathbf{Z}) - \nabla_{[\mathbf{X},\mathbf{Y}]}(\mathbf{Z})$$

and

$$T(\mathbf{X},\mathbf{Y}) = \nabla_{\mathbf{X}}\mathbf{Y} - \nabla_{\mathbf{Y}}\mathbf{X} - [\mathbf{X},\mathbf{Y}].$$

The following fact is needed in Chapter 5.

Fact A.2.3. *Let* $\mathbf{X}$, $\mathbf{Y}$, $\mathbf{Z}$ *and* $\mathbf{W}$ *be vector fields, then the curvature tensor satisfies (see [41], page 53)*

$$\langle R(\mathbf{X},\mathbf{Y})\mathbf{Z},\mathbf{W}\rangle = \langle R(\mathbf{W},\mathbf{Z})\mathbf{Y},\mathbf{X}\rangle.$$

A.3 Riemannian Manifolds and Connections

Definition A.3.1 (Riemannian Manifold). A *Riemannian manifold* is an n-dimensional differentiable manifold M together with a choice , for each $\mathbf{q} \in M$, of an inner product $\langle\ ,\ \rangle$ in $\mathrm{T}_{\mathbf{q}}M$ that varies differentiably with $\mathbf{q}$ in the following sense. For some (hence all) parametrization $\mathbf{q}_\alpha : U_\alpha \to M$ with $\mathbf{q} \in \mathbf{q}_\alpha(U_\alpha)$, the functions

$$g_{ij}(u_1,\ldots,u_n) = \langle \frac{\partial}{\partial u_i}, \frac{\partial}{\partial u_j}\rangle,\ i,j = 1,\ldots,n,$$

are differentiable at $\mathbf{q}_\alpha^{-1}(\mathbf{q})$; here $(u_1,\ldots,u_n)$ are the coordinates of $U_\alpha \subset \mathbb{R}^n$[84].

Remark A.3.1. A differentiable manifold with a positive definite quadratic form $\langle\cdot,\cdot\rangle$ on every tangent space $\mathrm{T}_{\mathbf{q}}M$ is called a *Riemannian Manifold*. $\langle\cdot,\cdot\rangle$, often written $g(\cdot,\cdot)$, is called a *Riemannian metric*.

Definition A.3.2 (Gradient Flows). Let f be a smooth function on a Riemannian manifold M with metric $g(\cdot,\cdot) = \langle \cdot, \cdot \rangle$. The *gradient flow* of f, $\mathrm{grad} f$, is the flow of the vector field defined by $\mathrm{d}f(\mathbf{v}) = \langle \mathrm{grad} f, \mathbf{v} \rangle$ for any $\mathbf{v} \in \mathrm{T}M$.

Definition A.3.3 (Reduced Bundle). Let M be a manifold with a Riemannian metric g. For each $\mathbf{q} \in M$, one can define a set of orthonormal bases for $\mathrm{T}_{\mathbf{q}}M$. A reduced bundle of the tangent bundle $\mathrm{T}M$ is one whose fibers are orthonormal bases and that has a structure group $\mathrm{O}(n)$ (the set of n dimensional orthogonal matrices.)

Definition A.3.4 (Riemannian Connections). A *Riemannian connection* (also called the *Levi-Civita connection*) is a unique affine connection on M, such that $\nabla g = 0$ and the torsion tensor T is identically zero. If the metric is given by $g = \sum g_{ij} \mathrm{d}q^i \mathrm{d}q^j$, then the connection coefficients are given by

$$\Gamma^i_{jk} = \sum_l \frac{1}{2} g^{il} \left[\frac{\partial g_{jl}}{\partial q^k} + \frac{\partial g_{ik}}{\partial q^j} + \frac{\partial g_{jk}}{\partial q^l} \right],$$

which are called the *Christoffel symbols*. g^{il} denotes the il-th element of the inverse of g.

A.4 Calculus of Variations on Manifolds

In this section, we introduce the notion of a variational vector field. This allows us to introduce the necessary notation and tools to derive the necessary conditions for apply the calculus of variations on manifolds.

Let M be a smooth ($\mathcal{C}^\infty$) n-dimensional Riemannian manifold with the Riemannian metric denoted by $\langle \cdot, \cdot \rangle$ at a point $\mathbf{q} \in M$. Thus the length of a tangent vector $\mathbf{v} \in \mathrm{T}_{\mathbf{q}}M$ is denoted by $\|\mathbf{v}\| = \langle \mathbf{v}, \mathbf{v} \rangle^{1/2}$, where $\mathrm{T}_{\mathbf{q}}M$ is the tangent space of M at $\mathbf{q}$. We take ∇ to be the Levi-Civita connection and is, hence, assumed to be symmetric throughout the entirety of this appendix.

We will use $\mathrm{D}/\mathrm{d}t$ and $\nabla_{\mathbf{v}}$ to denote the covariant time derivative. The manifold M is assumed to be parallelizable. That is, there exists vector fields $\mathbf{X}_1(\mathbf{q}), \ldots, \mathbf{X}_n(\mathbf{q}) \in \mathrm{T}_{\mathbf{q}}M$ at each point $\mathbf{q} \in M$ such that $\langle \mathbf{X}_i, \mathbf{X}_j \rangle = \delta_{ij}$ for all $\mathbf{q} \in M$, where δ is the Kronecker delta. In this appendix we take $\mathbf{X}_i$ to be the standard basis $\mathbf{X}_i = \partial_i = \frac{\partial}{\partial q_i}$, where $\mathbf{q} = (q_1, q_2, \ldots, q_n)$.

Let Ω be the set of all $\mathcal{C}^1$ piecewise smooth curves $\mathbf{q} : [0, T] \to M$ in M such that $\mathbf{q}(0) = \mathbf{q}_0$ and $\mathbf{q}(T) = \mathbf{q}_T$ are fixed. The set Ω is called the *admissible set*. For the class of $\mathcal{C}^1$ curves in Ω we introduce the $\mathcal{C}^1$ *piecewise smooth one-parameter variation* of a curve $\mathbf{q} \in \Omega$ by

$$\begin{aligned} \mathbf{q}_\epsilon : [0, T] \times (-\epsilon, \epsilon) &\to M \\ (t, u) &\to \mathbf{q}(t, \epsilon) = \mathbf{q}_\epsilon(t). \end{aligned}$$

A vector field $\mathbf{Y}$ along a variation $\mathbf{q}_\epsilon$ is defined as the mapping that assigns to each $(t, \epsilon) \in [0, T] \times (-\rho, \rho)$ a tangent vector $\mathbf{Y}(t, \epsilon) \in \mathrm{T}_{\mathbf{q}_\epsilon}M$. For example, the vector fields $\frac{\mathrm{D}\mathbf{q}_\epsilon}{\partial \epsilon}$ and $\frac{\mathrm{D}\mathbf{q}_\epsilon}{\partial t}$ are defined by

$$\frac{\mathrm{D}\mathbf{q}_\epsilon}{\partial \epsilon} f = \frac{\mathrm{D}}{\partial \epsilon} (f \circ \mathbf{q}_\epsilon) \text{ and } \frac{\mathrm{D}\mathbf{q}_\epsilon}{\partial t} f = \frac{\mathrm{D}}{\partial t} (f \circ \mathbf{q}_\epsilon),$$

respectively, where f is a $\mathcal{C}^\infty$ real-valued function on M. With $\epsilon = 0$, the vector fields $\frac{\mathrm{D}\mathbf{q}_\epsilon}{\partial \epsilon}$ and $\frac{\mathrm{D}\mathbf{q}_\epsilon}{\partial t}$ are now restricted to $\mathbf{q}$ and the $\mathcal{C}^1$ piecewise smooth vector field along $\mathbf{q}$, $\mathbf{v}(t) := \frac{\mathrm{D}}{\partial t}\mathbf{q}_\epsilon(t, 0)$, is the *velocity vector field along* $\mathbf{q}$. On the other hand, the $\mathcal{C}^1$ piecewise smooth vector field $\mathbf{W}_t = \mathbf{W}(t) := \frac{\mathrm{D}}{\partial \epsilon}\mathbf{q}_\epsilon(t, 0) \in \mathrm{T}_{\mathbf{q}}\Omega$ is called the *variational vector field* associated with $\mathbf{q}_\epsilon$ along $\mathbf{q}$.

The one-parameter variation $\mathbf{q}_\epsilon$ is characterized infinitesimally by the vector space $\mathrm{T}_{\mathbf{q}_\epsilon}\Omega$ by setting $\mathbf{q}_\epsilon(t) = \exp_{\mathbf{q}(t)}(\epsilon \mathbf{W}_t)$, where $\exp_{\mathbf{q}(t)}$ is the exponential map on M. $\mathbf{q}_\epsilon$ is said to be *admissible* if, for each $\epsilon \in (-\rho, \rho)$, the curve $\mathbf{q}_\epsilon$ satisfies the boundary

conditions

$$\begin{aligned}
\mathbf{q}_\epsilon(t,0) &= \mathbf{q}(t), \\
\frac{\mathrm{D}\mathbf{q}_\epsilon}{\partial\epsilon}(t,0) &= \mathbf{W}_t \\
\frac{\mathrm{D}\mathbf{q}_\epsilon}{\partial\epsilon}(0,0) &= \frac{\mathrm{D}\mathbf{q}_\epsilon}{\partial\epsilon}(T,0) = 0 \\
\frac{\mathrm{D}}{\mathrm{d}t}\frac{\mathrm{D}\mathbf{q}_\epsilon}{\partial\epsilon}(t,0) &= \frac{\mathrm{D}}{\mathrm{d}t}\mathbf{W}_t \text{ is continuous on } [0,T] \\
\frac{\mathrm{D}}{\mathrm{d}t}\frac{\mathrm{D}\mathbf{q}_\epsilon}{\partial\epsilon}(0,0) &= \frac{\mathrm{D}}{\mathrm{d}t}\frac{\mathrm{D}\mathbf{q}_\epsilon}{\partial\epsilon}(T,0) = 0.
\end{aligned} \tag{A-4.1}$$

The following two facts will be needed in Chapter 5.

Fact A.4.1. *A one-parameter variation* $\mathbf{q}_\epsilon(t,u)$ *satisfies (see [41], page 50)*

$$\frac{\mathrm{D}}{\partial\epsilon}\frac{\mathrm{D}\mathbf{q}_\epsilon}{\partial t} = \frac{\mathrm{D}}{\partial t}\frac{\mathrm{D}\mathbf{q}_\epsilon}{\partial\epsilon}.$$

Fact A.4.2. *Let* $\mathbf{Y}$ *be a vector field along* $\mathbf{q}_\epsilon$*, then (see [41], page 52)*

$$\frac{\mathrm{D}}{\partial\epsilon}\frac{\mathrm{D}}{\partial t}\mathbf{Y} - \frac{\mathrm{D}}{\partial t}\frac{\mathrm{D}}{\partial\epsilon}\mathbf{Y} = R\left(\frac{\mathrm{D}\mathbf{q}_\epsilon}{\partial\epsilon}, \frac{\mathrm{D}\mathbf{q}_\epsilon}{\partial t}\right)\mathbf{Y}.$$

APPENDIX B

Systems on Lie Groups

The purpose of this appendix is to discuss optimal control problems on Lie groups, especially the special orthogonal group SO(3). Though some of the results presented in Section (B.4) are new, to the author's knowledge, it also serves to set the stage for the more general optimal control problem discussed in Chapter 4.

We discuss basic properties of Lie groups. Specifically, we are interested in the group of rigid body motions SE(3) and its subgroups. We begin with basic nomenclature and definitions. More detailed discussions can be found in [93], [51], [49] and [92].

B.1 Nomenclature and Basic Definitions

This section relies heavily on Section 2 of [49]. Although the focus of this work is SE(3), in this section we study proper subgroups of SE(3), denoted by G with Lie algebra denoted by $\mathfrak{g}$. We often specialize the result to the SE(3) case directly. We begin by stating the equations of motion for a dynamical system with state $g \in G$. First, one can express the first time derivative of g as either a left or right control system:

$$\dot{g} = g\mathbf{V}^b, \qquad \text{or} \qquad \dot{g} = \mathbf{V}^s g, \tag{B-1.1}$$

respectively, where $\mathbf{V}^b \in \mathfrak{g}$ is the velocity in body frame and $\mathbf{V}^s \in \mathfrak{g}$ is the velocity in spatial frame. The system $\dot{g} = g\mathbf{V}^b$ is said to be *left-invariant* since it is invariant under left multiplication by constant matrices, while the system $\dot{g} = \mathbf{V}^s g$ is said to be *right-invariant* since it is invariant under right multiplication by constant matrices.

For all $g \in G$ and all $\mathbf{X}, \mathbf{Y} \in \mathfrak{g}$ the adjoint map Ad_g and the matrix commutator $\mathrm{ad}_{\mathbf{X}}$ are defined as

$$\begin{aligned} \mathrm{Ad}_g \mathbf{Y} &= g\mathbf{Y}g^{-1} \\ \mathrm{ad}_{\mathbf{X}} \mathbf{Y} &= [\mathbf{X}, \mathbf{Y}] = \mathbf{XY} - \mathbf{YX}. \end{aligned}$$

On SE(3), a group element g is represented as a pair $g = (R, p) \in \mathrm{SO}(3) \times \mathbb{R}^3$ and velocity by the pair $\mathbf{V} = (\hat{\omega}, v) \in \mathfrak{so}(3) \times \mathbb{R}^3$ using homogeneous coordinates (SO(3) is the special orthogonal group of rotations and $\mathfrak{so}(3)$ is its Lie algebra.) In matrix form, these are given by

$$g = \begin{bmatrix} R & p \\ 0 & 1 \end{bmatrix} \quad \text{and} \quad \mathbf{V} = \begin{bmatrix} \hat{\omega} & v \\ 0 & 0 \end{bmatrix}. \tag{B-1.2}$$

The operator $\hat{\cdot} : \mathbb{R}^3 \to \mathfrak{so}(3)$ is such that $\hat{\omega} y = \omega \times y$, $\times$ being the vector cross product. Viewing Ad_g and $\mathrm{ad}_{\mathbf{V}}$ to be acting on elements of $\mathfrak{g}$ written as column vectors in $\mathbb{R}^6$, one can show that

$$\mathrm{Ad}_g = \begin{bmatrix} R & 0 \\ \hat{p}R & R \end{bmatrix} \quad \text{and} \quad \mathrm{ad}_{\mathbf{V}} = \begin{bmatrix} \hat{\omega} & 0 \\ \hat{v} & \hat{\omega} \end{bmatrix}.$$

With the kinematics given by equation (B-1.1), the dynamic equation of motion is given by

$$\dot{\mathbf{V}}^b = f(g, \mathbf{V}^b) + \mathbf{U}, \tag{B-1.3}$$

where, for the sake of later sections, we only work in body coordinates (that is, with left invariant systems.) From now on, we dismiss the superscript b that denotes a

body-fixed frame and simply use $\mathbf{V}$. The vector field $f(g, \mathbf{V}) \in \mathfrak{se}(3)$ represents the system's internal drift and $\mathbf{U} \in \mathfrak{se}(3)$ is the control input. The drift term has the general form:

$$f(g, \mathbf{V}) = \begin{bmatrix} \hat{f}_r(g, \mathbf{V}) & f_t(g, \mathbf{V}) \\ 0 & 0 \end{bmatrix}, \tag{B-1.4}$$

where $\hat{f}_r \in \mathfrak{so}(3)$ corresponds to rotational drift and $f_t \in \mathbb{R}^3$ corresponds to translational drift. Likewise, we have

$$\mathbf{U} = \begin{bmatrix} \hat{\tau} & u \\ 0 & 0 \end{bmatrix}, \tag{B-1.5}$$

for the control input, where $\hat{\tau} \in \mathfrak{so}(3)$ is the input torque acting on the body and $u \in \mathbb{R}^3$ is the input force assumed acting at the body's center of mass. The vector fields $\hat{f}_r$, f_t, $\hat{\tau}$ and u take up the following forms:

$$\begin{aligned} \hat{f}_r(g, \mathbf{V}) &= \begin{bmatrix} 0 & -f_{r3}(g, \mathbf{V}) & f_{r2}(g, \mathbf{V}) \\ f_{r3}(g, \mathbf{V}) & 0 & -f_{r1}(g, \mathbf{V}) \\ -f_{r2}(g, \mathbf{V}) & f_{r1}(g, \mathbf{V}) & 0 \end{bmatrix}, \qquad f_t = \begin{bmatrix} f_{t1}(g, \mathbf{V}) \\ f_{t2}(g, \mathbf{V}) \\ f_{t3}(g, \mathbf{V}) \end{bmatrix}, \\ \hat{\tau} &= \begin{bmatrix} 0 & -\tau_3 & \tau_2 \\ \tau_3 & 0 & -\tau_1 \\ -\tau_2 & \tau_1 & 0 \end{bmatrix}, \qquad u = \begin{bmatrix} u_1 \\ u_2 \\ u_3 \end{bmatrix}. \end{aligned} \tag{B-1.6}$$

B.2 Preliminary Remarks on Metrics

Much of what is presented in this section can be found in [96] and [84]. If a bilinear form defined on the tangent space at each point on a manifold M is smooth, positive-definite and symmetric then it qualifies as a Riemannian metric and M is then called a Riemannian manifold. If a bilinear form is smooth, symmetric but indefinite, then the corresponding metric is called semi-Riemannian. On an n-dimensional manifold, a

metric $\langle \cdot, \cdot \rangle$ is locally characterized by an $n \times n$ matrix of $\mathcal{C}^\infty$ functions $g_{ij} = \langle \mathbf{X}_i, \mathbf{X}_j \rangle$, where $\mathbf{X}_i$, $i = 1, \ldots, n$, form basis-vector fields for the tangent space. If the metric is defined globally, then the matrix g_{ij} completely defines the metric.

On SE(3), an inner product on the Lie algebra $\mathfrak{se}(3)$ can be extended to a Riemannian metric over the manifold using left (or right) translations as follows. Let $\mathbf{W}$ be a positive-definite matrix, $S_1,\ S_2 \in \mathfrak{se}(3)$, let the inner product at the identity e be given by:

$$\langle S_1, S_2 \rangle \,|_e = s_1^T W s_2,$$

where s_i is the 6×1 matrix representation of S_i, $i = 1, 2$. If $\mathbf{V}_1$ and $\mathbf{V}_2$ are arbitrary vector fields at an arbitrary group element $g \in \mathrm{SE}(3)$, then the inner product $\left\langle \tilde{\mathbf{V}}_1, \tilde{\mathbf{V}}_2 \right\rangle \Big|_g$ on the tangent space $\mathrm{T}_g\mathrm{SE}(3)$ can be defined by a left-invariant metric given by:

$$\left\langle \tilde{\mathbf{V}}_1, \tilde{\mathbf{V}}_2 \right\rangle \Big|_g = \left\langle g^{-1}\tilde{\mathbf{V}}_1, g^{-1}\tilde{\mathbf{V}}_2 \right\rangle \Big|_e = \langle \mathbf{V}_1, \mathbf{V}_2 \rangle \Big|_e = v_1^T W v_2,$$

where v_i is the 6×1 matrix representation of $\mathbf{V}_i = g^{-1}\tilde{\mathbf{V}}_i$, $i = 1, 2$. A right-invariant metric is defined analogously.

B.3 The Exponential Map, the Logarithmic Map and Exponential Coordinates

We now make more definitions. For proofs, see [49]. On any proper subgroup of SE(3), the exponential map $\exp : \mathfrak{g} \to G$ is a surjective map and a local diffeomorphism, where $\mathfrak{g}$ is the Lie algebra associated with the proper subgroup G.

Lemma B.3.1 (Exponential Map, [49]). *Given* $\hat{\psi} \in \mathfrak{so}(3)$ *and* $\mathbf{X} = (\hat{\psi}, q) \in$

$\mathfrak{se}(3)$, *then we have Rodrigues' formula:*

$$\begin{aligned}\exp_{SO(3)}\left(\hat{\psi}\right) &= I + \sin\left(\|\psi\|\right)\frac{\hat{\psi}}{\|\psi\|} + \left(1-\cos\left(\|\psi\|\right)\right)\frac{\hat{\psi}^2}{\|\psi\|^2} \\ \exp_{\mathrm{SE}(3)}\left(\mathbf{X}\right) &= \begin{bmatrix} \exp_{SO(3)}\left(\hat{\psi}\right) & A(\psi)q \\ 0 & 1 \end{bmatrix},\end{aligned}$$

where $\|\cdot\|$ *is the standard Euclidean norm and*

$$A(\psi) = I + \left(\frac{1-\cos\left(\|\psi\|\right)}{\|\psi\|}\right)\frac{\hat{\psi}}{\|\psi\|} + \left(1-\frac{\sin\left(\|\psi\|\right)}{\|\psi\|}\right)\frac{\hat{\psi}^2}{\|\psi\|^2}.$$

$\mathbf{X} = \log(g) \in \mathfrak{g}$ is defined to be the exponential coordinates of the group element g in an open neighborhood of the origin (dense in) G. The logarithmic map is regarded as a local chart of the manifold G.

Lemma B.3.2 (Logarithmic Map, [49]). *Let* $(R,p) \in \mathrm{SO}(3)\times\mathbb{R}^3$ *be such that* $\mathrm{tr}(R) \neq -1$. *Then*

$$\log_{\mathrm{SO}(3)}(R) = \frac{\phi}{2\sin\phi}\left(R - R^T\right) \in \mathfrak{so}(3),$$

where ϕ *satisfies* $\cos\phi = \frac{1}{2}\left(\mathrm{tr}(R)-1\right)$ *and* $|\phi| < \pi$. *The logarithmic map on* $\mathrm{SE}(3)$ *is given by:*

$$\log_{\mathrm{SE}(3)}(R,p) = \begin{bmatrix} \hat{\psi} & A^{-1}(\psi)p \\ 0 & 0 \end{bmatrix} \in \mathfrak{se}(3), \tag{B-3.1}$$

where $\hat{\psi} = \log_{\mathrm{SO}(3)}(R)$ *and*

$$A^{-1}(\psi) = I - \frac{1}{2}\hat{\psi} + \left[1-\alpha(\|\psi\|)\right]\frac{\hat{\psi}^2}{\|\psi\|^2} \tag{B-3.2}$$

and $\alpha(y) := (y/2)\cot(y/2)$.

Elements of the Lie algebra $\mathfrak{se}(3)$ may either represent a velocity as in equation (B-1.1) (with a velocity element denoted by $\mathbf{V} = (\hat{\omega}, v)$) or the matrix logarithm of

the state as in equation (B-3.1) (with a velocity element denoted by $\mathbf{X} = (\hat{\psi}, q)$). With the latter view, elements of $\mathfrak{se}(3)$ are therefore also viewed as states. An element of SE(3) is given by $g = (R, p)$.

Remark B.3.1 ([49]). The following identities hold true:

$$\begin{aligned} A^{-1}(\psi)R(\psi) &= R(\psi)A^{-1}(\psi) = A(\psi)^{-T}, \\ A(\psi)R(\psi) &= R(\psi)A(\psi) = 2A(2\psi) - A(\psi), \\ \frac{\mathrm{d}}{\mathrm{d}\,\|\psi\|}A(\psi) &= \frac{1}{\|\psi\|}\left(R - A(\psi)\right), \end{aligned} \tag{B-3.3}$$

where $R(\psi) = \exp_{\mathrm{SO}(3)}(\hat{\psi})$.

Example B.3.1 (Exponential and Logarithmic Maps on $SE(2)$, [49]). The orientation angle θ has the skew symmetric matrix form

$$\hat{\theta} = \begin{bmatrix} 0 & -\theta \\ \theta & 0 \end{bmatrix} \in \mathfrak{so}(2).$$

Let $\mathbf{X} = (\hat{\theta}, q) \in \mathfrak{se}(2)$. Then we have

$$\begin{aligned} \exp_{\mathrm{SO}(2)}(\hat{\theta}) &= \begin{bmatrix} \cos\theta & -\sin\theta \\ \sin\theta & \cos\theta \end{bmatrix} \\ \exp_{SE(2)}(\mathbf{X}) &= \begin{bmatrix} \exp_{\mathrm{SO}(2)}(\hat{\theta}) & A(\theta)q \\ 0 & 1 \end{bmatrix}, \end{aligned}$$

where

$$A(\theta) = \frac{1}{\theta}\begin{bmatrix} \sin\theta & -(1-\cos\theta) \\ (1-\cos\theta) & \sin\theta \end{bmatrix}.$$

For $SE(2)$, the singularity occurs at $\mathrm{tr}(R) = -2$ as opposed to $\mathrm{tr}(R) = -1$ for SE(3). Let $(R, p) \in \mathrm{SO}(2) \times \mathbb{R}^2$ be such that $\mathrm{tr}(R) \neq -2$. Then $\log_{\mathrm{SO}(2)}(R) = \hat{\theta}$,

where $\cos\theta = R_{11}$, $\sin\theta = R_{21}$ and $|\theta| < \pi$. Then we have:

$$\log_{SE(2)}(R,p) = \begin{bmatrix} \hat{\theta} & A^{-1}(\theta)p \\ 0 & 1 \end{bmatrix} \in \mathfrak{se}(2),$$

where $\hat{\theta} = \log_{\mathrm{SO}(2)}(R)$ and $A^{-1}(\theta) = \begin{bmatrix} \alpha(\theta) & \theta/2 \\ -\theta/2 & \alpha(\theta) \end{bmatrix}$, with $\alpha(\cdot)$ as defined above.

The results stated next give explicit formulas that relate the time derivative of $\mathbf{X}(t) = \log(g(t))$ with the body and spatial velocities $\mathbf{V}^b$ and $\mathbf{V}^s$, respectively. For the linear time-dependent case $\mathbf{X}(t) = t\mathbf{Y}$, it can be shown that that $\dot{\mathbf{X}} = \mathbf{Y} = \mathbf{V}^b = \mathbf{V}^s$. In fact we have: $\mathbf{Y} = \dot{\mathbf{X}} = \frac{\mathrm{d}\log(g(t))}{\mathrm{d}t} = \frac{\mathrm{d}\log(g)}{\mathrm{d}g}\dot{g} = g^{-1}\dot{g} = \mathbf{V}^b$. Since $\mathbf{V}^s = \dot{g}g^{-1} = gg^{-1}\dot{g}g^{-1} = g\mathbf{V}^b g^{-1} = \mathrm{Ad}_g(\mathbf{V}^b)$, then $\mathbf{V}^s = \mathrm{Ad}_g(\mathbf{Y}) = \mathbf{Y}$. Hence, $\mathbf{Y} = \mathbf{V}^b = \mathbf{V}^s$. For the general case, the results are not straight forward and will be the subject of the next paragraphs.

The first result expresses the body and spatial velocities as integral functions of the time derivative of $\mathbf{X}(t)$, the exponential coordinates of $g(t)$.

Theorem B.3.1 (Integral Formulas). *Let $g(t)$ be a smooth curve on G, $\mathbf{X}(t) = \log(g(t))$ be the exponential coordinates of $g(t)$, $\mathbf{V}^b = g^{-1}\dot{g}$ the body velocity and $\mathbf{V}^s = \dot{g}g^{-1}$ the spatial velocity. Then $\dot{\mathbf{X}}$ is related to $\mathbf{V}^b$ and $\mathbf{V}^s$ through:*

$$\begin{aligned} \mathbf{V}^b &= \int_0^1 \mathrm{Ad}_{\exp(-\lambda\mathbf{X}(t))}\left(\dot{\mathbf{X}}\right)\mathrm{d}\lambda \\ \mathbf{V}^s &= \int_0^1 \mathrm{Ad}_{\exp(\lambda\mathbf{X}(t))}\left(\dot{\mathbf{X}}\right)\mathrm{d}\lambda. \end{aligned}$$

Proof Define $\mathbf{V}^b_\lambda$ such that it satisfies the differential equation:

$$\frac{\mathrm{d}}{\mathrm{d}t}\exp\left(\lambda\mathbf{X}(t)\right) = \exp\left(\lambda\mathbf{X}(t)\right)\left(\lambda\mathbf{V}^b_\lambda\right),$$

where $\lambda \in [0,1]$. Note that if we set $\lambda = 1$, we have:

$$\dot{g} = \frac{\mathrm{d}}{\mathrm{d}t}\exp\left(\mathbf{X}(t)\right) = \exp\left(\lambda\mathbf{X}(t)\right)\left(\mathbf{V}^b_1\right) = g\mathbf{V}^b_1$$

such that $\mathbf{V}^b = \mathbf{V}_1^b$. Using the definition of $\mathbf{V}_\lambda^b$, we then have

$$\begin{aligned}\frac{\mathrm{d}}{\mathrm{d}\lambda}\left[\frac{\mathrm{d}}{\mathrm{d}t}\exp\left(\lambda\mathbf{X}(t)\right)\right] &= \frac{\mathrm{d}}{\mathrm{d}\lambda}\left[\exp\left(\lambda\mathbf{X}(t)\right)\left(\lambda\mathbf{V}_\lambda^b\right)\right] \\ &= \mathbf{X}(t)\exp\left(\lambda\mathbf{X}(t)\right)\left(\lambda\mathbf{V}_\lambda^b\right) + \exp\left(\lambda\mathbf{X}(t)\right)\frac{\mathrm{d}}{\mathrm{d}\lambda}\left(\lambda\mathbf{V}_\lambda^b\right). \\ &= \mathbf{X}(t)\frac{\mathrm{d}}{\mathrm{d}t}\left[\exp\left(\lambda\mathbf{X}(t)\right)\right] + \exp\left(\lambda\mathbf{X}(t)\right)\frac{\mathrm{d}}{\mathrm{d}\lambda}\left(\lambda\mathbf{V}_\lambda^b\right).\end{aligned}$$

But this is also equal to:

$$\begin{aligned}\frac{\mathrm{d}}{\mathrm{d}t}\left[\frac{\mathrm{d}}{\mathrm{d}\lambda}\exp\left(\lambda\mathbf{X}(t)\right)\right] &= \frac{\mathrm{d}}{\mathrm{d}t}\left[\mathbf{X}(t)\exp\left(\lambda\mathbf{X}(t)\right)\right] \\ &= \dot{\mathbf{X}}\exp\left(\lambda\mathbf{X}(t)\right) + \mathbf{X}(t)\frac{\mathrm{d}}{\mathrm{d}t}\exp\left(\lambda\mathbf{X}(t)\right).\end{aligned}$$

Hence, we have:

$$\exp\left(\lambda\mathbf{X}(t)\right)\frac{\mathrm{d}}{\mathrm{d}\lambda}\left(\lambda\mathbf{V}_\lambda^b\right) = \dot{\mathbf{X}}\exp\left(\lambda\mathbf{X}(t)\right)$$

implying that:

$$\frac{\mathrm{d}}{\mathrm{d}\lambda}\left(\lambda\mathbf{V}_\lambda^b\right) = \exp\left(-\lambda\mathbf{X}(t)\right)\dot{\mathbf{X}}\exp\left(\lambda\mathbf{X}(t)\right) = \mathrm{Ad}_{\exp(-\lambda\mathbf{X}(t))}\dot{\mathbf{X}}$$

Integrating this equation over λ from $\lambda = 0$ to $\lambda = 1$, we get:

$$\mathbf{V}^b = \int_0^1 \frac{\mathrm{d}}{\mathrm{d}\lambda}\left(\lambda\mathbf{V}_\lambda^b\right)\mathrm{d}\lambda = \mathbf{V}_1^b = \int_0^1 \mathrm{Ad}_{\exp(-\lambda\mathbf{X}(t))}\dot{\mathbf{X}}\mathrm{d}\lambda.$$

Finally, since $\mathbf{V}^s = \mathrm{Ad}_g\mathbf{V}^b$, then:

$$\begin{aligned}\mathbf{V}^s &= \mathrm{Ad}_g\mathbf{V}^b = \mathrm{Ad}_{\exp\mathbf{X}(t)}\int_0^1 \mathrm{Ad}_{\exp(-\lambda\mathbf{X}(t))}\dot{\mathbf{X}}\mathrm{d}\lambda \\ &= \int_0^1 \mathrm{Ad}_{\exp(\mathbf{X}(t))\exp(-\lambda\mathbf{X}(t))}\dot{\mathbf{X}}\mathrm{d}\lambda \\ &= \int_0^1 \mathrm{Ad}_{\exp(\mathbf{X}(t)-\lambda\mathbf{X}(t))}\dot{\mathbf{X}}\mathrm{d}\lambda \\ &= \int_0^1 \mathrm{Ad}_{\exp((1-\lambda)\mathbf{X}(t))}\dot{\mathbf{X}}\mathrm{d}\lambda.\end{aligned}$$

Letting $\mu = 1 - \lambda$, then we have:

$$\mathbf{V}^s = -\int_0^1 \mathrm{Ad}_{\exp(\mu \mathbf{X}(t))} \dot{\mathbf{X}} \mathrm{d}\mu.$$

The theorem is proven.

■

Theorem B.3.2 (Derivative of the Exponential Coordinates). *Let $g(t)$ be a smooth curve on G, $\mathbf{X}(t) = \log(g(t))$ be the exponential coordinates of $g(t)$, $\mathbf{V}^b = g^{-1}\dot{g}$ the body velocity and $\mathbf{V}^s = \dot{g}g^{-1}$ the spatial velocity. Then $\dot{\mathbf{X}}$ is related to $\mathbf{V}^b$ and $\mathbf{V}^s$ through:*

$$\begin{aligned} \dot{\mathbf{X}} &= \sum_{i=0}^{\infty} \frac{(-1)^n B_i}{i!} \mathrm{ad}^i_{\mathbf{X}} \left(\mathbf{V}^b\right) \\ &= \sum_{i=0}^{\infty} \frac{B_i}{i!} \mathrm{ad}^i_{\mathbf{X}} \left(\mathbf{V}^s\right), \end{aligned}$$

where $\{B_i\}$ are the Bernoulli numbers[1]*. The first of these equations could be written in the form $\dot{\mathbf{X}} = \mathcal{B}_{\mathbf{X}} \mathbf{V}^b$, where the symbols $\mathcal{B}_{\mathbf{X}}$ denote:*

$$\mathcal{B}_{\mathbf{X}} = \sum_{i=0}^{\infty} \frac{(-1)^n B_i}{i!} \mathrm{ad}^i_{\mathbf{X}}.$$

Remark B.3.2. Noting that $B_{2k+1} = 0$ for all $k > 0$ and that $B_0 = 1$, $B_1 = -1/2$,

---

[1]The Bernoulli numbers $\{B_i\}$ are a sequence of signed rational numbers that can be defined by the identity

$$\frac{x}{e^x - 1} = \sum_{i=0}^{\infty} \frac{B_n x^i}{i!}.$$

$B_2 = 1/6$ and $B_4 = -1/30$, then the first three terms for $\dot{\mathbf{X}}$ are given by:

$$\begin{aligned}\dot{\mathbf{X}} &= \mathbf{V}^b - \frac{B_1}{2}\mathrm{ad}_{\mathbf{X}}\mathbf{V}^b + \sum_{m=1}^{\infty}\frac{B_{2m}}{(2m)!}\mathrm{ad}_{\mathbf{X}}^{2m}\mathbf{V}^b = \mathbf{V}^b + \frac{1}{2}\mathrm{ad}_{\mathbf{X}}\mathbf{V}^b \\ &\quad + \frac{1}{12}\mathrm{ad}_{\mathbf{X}}^2\mathbf{V}^b - \frac{1}{120}\mathrm{ad}_{\mathbf{X}}^4\mathbf{V}^b + \dots \\ &= \mathbf{V}^s + \frac{B_1}{2}\mathrm{ad}_{\mathbf{X}}\mathbf{V}^s + \sum_{m=1}^{\infty}\frac{B_{2m}}{(2m)!}\mathrm{ad}_{\mathbf{X}}^{2m}\mathbf{V}^s = \mathbf{V}^s - \frac{1}{2}\mathrm{ad}_{\mathbf{X}}\mathbf{V}^s \\ &\quad + \frac{1}{12}\mathrm{ad}_{\mathbf{X}}^2\mathbf{V}^s - \frac{1}{120}\mathrm{ad}_{\mathbf{X}}^4\mathbf{V}^s + \dots\end{aligned}$$

and that the two expressions differ only in the second term. Note that for small $\mathbf{X}$, the matrix series is full rank and absolutely convergent. In particular at $\mathbf{X} = 0$ we have $\dot{\mathbf{X}} = \mathbf{V}^b = \mathbf{V}^s$.

Remark B.3.3. For a generic group G, let the finite dimension of G be given by n. Therefore, the rank of the linear operator $\mathrm{ad}_{\mathbf{X}}$ is at most n and by the Cayley-Hamilton theorem there exist functions $h_i(\mathbf{X})$, $i = 1, \dots, n$, such that $\mathrm{ad}_{\mathbf{X}}^{n+1} = \sum_{i=1}^{n} h_i(\mathbf{X})\mathrm{ad}_{\mathbf{X}}^i$. But since $\mathrm{ad}_{\mathbf{X}}\mathbf{X} = 0$ for any $\mathbf{X} \in \mathfrak{g}$, then the rank of $\mathrm{ad}_{\mathbf{X}}$ is at most $n - 1$.

Lemma B.3.3 (Time Derivative of Exponential Coordinates on SO(3), [49]). *Let $R(t)$ be a smooth curve on SO(3) such that $\mathrm{tr}(R(t)) \neq -1$. Let $\hat{\psi}(t) = \log(R(t))$ be the exponential coordinates of $R(t)$ and $\hat{\omega} = R^{-1}\dot{R}$ the body angular velocity. Then we have:*

$$\begin{aligned}\dot{\psi} &= \omega_{\|} + \frac{1}{2}(\psi \times \omega) + \alpha(\|\psi\|)\omega_{\perp} \\ &= \left(I + \frac{1}{2}\hat{\psi} + (1 - \alpha(\|\psi\|))\frac{\hat{\psi}^2}{\|\psi\|^2}\right)\omega,\end{aligned}$$

where $\alpha(y) = (y/2)\cot(y/2)$ and $\omega = \omega_{\|} + \omega_{\perp}$ is the orthogonal decomposition of ω along $\mathrm{span}\{\psi\}$ and $\mathrm{span}\{\psi\}^{\perp}$.

Lemma B.3.4 (Time Derivative of Exponential Coordinates on $\mathrm{SE}(3)$, [49]). *Let $g(t) = (R(t), p(t))$ be a smooth curve on $\mathrm{SE}(3)$ such that $\mathrm{tr}(R(t)) \neq -1$. Let $\mathbf{X}(t) = \left(\hat{\psi}, q\right) = \log(g(t))$ be the exponential coordinates of $g(t)$ and $\mathbf{V}^b = g^{-1}\dot{g}$ be the body velocity. Then we have:*

$$\begin{aligned} \dot{\mathbf{X}} &= \mathcal{B}\mathbf{V}^b \\ &= \left(\mathrm{id} + \frac{1}{2}\mathrm{ad}_{\mathbf{X}} + A\left(\|\psi\|\right)\mathrm{ad}_{\mathbf{X}}^2 + B\left(\|\psi\|\right)\mathrm{ad}_{\mathbf{X}}^4\right)\mathbf{V}^b, \end{aligned} \tag{B-3.4}$$

where

$$\begin{aligned} y^2 A(y) &= 2\left[1 - \alpha(y)\right] + \frac{1}{2}\left[\alpha(y) - \beta(y)\right], \\ y^4 B(y) &= \left[1 - \alpha(y)\right] + \frac{1}{2}\left[\alpha(y) - \beta(y)\right] \end{aligned}$$

and $\alpha(y) = (y/2)\cot(y/2)$ and $\beta(y) = (y/2)^2/\sin^2(y/2)$. Additionally, the operator $\mathcal{B}_{\mathbf{X}}$ can be written as:

$$\mathcal{B}_{\mathbf{X}} = \begin{bmatrix} A(\psi)^{-T} & 0 \\ \star & A(\psi)^{-T} \end{bmatrix}.$$

Remark B.3.4. The $\star$ notation signifies that we do not care what the corresponding element is. We do not care about the (2,1) and (2,2) blocks of $\mathcal{B}_{\mathbf{X}}$ since these contribute to the zero elements (2,1) and (2,2) of the exponential coordinate $\dot{\mathbf{X}}$, which is also in $\mathfrak{se}(3)$ and, hence, ought to be zero regardless of what the second row in $\mathcal{B}_{\mathbf{X}}$ is.

Lemma B.3.5 (Time Derivative of Exponential Coordinates on $SE(2)$, [49]). *Let $g(t) = (R(t), p(t))$ be a smooth curve on $\mathrm{SE}(3)$ such that $\mathrm{tr}(R(t)) \neq -2$. Let $\mathbf{X}(t) = \left(\hat{\theta}, q\right) = \log(g(t))$ be the exponential coordinates of $g(t)$ and $\mathbf{V}^b = g^{-1}\dot{g} =$*

$(\hat{\omega}, v)$ be the body velocity. Then we have:

$$\begin{aligned}
\dot{\theta} &= \omega \\
\dot{q} &= \frac{\omega}{\theta}\left(I - A(\theta)^{-T}\right) q + A(\theta)^{-T} v \\
&= \omega \begin{bmatrix} (1-\alpha(\theta))/\theta & -1/2 \\ 1/2 & (1-\alpha(\theta))/\theta \end{bmatrix} q + \begin{bmatrix} \alpha(\theta) & \theta/2 \\ -\theta/2 & \alpha(\theta) \end{bmatrix} v.
\end{aligned}$$

B.4 Optimal Control of the Rigid Body

B.4.1 Metric on $\mathfrak{so}(3)$

For the subgroup SO(3) $\subset$ SE(3), one uses the Killing form, denoted $\langle \cdot, \cdot \rangle_K$, to define an inner product on its Lie algebra $\mathfrak{so}(3)$ as follows. On any Lie group G with Lie algebra $\mathfrak{g}$, the Killing form $\langle \cdot, \cdot \rangle_K$ is defined as the bilinear operator on $\mathfrak{g} \times \mathfrak{g}$:

$$\langle \mathbf{X}, \mathbf{Y} \rangle_K \triangleq \mathrm{tr}(\mathrm{ad}_{\mathbf{X}} \cdot \mathrm{ad}_{\mathbf{Y}}) \tag{B-4.1}$$

for all $\mathbf{X}, \mathbf{Y} \in \mathfrak{g}$. The group G is said to be *semi-simple* if $\langle \cdot, \cdot \rangle_K$ is non-degenerate. For a compact Lie group, $\langle \cdot, \cdot \rangle_K$ is both non-degenerate and negative definite. Hence, for a compact Lie group G, an inner product on the Lie algebra $\mathfrak{g}$ can be defined by $\langle \cdot, \cdot \rangle \triangleq -\alpha \langle \cdot, \cdot \rangle_K$, $\alpha > 0$. For SO(3) we set $\alpha = \frac{1}{2}$ so that $\langle \Omega_1, \Omega_2 \rangle = -\frac{1}{2}\mathrm{Tr}(\Omega_1 \Omega_2) = \langle \omega_1, \omega_2 \rangle_{\mathbb{R}^3}$ with $\Omega_1 = \hat{\omega}_1 \in \mathfrak{so}(3)$, $\Omega_2 = \hat{\omega}_2 \in \mathfrak{so}(3)$ and $\omega_1, \omega_2 \in \mathbb{R}^3$. It can be shown that $\langle \cdot, \cdot \rangle$ is Ad-invariant. That is, $\langle \cdot, \cdot \rangle$ satisfies:

$$\langle \mathbf{X}, \mathbf{Y} \rangle = \langle \mathrm{Ad}_g \mathbf{X}, \mathrm{Ad}_g \mathbf{Y} \rangle \tag{B-4.2}$$

for all $g \in G$. Moreover, the matrix commutator satisfies:

$$\langle \mathrm{ad}_{\mathbf{Z}} \mathbf{X}, \mathbf{Y} \rangle = -\langle \mathbf{X}, \mathrm{ad}_{\mathbf{Z}} \mathbf{Y} \rangle$$

for all $\mathbf{X}, \mathbf{Y}, \mathbf{Z} \in \mathfrak{g}$. To get a Riemannian manifold structure on G, the Ad-invariant inner product $\langle \cdot, \cdot \rangle$ on the algebra $\mathfrak{g}$ induces and Ad-invariant metric on G by either a left or right translation.

We now derive some basic results and relate these results to previously published ones.

B.4.2 Euler's Equation as a Constrained Optimal Control Problem

EOMs in body-fixed frame

In this section we derive Euler's equations (the rotational equations of motion) for the rigid body starting with the kinematic equation of motion (in body-fixed frame):

$$\dot{R} = R\Omega^b, \tag{B-4.3}$$

where R is the body's rotation matrix and $\Omega^b \in \mathfrak{so}(3)$ is the body's angular velocity expressed as a matrix in the Lie algebra. With ω^b the body's angular velocity, $\Omega^b = \hat{\omega}^b$. To derive Euler's equations, we minimize the kinetic energy:

$$\mathcal{J} = \int_0^T \frac{1}{2} \left\langle \Omega^b, \mathbf{J}(\Omega^b) \right\rangle \mathrm{d}t \tag{B-4.4}$$

subject to the constraint given by equation (B-4.3) and the boundary conditions:

$$R(0) = R_0,\ R(T) = R_T, \tag{B-4.5}$$

where the inner product $\langle \cdot, \cdot \rangle$ corresponds to the Killing form as defined in Section (B.4.1). $\mathbf{J} : \mathfrak{so}(3) \to \mathfrak{so}(3)$ is the symmetric[2], positive definite, and, hence, invertible operator defined by:

$$\mathbf{J}(\Omega) = J\Omega + \Omega J,\ \forall \Omega \in \mathfrak{so}(3), \tag{B-4.6}$$

where J is a diagonal matrix satisfying $J_i + J_j > 0$ for all $i \neq j$. The elements of J are related to the standard diagonal moment of inertia tensor I by $I_1 = J_2 + J_3$,

[2] J is symmetric with respect to the inner product $\langle \cdot, \cdot \rangle$ defined by the Killing form.

$I_2 = J_3 + J_1$ and $I_3 = J_1 + J_2$ (see [42], page 349.) Hence, for any $\mathbf{Z} \in \mathfrak{so}(3)$, it is easy to check that

$$\mathbf{J}(\mathbf{Z}) = \begin{bmatrix} 0 & -z_3(J_1+J_2) & z_2(J_1+J_3) \\ z_3(J_1+J_2) & 0 & -z_1(J_2+J_3) \\ -z_2(J_1+J_3) & z_1(J_2+J_3) & 0 \end{bmatrix} = \begin{bmatrix} 0 & -I_3 z_3 & I_2 z_2 \\ I_3 z_3 & 0 & -I_1 z_1 \\ -I_2 z_2 & I_1 z_1 & 0 \end{bmatrix}.$$

Using the calculus of variations, we append the cost function (B-4.4) with the constraint (B-4.3) to obtain the modified cost functional:

$$\mathcal{J} = \int_0^T \frac{1}{2} \left\langle \Omega^b, \mathbf{J}(\Omega^b) \right\rangle + \left\langle \Lambda^b, R^T \dot{R} - \Omega^b \right\rangle \mathrm{d}t \tag{B-4.7}$$

where Λ^b is a Lagrange multiplier matrix. Though adjoint variables (that is, Lagrange multipliers) belong to the cotangent space $so^*(3)$, an element of the cotangent space is identified with an element of the tangent space through $\Lambda^*(\cdot) = \langle \Lambda, \cdot \rangle$, where $\Lambda^* \in so^*(3)$. In equation (B-4.7), we have appended the cost with equation (B-4.3) expressed as an element of $\mathfrak{so}(3)$: $R^T\dot{R} - \Omega^b = 0$, where $R^T\dot{R} \in \mathfrak{so}(3)$ and $\Omega^b \in \mathfrak{so}(3)$.

In what follows, $v_\epsilon(t) = v_\epsilon(t, \epsilon)$ denotes a variation of the variable v such that $v_\epsilon(t, 0) = v(t)$. Hence we have:

$$\begin{aligned} \frac{\partial}{\partial \epsilon} \mathcal{J}_\epsilon &= \int_0^T \left\langle \delta\Omega^b + B(\mathbf{W}, \Omega^b), \mathbf{J}(\Omega^b) \right\rangle + \left\langle \Lambda^b, \frac{\mathrm{D}}{\partial \epsilon} \left(R_\epsilon^T \dot{R}_\epsilon \right) - \frac{\mathrm{D}}{\partial \epsilon} \Omega_\epsilon^b \right\rangle \mathrm{d}t \\ &= \int_0^T \left\langle \delta\Omega^b, \mathbf{J}(\Omega^b) - \Lambda^b \right\rangle \mathrm{d}t \\ &\quad + \int_0^T \left\langle B(\mathbf{W}^b, \Omega^b), \mathbf{J}(\Omega^b) - \Lambda^b \right\rangle + \left\langle -\frac{\mathrm{D}\Lambda^b}{\mathrm{d}t} + [\Lambda^b, \Omega^b], \mathbf{W}^b \right\rangle \mathrm{d}t, \end{aligned} \tag{B-4.8}$$

where $\mathcal{J}_\epsilon = \mathcal{J}(R_\epsilon, v_\epsilon, \Omega_\epsilon)$,

$$\delta\Omega^b(t) = \sum_{i=1}^3 \frac{\partial \omega_{\epsilon i}^b}{\partial \epsilon}(t, 0) \mathbf{X}_i \in \mathfrak{so}(3),$$

and

$$B(\mathbf{W}^b, \Omega^b) = \sum_{i=1}^3 \omega_i^b(t) \nabla_{\mathbf{W}^b} \mathbf{X}_i \in \mathfrak{so}(3).$$

$\mathbf{W}^b$ is the variational vector field that is defined as follows (see [50], page 41, for a right control system.) For a perturbed element $R_\epsilon(t,\epsilon)$ that satisfies $R_\epsilon(t,0) = R(t)$, we have an analogous expression to (B-4.3) such that for some $\mathbf{W}^b \in \mathfrak{so}(3)$ we have $\partial R/\partial\epsilon\big|_{\epsilon=0} = RW^b \in \mathrm{T}_R\mathrm{SO}(3)$. $[\cdot,\cdot]$ denotes the Lie bracket, and ∇ is the covariant derivative. Here, $\mathbf{X}_i$ $(i = 1,2,3)$ is a set of basis vector fields for $\mathfrak{so}(3)$ and ω_i^b $(i = 1,2,3)$ are the components of Ω^b such that $\Omega^b = \sum_{i=1}^3 \omega_i^b \mathbf{X}_i$. In deriving the above expressions use has been made of the following identities: $\langle B, \mathbf{J}(C)\rangle = \langle \mathbf{J}(B), C\rangle$ and $\langle [B,C], D\rangle = \langle B, [C,D]\rangle$ for all $A \in \mathrm{SO}(3)$ and $B,C,D \in \mathfrak{so}(3)$[3]. We have also integrated by parts:

$$\begin{aligned}
\int_0^T \left\langle \Lambda^b, \frac{\mathrm{D}\mathbf{W}^b}{\mathrm{d}t} \right\rangle \mathrm{d}t &= \int_0^T \left(\Lambda^b\right)^* \left(\frac{\mathrm{D}\mathbf{W}^b}{\mathrm{d}t}\right) \mathrm{d}t \\
&= -\int_0^T \frac{\mathrm{D}\left(\Lambda^b\right)^*}{\mathrm{d}t}\left(\mathbf{W}^b\right) \mathrm{d}t + \left[\left\langle \Lambda^b, \mathbf{W}^b \right\rangle\right]_0^T \\
&= -\int_0^T \left\langle \frac{\mathrm{D}\Lambda^b}{\mathrm{d}t}, \mathbf{W}^b \right\rangle \mathrm{d}t,
\end{aligned}$$

where $\mathbf{W}(0) = \mathbf{W}(T) = 0$ by virtue of the boundary conditions (B-4.5).

First order necessary conditions for optimality are obtained by setting $\partial\mathcal{J}_\epsilon/\partial\epsilon\big|_{\epsilon=0} = 0$. By the independence of $\delta\Omega^b$ and $\mathbf{W}^b$ in equation (B-4.8), the first integral in the equation is zero and we get:

$$\Lambda^b = \mathbf{J}(\Omega^b). \tag{B-4.9}$$

Hence, we have $\left\langle B(\mathbf{W}^b, \Omega^b), \mathbf{J}(\Omega^b) - \Lambda^b \right\rangle = 0$ and (B-4.8) implies

$$\frac{\mathrm{D}\Lambda^b}{\mathrm{d}t} = [\Lambda^b, \Omega^b]. \tag{B-4.10}$$

---

[3]For all $A \in \mathrm{SO}(3)$ and $B,C,D \in \mathfrak{so}(3)$, using simple properties of the trace operator we have $\langle B, \mathbf{J}(C)\rangle = -\frac{1}{2}\mathrm{Tr}\left(B\mathbf{J}(C)\right) = -\frac{1}{2}\mathrm{Tr}\left(B(JC + CJ)\right) = -\frac{1}{2}\left[\mathrm{Tr}\left(BJC\right) + \mathrm{Tr}\left(BCJ\right)\right] = -\frac{1}{2}\left[\mathrm{Tr}\left(BJC\right) + \mathrm{Tr}\left(JBC\right)\right] = -\frac{1}{2}\mathrm{Tr}\left((BJ + JB)C\right) = \langle \mathbf{J}(B), C\rangle$. For the identity $\langle [B,C], D\rangle = \langle B, [C,D]\rangle$, see Theorem (21.3) on page 113 in [41] for the generic compact Lie group case. For the case at hand, we have: $\langle [B,C], D\rangle = -\frac{1}{2}\mathrm{Tr}(BCD - CBD) = -\frac{1}{2}\mathrm{Tr}(BCD - BDC) = -\frac{1}{2}\mathrm{Tr}(B(CD - DC)) = \langle B, [C,D]\rangle$.

Recalling that the angular momentum is defined as $M^b = \mathbf{J}(\Omega^b)$, then equation (B-4.10) can be re-written in the familiar form of Euler's equation:

$$\frac{\mathrm{D}M^b}{\mathrm{d}t} = \left[M^b, \Omega^b\right]. \tag{B-4.11}$$

Two final remarks are in order. Firstly, in the above discussion we have reserved the covariant time differentiation $\frac{\mathrm{D}}{\mathrm{d}t}$ for vector fields (such as M^b and Ω^b) but have used a simple time derivative (the dot over a variable) for coordinate variables (namely, the variable R.) This is a standard notation that we adopt here. Secondly, if $M^b = \hat{m}^b$, then equation (B-4.11) is written in the more familiar form:

$$\dot{m}^b = m^b \times \omega^b.$$

Euler's equation is of course expressed in the body-fixed frame. In a space-fixed frame, we have $\dot{m}^s = m^b + \omega^b \times m^b = m^b \times \omega^b + \omega^b \times m^b = 0$. That is, in a space-faxed frame, angular momentum is conserved, which is a standard result.

We now derive the same result using an alternative approach using the calculus of variations that does not rely on the use of Lagrange multipliers. If we replace Ω^b in the cost function with $R^T\dot{R}$ and take variations, we get

$$\begin{aligned}
\left.\frac{\partial \mathcal{J}_\epsilon}{\partial \epsilon}\right|_{\epsilon=0} &= \int_0^T \left\langle \left[\Omega^b, \mathbf{W}^b\right] + \frac{\mathrm{D}\mathbf{W}^b}{\mathrm{d}t}, \mathbf{J}\left(\Omega^b\right) \right\rangle \mathrm{d}t \\
&= \int_0^T \left\langle \mathbf{W}^b, -\left[\Omega^b, \mathbf{J}\left(\Omega^b\right)\right] - \frac{\mathrm{D}\mathbf{J}\left(\Omega^b\right)}{\mathrm{d}t} \right\rangle \mathrm{d}t,
\end{aligned}$$

which when set equal to zero gives the same result as before.

EOMs in space-fixed frame

Let us derive the equations of motions in a space-fixed frame. As noted at the end of the previous section, we now ought to obtain the basic result that angular momentum, which, as we shall see, turns out to have a more complex expression, is

conserved. Hence, in this section we study the rigid body expressing its kinematic equation in space-fixed frame:

$$\dot{R} = \Omega^s R. \tag{B-4.12}$$

We wish to minimize the same cost functional given by equation (B-4.4) (that is, the kinetic energy) subject to the kinematics given by equation (B-4.12) and some boundary conditions as given by equation (B-4.5). First, since $\dot{R} = R\Omega^b = \Omega^s R$, then we have:

$$\Omega^s = R\Omega^b R^T. \tag{B-4.13}$$

Hence, we have

$$\mathbf{J}(\Omega^b) = JR^T\Omega^s R + R^T\Omega^s RJ =: \mathbf{J}(R, \Omega^s) \tag{B-4.14}$$

and the cost functional is given by the more complicated expression:

$$\mathcal{J} = \int_0^T \frac{1}{2} \left\langle \Omega^s, RJR^T\Omega^s + \Omega^s RJR^T \right\rangle \mathrm{d}t.$$

Appending the cost by the term $\left\langle \Lambda^s, \dot{R}R^T - \Omega^s \right\rangle$ and performing the computation as in the previous section (except that it now requires a bit more strenuous effort), we obtain:

$$\begin{aligned} \left.\frac{\partial \mathcal{J}_\epsilon}{\partial \epsilon}\right|_{\epsilon=0} &= \int_0^T \left\langle \delta\Omega^s, \left(RJR^T\Omega^s + \Omega^s RJR^T\right) - \Lambda^s \right\rangle \mathrm{d}t \\ &\quad + \int_0^T \left\langle B(\mathbf{W}^s, \Omega^s), \left(RJR^T\Omega^s + \Omega^s RJR^T\right) - \Lambda^s \right\rangle \mathrm{d}t - \int_0^T \left\langle \frac{\mathrm{D}\Lambda^s}{\mathrm{d}t}, \mathbf{W}^s \right\rangle \mathrm{d}t, \end{aligned}$$

where now we define the right variation vector field $\mathbf{W}^s$ by $\partial R_\epsilon/\partial\epsilon = \mathbf{W}^s R_\epsilon$. Hence, the necessary optimality conditions are given by:

$$\begin{aligned} M^s &:= \Lambda^s = RJR^T\Omega^s + \Omega^s RJR^T \\ \frac{\mathrm{D}M^s}{\mathrm{d}t} &= 0, \end{aligned} \tag{B-4.15}$$

where M^s is the angular momentum as expressed in a space-fixed frame. The second of equations (B-4.15) expresses the fact that angular momentum is conserved in an inertial (Newtonian, or space-fixed) frame.

B.4.3 Second Order Optimal Control Problem

In body-fixed frame

We now study the minimum control problem in body-fixed variables, minimizing

$$\mathcal{J} = \int_0^T \frac{1}{2} \left\langle \hat{\tau}^b, \hat{\tau}^b \right\rangle \mathrm{d}t \tag{B-4.16}$$

subject to the second order dynamics:

$$\begin{aligned} \dot{R} &= R\Omega^b \\ \frac{\mathrm{D}M^b}{\mathrm{d}t} &= \left[M^b, \Omega^b\right] + \hat{\tau}^b \end{aligned} \tag{B-4.17}$$

and the boundary conditions:

$$R(0) = R_0,\ \Omega^b(0) = \Omega_0^b,\ R(T) = R_T,\ \Omega^b(T) = \Omega_T^b \tag{B-4.18}$$

where $\hat{\tau}^b \in \mathfrak{so}(3)$ is the skew symmetric form of the torque vector $\tau^b \in R^3$. Note that if we set $J = \frac{1}{2}I$, then $M^b = \Omega^b$ and we are able to make connections to previously published results [30, 94, 55] for systems of the form:

$$\begin{aligned} \dot{x} &= \Omega \\ \frac{\mathrm{D}\Omega}{\mathrm{d}t} &= \hat{\tau}, \end{aligned} \tag{B-4.19}$$

where $x = R^T\dot{R}$.

We follow the same procedure as in the previous section by first formulating the appended cost functional:

$$\mathcal{J} = \int_0^T \frac{1}{2} \left\langle \hat{\tau}^b, \hat{\tau}^b \right\rangle + \left\langle \Lambda_1^b, R^T\dot{R} - \Omega^b \right\rangle + \left\langle \Lambda_2^b, \frac{\mathrm{D}M^b}{\mathrm{d}t} - \left[M^b, \Omega^b\right] - \hat{\tau}^b \right\rangle \mathrm{d}t.$$

Computing $\partial \mathcal{J}_\epsilon / \partial \epsilon$, we get:

$$\begin{aligned}
\left.\frac{\partial \mathcal{J}}{\partial \epsilon}\right|_{\epsilon=0} &= \int_0^T \left\langle \left.\frac{\mathrm{D}\hat{\tau}^b}{\mathrm{d}\epsilon}\right|_{\epsilon=0}, \hat{\tau}^b - \Lambda_2^b \right\rangle \mathrm{d}t \\
&\quad + \int_0^T \left\langle \left.\frac{\mathrm{D}\Omega^b}{\mathrm{d}\epsilon}\right|_{\epsilon=0}, -\Lambda_1^b - \mathbf{J}\left(\left[\Omega^b, \Lambda_2^b\right]\right) + \left[M^b, \Lambda_2^b\right] - \frac{\mathrm{D}}{\mathrm{d}t}\mathbf{J}\left(\Lambda_2^b\right) \right\rangle \mathrm{d}t \\
&\quad + \left\langle \mathbf{W}^b, -[\Omega^b, \Lambda_1^b] - \frac{\mathrm{D}\Lambda_1^b}{\mathrm{d}t} + \mathbf{R}\left(\mathbf{J}(\Lambda_2^b), \Omega^b\right)\Omega^b \right\rangle \Bigg] \mathrm{d}t, \qquad \text{(B-4.20)}
\end{aligned}$$

where $\mathbf{R}$ is the curvature tensor associated with SO(3). In obtaining equation (B-4.20), use of the following identities and the ones utilized in the previous section has been made:

$$\begin{aligned}
\frac{\mathrm{D}}{\mathrm{d}\epsilon}\frac{\mathrm{D}}{\mathrm{d}t}\Omega_\epsilon^b - \frac{\mathrm{D}}{\mathrm{d}t}\frac{\mathrm{D}}{\mathrm{d}\epsilon}\Omega_\epsilon^b &= \mathbf{R}(\mathbf{W}^b, \Omega_\epsilon^b)\Omega_\epsilon^b \\
\left\langle \mathbf{J}(\Lambda_2^b), \mathbf{R}(\mathbf{W}^b, \Omega^b)\Omega^b \right\rangle &= \left\langle \mathbf{W}^b, \mathbf{R}(\mathbf{J}(\Lambda_2^b), \Omega^b)\Omega^b \right\rangle
\end{aligned}$$

We have also used the linearity of the operator $\mathbf{J}$. We have, for example,

$$\frac{\partial}{\partial \epsilon}\mathbf{J}\left(\Omega_\epsilon^b\right) = \mathbf{J}\left(\frac{\partial \Omega_\epsilon^b}{\partial \epsilon}\right).$$

We then have the following theorem, which holds since in equation (B-4.20), arbitrary variations in $\hat{\tau}$, Ω and R are independent and, hence, their inner product terms must be zero for $\partial \mathcal{J}/\partial \epsilon\big|_{\epsilon=0} =$ to hold.

Theorem B.4.1. *Necessary optimality conditions for a trajectory $(R, \Omega, \hat{\tau})$ to be the optimal solution to the problem of minimizing (B-4.16) subject to the dynamics in equation (B-4.17) and the boundary conditions in equation (B-4.18) are given by*

$$\begin{aligned}
\dot{R} &= R\Omega^b \\
\frac{\mathrm{D}M^b}{\mathrm{d}t} &= \left[M^b, \Omega^b\right] + \Lambda_2^b \\
\hat{\tau}^b &= \Lambda_2^b \qquad \text{(B-4.21)} \\
\frac{\mathrm{D}\Lambda_1^b}{\mathrm{d}t} &= -[\Omega^b, \Lambda_1^b] + \mathbf{R}(\mathbf{J}(\Lambda_2^b), \Omega^b)\Omega^b \\
\frac{\mathrm{D}\mathbf{J}(\Lambda_2^b)}{\mathrm{d}t} &= [M^b, \Lambda_2^b] - \Lambda_1 - \mathbf{J}(\left[\Omega^b, \Lambda_2^b\right]).
\end{aligned}$$

and the boundary conditions (B-4.18).

We now make connections to previously published results under the assumption that $J = \frac{1}{2} I_{3\times 3}$, where $I_{3\times 3}$ is the 3×3 identity matrix. Let $x = R^T R$ and define the variation vector field $\mathbf{W}_x$ such that $\frac{\partial x_\epsilon}{\partial \epsilon}\big|_{\epsilon=0} = \mathbf{W}_x$. Then

$$\int_0^T \frac{\mathrm{D}\mathbf{W}_x}{\mathrm{d}t}\mathrm{d}t = \int_0^T \left.\frac{\partial \dot{x}_\epsilon}{\partial \epsilon}\right|_{\epsilon=0} \mathrm{d}t = \int_0^T \left.\frac{\partial}{\partial \epsilon} R_\epsilon^T \dot{R}_\epsilon\right|_{\epsilon=0} \mathrm{d}t = \int_0^T \left[\Omega, \mathbf{W}^b\right] + \frac{\mathrm{D}\mathbf{W}^b}{\mathrm{d}t}\mathrm{d}t.$$

Thus $\mathbf{W}^b$ and $\mathbf{W}_x$ are related by

$$\mathbf{W}_x = \mathbf{W}^b + \int_0^T \left[\Omega, \mathbf{W}^b\right] \mathrm{d}t.$$

With this one can show that equation (B-4.20) can be written in terms of $\mathbf{W}_x$ as

$$\begin{aligned} \left.\frac{\partial \mathcal{J}}{\partial \epsilon}\right|_{\epsilon=0} \quad = \quad & \int_0^T \left\langle \left.\frac{\mathrm{D}\hat{\tau}^b}{\mathrm{d}\epsilon}\right|_{\epsilon=0}, \hat{\tau}^b - \Lambda_2^b \right\rangle \mathrm{d}t + \left\langle \left.\frac{\mathrm{D}\Omega^b}{\mathrm{d}\epsilon}\right|_{\epsilon=0}, -\Lambda_1^b - \frac{\mathrm{D}\Lambda_2^b}{\mathrm{d}t} \right\rangle \\ & + \left\langle \mathbf{W}_x, -\frac{\mathrm{D}\Lambda_1^b}{\mathrm{d}t} + \mathbf{R}\left(\Lambda_2^b, \Omega^b\right)\Omega^b \right\rangle \Bigg] \mathrm{d}t, \end{aligned}$$

which implies that the necessary conditions could be re-written as

$$\begin{aligned} \dot{x} &= \Omega^b \\ \frac{\mathrm{D}\Omega^b}{\mathrm{d}t} &= \Lambda_2^b \\ \hat{\tau}^b &= \Lambda_2^b \\ \frac{\mathrm{D}\Lambda_1^b}{\mathrm{d}t} &= \mathbf{R}(\Lambda_2^b, \Omega^b)\Omega^b \\ \frac{\mathrm{D}\Lambda_2^b}{\mathrm{d}t} &= -\Lambda_1^b. \end{aligned} \tag{B-4.22}$$

Differentiating the third equation one more time and using the second equation, the above necessary conditions for the special case when $J = \frac{1}{2} I$, we obtain the following standard result

$$\frac{\mathrm{D}^3\Omega^b}{\mathrm{d}t^3} + \mathbf{R}(\hat{\tau}^b, \Omega^b)\Omega^b = 0, \tag{B-4.23}$$

which is the standard geodesic equation first derived in [30]. Hence we have the following lemma.

Lemma B.4.1. *Under the assumption that $J = \frac{1}{2} I_{3\times 3}$, then the necessary conditions (B-4.21) are equivalently expressed as in equation (B-4.22) or equation (B-4.23).*

The result in [30] is only true for rigid bodies with symmetric inertia properties (up to a scalar multiple of the identity).

Example B.4.1 (Example on SO(2)). For SO(2), it is easy to verify that $[\mathbf{Z}, \mathbf{Y}] \equiv 0$ for all $\mathbf{X}, \mathbf{Y} \in \mathfrak{so}(2)$ and, hence, $\mathbf{R}(\mathbf{X}, \mathbf{Y})\mathbf{Z} = \frac{1}{4}\left[[\mathbf{X}, \mathbf{Y}]\, \mathbf{Z}\right] \equiv 0$, for all $\mathbf{X}, \mathbf{Y}, \mathbf{Z} \in \mathfrak{so}(2)$. Therefore, for the SO(2) case, the necessary conditions are:

$$\begin{aligned} \dot{R} &= R\Omega \\ \frac{\mathrm{D}M}{\mathrm{d}t} &= \Lambda_2 \\ \frac{\mathrm{D}\Lambda_1}{\mathrm{d}t} &= 0 \\ \frac{\mathrm{D}\mathbf{J}\left(\Lambda_2\right)}{\mathrm{d}t} &= -\Lambda_1 \\ \hat{\tau} &= \Lambda_2. \end{aligned}$$

If we let θ be the orientation of the planar body, then

$$\hat{\theta} = \log(R) = \begin{bmatrix} 0 & -\theta \\ \theta & 0 \end{bmatrix}.$$

This corresponds to

$$R = \exp\left(\hat{\theta}\right) = \begin{bmatrix} \cos\theta & -\sin\theta \\ \sin\theta & \cos\theta \end{bmatrix}.$$

Recall that in the general three dimensional case $\mathbf{J}\left(\Lambda_2\right) = J\Lambda_2 + \Lambda_2 J$, where J is a diagonal matrix with entries J_1, J_2 and J_3. In the two dimensional case, we have

$$\mathbf{J}\left(\Lambda_2\right) = \begin{bmatrix} 0 & -I_3\lambda_2 \\ I_3\lambda_2 & 0 \end{bmatrix}$$

and

$$M = \begin{bmatrix} 0 & -I_3\omega \\ I_3\omega & 0 \end{bmatrix},$$

where $\Lambda_2 = \hat{\lambda}_2$ and $\Omega = \hat{\omega}$. I_3 is the moment of inertia about the out-of-plane axis of the body. With the above identifications, the necessary conditions (B-4.24) are equivalently written as

$$\begin{bmatrix} \dot{\theta} \\ \dot{\omega} \\ \dot{\lambda}_1 \\ \dot{\lambda}_2 \end{bmatrix} = \begin{bmatrix} 0 & 1 & 0 & 0 \\ 0 & 0 & 0 & \frac{1}{I_3} \\ 0 & 0 & 0 & 0 \\ 0 & 0 & \frac{1}{I_3} & 0 \end{bmatrix} \begin{bmatrix} \theta \\ \omega \\ \lambda_1 \\ \lambda_2 \end{bmatrix}.$$

These equations may be solved analytically to obtain:

$$\begin{aligned} \theta(t) &= \frac{\lambda_1^0}{6I_3^2}t^3 + \frac{\lambda_2^0}{2I_3}t^2 + \omega_0 t + \theta_0 \\ \omega(t) &= \frac{\lambda_1^0}{2I_3^2}t^2 + \frac{\lambda_2^0}{I_3}t + \omega_0 \\ \lambda_1(t) &= \lambda_1^0 \\ \lambda_2(t) &= \frac{\lambda_1^0}{I_3}t + \lambda_2^0, \end{aligned}$$

where λ_1^0 and λ_2^0 are initial conditions on the Lagrange multipliers to satisfy the terminal conditions imposed on θ and ω. In this case these are given by

$$\begin{aligned} \lambda_1^0 &= \frac{21}{2}I_3^2T^3(\theta_T - \theta_0) - 3\frac{I_3^2}{T^2}\omega_0 + \frac{3}{2}\frac{I_3^2}{T^2}\omega_T \\ \lambda_2^0 &= \frac{3}{4}I_3T^2(\theta_T - \theta_0) + \frac{1}{2}\frac{I_3}{T}\omega_0 + \frac{1}{4}\frac{I_3}{T}\omega_T. \end{aligned}$$

If no terminal conditions were specified, then the above initial conditions on the multipliers will be replaced by the terminal conditions $\lambda_1(T) = \lambda_2(T) = 0$.

Say we wish to drive the system from an initial state $\theta(0) = \theta_0 = 0.5$ radians, $\omega(0) = \omega_0 = 0$ to the terminal state $\theta(T) = 0$ and $\omega(T) = 0$, where $T = 5\pi$ and

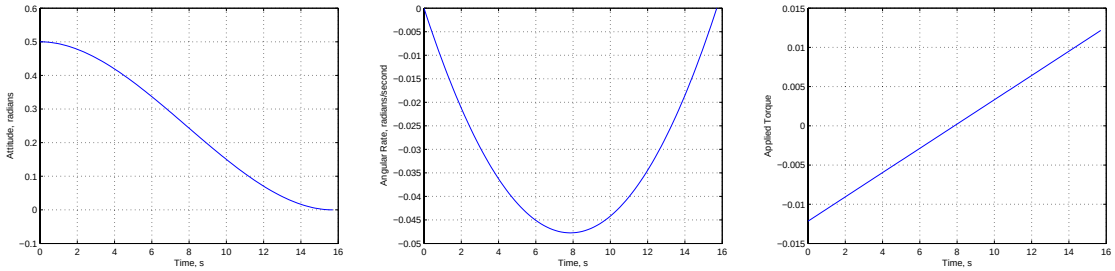

Figure B.1: Attitude (left), angular velocity (center) and applied torque (right.)

$I_3 = 1$. Figure (B.1) shows attitude, angular velocity and torque applied as a function of time on $[0, T]$. Note that the attitude converges to zero and the solution satisfies the desired boundary conditions.

In space-fixed frame

In the space-fixed frame formulation, we wish to minimize

$$\mathcal{J} = \int_0^T \frac{1}{2} \langle \hat{\tau}^s, \hat{\tau}^s \rangle \, \mathrm{d}t \tag{B-4.24}$$

subject to the second order dynamics:

$$\begin{aligned} \dot{R} &= R\Omega^s \\ \frac{\mathrm{D}M^s}{\mathrm{d}t} &= \hat{\tau}^s \end{aligned} \tag{B-4.25}$$

and the boundary conditions:

$$R(0) = R_0, \ \Omega^s(0) = \Omega^s_0, \ R(T) = R_T, \ \Omega^s(T) = \Omega^s_T \tag{B-4.26}$$

where $\hat{\tau}^s \in \mathfrak{so}(3)$ is the skew symmetric form of the torque vector $\tau^s \in R^3$. The corresponding variational vector fields are such that $\partial R_\epsilon / \partial \epsilon = \mathbf{W}^s R$. In the current

settings, we have:

$$\begin{aligned}
\left.\frac{\partial \mathcal{J}}{\partial \epsilon}\right|_{\epsilon=0} &= \int_0^T \langle \delta\hat{\tau}^s, \hat{\tau}^s - \Lambda_2^s \rangle \, \mathrm{d}t \\
&\quad + \int_0^T \left\langle \mathbf{W}^s, -\frac{\mathrm{D}\Lambda_1^s}{\mathrm{d}t} + [\Omega^s, \Lambda_1^s] + RJR^T \frac{\mathrm{D}\Omega^s}{\mathrm{d}t}\Lambda_2^s - \frac{\mathrm{D}\Omega^s}{\mathrm{d}t}\Lambda_2^s RJR^T \right. \\
&\quad \left. + RJR^T\Lambda_2^s \frac{\mathrm{D}\Omega^s}{\mathrm{d}t} - \Lambda_2^s \frac{\mathrm{D}\Omega^s}{\mathrm{d}t} RJR^T + \mathbf{R}(RJR^T\Lambda_2^s + \Lambda_2^s RJR^T, \Omega^s)\Omega^s \right\rangle \mathrm{d}t \\
&\quad + \int_0^T \left\langle \left.\frac{\mathrm{D}\Omega^s}{\mathrm{d}\epsilon}\right|_{\epsilon=0}, -\Lambda_1^s - \frac{\mathrm{D}}{\mathrm{d}t}\left(RJR^T\Lambda_2^s + \Lambda_2^s RJR^T\right) \right\rangle \mathrm{d}t.
\end{aligned}$$

Hence, the necessary optimality conditions are given by:

$$\begin{aligned}
\hat{\tau}^s &= \Lambda_2^s \\
\frac{\mathrm{D}\Lambda_1^s}{\mathrm{d}t} &= [\Omega^s, \Lambda_1^s] + RJR^T \frac{\mathrm{D}\Omega^s}{\mathrm{d}t}\Lambda_2^s \\
&\quad - \frac{\mathrm{D}\Omega^s}{\mathrm{d}t}\Lambda_2^s RJR^T + RJR^T\Lambda_2^s \frac{\mathrm{D}\Omega^s}{\mathrm{d}t} \\
&\quad - \Lambda_2^s \frac{\mathrm{D}\Omega^s}{\mathrm{d}t} RJR^T + \mathbf{R}(RJR^T\Lambda_2^s + \Lambda_2^s RJR^T, \Omega^s)\Omega^s \\
\frac{\mathrm{D}}{\mathrm{d}t}\left(RJR^T\Lambda_2^s + \Lambda_2^s RJR^T\right) &= -\Lambda_1^s.
\end{aligned}$$

B.5 Optimal Trajectory Tracking

In this section we study the optimal trajectory tracking problem. That is, we wish to minimize the weighted sum of the control effort and the deviation of the configuration of the body from a nominal trajectory, where the system is subject to the dynamic constraints given by equations (B-1.1) and (B-1.3) and some initial and terminal constraints. As was done before, we will study the problem on SO(n) ($n = 2, 3$) first with some illustrations and then generalize the study to the $SE(n)$ ($n = 2, 3$) case. Illustrative examples will be given for $SE(2)$.

B.5.1 Trajectory tracking on SO(n)

In this section we carry out the analysis in body-fixed variables. Hence, we will drop the superscript b that identifies a body-fixed variable. Let $R_d(T) \in \mathrm{SO}(n)$ be a

given trajectory to be tracked and, as above, the body's configuration be denoted by $R(t) \in \mathrm{SO}(n)$. Before embarking on deriving the main result, we have to decide on a choice for the error signal. The error signal we choose is $e(t) = R_d(t)^T R(t)$. It is easy to see that $e(t) \in \mathrm{SO}(n)$: $e^T e = R^T R_d R_d^T R = I$, the identity, and $\det\left(R_d^T R\right) = \det\left(R_d^T\right)\det\left(R\right) = \det\left(R_d\right)\det\left(R\right) = 1$. When $R(t) = R_d(t)$ for any $t \in [0, T]$, then $e(t) = I$. Hence, we desire to have e as small as possible. Next, we have to quantify the smallness of of e. That is, we need to define a distance function on $\mathrm{SO}(n)$ to be able to measure how far away $e(t)$ is from identity. We have the following result.

Proposition B.5.1 (Distance Metric on SO(n), [49]). *With respect to an* Ad*-invariant metric $\langle \cdot, \cdot \rangle$, the distance between an element $g \in G$ and the identity $e_G \in G$ of a compact Lie group G is given by the norm of the logarithmic function: $\langle \log(g), \log(g) \rangle^{1/2}$.*

Hence, a measure of the tracking error is given by $\langle \log(e), \log(e) \rangle$. With these definitions, the optimal trajectory tracking problem is given by:

Problem B.5.1. *Minimize*

$$\mathcal{J} = \int_0^T \frac{1}{2}\left\langle \hat{\tau}, \hat{\tau} \right\rangle + \frac{\beta}{2}\left\langle \log\left(R_d^T(t)R(t)\right), \log\left(R_d^T(t)R(t)\right)\right\rangle \mathrm{d}t \tag{B-5.1}$$

subject to the second order attitude dynamics

$$\begin{aligned} \dot{R} &= R\Omega \\ \frac{\mathrm{D}M}{\mathrm{d}t} &= [M, \Omega] + \hat{\tau} \end{aligned} \tag{B-5.2}$$

and the boundary conditions

$$R(0) = R_0,\ \Omega(0) = \Omega_0,\ R(T) = R_T,\ \Omega(T) = \Omega_T. \tag{B-5.3}$$

$\beta \geq 0$ is a weighting parameter.

Before embarking on deriving the necessary optimality conditions, we need the following result.

Theorem B.5.1 (Derivative of the Distance Function, [49, 97]). *Let G be a compact Lie group with a bi-invariant metric $\langle \cdot, \cdot \rangle$. Consider a trajectory $g(\lambda) \in G$ parameterized by the variable λ, such that $g(\lambda)$ never passes through a singularity of the exponential map. Then*

$$\frac{1}{2} \frac{\mathrm{d}}{\mathrm{d}\lambda} \|g\|_G^2 = \langle \log(g), \mathbf{Z} \rangle \,, \tag{B-5.4}$$

where $\|\cdot\|_G$ denotes the distance metric on G: $\|\cdot\|_G = \langle \cdot, \cdot \rangle^{1/2}$. $\mathbf{Z}$ is a vector field that satisfies $\frac{\partial}{\partial \lambda} g(\lambda) = g\mathbf{Z}$.

The variable λ may either denote the time variable t or the perturbation variable ϵ. In applications such as PD control on the Euclidean group [49], λ denotes the time variable. On the other hand, in the calculus of variations and the current setting, λ denotes the perturbation variable ϵ. Indeed, note that the perturbed error is given by $e_\epsilon(t) = R_d^T(t) R_\epsilon(t)$. Hence, we have: $\frac{\partial}{\partial \epsilon} e_\epsilon = e_\epsilon(t) \mathbf{W}(t)$, where $\mathbf{W}(t)$ is the left-invariant variation vector field associated with the curve $R(t)$: $\frac{\partial}{\partial \epsilon} R_\epsilon(t) \big|_{\epsilon=0} = R(t)\mathbf{W}(t)$.

With the above definitions, we are in a position to formulate the appended cost functional:

$$\mathcal{J} = \frac{1}{2} \langle \hat{\tau}, \hat{\tau} \rangle + \frac{\beta}{2} \left\langle \log\left(R_d^T R\right), \log\left(R_d^T R\right) \right\rangle + \left\langle \Lambda_1, R^T \dot{R} - \Omega \right\rangle + \left\langle \Lambda_2, \frac{\mathrm{D}M}{\mathrm{d}t} - [M, \Omega] - \hat{\tau} \right\rangle .$$

Taking variations of this expression and using Theorem (B.5.1), we obtain

$$\begin{aligned} \left. \frac{\partial \mathcal{J}_\epsilon}{\partial \epsilon} \right|_{\epsilon=0} = & \left\langle \left. \frac{\mathrm{D}\hat{\tau}_\epsilon}{\mathrm{d}\epsilon} \right|_{\epsilon=0}, \hat{\tau} - \Lambda_2 \right\rangle + \left\langle \mathbf{W}, \beta \log\left(R_d^T R\right) - [\Omega, \Lambda_1] - \frac{\mathrm{D}\lambda_1}{\mathrm{d}t} + \mathbf{R}\left(\Lambda_2, \Omega\right) M \right\rangle \\ & + \left\langle \left. \frac{\mathrm{D}\Omega_\epsilon}{\mathrm{d}\epsilon} \right|_{\epsilon=0}, -\Lambda_1 - \frac{\mathrm{D}\mathbf{J}\left(\Lambda_2\right)}{\mathrm{d}t} - \mathbf{J}\left([\Omega, \Lambda_2]\right) + [M, \Lambda_2] \right\rangle \mathrm{d}t. \end{aligned}$$

$\mathbf{R}$ is the riemannian curvature tensor associated with the special orthogonal group. For any compact Lie group (such as the special orthogonal group) we have

Lemma B.5.1 (Riemannian Curvature Tensor for Compact Lie Groups, [41]). *Let G be a Lie group with a bi-invariant Riemannian metric. If $\mathbf{X}, \mathbf{Y}, \mathbf{Z}$ are left invariant vector fields on G, then $\mathbf{R}(\mathbf{X}, \mathbf{Y})\mathbf{Z} = \frac{1}{4}[[\mathbf{X}, \mathbf{Y}], \mathbf{Z}]$.*

Hence, we have the following theorem.

Theorem B.5.2. *The first order necessary optimality conditions for the problem (B.5.1) are given by:*

$$\begin{aligned}
\dot{R} &= R\Omega \\
\frac{\mathrm{D}M}{\mathrm{d}t} &= [M, \Omega] + \Lambda_2 \\
\frac{\mathrm{D}\Lambda_1}{\mathrm{d}t} &= \beta \log\left(R_d^T R\right) - [\Omega, \Lambda_1] + \frac{1}{4}[[\Lambda_2, \Omega], M] \\
\frac{\mathrm{D}\mathbf{J}(\Lambda_2)}{\mathrm{d}t} &= -\Lambda_1 - \mathbf{J}([\Omega, \Lambda_2]) + [M, \Lambda_2] \\
\hat{\tau} &= \Lambda_2.
\end{aligned}$$

We now study this result for the two cases of interest: SO(2) and SO(3).

Trajectory Tracking on SO(2)

For SO(2), it is easy to verify that $[\mathbf{Z}, \mathbf{Y}] \equiv 0$ for all $\mathbf{X}, \mathbf{Y} \in \mathfrak{so}(2)$ and, hence, $\mathbf{R}(\mathbf{X}, \mathbf{Y})\mathbf{Z} = \frac{1}{4}[[\mathbf{X}, \mathbf{Y}]\mathbf{Z}] \equiv 0$, for all $\mathbf{X}, \mathbf{Y}, \mathbf{Z} \in \mathfrak{so}(2)$. Therefore for the SO(2) case,

the necessary conditions are:

$$\begin{aligned} \dot{R} &= R\Omega \\ \frac{\mathrm{D}M}{\mathrm{d}t} &= \Lambda_2 \\ \frac{\mathrm{D}\Lambda_1}{\mathrm{d}t} &= \beta \log\left(R_d^T R\right) \\ \frac{\mathrm{D}\mathbf{J}\left(\Lambda_2\right)}{\mathrm{d}t} &= -\Lambda_1 \\ \hat{\tau} &= \Lambda_2. \end{aligned} \tag{B-5.5}$$

If we let θ be the orientation of the planar body, then

$$\hat{\theta} = \log(R) = \begin{bmatrix} 0 & -\theta \\ \theta & 0 \end{bmatrix}.$$

This corresponds to

$$R = \exp\left(\hat{\theta}\right) = \begin{bmatrix} \cos\theta & -\sin\theta \\ \sin\theta & \cos\theta \end{bmatrix}.$$

Similar expressions are obtained for the desired rotation matrix R_d but replacing the orientation θ with the desired orientation angle θ_d. Since

$$R_d^T R = \begin{bmatrix} \cos(\theta - \theta_d) & -\sin(\theta - \theta_d) \\ \sin(\theta - \theta_d) & \cos(\theta - \theta_d) \end{bmatrix}$$

and, hence,

$$\log(R_d^T R) = \begin{bmatrix} 0 & -(\theta - \theta_d) \\ \theta - \theta_d & 0 \end{bmatrix}.$$

Recall that in the general three dimensional case $\mathbf{J}\left(\Lambda_2\right) = J\Lambda_2 + \Lambda_2 J$, where J is a diagonal matrix with entries J_1, J_2 and J_3. In the two dimensional case, we have

$$\mathbf{J}\left(\Lambda_2\right) = \begin{bmatrix} 0 & -I_3\lambda_2 \\ I_3\lambda_2 & 0 \end{bmatrix}$$

and

$$M = \begin{bmatrix} 0 & -I_3\omega \\ I_3\omega & 0 \end{bmatrix},$$

where $\Lambda_2 = \hat{\lambda}_2$ and $\Omega = \hat{\omega}$. I_3 is the moment of inertia about the out-of-plane axis of the body. With the above identifications, the necessary conditions (B-5.5) are equivalently written as

$$\begin{bmatrix} \dot{\theta} \\ \dot{\omega} \\ \dot{\lambda}_1 \\ \dot{\lambda}_2 \end{bmatrix} = \begin{bmatrix} 0 & 1 & 0 & 0 \\ 0 & 0 & 0 & \frac{1}{I_3} \\ \beta & 0 & 0 & 0 \\ 0 & 0 & -\frac{1}{I_3} & 0 \end{bmatrix} \begin{bmatrix} \theta \\ \omega \\ \lambda_1 \\ \lambda_2 \end{bmatrix} + \begin{bmatrix} 0 \\ 0 \\ -\beta \\ 0 \end{bmatrix} \theta_d(t). \tag{B-5.6}$$

Note here that the closed-loop system is unstable with eigenvalues given by

$$\pm \frac{1}{2}\sqrt{\frac{2}{I_3}}\beta^{1/4}(1-\imath), \;\; \pm \frac{1}{2}\sqrt{\frac{2}{I_3}}\beta^{1/4}(1+\imath). \tag{B-5.7}$$

This observation, of course, is an example that represents the difficulty with extending the present work to an infinite-time horizon even for the two-dimensional case. For linear systems, such as the two-dimensional problem we consider here, the instability does not pose a problem in the finite-horizon since linear systems do not have a finite escape time. On the other hand, for the infinite-time horizon problem we need to satisfy the Ricatti condition to ensure stability of the closed loop system. For a nonlinear system, however, the system possesses a finite escape time and, for the finite horizon time, we need to ensure that the terminal maneuver time T is smaller than the escape time.

We now consider an example. Say we wish to drive the system from an initial state $\theta(0) = \theta_0 = 0.5$ radians, $\omega(0) = \omega_0 = 0$ to the terminal state $\theta(T) = 0.2\cos T$ and $\omega(T) = 0$, where $T = 5\pi$. The trajectory to be tracked is given by $\theta_d(t) = 0.2\cos t$.

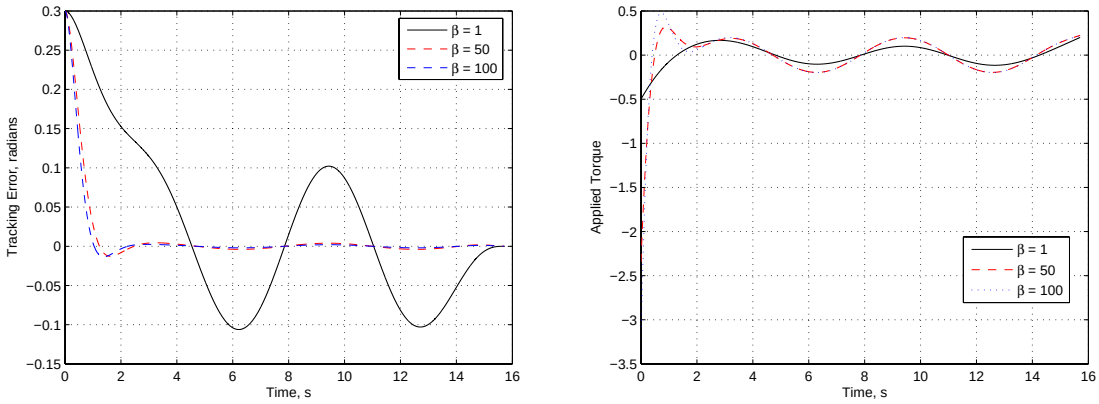

Figure B.2: Tracking error (left) and applied torque (right) for three different values of β: $\beta = 1,\ 50,\ 100$.

This is a two point boundary value problem. We use Matlab®'s bvp4c boundary value solver. The tracking error is plotted in Figure (B.2). Note that the error converges to zero and the solution satisfies the desired terminal conditions.

APPENDIX C

Optimal Control on Riemannian Manifolds with Potential Fields

This appendix is an extension of the work done by the author in Chapter 5 and in [40], where necessary conditions for minimizing the cost function for a trajectory that evolves on a Riemannian manifold and satisfies a second order differential equation together with some interpolation, smoothness and motion constraints were derived. In this appendix, we investigate the inclusion of a generalized potential field in the dynamics. This problem is motivated by two-spacecraft interferometric imaging applications, where the formation is evolving in some generalized potential field. The corresponding necessary conditions are derived and connections are made with previous results. The appendix is concluded with an example.

C.1 Problem Statement

In this appendix we consider systems that satisfy dynamics of the form:

$$\begin{aligned} \frac{\mathrm{D}\mathbf{q}}{\mathrm{d}t}(t) &= \mathbf{v}(t) \\ \frac{\mathrm{D}\mathbf{v}}{\mathrm{d}t}(t) &= \mathbf{u}(t) + \Delta_{\mathbf{q}(t)}\left(V\left(\mathbf{q}\left(t\right)\right)\right), \end{aligned} \tag{C-1.1}$$

where $\mathbf{q} : [0, T] \to M$ is a curve on M, $\mathbf{v}(t) \in T_{\mathbf{q}(t)}M$, $\mathbf{u}(t) \in TT_{\mathbf{q}(t)}M$ and $V : M \to \mathbb{R}$ is the potential energy function. $\Delta_{\mathbf{q}(t)}(\cdot)$ denotes the gradient with respect to the

metric g computed at the point $\mathbf{q}(t)$. $\Delta_{\mathbf{q}(t)}\left(V\left(\mathbf{q}\left(t\right)\right)\right)$ may equivalently be written in the form $[\mathrm{d}V]^{\#}_{\mathbf{q}(t)}$, where d denotes the exterior derivative and $\boldsymbol{\omega}^{\#}$ denotes the sharp operator acting on the form $\boldsymbol{\omega}$ to yield a vector field (see pages 85 and 95 in [42] and page 58-9 in [88] for a discussion on the gradient field and treating potential fields.) Moreover, let $\mathbf{u}(t) \in TT_{\mathbf{q}(t)}M$ be given by

$$\mathbf{u}(t) = \sum_{i=1}^{m} u_i(t)\mathbf{X}_i(\mathbf{q}(t)), \tag{C-1.2}$$

where $m \leq n$ and $\mathbf{X}_j$, $j = 1, \ldots, n$, satisfy $\langle \mathbf{X}_j, \mathbf{X}_k \rangle = \delta_{jk}$. In other words, $\mathbf{X}_j$ is an orthonormal set of vector fields on $T_{\mathbf{q}(t)}M$. Mathematically, this assumption limits the class of manifolds we consider (to parallelizable manifolds) for the general problem formulation, but is satisfied for the special case where we deal with real life systems of particles in space. Thus, we have:

$$\langle \mathbf{u}(t), \mathbf{u}(t) \rangle = \sum_{i=1}^{m} \mathbf{u}_i^2(t). \tag{C-1.3}$$

$m = n$ corresponds to the fully actuated system, whereas $m < n$ corresponds to the under-actuated situation. Here is a statement of the problem we are considering.

Problem C.1.1. *Find critical values of*

$$\mathcal{J}^{\tau}(\mathbf{q}) = \frac{1}{2}\int_0^T \left[\langle \mathbf{u}, \mathbf{u} \rangle + \tau^2 \left\langle \frac{\mathrm{D}\mathbf{q}(t)}{\mathrm{d}t}, \frac{\mathrm{D}\mathbf{q}(t)}{\mathrm{d}t} \right\rangle\right] \mathrm{d}t, \tag{C-1.4}$$

over the set Ω *of* $\mathcal{C}^1$*-paths* $\mathbf{q}$ *on* M*, satisfying*

- *the* dynamic constraints *(C-1.1),*
- $\mathbf{q}\big|_{[0,T]}$ *is smooth,*
- boundary conditions

$$\mathbf{q}(0) = \mathbf{q}_0,\ \mathbf{q}(T) = \mathbf{q}_T,\ \mathbf{v}(0) = \mathbf{v}_0,\ \mathbf{v}(T) = \mathbf{v}_T, \tag{C-1.5}$$

- *and the* motion constraints

$$\left\langle \frac{\mathrm{D}\mathbf{q}}{dt}, \mathbf{X}_i(\mathbf{q}) \right\rangle = k_i,\ i = 1, \ldots, l\ (l < n) \tag{C-1.6}$$

for $\mathbf{X}_i,\ i = 1, \ldots, n$, *linearly independent vector fields in some neighborhood of* $\mathbf{q}$ *and given constants* $k_i,\ i = 1, \ldots, l$.

In Chapter 5, we assumed that the system is evolving in a gravity-free space. Here we extend this work by including a potential field in the formulation. This has applications where the formation is evolving in a gravitational field such as in the vicinity of a libration point or when under the effect of planetary gravitational fields. It is also worth noting that the use of geometric control methods for spacecraft formation flying has received little attention, whereas extensive investigations have been conducted in the field of of robotic path planning (for more on this issue, see Section (IV) in [8].) This work is an attempt to use geometric optimal control theory for spacecraft formation motion planning.

When $m < n$ and the control variables belong not to TTM but to TM and directly control the system speeds as opposed to the accelerations, the problem is known at the SubRiemmannian optimal control problem. See for example [98], [99] and [42] and references therein for the treatment of these kinematic control problems. In this appendix we restrict our attention to the fully actuated dynamic version of the problem.

Assumption C.1.1. Each particle is fully actuated in all n directions. That is to say $m = n$.

Moreover, we may ignore the motion constraints (C-1.6). As shown in Chapter 5 and in [40], these constraints are automatically appended to the final expression for

the necessary conditions corresponding to the unconstrained problem. Here, again, once the necessary conditions are obtained for systems with a potential field, the motion constraints are simply appended to the necessary conditions. In Section (C.3) we derive the necessary conditions for the full problem (C.1.1).

C.2 Necessary Conditions for Optimality

As in [35], in this section we follow a Lagrangian approach to obtaining the first order necessary conditions that provide an optimal solution to the optimal control problem (C.1.1) without the motion constraints (C-1.6). We also show that the Lagrangian approach yields results identical to those obtained by purely variational approaches. In Section (C.3) we derive the necessary conditions for the full problem, including motion constraints. We now derive the necessary conditions using a Lagrangian approach.

Appending the Lagrangian with the dynamic equations of motion, one obtains:

$$\begin{aligned}\mathcal{J}^\tau(\mathbf{q},\mathbf{v},\boldsymbol{\lambda}_1,\boldsymbol{\lambda}_2,\mathbf{u}) &= \int_0^T \boldsymbol{\lambda}_1\left(\frac{\mathrm{D}\mathbf{q}}{\mathrm{d}t}-\mathbf{v}\right)+\boldsymbol{\lambda}_2\left(\frac{\mathrm{D}\mathbf{v}}{\mathrm{d}t}-\mathbf{u}-\Delta V\right)\\ &\quad +\frac{1}{2}\langle\mathbf{u},\mathbf{u}\rangle+\frac{1}{2}\tau^2\left\langle\frac{\mathrm{D}\mathbf{q}}{\mathrm{d}t},\frac{\mathrm{D}\mathbf{q}}{\mathrm{d}t}\right\rangle\mathrm{d}t,\end{aligned}$$

where $\boldsymbol{\lambda}_i \in T^*_{\mathbf{q}(t)}M$, $i=1,2$, are the one-form Lagrange multipliers. We now proceed by taking variations of $\mathcal{J}^\tau$ to obtain

$$\begin{aligned}\frac{\partial}{\partial\epsilon}\mathcal{J}^\tau\Big|_{\epsilon=0} &= \int_0^T\left[\boldsymbol{\lambda}_1\left(\frac{\mathrm{D}}{\partial\epsilon}\frac{\mathrm{D}\mathbf{q}(t,\epsilon)}{\mathrm{d}t}-\frac{\mathrm{D}\mathbf{v}}{\partial\epsilon}(t,\epsilon)\right)+\boldsymbol{\lambda}_2\left(\frac{\mathrm{D}}{\partial\epsilon}\frac{\mathrm{D}\mathbf{v}(t,\epsilon)}{\mathrm{d}t}-\frac{\mathrm{D}\mathbf{u}}{\partial\epsilon}-\frac{\mathrm{D}}{\partial\epsilon}\Delta V\right)\right.\\ &\quad \left.+\left\langle\mathbf{u},\frac{\mathrm{D}\mathbf{u}}{\partial\epsilon}\right\rangle+\tau^2\left\langle\frac{\mathrm{D}\mathbf{q}(t,\epsilon)}{\mathrm{d}t},\frac{\mathrm{D}}{\partial\epsilon}\frac{\mathrm{D}\mathbf{q}(t,\epsilon)}{\mathrm{d}t}\right\rangle\right]\mathrm{d}t\Big|_{\epsilon=0}\\ &= \int_0^T\boldsymbol{\lambda}_1\left(\frac{\mathrm{D}\mathbf{W}}{\mathrm{d}t}-\delta\mathbf{v}-\mathbf{B}(\mathbf{W},\mathbf{v})\right)\\ &\quad +\boldsymbol{\lambda}_2\left(\frac{\mathrm{D}}{\partial\epsilon}\frac{\mathrm{D}\mathbf{v}(t,\epsilon)}{\mathrm{d}t}\Big|_{\epsilon=0}-\delta\mathbf{u}-\mathbf{B}(\mathbf{W},\mathbf{u})-\nabla_{\mathbf{W}}\Delta V\right)\\ &\quad +\langle\mathbf{u},\delta\mathbf{u}+\mathbf{B}(\mathbf{W},\mathbf{u})\rangle+\tau^2\left\langle\frac{\mathrm{D}\mathbf{q}}{\mathrm{d}t},\frac{\mathrm{D}\mathbf{W}}{\mathrm{d}t}\right\rangle\mathrm{d}t.\end{aligned}$$

Integrating by parts and the fact that $\mathbf{W}(0) = \mathbf{W}(T) = 0$, one obtains

$$\int_0^T \boldsymbol{\lambda}_1 \left(\frac{\mathrm{D}\mathbf{W}}{\mathrm{d}t} \right) \mathrm{d}t \;=\; -\int_0^T \frac{\mathrm{D}\boldsymbol{\lambda}_1}{\mathrm{d}t} (\mathbf{W}) \, \mathrm{d}t \tag{C-2.1}$$

and

$$\int_0^T \tau^2 \left\langle \frac{\mathrm{D}\mathbf{q}}{\mathrm{d}t}, \frac{\mathrm{D}\mathbf{W}}{\mathrm{d}t} \right\rangle \mathrm{d}t = -\int_0^T \tau^2 \left\langle \frac{\mathrm{D}^2\mathbf{q}}{\mathrm{d}t^2}, \mathbf{W} \right\rangle \mathrm{d}t. \tag{C-2.2}$$

Let $\mathbf{Y}$ be a vector field along $\mathbf{q}(t, \epsilon)$, then we have the standard property [55]

$$\frac{\mathrm{D}}{\partial \epsilon} \frac{\mathrm{D}}{\partial t} \mathbf{Y} - \frac{\mathrm{D}}{\partial t} \frac{\mathrm{D}}{\partial \epsilon} \mathbf{Y} = \mathbf{R} \left(\frac{\mathrm{D}\mathbf{q}}{\partial \epsilon}, \frac{\mathrm{D}\mathbf{q}}{\partial t} \right) \mathbf{Y}. \tag{C-2.3}$$

Using this property and integrating by parts we have

$$\begin{aligned} \int_0^T \boldsymbol{\lambda}_2 \left(\frac{\mathrm{D}^2\mathbf{v}}{\partial \epsilon \partial t} \right) \mathrm{d}t \;&=\; \int_0^T \boldsymbol{\lambda}_2 \left(\mathbf{R}(\mathbf{W}, \mathbf{v})\mathbf{v} + \frac{\mathrm{D}^2\mathbf{v}}{\partial t \partial \epsilon} \right) \mathrm{d}t \\ &=\; \int_0^T \boldsymbol{\lambda}_2 \left(\mathbf{R}(\mathbf{W}, \mathbf{v})\mathbf{v} \right) - \frac{\mathrm{D}\boldsymbol{\lambda}_2}{\mathrm{d}t} \left(\delta\mathbf{v} + \mathbf{B}(\mathbf{W}, \mathbf{v}) \right) \mathrm{d}t. \end{aligned} \tag{C-2.4}$$

Using equations (C-2.1-C-2.4) and separating expressions involving $\mathbf{W}$, $\delta\mathbf{v}$ and $\delta\mathbf{u}$, we now have

$$\begin{aligned} \left. \frac{\partial \mathcal{J}^\tau}{\partial \epsilon} \right|_{\epsilon=0} \;=\; & \int_0^T \Bigg[-\frac{\mathrm{D}\boldsymbol{\lambda}_1}{\mathrm{d}t} (\mathbf{W}) - \boldsymbol{\lambda}_1 \left(\mathbf{B}(\mathbf{W}, \mathbf{v}) \right) \\ & -\frac{\mathrm{D}\boldsymbol{\lambda}_2}{\mathrm{d}t} \left(\mathbf{B}(\mathbf{W}, \mathbf{v}) \right) + \boldsymbol{\lambda}_2 \left(\mathbf{R}(\mathbf{W}, \mathbf{v})\mathbf{v} \right) - \boldsymbol{\lambda}_2 \left(\mathbf{B}(\mathbf{W}, \mathbf{u}) \right) \\ & -\boldsymbol{\lambda}_2 \left(\nabla_{\mathbf{W}} \Delta V \right) + \langle \mathbf{u}, \mathbf{B}(\mathbf{W}, \mathbf{u}) \rangle - \tau^2 \left\langle \mathbf{W}, \frac{\mathrm{D}^2\mathbf{q}}{\mathrm{d}t^2} \right\rangle \Bigg] \mathrm{d}t \\ & + \int_0^T -\boldsymbol{\lambda}_1 \left(\delta\mathbf{v} \right) - \frac{\mathrm{D}\boldsymbol{\lambda}_2}{\mathrm{d}t} \left(\delta\mathbf{v} \right) \mathrm{d}t + \int_0^T -\boldsymbol{\lambda}_2 \left(\delta\mathbf{u} \right) + \langle \mathbf{u}, \delta\mathbf{u} \rangle \, \mathrm{d}t. \end{aligned} \tag{C-2.5}$$

For an optimal solution, the first order necessary condition is that

$$\left. \frac{\partial \mathcal{J}}{\partial \epsilon} (\mathbf{q}(t, \epsilon), \mathbf{u}(t, \epsilon), t) \right|_{\epsilon=0} = 0 \tag{C-2.6}$$

Using this condition and the fact that $\mathbf{W}$, $\delta\mathbf{u}$ and $\delta\mathbf{v}$ are independent and arbitrary for arbitrary ϵ, the last integral in equation (2.6) implies that $\mathbf{u} = \boldsymbol{\lambda}_2^\sharp$. The second integral and condition (C-2.6) imply that

$$\frac{\mathrm{D}\boldsymbol{\lambda}_2}{\mathrm{d}t} (\mathbf{X}) = -\boldsymbol{\lambda}_1(\mathbf{X}) \tag{C-2.7}$$

for an arbitrary vector field $\mathbf{X}$. $\mathbf{u} = \boldsymbol{\lambda}_2^\sharp$ implies that $\boldsymbol{\lambda}_2 \left(\mathbf{R}(\mathbf{W}, \mathbf{v})\mathbf{v}\right) = \langle \mathbf{u}, \mathbf{R}(\mathbf{W}, \mathbf{v})\mathbf{v} \rangle = \langle \mathbf{W}, \mathbf{R}(\mathbf{u}, \mathbf{v})\mathbf{v} \rangle$, using the standard properties of the curvature tensor [41]. This and the fact that the first integral in equation (2.6) is zero for arbitrary $\mathbf{W}$ imply that

$$\frac{\mathrm{D}\boldsymbol{\lambda}_1}{\mathrm{d}t}(\mathbf{X}) = \left\langle \mathbf{R}(\mathbf{u}, \mathbf{v})\mathbf{v} - \tau^2 \frac{\mathrm{D}\mathbf{v}}{\mathrm{d}t}, \mathbf{X} \right\rangle - \boldsymbol{\lambda}_2 \left(\nabla_{\mathbf{X}} \Delta V\right) \tag{C-2.8}$$

for an arbitrary vector field $\mathbf{X}$. Equations (C-1.1), (C-2.7), (C-2.8) and $\mathbf{u} = \boldsymbol{\lambda}_2^\sharp$ give us the main theorem of this appendix.

Theorem C.2.1. *The extremals of the optimal control problem (C.1.1), without the motion constraints (C-1.6), must necessarily satisfy the following necessary conditions for an arbitrary vector field* $\mathbf{X}$*:*

$$\begin{aligned}
\frac{\mathrm{D}\mathbf{q}}{\mathrm{d}t} &= \mathbf{v} \\
\frac{\mathrm{D}\mathbf{v}}{\mathrm{d}t} &= \boldsymbol{\lambda}_2^\# + \Delta V \\
\frac{\mathrm{D}\boldsymbol{\lambda}_1}{\mathrm{d}t}(\mathbf{X}) &= \left(\mathbf{R}(\mathbf{u}, \mathbf{v})\mathbf{v} - \tau^2 \frac{\mathrm{D}\mathbf{v}}{\mathrm{d}t}\right)^\flat (\mathbf{X}) - \boldsymbol{\lambda}_2 \left(\nabla_{\mathbf{X}} \Delta V\right) \\
\frac{\mathrm{D}\boldsymbol{\lambda}_2}{\mathrm{d}t}(\mathbf{X}) &= -\boldsymbol{\lambda}_1(\mathbf{X}) \\
\mathbf{u} &= \boldsymbol{\lambda}_2^\#,
\end{aligned}$$

where $\mathbf{Y}^\flat$ *denotes the flat operator acting on the vector field* $\mathbf{Y}$*:* $\mathbf{Y}^\flat(\cdot) = \langle \mathbf{Y}, \cdot \rangle$*.*

Remark C.2.1. In the proof for Theorem (C.2.1) we have not taken variations in the multipliers $\boldsymbol{\lambda}_i$, $i = 1, 2$. The reason is that taking variations in these terms results in

$$\begin{aligned}
&\int_0^T \delta\boldsymbol{\lambda}_1 \left(\frac{\mathrm{D}\mathbf{q}}{\mathrm{d}t} - \mathbf{v}\right) + \left(\mathbf{B}(\mathbf{W}, \boldsymbol{\lambda}_1)\right) \left(\frac{\mathrm{D}\mathbf{q}}{\mathrm{d}t} - \mathbf{v}\right) \\
&+\delta\boldsymbol{\lambda}_2 \left(\frac{\mathrm{D}\mathbf{v}}{\mathrm{d}t} - \mathbf{u}\right) + \left(\mathbf{B}(\mathbf{W}, \boldsymbol{\lambda}_2)\right) \left(\frac{\mathrm{D}\mathbf{v}}{\mathrm{d}t} - \mathbf{u} - \Delta_c V\right) \mathrm{d}t
\end{aligned}$$

in addition to terms involving variations of the arguments in the parentheses, which we have used in the proof of the theorem. By the independence of $\delta\boldsymbol{\lambda}_i$, $i = 1, 2$,

their arguments must be zero. This yields the dynamic constraints (C-1.1). Hence, the second and fourth terms in the above expression are zero since the arguments in parentheses are zero. Thus, we omit taking variations of the multipliers though, formally, we should have.

We now derive an alternative form to the above necessary conditions analogous to that obtained in Chapter 5, [40] and [35]. In Section (C.3), we derive this alternate form following a procedure found in in Chapter 5 and in [40], [33] and [55] including the motion constraints (C-1.6).

Theorem C.2.2. *The necessary conditions of Theorem (C.2.1) can equivalently be written as*

$$\left\langle \mathbf{Z}, \frac{\mathrm{D}^3\mathbf{v}}{\mathrm{d}t^3} + \mathbf{R}(\mathbf{u},\mathbf{v})\mathbf{v} - \tau^2\frac{\mathrm{D}\mathbf{v}}{\mathrm{d}t} - \frac{\mathrm{D}^2\Delta V}{\mathrm{d}t^2} \right\rangle = \langle \mathbf{u}, \nabla_{\mathbf{Z}}\Delta V\rangle$$

for any arbitrary vector field $\mathbf{Z}$.

Proof Let $\mathbf{Z}$ be an arbitrary vector field. Then, by the fourth and fifth equations in Theorem (C.2.1) we have:

$$\frac{\mathrm{D}^2\boldsymbol{\lambda}_2}{\mathrm{d}t^2}(\mathbf{Z}) = -\frac{\mathrm{D}\boldsymbol{\lambda}_1}{\mathrm{d}t}(\mathbf{Z}) \quad = \quad \left\langle \mathbf{Z}, -\mathbf{R}(\mathbf{u},\mathbf{v})\mathbf{v} + \tau^2\frac{\mathrm{D}^2\mathbf{q}}{\mathrm{d}t^2} \right\rangle + \langle \mathbf{u}, \nabla_{\mathbf{Z}}\Delta V\rangle \,. \quad \text{(C-2.9)}$$

Since $\mathbf{u} = \boldsymbol{\lambda}_2^\sharp$

$$\frac{\mathrm{D}^2\boldsymbol{\lambda}_2}{\mathrm{d}t^2}(\mathbf{Z}) = \left\langle \mathbf{Z}, \frac{\mathrm{D}^2\mathbf{u}}{\mathrm{d}t^2} \right\rangle = \left\langle \mathbf{Z}, \frac{\mathrm{D}^3\mathbf{v}}{\mathrm{d}t^3} - \frac{\mathrm{D}^2\Delta V}{\mathrm{d}t^2} \right\rangle . \quad \text{(C-2.10)}$$

The statement of the theorem follows immediately from Equations (C-2.9) and (C-2.10).

■

Note here that Theorem (C.2.2) is slightly different from that obtained in Chapter 5 and in [40] in that the control $\mathbf{u}$ appears directly in the equation as opposed to

the acceleration $\frac{\mathrm{D}^2\mathbf{q}}{\mathrm{d}t^2}$. Note also that if we set $\Delta V = 0$, we retrieve the gravity-free necessary conditions appearing in [30, 40]:

$$\frac{\mathrm{D}^3\mathbf{v}}{\mathrm{d}t^3} + \mathbf{R}\left(\frac{\mathrm{D}\mathbf{v}}{\mathrm{d}t}, \mathbf{v}\right)\mathbf{v} - \tau^2\frac{\mathrm{D}\mathbf{v}}{\mathrm{d}t} = 0. \tag{C-2.11}$$

C.3 Motion Constraints

In this section, we briefly re-derive Theorem (C.2.2) following a direct variational procedure as in [40], [33] and [55]. For completeness, we also generalize the result to the case of motion constraints given by equation (C-1.6).

As in [33], define the one forms $\boldsymbol{\omega}_i(\mathbf{Y}) = \langle \mathbf{X}_i, \mathbf{Y}\rangle$ and the two forms $\mathrm{d}\boldsymbol{\omega}_i$, $i = 1, \ldots, l$, where d is the exterior derivative. Defining $\lrcorner$ as the contraction operator, the 1-form $\mathbf{X}\lrcorner\mathrm{d}\boldsymbol{\omega}_i$ satisfies: $\mathbf{X}\lrcorner\mathrm{d}\boldsymbol{\omega}_i(\mathbf{Y}) = \mathrm{d}\boldsymbol{\omega}_i(\mathbf{X}, \mathbf{Y})$. One may define tensors S_i such that $S_{i_\mathbf{q}} : T_\mathbf{q}M \to T_\mathbf{q}M$, by setting $\mathrm{d}\boldsymbol{\omega}_i(\mathbf{X}, \mathbf{Y}) = \langle S_i(\mathbf{X}), \mathbf{Y}\rangle = -\langle S_i(\mathbf{Y}), \mathbf{X}\rangle$.

Augmenting the cost function by the motion constraints

$$\sum_{i=1}^{l} \boldsymbol{\eta}_i \left\langle \frac{\mathrm{D}\mathbf{q}}{\mathrm{d}t}, \mathbf{X}_i(\mathbf{q}) \right\rangle = \sum_{i=1}^{l} \boldsymbol{\eta}_i \boldsymbol{\omega}_i \left(\frac{\mathrm{D}\mathbf{q}}{\mathrm{d}t}\right),$$

the perturbed cost function is given by

$$\mathcal{J}_\epsilon^\tau = \frac{1}{2}\int_0^T \langle \mathbf{u}(t,\epsilon), \mathbf{u}(t,\epsilon)\rangle + \tau^2 \left\langle \frac{\mathrm{D}\boldsymbol{\alpha}}{\partial t}, \frac{\mathrm{D}\boldsymbol{\alpha}}{\partial t} \right\rangle + \sum_{i=1}^{l} \boldsymbol{\eta}_i \left\langle \frac{\mathrm{D}\boldsymbol{\alpha}}{\mathrm{d}t}, \mathbf{X}_i(\boldsymbol{\alpha}) \right\rangle \mathrm{d}t,$$

where $\boldsymbol{\alpha}$ denotes the perturbed trajectory $\mathbf{q}(t,\epsilon)$. Taking variations of the cost function and using the dynamics (C-1.1), we have

$$\begin{aligned}\frac{\partial \mathcal{J}^\tau}{\partial \epsilon} &= \int_0^T \left\langle \mathbf{u}(t,\epsilon), \frac{\mathrm{D}}{\partial\epsilon}\frac{\mathrm{D}^2\boldsymbol{\alpha}}{\partial t^2} \right\rangle - \left\langle \mathbf{u}(t,\epsilon), \frac{\mathrm{D}}{\partial\epsilon}\Delta_{\boldsymbol{\alpha}} V(\boldsymbol{\alpha}) \right\rangle + \tau^2 \left\langle \frac{\mathrm{D}^2\boldsymbol{\alpha}}{\partial\epsilon\partial t}, \frac{\mathrm{D}\boldsymbol{\alpha}}{\partial t} \right\rangle \\ &\quad + \sum_{i=1}^{l} \boldsymbol{\eta}_i \left[\left\langle \frac{\mathrm{D}}{\partial t}\frac{\mathrm{D}\boldsymbol{\alpha}}{\partial\epsilon}, \mathbf{X}_i(\boldsymbol{\alpha}) \right\rangle + \left\langle \frac{\mathrm{D}\boldsymbol{\alpha}}{\partial t}, \frac{\mathrm{D}}{\partial\epsilon}\mathbf{X}_i(\boldsymbol{\alpha}) \right\rangle \right] \mathrm{d}t.\end{aligned}$$

By the identity (C-2.3), we have

$$\begin{aligned}\left.\frac{\partial \mathcal{J}^\tau}{\partial \epsilon}\right|_{\epsilon=0} &= \int_0^T \left\langle \mathbf{u}, \frac{\mathrm{D}^2}{\partial t^2}\mathbf{W} \right\rangle + \langle \mathbf{u}(t), \mathbf{R}\left(\mathbf{W}, \mathbf{v}\right)\mathbf{v}\rangle \\ &\quad - \langle \mathbf{u}(t), \nabla_{\mathbf{W}} \Delta V\rangle + \tau^2 \left\langle \frac{\mathrm{D}^2\boldsymbol{\alpha}}{\partial\epsilon\partial t}, \frac{\mathrm{D}\boldsymbol{\alpha}}{\partial t} \right\rangle \Bigg|_{\epsilon=0} \\ &\quad + \sum_{i=1}^{l} \boldsymbol{\eta}_i \left[\left\langle \frac{\mathrm{D}\mathbf{W}}{\partial t}, \mathbf{X}_i \right\rangle + \left\langle \frac{\mathrm{D}\mathbf{q}}{\partial t}, \nabla_W X_i \right\rangle \right] \mathrm{d}t.\end{aligned}$$

For the first term, we integrate twice by parts and apply boundary conditions (C-1.5) to obtain

$$\int_0^T \left\langle \mathbf{u}, \frac{\mathrm{D}^2\mathbf{W}}{\partial t^2} \right\rangle \mathrm{d}t = \int_0^T \left\langle \frac{\mathrm{D}^2\mathbf{u}}{\mathrm{d}t^2}, \mathbf{W} \right\rangle \mathrm{d}t.$$

For the third term, we use the property $\langle \mathbf{Z}_1, \mathbf{R}(\mathbf{Z}_2, \mathbf{Z}_3)\mathbf{Z}_4\rangle = \langle \mathbf{Z}_2, \mathbf{R}(\mathbf{Z}_1, \mathbf{Z}_4)\mathbf{Z}_3\rangle$ to obtain $\langle \mathbf{u}, \mathbf{R}\left(\mathbf{W}, \mathbf{v}\right)\mathbf{v}\rangle = \langle \mathbf{W}, \mathbf{R}\left(\mathbf{u}, \mathbf{v}\right)\mathbf{v}\rangle$. For the fifth term we integrate by parts once and use the boundary conditions (C-1.5) to obtain

$$\int_0^T \tau^2 \left\langle \frac{\mathrm{D}^2\boldsymbol{\alpha}}{\partial\epsilon\partial t}, \frac{\mathrm{D}\boldsymbol{\alpha}}{\partial t} \right\rangle \mathrm{d}t = -\int_0^T \tau^2 \left\langle \mathbf{W}, \frac{\mathrm{D}^2\mathbf{q}}{\mathrm{d}t^2} \right\rangle \mathrm{d}t.$$

As for the first term under the summation in the cost function, integrate by parts to obtain

$$\int_0^T \sum_{i=1}^{l} \boldsymbol{\eta}_i \left\langle \frac{\mathrm{D}}{\partial t}\frac{\mathrm{D}\boldsymbol{\alpha}}{\partial \epsilon}, \mathbf{X}_i(\boldsymbol{\alpha}) \right\rangle \Bigg|_{\epsilon=0} \mathrm{d}t = -\int_0^T \sum_{i=1}^{l} \frac{\mathrm{d}\boldsymbol{\eta}_i}{\mathrm{d}t} \langle \mathbf{W}, \mathbf{X}_i(\mathbf{q})\rangle + \boldsymbol{\eta}_i \left\langle \mathbf{W}, \frac{\mathrm{D}\mathbf{X}_i(\mathbf{q})}{\mathrm{d}t} \right\rangle \mathrm{d}t.$$

Note that $\boldsymbol{\eta}$ is a scalar function (that is, it is neither a vector or a co-vector field) and, therefore, we are justified in writing $\mathrm{D}\boldsymbol{\eta}/\mathrm{d}t = \mathrm{d}\boldsymbol{\eta}/\mathrm{d}t = \dot{\boldsymbol{\eta}}$. We now study the sum of the second term in this expression and the last term in the integrand. Making use of some of the properties of the Riemannian connection and recalling the definition of the exterior derivative of a one form $\boldsymbol{\omega}$: $\mathrm{d}\boldsymbol{\omega}(\mathbf{X}, \mathbf{Y}) = \mathbf{X}\boldsymbol{\omega}(\mathbf{Y}) - \mathbf{Y}\boldsymbol{\omega}(\mathbf{X}) - \boldsymbol{\omega}\left([\mathbf{X}, \mathbf{Y}]\right)$ for all vector fields $\mathbf{X}$ and $\mathbf{Y}$ on M, then, for the one forms $\boldsymbol{\omega}_i$ such that $\boldsymbol{\omega}_i(\mathbf{W}) = \langle \mathbf{W}, \mathbf{X}_i\rangle$, one has $\mathrm{d}\boldsymbol{\omega}_i\left(\mathbf{X}, \mathbf{Y}\right) = \langle \nabla_{\mathbf{X}}\mathbf{X}_i, \mathbf{Y}\rangle - \langle \nabla_Y X_i, \mathbf{X}\rangle$. Setting $\mathbf{X} = \frac{\mathrm{D}\mathbf{q}}{\mathrm{d}t}$ and

$\mathbf{Y} = \mathbf{W}$, we thus have

$$-\sum_{i=1}^{l} \boldsymbol{\eta}_i \left\langle \mathbf{W}, \frac{\mathrm{D}\mathbf{X}_i(\mathbf{q})}{\mathrm{d}t} \right\rangle \quad + \quad \sum_{i=1}^{l} \boldsymbol{\eta}_i \left\langle \frac{\mathrm{D}\mathbf{q}}{\mathrm{d}t}, \nabla_{\mathbf{W}} \mathbf{X}_i \right\rangle$$
$$= -\sum_{i=1}^{l} \boldsymbol{\eta}_i \mathrm{d}\boldsymbol{\omega}_i \left(\frac{\mathrm{D}\mathbf{q}}{\mathrm{d}t}, \mathbf{W} \right) = -\left\langle \sum_{i=1}^{l} \boldsymbol{\eta}_i S_i \left(\frac{\mathrm{D}\mathbf{q}}{\mathrm{d}t} \right), \mathbf{W} \right\rangle.$$

The above discussion implies that for $\frac{\partial \mathcal{J}^\tau}{\partial \epsilon}\big|_{\epsilon=0}$ to be zero, we must have

$$\left\langle \mathbf{W}, \frac{\mathrm{D}^2\mathbf{u}}{\mathrm{d}t^2} + \mathbf{R}(\mathbf{u}, \mathbf{v})\,\mathbf{v} - \tau^2 \frac{\mathrm{D}^2\mathbf{q}}{\mathrm{d}t^2} - \sum_{i=1}^{l} \left[\dot{\boldsymbol{\eta}}_i X_i + \boldsymbol{\eta}_i S_i \left(\frac{\mathrm{D}\mathbf{q}}{\mathrm{d}t} \right) \right] \right\rangle - \langle \mathbf{u}, \nabla_{\mathbf{W}} \Delta V \rangle = 0.$$

Since $\mathbf{W}$ is an arbitrary vector field, then the following theorem must hold true.

Theorem C.3.1. *A necessary condition for an extremal, $\mathbf{q}(t)$, of the optimal control problem (C.1.1), with the motion constraints (C-1.6), is:*

$$\left\langle \mathbf{Z}, \frac{\mathrm{D}^2\mathbf{u}}{\mathrm{d}t^2} + \mathbf{R}(\mathbf{u}, \mathbf{v})\,\mathbf{v} - \tau^2 \frac{\mathrm{D}\mathbf{v}}{\mathrm{d}t} - \sum_{i=1}^{l} \left[\dot{\boldsymbol{\eta}}_i X_i + \boldsymbol{\eta}_i S_i(\mathbf{v}) \right] \right\rangle = \langle \mathbf{u}, \nabla_{\mathbf{Z}} \Delta V \rangle$$

for any arbitrary vector field $\mathbf{Z}$.

Theorem (C.3.1) is a generalization of results found in [55] and [30] in that a drift vector field is included in the model. We note that, without the motion constraints (C-1.6) the resulting necessary condition is identical to that of Theorem (C.2.2), where $\frac{\mathrm{D}^2\mathbf{u}}{\mathrm{d}t^2} = \frac{\mathrm{D}^3\mathbf{v}}{\mathrm{d}t^3}$.

C.4 Example

As an illustration for the above notions, we consider the execution of a two-spacecraft spiral maneuver as in Chapter 5 and [45].

Here we study the problem in $\mathbb{R}^3$ and treat the spiral constraint as a motion constraint and set M to be a sphere of constant radius ρ. M has dimension equal to 2. Thus, we choose to work with the spherical coordinates θ and ϕ (see Figure

(C.1).) We may now consider the following equations of motion for spacecraft # 2:

$$\ddot{\theta} = u_\theta + f_\theta, \text{ and } \ddot{\phi} = u_\phi + f_\phi, \tag{C-4.1}$$

where u_θ and u_ϕ are the control variables and f_θ and f_ϕ are components of the potential field. We then impose the spiral constraint (C-1.6) in terms of the coordinates θ and ϕ as follows. Let r be the projection of ρ onto the x-y plane: $r = \rho \sin\phi$. The spiral constraint can be expressed in (spherical coordinate) differential form as

$$-k\mathrm{d}\theta + \rho\cos\phi\mathrm{d}\phi = 0, \tag{C-4.2}$$

where k is some constant (see Chapter 6 for further details.)

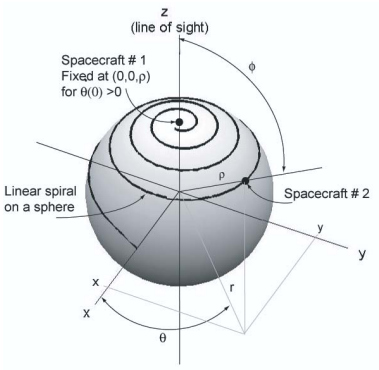

Figure C.1: Variable definition for example.

Let $\mathbf{q} = (\theta, \phi)$. It is desired to solve problem (C.1.1), where we aim at minimizing $\mathcal{J}^\tau$ subject to the *motion* constraint:

$$\langle \mathbf{v}, \mathbf{X}_1(\mathbf{q}) \rangle = 0, \tag{C-4.3}$$

the boundary conditions:

$$\theta(0) = \theta_0,\ \phi(0) = \phi_0,\ \theta(T) = \theta_T, \text{ and } \phi(T) = \phi_T \tag{C-4.4}$$

and the dynamics (C-4.1), where $\mathbf{X}_1(\mathbf{q})$ is given by

$$\mathbf{X}_1 = -k\,(\partial/\partial\theta) + \rho\cos\phi\,(\partial/\partial\phi)$$

and the values of $\theta(0) = \theta_0,\ \phi(0) = \phi_0,\ \theta(T) = \theta_T$, and $\phi(T) = \phi_T$ are defined to satisfy the motion constraint *and* lie on M at times 0 and T. We are only interested in the projection of the motion onto a plane parallel to the x-y plane, where $x = r\cos\theta$ and $y = r\sin\theta$. With spacecraft # 2 moving on one hemisphere, spacecraft # 1 will be fixed at $(0, 0, +\rho)$ or $(0, 0, -\rho)$ if $\dot{\theta}(0) > 0$ or $\dot{\theta}(0) < 0$, respectively.

First, we need to compute the curvature vector field $\mathbf{R}(\mathbf{u}, \mathbf{v})\,\mathbf{v}$ for this problem. Following standard methods for computing the curvature tensor (see, for instance, [59, 60]), one finds that

$$\mathbf{R}(\mathbf{u}, \mathbf{v})\,\mathbf{v} = -u_\theta\dot{\phi}\left(\dot{\theta} - \dot{\phi}\right)\sin^2\phi\,(\partial/\partial\phi)\,.$$

The corresponding differential form for the constraint (C-4.2) is given by $\boldsymbol{\omega}_1 = -k\mathrm{d}\theta + \rho\cos\phi\mathrm{d}\phi$. The two form $\mathrm{d}\boldsymbol{\omega}_1$ is, therefore, $\mathrm{d}\boldsymbol{\omega}_1 = 0$. Since $l = 1$, then set $\eta_1 = \eta$. The second time derivative of u is given by:

$$\frac{\mathrm{D}^2\mathbf{u}}{\mathrm{d}t^2} = \left[\dot{h}_1 + \frac{h_1\dot{\phi} + h_2\dot{\theta}}{\tan\phi}\right]\frac{\partial}{\partial\theta} + \left[\dot{h} - h_1\dot{\theta}\sin\phi\cos\phi\right]\frac{\partial}{\partial\phi},$$

where

$$h_1 = \dot{u}_\theta + \frac{u_\theta\dot{\phi} + u_\phi\dot{\theta}}{\tan\phi} \text{ and } h_2 = \dot{u}_\phi - u_\theta\dot{\theta}\sin\phi\cos\phi.$$

Next, we need to compute the first time derivative of $\mathbf{v}$, which is found to be

$$\frac{\mathrm{D}\mathbf{v}}{\mathrm{d}t} = \left(\ddot{\theta} + \frac{2\dot{\theta}\dot{\phi}}{\tan\phi}\right)\frac{\partial}{\partial\theta} + \left(\ddot{\phi} - \dot{\theta}^2\sin\phi\cos\phi\right)\frac{\partial}{\partial\phi}.$$

Finally, let $\mathbf{Z} = z_\theta\frac{\partial}{\partial\theta} + z_\phi\frac{\partial}{\partial\phi}$ be an arbitrary vector field, where z_θ and z_ϕ are arbitrary scalar functions. Then, after a simple computation we have

$$\begin{aligned}\langle\mathbf{u}, \nabla_{\mathbf{Z}}\Delta V\rangle \;=\; & u_\theta\left[z_\theta\left(\frac{\partial f_\theta}{\partial\theta} + \frac{f_\phi}{\tan\phi}\right) + z_\phi\left(\frac{\partial f_\theta}{\partial\phi} + \frac{f_\theta}{\tan\phi}\right)\right] \\ & + u_\phi\left[z_\theta\left(\frac{\partial f_\phi}{\partial\theta} - f_\theta\sin\phi\cos\phi\right) + z_\phi\frac{\partial f_\phi}{\partial\phi}\right].\end{aligned}$$

We are now in a position to state the necessary condition from Theorem (C.3.1) in coordinate form:

$$\begin{aligned}
0 &= z_\theta\Bigg[- u_\theta \left(\frac{\partial f_\theta}{\partial \theta} + \frac{f_\phi}{\tan\phi} \right) - u_\phi \left(\frac{\partial f_\phi}{\partial \theta} - f_\theta \sin\phi\cos\phi \right) \\
&\quad + \frac{\mathrm{d}h_1}{\mathrm{d}t} + \frac{h_1\dot{\phi} + h_2\dot{\theta}}{\tan\phi} - \tau^2 \left(\ddot{\theta} + \frac{2\dot{\theta}\dot{\theta}}{\tan\phi} \right) + k\dot{\eta} \Bigg] \\
&\quad + z_\phi\Bigg[- u_\theta \left(\frac{\partial f_\theta}{\partial \phi} + \frac{f_\theta}{\tan\phi} \right) - u_\phi \frac{\partial f_\phi}{\partial \phi} + \frac{\mathrm{d}h_2}{\mathrm{d}t} - h_1\dot{\theta}\sin\phi\cos\phi \\
&\quad - u_\theta\dot{\phi}\left(\dot{\theta} - \dot{\phi}\right)\sin^2\phi - \tau^2\left(\ddot{\phi} - \dot{\theta}^2\sin\phi\cos\phi\right) - \rho\cos\phi\dot{\eta} \Bigg].
\end{aligned}$$

However, since z_θ and z_ϕ are arbitrary and independent functions, then their coefficients in the above equation must be zero:

$$\begin{aligned}
\dot{h}_1 &= u_\theta \left(\frac{\partial f_\theta}{\partial \theta} + \frac{f_\phi}{\tan\phi} \right) + u_\phi \left(\frac{\partial f_\phi}{\partial \theta} - f_\theta \sin\phi\cos\phi \right) \\
&\quad - \frac{h_1\dot{\phi} + h_2\dot{\theta}}{\tan\phi} + \tau^2 \left(\ddot{\theta} + \frac{2\dot{\theta}\dot{\theta}}{\tan\phi} \right) - k\dot{\eta} \\
\dot{h}_2 &= u_\theta \left(\frac{\partial f_\theta}{\partial \phi} + \frac{f_\theta}{\tan\phi} \right) + u_\phi \frac{\partial f_\phi}{\partial \phi} + h_1\dot{\theta}\sin\phi\cos\phi \\
&\quad - u_\theta\dot{\phi}\left(\dot{\theta} - \dot{\phi}\right)\sin^2\phi + \tau^2\left(\ddot{\phi} - \dot{\theta}^2\sin\phi\cos\phi\right) + \rho\cos\phi\dot{\eta}.
\end{aligned}$$

These are the necessary conditions for optimality.

One would have obtained the same necessary conditions if one had treated the problem on $\mathbb{R}^3$ with the spiral and spherical constraints imposed on the state (namely, the spherical coordinates.) However, working on the constrained manifold in the coordinate free setting discussed in this appendix is both efficient and easier. For more on this, we refer the reader to the remarks in Chapter 6.

C.5 Conclusion

As an extension to the work done by the authors in Chapter 5, in this appendix we investigate the inclusion of a generalized potential field in the dynamics. This

problem is motivated by two-spacecraft interferometric imaging applications, where the formation is evolving in some generalized potential field. The corresponding necessary conditions are derived and results are re-derived using alternative formalisms.

APPENDIX D

Optimal control of under-actuated systems with application to Lie groups

In this appendix we study a class of optimal control problems know as the τ-elastic variational problem for second order, under-actuated systems. After introducing and stating the problem, we derive the necessary optimality conditions using two approaches. The first approach is purely variational where the resulting necessary conditions are represented by a single fourth order differential equation. In the second approach, we use the Lagrange multiplier technique. In this case, the necessary conditions are represented by a set of four first order differential equations. We show that the two results are equivalent. Finally, we further specialize the result for the compact semi-simple Lie group case and use SO(3) as an example. We also make some remarks on the SE(3) case, which is the subject of current research.

D.1 Introduction

In this appendix we use differential geometric techniques on Riemannian manifolds to obtain necessary conditions for a class of optimal control problems. This class of optimal control problems is known in the mathematical literature as τ-elastic variational problems (see Chapter 5, [55] and [40] and references therein for more on the τ-elastic variational problem.) Interest in the τ-elastic variational problem is

two-fold. The first is pure interest in the mathematical and theoretical implications of this problem as the resulting necessary conditions represent elastic curves that deviate from geodesic curves joining the boundary points.

Secondly, the authors are generally interested in applying the results to multi-spacecraft, especially dual spacecraft, formation flying for imaging applications. As will be seen in the next section, the cost functional in the τ-elastic variational problem is a weighted sum of fuel expenditure and the relative speed between the spacecraft pair. In interferometric imaging, relative speed is inversely proportional to the attained signal-to-noise ratio (see Chapter 2, [5] and [45] and references therein.) Hence, the optimal control problem is suitable for the motion path planning problem of a two-spacecraft formation. Modeling the formation as a pair of fully-actuated point particles has been treated in Chapters 5 and 3, [40] and [38]. One may also model the two-spacecraft as a pair of rigid bodies evolving in three-dimensional space and, hence, as a system in SE(3)$\times$ SE(3) (two copies of the three-dimensional special Euclidean group.) This however is a much harder problem and is subject to current investigation.

We focus our attention on the case where the system is under-actuated, that is, when the control vector spans a subspace of the tangent space at a point on the manifold. Optimal kinematic control problems on Riemannian manifolds with under-actuated systems are known in the literature as the sub-Riemannian optimal control problem ([99].) In [99], the authors study a restricted version of the cost functional we consider in this appendix (setting $\tau = 0$.) Moreover, the authors in that paper consider systems satisfying first order (that is, kinematic) differential equations. We, on the other hand, study second order (dynamic) systems.

Here is how the appendix is organized. In Section (D.2), we state the problem and

describe it in more detail. In Section (D.3), we provide some preliminary definitions, facts and lemmas. In Section (D.4), we derive the necessary conditions for the general problem. This is done following two approaches where one results in a single fourth order differential equation and the second in four first order differential equations as necessary conditions. We show that these results are indeed equivalent. In Section (D.5), we specialize the result to the compact semi-simple Lie group case, where we relate current results to those obtain previously in the literature. We use the SO(3) Lie group case as an example. We conclude the appendix with a summary and final remarks on future research in Section (D.6).

D.2 Problem Statement

In this appendix we consider systems that satisfy dynamics of the form:

$$\begin{aligned} \frac{\mathrm{D}\mathbf{q}}{\mathrm{d}t}(t) &= \frac{\mathrm{d}\mathbf{q}}{\mathrm{d}t}(t) = \mathbf{v}(t) \\ \frac{\mathrm{D}\mathbf{v}}{\mathrm{d}t}(t) &= \mathbf{u}(t), \end{aligned} \tag{D-2.1}$$

where we now view $\mathbf{q} : [0, T] \to M$ as a curve on M, $\mathbf{v}(t) \in T_{\mathbf{q}(t)}M$ and $\mathbf{u}(t) \in TT_{\mathbf{q}(t)}M$. In this appendix, we are interested in the situation where $\mathbf{u}(t)$ be given by

$$\mathbf{u}(t) = \sum_{i=1}^{m} u_i(t)\mathbf{X}_i(\mathbf{q}(t)), \tag{D-2.2}$$

where $m < n$. Thus, we have:

$$\langle \mathbf{u}(t), \mathbf{u}(t) \rangle = \sum_{i=1}^{m} u_i^2(t). \tag{D-2.3}$$

$m = n$ corresponds to the fully actuated system, whereas $m < n$ corresponds to the under-actuated system. Different versions of the the optimal control problem with $m = n$ have been treated in the past. See, for example, [30], [33], [35], [35] and [38, 43, 40]. The case where $m < n$ has been treated in [98] and [99] for kinematic

systems. In Section (D.1), we briefly described how our present work differs from that in [99]. We now state the optimal control problem.

Problem D.2.1. *Find critical values of*

$$\mathcal{J}^{\tau}(\mathbf{q}) = \frac{1}{2}\int_0^T \left[\langle \mathbf{u}, \mathbf{u}\rangle + \tau^2 \langle \mathbf{v}, \mathbf{v}\rangle\right] \mathrm{d}t, \tag{D-2.4}$$

over the set Ω *of* $\mathcal{C}^1$*-paths* $\mathbf{q}$ *on* M*, satisfying*

- *the* dynamic constraints *(D-2.1),*
- $\mathbf{q}(t)$ *is smooth for all* $t \in [0, T]$*,*
- boundary conditions

$$\begin{aligned} \mathbf{q}(0) &= \mathbf{q}_0 \quad \mathbf{q}(T) = \mathbf{q}_T \\ \mathbf{v}(0) &= \mathbf{v}_0 \quad \mathbf{v}(T) = \mathbf{v}_T, \end{aligned} \tag{D-2.5}$$

- *and the* motion constraints

$$\left\langle \frac{\mathrm{D}\mathbf{q}}{\mathrm{d}t}, \mathbf{X}_i(\mathbf{q}) \right\rangle = k_i, \ i = 1, \ldots, l \ (l < n) \tag{D-2.6}$$

for $\mathbf{X}_i, \ i = 1, \ldots, n$*, linearly independent vector fields in some neighborhood of* $\mathbf{q}(t)$ *and given constants* $k_i, \ i = 1, \ldots, l$*.*

The above cost function is still motivated by optimal path planning for dual spacecraft interferometric imaging formations. The results presented in Section (D.4) are general enough to be applied to the multi-spacecraft interferometric imaging problem, where the formation can be treated as either a set of two point particles or two bodies. In the latter case, the formation evolves on SE(3), which is a non-compact Lie group and is subject of current research.

The compact Lie group case is also of interest in that many previous results (e.g., [99]) study the optimal control problem for Lie groups. It would be interesting

and instructive to compare our current generalized results with those appearing in previous literature. We do this in Section (D.5).

We may ignore the motion constraints (D-2.6). As shown in Chapter 5, these constraints are automatically appended to the final expression for the necessary conditions corresponding to the unconstrained problem. Here, again, once the necessary conditions are obtained for systems with a potential field, the motion constraints are simply appended to the necessary conditions.

D.3 Preliminaries

For basic notation and definitions, refer to Appendix A. In addition the results found in Appendix A, we also need the following lemma.

Lemma D.3.1. *Let* $\mathbf{Z}$ *be an arbitrary vector,* $\mathbf{W}$ *be a variational vector field and* $\mathbf{v}$ *be the velocity vector field. Then, we have*

$$\mathbf{Z}\left(\langle \mathbf{v}, \mathbf{W} \rangle\right) = 0.$$

Proof In local coordinates, let $\mathbf{Z} = \sum_{k=1}^{n} \zeta_k \partial_k$, $\mathbf{v} = \sum_{i=1}^{n} v_i \partial_i$ and $\mathbf{W} = \sum_{j=1}^{n} w_j \partial_j$. Note that $w_j = \frac{\partial}{\partial \epsilon} q_j(t, \epsilon)$. Then we have:

$$\begin{aligned} \mathbf{Z}\left(\langle \mathbf{v}, \mathbf{W} \rangle\right) &= \sum_{k=1}^{n} \zeta_k \frac{\partial}{\partial q_k} \left(\sum_{i=1}^{n} v_i \frac{\partial q_i}{\partial \epsilon} \right) \\ &= \sum_{k=1}^{n} \zeta_k \sum_{i=1}^{n} v_i \frac{\partial^2 q_i}{\partial q_k \partial \epsilon} \\ &= 0, \end{aligned}$$

where $\frac{\partial^2}{\partial q_k \partial \epsilon} q_i(t, \epsilon) = \frac{\partial^2}{\partial \epsilon \partial q_k} q_i(t, \epsilon) = \frac{\partial}{\partial \epsilon} \delta_{ik} = 0$ and $\frac{\partial v_i}{\partial q_k} = 0$ since the components of the velocity vector field $\mathbf{v}$ are independent of the local coordinates $q_1, \ldots, q_n$.

■

Lemma D.3.2. *Let* $\mathbf{Z}$ *be an arbitrary vector,* $\mathbf{W}$ *be a variational vector field,* $\mathbf{v}$ *be the velocity vector field and* $\mathbf{u} = \frac{\mathrm{D}\mathbf{v}}{\mathrm{d}t}$ *be the control vector field. Then, we have*

$$\mathbf{Z}\left(\langle \mathbf{u}, \mathbf{W} \rangle\right) = 0.$$

Proof of Lemma (D.3.2) is analogous to that of Lemma (D.3.1). Lemmas (D.3.1) and (D.3.2) and the identity

$$\mathbf{X}\left(\langle \mathbf{Y}, \mathbf{Z} \rangle\right) = \langle \nabla_{\mathbf{X}} \mathbf{Y}, \mathbf{Z} \rangle + \langle \mathbf{Y}, \nabla_{\mathbf{X}} \mathbf{Z} \rangle$$

for arbitrary vector fields $\mathbf{X}$, $\mathbf{Y}$ and $\mathbf{Z}$, imply

$$\langle \mathbf{v}, \nabla_{\mathbf{Z}} \mathbf{W} \rangle = -\langle \nabla_{\mathbf{Z}} \mathbf{v}, \mathbf{W} \rangle \tag{D-3.1}$$

and

$$\langle \mathbf{u}, \nabla_{\mathbf{Z}} \mathbf{W} \rangle = -\langle \nabla_{\mathbf{Z}} \mathbf{u}, \mathbf{W} \rangle . \tag{D-3.2}$$

D.4 Necessary Conditions for Optimality

In this section we first pursue a purely variational approach in deriving the necessary conditions for the problem (D.2.1) without the motion constraints (D-2.6). That is, Lagrange multipliers will not be introduced to the Lagrangian. This purely variational approach is used to derive necessary conditions in Chapter 5, [40], [99] and [33]. However, to take into account the constraint that the control vector field $\mathbf{u}$ only spans a subspace of the tangent space to M at some point $\mathbf{q} \in M$, the following vector field will be introduced:

$$\mathbf{Z}_t = \sum_{k=m+1}^{n} \zeta_k(t) \mathbf{X}_k$$

such that

$$\left\langle \mathbf{X}_k, \frac{\mathrm{D}\mathbf{v}}{\mathrm{d}t} \right\rangle = \langle \mathbf{X}_k, \mathbf{u} \rangle = 0, \;\; k = m+1, \ldots, n \tag{D-4.1}$$

and

$$\langle \mathbf{Z}_t, \mathbf{u} \rangle = 0. \tag{D-4.2}$$

We will drop the subscript t in $\mathbf{Z}_t$ to become $\mathbf{Z}$.

Appending the cost function by the term (D-4.2), one obtains:

$$\mathcal{J}^\tau = \int_0^T \frac{1}{2} \langle \mathbf{u}, \mathbf{u} \rangle + \frac{\tau^2}{2} \langle \mathbf{v}, \mathbf{v} \rangle + \langle \mathbf{Z}, \mathbf{u} \rangle \, \mathrm{d}t. \tag{D-4.3}$$

A control vector $\mathbf{u}$ solves

$$\min_{\mathbf{u}} \mathcal{J}^\tau (\mathbf{q}, \mathbf{v}, \mathbf{u}) \tag{D-4.4}$$

only if

$$\frac{\partial}{\partial \epsilon} \mathcal{J}^\tau (\mathbf{q}_\epsilon(t,\epsilon), \mathbf{v}_\epsilon(t,\epsilon), \mathbf{u}_\epsilon(t,\epsilon)) \Big|_\epsilon = 0, \tag{D-4.5}$$

where $\mathbf{v}_\epsilon(t,\epsilon)$ and $\mathbf{u}_\epsilon(t,\epsilon)$ are defined analogous to $\mathbf{q}_\epsilon(t,\epsilon)$ in the previous section. Replacing $\mathbf{u}$ with $\nabla_{\mathbf{v}}\mathbf{v}$ in Equation (D-4.3) and taking variations with respect to ϵ, one obtains:

$$\frac{\partial \mathcal{J}^\tau}{\partial \epsilon}\Big|_{\epsilon=0} = \int_0^T \left[\left\langle \frac{\mathrm{D}\mathbf{v}}{\partial t}, \frac{\mathrm{D}^2 \mathbf{v}_\epsilon}{\partial \epsilon \partial t} \right\rangle + \tau^2 \left\langle \mathbf{v}, \frac{\mathrm{D}\mathbf{v}_\epsilon}{\partial \epsilon} \right\rangle + \left\langle \frac{\mathrm{D}\mathbf{Z}}{\partial \epsilon}, \mathbf{u}_\epsilon \right\rangle + \left\langle \mathbf{Z}, \frac{\mathrm{D}^2 \mathbf{v}_\epsilon}{\partial \epsilon \partial t} \right\rangle \right]_{\epsilon=0} \mathrm{d}t.$$

We now set $\frac{\partial \mathbf{q}_\epsilon}{\partial \epsilon}\big|_{\epsilon=0} = \mathbf{W}$, use Facts (A.4.1) and (A.4.2) and the standard connection ∇ property $\frac{\mathrm{D}\mathbf{Z}}{\mathrm{d}\epsilon} = \nabla_{\mathbf{W}}\mathbf{Z} = \nabla_{\mathbf{Z}}\mathbf{W} + [\mathbf{W}, \mathbf{Z}]$ such that the right hand side of the above equation becomes

$$\int_0^T \left\langle \frac{\mathrm{D}\mathbf{v}}{\partial t} + \mathbf{Z}, \mathbf{R}(\mathbf{W}, \mathbf{v})\mathbf{v} + \frac{\mathrm{D}}{\partial t}\frac{\mathrm{D}\mathbf{v}}{\partial \epsilon} \right\rangle + \tau^2 \left\langle \mathbf{v}, \frac{\mathrm{D}}{\partial t}\mathbf{W} \right\rangle + \langle \nabla_{\mathbf{Z}}\mathbf{W} + [\mathbf{W}, \mathbf{Z}], \mathbf{u} \rangle \, \mathrm{d}t.$$

Using Fact (A.2.3) for the curvature in the first term, integrating the τ^2 term by parts and applying Lemma (D.3.2) (and the remarks thereafter) to the last term in the integrand we obtain

$$\begin{aligned} &\int_0^T \left\langle \mathbf{W}, \mathbf{R}\left(\frac{\mathrm{D}\mathbf{v}}{\partial t} + \mathbf{Z}, \mathbf{v}\right)\mathbf{v} \right\rangle + \left\langle \frac{\mathrm{D}\mathbf{v}}{\partial t} + \mathbf{Z}, \frac{\mathrm{D}}{\partial t}\frac{\mathrm{D}}{\partial t}\mathbf{W} \right\rangle - \tau^2 \left\langle \frac{\mathrm{D}\mathbf{v}}{\partial t}, \mathbf{W} \right\rangle \\ &+\mathbf{Z}\left(\left\langle \mathbf{W}, \frac{\mathrm{D}\mathbf{v}}{\partial t} \right\rangle \right) - \left\langle \mathbf{W}, \nabla_{\mathbf{Z}}\frac{\mathrm{D}\mathbf{v}}{\partial t} \right\rangle + \langle -[\mathbf{Z}, \mathbf{W}], \mathbf{u} \rangle \, \mathrm{d}t. \end{aligned}$$

Recall that the Lie bracket is skew-symmetric: $[\mathbf{W}, \mathbf{Z}] = -[\mathbf{Z}, \mathbf{W}]$ and that

$$\mathcal{L}_{\mathbf{Z}} \left\langle \mathbf{W}, \frac{\mathrm{D}}{\partial t}\mathbf{v} \right\rangle = \langle \mathcal{L}_{\mathbf{Z}}\mathbf{W}, \mathbf{u}\rangle + \langle \mathbf{W}, \mathcal{L}_{\mathbf{Z}}\mathbf{u}\rangle .$$

Observe, however, that

$$\mathcal{L}_{\mathbf{Z}} (\langle \mathbf{W}, \mathbf{u}\rangle) = \mathbf{Z} (\langle \mathbf{W}, \mathbf{u}\rangle) = 0$$

by Lemma (D.3.2). Hence, we have $\langle [\mathbf{Z}, \mathbf{W}], \mathbf{u}\rangle = \langle \mathcal{L}_{\mathbf{Z}}\mathbf{W}, \mathbf{u}\rangle = -\langle \mathbf{W}, \mathcal{L}_{\mathbf{Z}}\mathbf{u}\rangle$. From this and the integration of the second inner product in the integrand twice by parts, we obtain

$$\int_0^T \langle \mathbf{W}, \mathbf{R}(\mathbf{u}+\mathbf{Z}, \mathbf{v})\,\mathbf{v}\rangle + \left\langle \nabla^3_{\mathbf{v}}\mathbf{v} + \nabla^2_{\mathbf{v}}\mathbf{Z}, \mathbf{W} \right\rangle - \tau^2 \left\langle \frac{\mathrm{D}\mathbf{v}}{\partial t}, \mathbf{W} \right\rangle$$
$$- \langle \mathbf{W}, \nabla_{\mathbf{Z}}\mathbf{u}\rangle + \langle \mathbf{W}, \mathcal{L}_{\mathbf{Z}}\mathbf{u}\rangle \,\mathrm{d}t.$$

Collecting terms, we finally obtain

$$\left.\frac{\partial \mathcal{J}^\tau}{\partial \epsilon}\right|_{\epsilon=0} = \int_0^T \left\langle \mathbf{W}, \mathbf{R}(\mathbf{u}+\mathbf{Z}, \mathbf{v})\,\mathbf{v} + \nabla^3_{\mathbf{v}}\mathbf{v} + \nabla^2_{\mathbf{v}}\mathbf{Z} \right.$$
$$\left. -\tau^2 \frac{\mathrm{D}\mathbf{v}}{\partial t} - \nabla_{\mathbf{Z}}\mathbf{u} + [\mathbf{Z}, \mathbf{u}] \right\rangle \mathrm{d}t. \qquad \text{(D-4.6)}$$

In obtaining Equation (D-4.6), repeated use has been made of the integration by parts identity, for example,

$$\int_0^T \left\langle \frac{\mathrm{D}}{\partial t}\mathbf{W}, \frac{\mathrm{D}\mathbf{v}}{\partial t} \right\rangle = -\int_0^T \left\langle \mathbf{W}, \frac{\mathrm{D}}{\partial t}\frac{\mathrm{D}\mathbf{v}}{\partial t} \right\rangle \mathrm{d}t,$$

and the fact that the variational vector field $\mathbf{W}$ is fixed at the boundary points 0 and T.

Since $\mathbf{W}$ is an arbitrary variational vector field, the condition (D-4.5) and Equation (D-4.6) immediately result in the main theorem of this appendix.

Theorem D.4.1. *A necessary condition for a control law* $\mathbf{u}(t)$ *to be an optimal solution for the problem (D.2.1) without the motion constraints (D-2.6), is that it satisfies the differential equation:*

$$\frac{\mathrm{D}^2\mathbf{u}}{\mathrm{d}t^2} + \mathbf{R}\left(\mathbf{u}+\mathbf{Z},\mathbf{v}\right)\mathbf{v} + \frac{\mathrm{D}^2\mathbf{Z}}{\mathrm{d}t^2} - \tau^2\mathbf{u} - \nabla_{\mathbf{Z}}\mathbf{u} + [\mathbf{Z},\mathbf{u}] = 0$$

and the condition (D-4.2).

It can be easily checked that this result reduces to previously published results in the literature. For example, if $m = n$, one can set $\mathbf{Z} = 0$ in the above theorem to obtain the necessary conditions for the fully actuated τ-elastic variational problem (see Chapter 5, [40] and [33].)

We now derive the necessary conditions following the Lagrange multiplier approach and show that these are equivalent to those obtained in Theorem (D.4.1).

First, we define a bilinear form $\mathbf{B}\left(\cdot,\cdot\right)$ that, for any vector field $\mathbf{Y} = \sum_{i=1}^{n} y_i\mathbf{X}_i$, satisfies:

$$\begin{aligned}\nabla_{\mathbf{v}}\mathbf{Y} &= \dot{\mathbf{Y}} + \mathbf{B}\left(\mathbf{v},\mathbf{Y}\right)\\ \nabla_{\mathbf{W}}\mathbf{Y} &= \delta\mathbf{Y} + \mathbf{B}\left(\mathbf{W},\mathbf{Y}\right),\end{aligned}$$

where $\dot{\mathbf{Y}} = \sum_{i=1}^{n} \dot{y}_i\mathbf{X}_i$, $\delta\mathbf{Y} = \sum_{i=1}^{n} \frac{\partial y_i}{\partial\epsilon}\mathbf{X}_i$, $\mathbf{B}\left(\mathbf{v},\mathbf{Y}\right) = \sum_{i,j,k=1}^{n} v_i y_j \Gamma_{ij}^{k}\mathbf{X}_k$, $\mathbf{B}\left(\mathbf{W},\mathbf{Y}\right) = \sum_{i,j,k=1}^{n} w_i y_j \Gamma_{ij}^{k}\mathbf{X}_k$, and $\mathbf{W} = \sum_{i=1}^{n} w_i\mathbf{X}_i = \sum_{i=1}^{n} \frac{\partial q_{\epsilon_i}}{\partial\epsilon}\mathbf{X}_i$ is the variation vector field corresponding to the curve $\mathbf{q}(t)$. $\mathbf{B}(\mathbf{W},\cdot)$ is introduced in order to be able to separate variations in the components of a vector field, $\delta\mathbf{Y}$, from variations in the basis vector fields, which are contained in $\mathbf{B}\left(\mathbf{W},\mathbf{Y}\right)$. It is important to separate these terms since the variations $\delta\mathbf{Y}$ are independent from $\mathbf{W}$. This is true especially when $\mathbf{Y} = \mathbf{v}$ or $\mathbf{u}$. As for $\mathbf{B}\left(\mathbf{v},\cdot\right)$, introducing this notation will be appreciated in the next section when we treat the Lie group case.

We append the Lagrangian in Equation (D-2.4) with the dynamics (D-2.1) and the constraints (D-4.1) to obtain

$$\mathcal{J}^\tau = \int_0^T \frac{1}{2}\langle \mathbf{u}, \mathbf{u}\rangle + \frac{\tau^2}{2}\langle \mathbf{v}, \mathbf{v}\rangle + \boldsymbol{\lambda}_1\left(\frac{\mathrm{d}\mathbf{q}}{\mathrm{d}t} - \mathbf{v}\right) + \boldsymbol{\lambda}_2\left(\frac{\mathrm{D}\mathbf{v}}{\mathrm{d}t} - \mathbf{u}\right) + \left\langle \mathbf{Z}, \frac{\mathrm{D}\mathbf{v}}{\mathrm{d}t}\right\rangle \mathrm{d}t. \tag{D-4.7}$$

Taking variations of this expression, one obtains

$$\begin{aligned}\frac{\partial \mathcal{J}^\tau}{\partial \epsilon} &= \int_0^T \langle \mathbf{u}, \delta\mathbf{u} + \mathbf{B}(\mathbf{W}, \mathbf{u})\rangle + \tau^2 \langle \mathbf{v}, \delta\mathbf{v} + \mathbf{B}(\mathbf{W}, \mathbf{v})\rangle \\ &\quad + \boldsymbol{\lambda}_1\left(\frac{\mathrm{D}\mathbf{W}}{\mathrm{d}t} - \delta\mathbf{v} - \mathbf{B}(\mathbf{W}, \mathbf{v})\right) + \boldsymbol{\lambda}_2\left(\frac{\mathrm{D}^2\mathbf{v}}{\partial\epsilon\partial t} - \delta\mathbf{u} - \mathbf{B}(\mathbf{W}, \mathbf{u})\right) \\ &\quad + \langle \nabla_{\mathbf{W}}\mathbf{Z}, \mathbf{u}\rangle + \langle \mathbf{Z}, \delta\mathbf{u} + \mathbf{B}(\mathbf{W}, \mathbf{u})\rangle \,\mathrm{d}t. \end{aligned} \tag{D-4.8}$$

Now, note that

$$\begin{aligned}\int_0^T \boldsymbol{\lambda}_1\left(\frac{\mathrm{D}\mathbf{W}}{\mathrm{d}t}\right)\mathrm{d}t &= -\int_0^T \frac{\mathrm{D}\boldsymbol{\lambda}_1}{\mathrm{d}t}(\mathbf{W})\,\mathrm{d}t, \\ \int_0^T \boldsymbol{\lambda}_2\left(\frac{\mathrm{D}^2\mathbf{v}}{\partial\epsilon\partial t}\right)\mathrm{d}t &= \int_0^T \boldsymbol{\lambda}_2\left(\frac{\mathrm{D}^2\mathbf{v}}{\partial t\partial\epsilon} + \mathbf{R}(\mathbf{W}, \mathbf{v})\,\mathbf{v}\right) \\ &= \int_0^T -\frac{\mathrm{D}\boldsymbol{\lambda}_2}{\mathrm{d}t}(\delta\mathbf{v} + \mathbf{B}(\mathbf{W}, \mathbf{u})) + \boldsymbol{\lambda}_2(\mathbf{R}(\mathbf{W}, \mathbf{v})\,\mathbf{v})\,\mathrm{d}t \\ \langle \nabla_{\mathbf{W}}\mathbf{Z}, \mathbf{u}\rangle &= \langle \nabla_{\mathbf{Z}}\mathbf{W} + [\mathbf{W}, \mathbf{Z}], \mathbf{u}\rangle = -\langle \mathbf{W}, \nabla_{\mathbf{Z}}\mathbf{u}\rangle + \langle \mathbf{W}, [\mathbf{Z}, \mathbf{u}]\rangle. \end{aligned}$$

Hence, we have

$$\begin{aligned}\frac{\partial \mathcal{J}^\tau}{\partial \epsilon} &= \int_0^T \langle \mathbf{u} + \mathbf{Z}, \delta\mathbf{u}\rangle - \boldsymbol{\lambda}_2(\delta\mathbf{u})\,\mathrm{d}t + \int_0^T \tau^2\langle \mathbf{v}, \delta\mathbf{v}\rangle - \boldsymbol{\lambda}_1(\delta\mathbf{v}) - \frac{\mathrm{D}\boldsymbol{\lambda}_2}{\mathrm{d}t}(\delta\mathbf{v}) + \langle \mathbf{u}, \delta\mathbf{u}\rangle \\ &\quad + \tau^2\langle \mathbf{v}, \mathbf{B}(\mathbf{W}, \mathbf{v})\rangle - \boldsymbol{\lambda}_1(\mathbf{B}(\mathbf{W}, \mathbf{v})) - \boldsymbol{\lambda}_2(\mathbf{B}(\mathbf{W}, \mathbf{u})) + \langle \mathbf{Z}, \mathbf{B}(\mathbf{W}, \mathbf{u})\rangle \\ &\quad - \frac{\mathrm{D}\boldsymbol{\lambda}_2}{\mathrm{d}t}(\delta\mathbf{v}) + \langle \mathbf{W}, [\mathbf{Z}, \mathbf{u}]\rangle - \frac{\mathrm{D}\boldsymbol{\lambda}_1}{\mathrm{d}t}(\mathbf{W}) - \langle \mathbf{W}, \nabla_{\mathbf{Z}}\mathbf{u} + \mathbf{R}(\mathbf{u} + \mathbf{Z}, \mathbf{v})\,\mathbf{v}\rangle\,\mathrm{d}t. \end{aligned}$$

By the independence of $\mathbf{W}$, $\delta\mathbf{v}$ and $\delta\mathbf{u}$, we have the following theorem.

Theorem D.4.2. *A necessary condition for a control law $\mathbf{u}(t)$ to be an optimal solution for the problem (D.2.1) without the motion constraints (D-2.6), is that the*

first order differential equations:

$$\begin{aligned}
\frac{\mathrm{d}\mathbf{q}}{\mathrm{d}t} &= \mathbf{v} \\
\frac{\mathrm{D}\mathbf{v}}{\mathrm{d}t} &= \mathbf{u} \\
\frac{\mathrm{D}\boldsymbol{\lambda}_1}{\mathrm{d}t} &= \left([\mathbf{Z},\mathbf{u}] - \nabla_{\mathbf{Z}}\mathbf{u} + \mathbf{R}(\mathbf{u}+\mathbf{Z},\mathbf{V})\mathbf{v}\right)^{\flat} \\
\frac{\mathrm{D}\boldsymbol{\lambda}_2}{\mathrm{d}t} &= -\boldsymbol{\lambda}_1 + \tau^2\left(\mathbf{v}\right)^{\flat} \\
\mathbf{u}+\mathbf{Z} &= \boldsymbol{\lambda}_2^{\sharp} \\
\langle \mathbf{Z},\mathbf{u}\rangle &= 0
\end{aligned}$$

be satisfied on $[0,T]$.

In Theorem (D.4.2), $\sharp$ and $\flat$ denote the sharp and flat operators (see [42] for definitions.) In the above, the Lagrange multipliers $\boldsymbol{\lambda}_i$, $i = 1,2$, are viewed as elements in the cotangent space T^*M.

We now show that the necessary conditions from Theorem (D.4.2) are equivalent to those of Theorem (D.4.1). First note that for an arbitrary vector field $\mathbf{Y}$, Theorem (D.4.2) implies that

$$\frac{\mathrm{D}^2\boldsymbol{\lambda}_2}{\mathrm{d}t^2}(\mathbf{Y}) = \left\langle \frac{\mathrm{D}^2(\mathbf{u}+\mathbf{Z})}{\mathrm{d}t^2}, \mathbf{Y} \right\rangle.$$

and that

$$\begin{aligned}
\frac{\mathrm{D}^2\boldsymbol{\lambda}_2}{\mathrm{d}t^2}(\mathbf{Y}) &= -\frac{\mathrm{D}\boldsymbol{\lambda}_1}{\mathrm{d}t}(\mathbf{Y}) + \tau^2\langle \mathbf{v},\mathbf{Y}\rangle \\
&= \left\langle -[\mathbf{Z},\mathbf{u}] + \nabla_{\mathbf{Z}}\mathbf{u} - \mathbf{R}(\mathbf{u}+\mathbf{Z},\mathbf{V})\mathbf{v} + \tau^2\mathbf{v},\mathbf{Y}\right\rangle.
\end{aligned}$$

Equating these two expressions immediately result in the fourth order necessary condition given in Theorem (D.4.1). Hence, we have the following Lemma.

Lemma D.4.1. *The necessary conditions of Theorem (D.4.2) are equivalent to those of Theorem (D.4.1).*

D.5 Optimal Control on Compact Semi-Simple Lie Groups

In this section we derive the necessary conditions from Theorem (D.4.1) where the manifold M is a compact semi-simple Lie group G. Let $\mathfrak{g}$ denote the Lie algebra of G and define the metric such that $\ll \cdot, \cdot \gg: -\frac{1}{2}\kappa(\cdot, \cdot)$, where κ denotes the Killing form on $\mathfrak{g}$. Recall that for semi-simple Lie groups, the Killing form is non-degenerate.

Let $J : \mathfrak{g} \to \mathfrak{g}$ be a positive definite linear mapping (the inertia tensor) that satisfies:

$$\begin{aligned} \ll J\mathbf{X}, \mathbf{Y} \gg &= \ll \mathbf{X}, J\mathbf{Y} \gg \\ \ll J\mathbf{X}, \mathbf{X} \gg &= 0 \text{ if and only if } \mathbf{X} = 0. \end{aligned}$$

Let $R_{\mathbf{g}}$ denote the right translation on G by $\mathbf{g} \in G$. If $\mathbf{X}, \mathbf{Y} \in \mathfrak{g}$, then the corresponding right invariant vector fields are given by $\mathbf{X}^r_{\mathbf{g}} = \mathbf{X}^r(\mathbf{g}) = R_{\mathbf{g}^*}\mathbf{X}$ and $\mathbf{Y}^r_{\mathbf{g}} = \mathbf{Y}^r(\mathbf{g}) = R_{\mathbf{g}^*}\mathbf{Y}$, respectively. Hence a right invariant metric on G may be defined as

$$\langle \mathbf{X}^r(\mathbf{g}), \mathbf{Y}^r(\mathbf{g}) \rangle := \ll \mathbf{X}, J\mathbf{Y} \gg . \tag{D-5.1}$$

Corresponding to this metric there exists a unique Riemannian connection ∇, which, in turn, defines the bilinear form:

$$(\mathbf{X}, \mathbf{Y}) \to \mathbf{B}(\mathbf{X}, \mathbf{Y}) = \frac{1}{2}\big\{ [\mathbf{X}, \mathbf{Y}] + J^{-1}[\mathbf{X}, J\mathbf{Y}] + J^{-1}[\mathbf{Y}, J\mathbf{X}] \big\}, \tag{D-5.2}$$

for any $\mathbf{X},\ \mathbf{Y} \in \mathfrak{g}$. If J were the identity, then $\mathbf{B}(\mathbf{X}, \mathbf{Y}) = \frac{1}{2}[\mathbf{X}, \mathbf{Y}]$. In this appendix we make the simplifying assumption $J = I$ is the identity. The reason for doing this is that the derivation becomes very cumbersome and lengthy in the general case, which will be the focus of future work. We will drop the superscript r for right invariant vector fields in the rest of the appendix.

With $\dot{\mathbf{q}} = \mathbf{v} = \sum_{i=1}^{n} v_i \mathbf{X}_i$, then we have:

$$\begin{aligned}
\frac{\mathrm{D}\mathbf{v}}{\mathrm{d}t} &= \sum_{i=1}^{n} \dot{v}_i \mathbf{X}_i + \sum_{i,j=1}^{n} \frac{1}{2} v_i v_j [\mathbf{X}_i, \mathbf{X}_j] = \sum_{i=1}^{m} \dot{v}_i \mathbf{X}_i \\
\frac{\mathrm{D}^2\mathbf{v}}{\mathrm{d}t^2} &= \sum_{i=1}^{n} \ddot{v}_i \mathbf{X}_i + \frac{1}{2} \sum_{j,k=1}^{n} v_i \dot{v}_k \left[\mathbf{X}_i, \mathbf{X}_k\right] \\
\frac{\mathrm{D}^3\mathbf{v}}{\mathrm{d}t^3} &= \sum_{i=1}^{n} \dddot{v}_i \mathbf{X}_i + \sum_{i,j=1}^{n} \ddot{v}_i v_j \left[\mathbf{X}_j, \mathbf{X}_j\right] \\
&\quad + \frac{1}{4} \sum_{i,j,k=1}^{n} v_i \dot{v}_j v_k \left[\mathbf{X}_k, \left[\mathbf{X}_i, \mathbf{X}_j\right]\right],
\end{aligned} \tag{D-5.3}$$

where $\mathbf{B}(\mathbf{v}, \mathbf{v}) = \nabla_{\mathbf{v}}\mathbf{v} = \sum_{i,j=1}^{n} \frac{1}{2} v_i v_j [\mathbf{X}_i, \mathbf{X}_j] = 0$ by the skew-symmetry of the Lie bracket. Note here that $\dot{v}_i = 0$ for $i = m+1, \ldots, n$. This is a standard result that can be found in [32]. We also need to compute $[\mathbf{Z}, \mathbf{u}]$:

$$[\mathbf{Z}, \mathbf{u}] = \sum_{i=m+1}^{n} \sum_{j=1}^{m} \zeta_i u_j \left[\mathbf{X}_i, \mathbf{X}_j\right]. \tag{D-5.4}$$

We now determine $\mathbf{R}\left(\mathbf{u} + \mathbf{Z}, \mathbf{v}\right)\mathbf{v}$:

$$\begin{aligned}
\mathbf{R}\left(\mathbf{u} + \mathbf{Z}, \mathbf{v}\right)\mathbf{v} &= \frac{1}{4}\left[\left[\mathbf{u} + \mathbf{Z}, \mathbf{v}\right], \mathbf{v}\right] \\
&= \frac{1}{4} \sum_{j,k=1}^{n} v_j v_k \left[\left[\sum_{i=1}^{m} u_i \mathbf{X}_i + \sum_{l=m+1}^{n} \zeta_l \mathbf{X}_l, \mathbf{X}_j\right], \mathbf{X}_k\right].
\end{aligned} \tag{D-5.5}$$

Finally, we need to compute the second-order time derivative of $\mathbf{Z}$. This is easily found to be:

$$\begin{aligned}
\frac{\mathrm{D}^2\mathbf{Z}}{\mathrm{d}t^2} &= \sum_{i=m+1}^{n} \ddot{\zeta}_i \mathbf{X}_i + \sum_{i=m+1}^{n} \sum_{j=1}^{n} \dot{\zeta}_i v_j \left[\mathbf{X}_j, \mathbf{X}_i\right] + \frac{1}{2} \sum_{i=m+1}^{n} \sum_{j=1}^{n} \zeta_i \dot{v}_j \left[\mathbf{X}_j, \mathbf{X}_i\right] \\
&\quad + \frac{1}{4} \sum_{i=m+1}^{n} \sum_{j,k=1}^{n} \zeta_i v_j v_k \left[\mathbf{X}_k, \left[\mathbf{X}_j, \mathbf{X}_i\right]\right].
\end{aligned} \tag{D-5.6}$$

We are now in a position to state the necessary optimality conditions for the problem (D.2.1). By Theorem (D.4.1), the necessary conditions are stated as:

$$\begin{aligned}
0 &= \dddot{v}_i \mathbf{X}_i - \tau^2 u_k \mathbf{X}_k + \ddot{v}_i v_j \left[\mathbf{X}_j, \mathbf{X}_i\right] + \ddot{\zeta}_l \mathbf{X}_l + \dot{\zeta}_l v_i \left[\mathbf{X}_i, \mathbf{X}_l\right] + \zeta_l u_k \left[\mathbf{X}_l, \mathbf{X}_k\right] \\
&\quad + \frac{1}{4}\Big\{ v_h v_i v_j \left[\mathbf{X}_j, \left[\mathbf{X}_h, \mathbf{X}_i\right]\right] + v_i v_j \left[\left[u_k \mathbf{X}_k + \zeta_l \mathbf{X}_l, \mathbf{X}_i\right], \mathbf{X}_j\right] + \zeta_l v_i v_j \left[\mathbf{X}_j, \left[\mathbf{X}_i, \mathbf{X}_l\right]\right] \Big\},
\end{aligned} \tag{D-5.7}$$

where we note that $\nabla_{\mathbf{Z}}\mathbf{u} = \mathbf{B}(\mathbf{Z},\mathbf{u}) = \frac{1}{2}[\mathbf{Z},\mathbf{u}]$ since $\mathbf{Z}$ and $\mathbf{u}$ are independent of the coordinate $\mathbf{q}$. We also used the fact that $\frac{\mathrm{D}^2\mathbf{u}}{\mathrm{d}t^2} = \frac{\mathrm{D}^3\mathbf{u}}{\mathrm{d}t^3}$. In Equation (D-5.7), we use the Einstein convention of summation over each (individual) term, where the indexes h, i, j are summed over $1, \ldots, n$, k over $1, \ldots, m$ and l over $m+1, \ldots, n$. Finally, note that the first term inside the curly brackets is zero, again, by the skew-symmetry of the Lie bracket. Hence, in final form, the necessary conditions are given by:

$$\begin{aligned} 0 &= \dddot{v}_i\mathbf{X}_i - \tau^2 u_k\mathbf{X}_k + \ddot{v}_i v_j[\mathbf{X}_j,\mathbf{X}_i] + \ddot{\zeta}_l\mathbf{X}_l + \dot{\zeta}_l v_i[\mathbf{X}_i,\mathbf{X}_l] + \zeta_l u_k[\mathbf{X}_l,\mathbf{X}_k] \\ &\quad + \frac{1}{4}\Big\{ v_i v_j[[u_k\mathbf{X}_k + \zeta_l\mathbf{X}_l,\mathbf{X}_i],\mathbf{X}_j] + \zeta_l v_i v_j[\mathbf{X}_j,[\mathbf{X}_i,\mathbf{X}_l]] \Big\}, \end{aligned} \tag{D-5.8}$$

If we set $\tau = 0$, this is the second order, dynamic version of the first order, kinematic problem found in [32] (Theorem 6) and [99]. Moreover, if we set $m = n$ (hence, $\mathbf{Z} = 0$) and $\tau = 0$, then the above equation reduces to:

$$\begin{aligned} 0 &= \dddot{v}_i\mathbf{X}_i + \ddot{v}_i v_j[\mathbf{X}_j,\mathbf{X}_i] + \frac{1}{4}\Big\{ v_i v_j v_k[[\mathbf{X}_k,\mathbf{X}_i],\mathbf{X}_j] \Big\} \\ &= \dddot{v}_i\mathbf{X}_i + \ddot{v}_i v_j[\mathbf{X}_j,\mathbf{X}_i], \end{aligned}$$

where the term in curly brackets before the first equality sign is zero by the skew-symmetry of the Lie bracket. This is exactly what is found in [30] and Lemma 4 in [32].

Using the first equation in (D-5.3) as well as Equations (D-5.4) and (D-5.5), it is easy to derive the first order form of the necessary conditions as given in Theorem

(D.4.2). In the form of Theorem (D.4.2), the necessary conditions are:

$$\begin{aligned}
\sum_{i=1}^{n} \dot{q}_i \mathbf{X}_i &= \sum_{i=1}^{n} v_i \mathbf{X}_i \\
\sum_{i=1}^{m} \dot{v}_i \mathbf{X}_i &= \sum_{i=1}^{m} u_i \mathbf{X}_i \\
\left(\frac{\mathrm{D}\boldsymbol{\lambda}_1}{\mathrm{d}t} \right)^{\sharp} &= \frac{1}{2} \sum_{i=m+1}^{n} \sum_{j=1}^{m} \zeta_i u_j \left[\mathbf{X}_i, \mathbf{X}_j \right] \\
&\quad + \frac{1}{4} \sum_{j,k=1}^{n} v_j v_k \left[\left[\sum_{i=1}^{m} u_i \mathbf{X}_i + \sum_{l=m+1}^{n} \zeta_l \mathbf{X}_l, \mathbf{X}_j \right], \mathbf{X}_k \right] \\
\frac{\mathrm{D}\boldsymbol{\lambda}_2}{\mathrm{d}t} &= -\sum_{i} \boldsymbol{\lambda}_1^i \boldsymbol{\Upsilon}_i + \tau^2 \sum_{i=1}^{n} v_i \boldsymbol{\Upsilon}_i,
\end{aligned}$$

where $\boldsymbol{\lambda}_1 = \sum_{i=1}^{n} \boldsymbol{\lambda}_1^i \boldsymbol{\Upsilon}_i$ and $\boldsymbol{\lambda}_2 = \sum_{i=1}^{n} \boldsymbol{\lambda}_2^i \boldsymbol{\Upsilon}_i$ and $\boldsymbol{\Upsilon}_i$, $i = 1, \ldots, n$, is the co-frame for T^*M such that $\Upsilon_i \left(\mathbf{X}_j \right) = \delta_{ij}$.

We now give an example on the three dimensional group of rigid body rotations SO(3). In this case, we have $[\mathbf{X}_1, \mathbf{X}_2] = \mathbf{X}_3$, $[\mathbf{X}_2, \mathbf{X}_3] = \mathbf{X}_1$ and $[\mathbf{X}_3, \mathbf{X}_1] = \mathbf{X}_2$. We note, of course, that for the optimal control problem to be well defined, the system we consider must be controllable. For example, the under-actuated system:

$$\begin{aligned}
\dot{\mathbf{q}} &= v_1 \mathbf{X}_1 + v_2 \mathbf{X}_2 + v_3 \mathbf{X}_3 \\
\tfrac{\mathrm{D}\mathbf{v}}{\mathrm{d}t} &= u_1 \mathbf{X}_1
\end{aligned} \tag{D-5.9}$$

is not controllable and, hence, the system can not be steered between any two arbitrary states. However, the system:

$$\begin{aligned}
\dot{\mathbf{q}} &= v_1 \mathbf{X}_1 + v_2 \mathbf{X}_2 + v_3 \mathbf{X}_3 \\
\tfrac{\mathrm{D}\mathbf{v}}{\mathrm{d}t} &= u_1 \mathbf{X}_1 + u_2 \mathbf{X}_2
\end{aligned} \tag{D-5.10}$$

is controllable. For this case we have $\mathbf{Z} = \zeta_3 \mathbf{X}_3$. After a long derivation, the fourth

order necessary conditions in Equation (D-5.8) for SO(3) can be shown to be:

$$\begin{aligned}
\dddot{v}_1 &- \tau^2 u_1 + \dot{\zeta}_3 v_2 - \zeta_3 u_2 \\
&+ \frac{1}{4}\left[v_1 v_2 u_2 + v_1 v_3 \zeta_3 - u_1\left(v_2^2 + v_3^2\right)\right] = 0 \\
\dddot{v}_2 &- \tau^2 u_2 - \dot{\zeta}_3 v_1 + \zeta_3 u_1 \\
&+ \frac{1}{4}\left[v_1 v_2 u_1 + v_2 v_3 \zeta_3 - u_2\left(v_1^2 + v_3^2\right)\right] = 0 \\
\dddot{v}_3 &+ \ddot{\zeta}_3 + \frac{1}{4}\left[v_1 v_3 u_3 + v_2 v_3 u_2 - \zeta_3\left(v_1^2 + v_2^2\right)\right] = 0.
\end{aligned}$$

D.6 Conclusion

In this appendix, we use geometric tools to derive coordinate-free necessary conditions for an optimal control problem, where the system is under-actuated and evolves on a Riemannian manifold. We apply the results to semi-simple compact Lie groups and relate our results to those appearing previously in the literature. Current research focuses on the non-compact Lie group case, such as SE(3). Future research will focus on adding more complexity to the model. Of particular interest are adding a drift (gravitation) term and the treatment of additional holonomic and/or nonholonomic constraints to the problem (D.2.1).

APPENDIX E

Subject Index

Index

BIBLIOGRAPHY

BIBLIOGRAPHY

[1] "Nasa origins program," URL: http://origins.jpl.nasa.gov, 2004.

[2] "Planet quest," URL: http://planetquest.jpl.nasa.gov/index.html, 2004.

[3] *The Terrestrial Planet Finder: A NASA Origins Program to Search for Habitable Planets*. Jet Propulsion Laboratory Publication 99-003, May 1999.

[4] M. Born and E. Wolf, *Principles of Optics*. New York, NY: Pergamon Press, 1964.

[5] S. Chakravorty, "Design and optimal control of multi-spacecraft interferometric imaging systems," Ph.D. dissertation, Aerospace Engineering, University of Michigan, 2004.

[6] D. C. Hyland, "Interferometric imaging concepts with reduced formation-keeping constraints," *AIAA Space 2001 Conference*, August 2001.

[7] ——, "The inverse huygens-fresnel principle and its implications for interferometric imaging," *The Journal of the Astronautical Sciences*, 2003, under review.

[8] D. P. Scharf, F. Y. Hadaegh, and S. R. Ploen, "A survey of spacecraft formation flying guidance and control (part i): Guidance," *Proceedings of the American Control Conference*, pp. 1733–1739, June 2003.

[9] V. Kapila, A. G. Sparks, J. M. Buffington, and Q. Yan, "Spacecraft formation flying: Dynamics and control," *Proceedings of the American Control Conference*, pp. 4137–4141, June 1999.

[10] S. Marcio, V. Kapila, and Q. Yan, "Adaptive nonlinear control of multiple spacecraft formation flying," *Journal of Guidance, Control, and Dynamics*, vol. 23, no. 3, pp. 385–390, May-June 2000.

[11] J. Lawton, R. W. Beard, and F. Y. Hadaegh, "An adaptive approach to satellite formation flying with relative distance constraints," *Proceedings of the American Control Conference*, pp. 1545–1549, June 1999.

[12] P. K. C. Wang and J. Yee, "Synchronized rotation of multiple autonomous spacecraft with rule-based controls: Experimental study," *Journal of Guidance, Control and Dynamics*, vol. 24, no. 2, pp. 352–359, March-April 2001.

[13] P. K. C. Wang, F. Y. Hadaeg, and K. Lau, "Synchronized formation rotation and attitude control of multiple free-flying spacecraft," *Journal of Guidance, Control and Dynamics*, vol. 22, no. 1, pp. 28–35, January-February 1999.

[14] R. W. Beard and F. Y. Hadaegh, "Finite thrust control for satellite formation flying with state constraints," *Proceedings of the American Control Conference*, pp. 4383–4387, June 1999.

[15] ——, "Fuel optimized rotation for satellite formations in free space," *Proceedings of the American Control Conference*, pp. 2975–2979, June 1999.

[16] R. W. Beard, T. W. McLain, and F. Y. Hadaegh, "Fuel equalized retargeting for separated spacecraft interferometry," *Proceedings of the American Control Conference*, pp. 1580–1584, June 1998.

[17] E. M. C. Kong, D. W. Miller, and R. J. Sedwick, "Exploiting orbital dynamics for interstellar separated spacecraft interferometry," *Proceedings of the 1999 American Control Conference*, pp. 4153–4157, June 2-4 1999.

[18] I. I. Hussein, D. J. Scheeres, and D. C. Hyland, "Interferometric observatories in earth orbit," *2003 AAS/AIAA Space Flight Mechanics Meeting*, February 9–13 2003.

[19] ——, "Interferometric observatories in earth orbit," *Journal of Guidance, Control and Dynamics*, vol. 27, no. 2, pp. 297–301, 2004.

[20] I. I. Hussein and D. J. Scheeres, "Effects of orbit perturbations on a class of earth-orbiting interferometric observatories," *2004 AAS/AIAA Space Flight Mechanics Meeting*, February 2004, paper No. AIAA04-210.

[21] R. H. Vassar and R. B. Sherwood, "Formationkeeping for a pair of satellites in a circular orbit," *Journal of Guidance*, vol. 8, no. 2, pp. 235–242, 1985.

[22] A. B. DeCou, "Orbital station-keeping for multiple spacecraft interferometry," *The Journal of the Astronautical Sciences*, vol. 39, no. 3, pp. 283–297, July-September 1991.

[23] H. Schaub and K. T. Alfriend, "j_2 invariant relative orbits for spacecraft formations," *Celestial Mechanics and Dynamical Astronomy*, vol. 79, pp. 77–95, 2001.

[24] H. Schaub, S. R. Vadali, J. L. Junkins, and K. T. Alfriend, "Spacecraft formation flying control using mean orbital elements," *The Journal of the Astronautical Sciences*, vol. 48, no. 1, pp. 69–87, 2000.

[25] A. Robertson, T. Corazzini, and J. P. How, "Formation sensing and control techniques for a separated spacecraft interferometer," *Proceedings of the American Control Conference*, pp. 1574–1579, 1998.

[26] K. Lau, S. Lichten, L. Young, and B. Haines, "An innovative deep space application of gps technology for formation flying spacecraft," *Guidance, Navigation and Control Conference*, pp. 3819–3828, July 1996.

[27] J. R. Carpenter, "A preliminary investigation of decentralized control for satellite formations," *IEEE Aerospace Conference Proceedings*, vol. 7, pp. 63–74, 2000.

[28] W. Kang, A. Sparks, and S. Banda, "Coordinated control of multisatellite systems," *Journal of Guidance, Control and Dynamics*, vol. 24, no. 2, pp. 360–368, March-April 2001.

[29] I. I. Hussein, D. J. Scheeres, and D. C. Hyland, "Optimal formation control for imaging and fuel usage," *2005 AAS/AIAA Space Flight Mechanics Meeting*, 2005, to appear.

[30] L. Noakes, G. Heinzinger, and B. Paden, "Cubic splines on curved spaces," *IMA Journal of Mathematical Control and Information*, vol. 6, no. 4, pp. 465–473, 1989.

[31] P. Crouch and J. W. Jackson, "Dynamic interpolation for linear systems," *29th IEEE Conference on Decision and Control*, pp. 2312–2314, 1990.

[32] P. Crouch and F. Silva-Leite, "Geometry and the dynamic interpolation problem," *Proceedings of the 1991 American Control Conference*, pp. 1131–1136, 1991.

[33] ——, "The dynamic interpolation problem: On riemannian manifolds, lie groups and symmetric spaces," *Journal of Dynamic and Control Systems*, vol. 1, no. 2, pp. 177–202, 1995.

[34] P. Crouch, F. Silva-Leite, and M. Camarinha, "A second order riemannian variational problem from a hamiltonian perspective," 1998, pre-print of the Mathematics Department, University of Coimbra, N. 98-17, 1998.

[35] ——, "Hamiltonian structure of generalized cubic polynomials," *Proceedings of the IFAC Workshop on Lagrangian and Hamiltonian Methods for Nonlinear Control*, pp. 13–18, 2000.

[36] P. W. Gorham, W. M. Folkner, and G. H. Blackwood, "Enabling concepts for a dual spacecraft formation-flying optical interferometer for nasa's st3 mission," *Proc. of the 1999 Dana Pt. Conf. on Optical Interferometry*, vol. 194, p. 359, 1999.

[37] A. E. Bryson and Y. Ho, *Applied Optimal Control*. New York, NY: Hemisphere Publishing Corporation, 1975.

[38] I. I. Hussein and A. M. Bloch, "Dynamic coverage optimal control for interferometric imaging spacecraft formations," *43rd IEEE Conference on Decision and Control*, pp. 1812–1817, December 2004.

[39] ——, "Dynamic coverage optimal control for interferometric imaging spacecraft formations (part ii): The nonlinear case," *2005 American Control Conference*, 2005, to appear.

[40] ——, "Dynamic interpolation on riemannian manifolds: An application to interferometric imaging," *Proceedings of the 2004 American Control Conference*, pp. 413–418, July 2004.

[41] J. Milnor, *Morse Theory*. Princeton, NJ: Princeton University Press, 2002.

[42] A. Bloch, J. Baillieul, P. E. Crouch, and J. E. Marsden, *Nonholonomic Mechanics and Control*. New York, NY: Springer-Verlag, 2003.

[43] I. I. Hussein and A. M. Bloch, "Optimal control on riemannian manifolds with potential fields," *43rd IEEE Conference on Decision and Control*, December 2004, 1982–1987.

[44] I. I. Hussein, A. M. Bloch, D. J. Scheeres, and N. H. McClamroch, "Optimal fuel-image motion planning for a class of dual spacecraft formations," *2005 American Control Conference*, 2005, to appear.

[45] I. I. Hussein, D. J. Scheeres, and D. C. Hyland, "Control of a satellite formation for imaging applications," *Proceedings of the 2003 American Control Conference*, pp. 308–313, June 2003.

[46] J. S. Bay, *Fundamentals of Linear State Space Systems*. Boston, MA: McGraw-Hill, 1999.

[47] W. J. Koon, J. E. Marsden, J. Masdemont, and R. M. Murray, "j_2 dynamics and formation flight," *Proceedings of AIAA Guidance, Navigation, and Control Conference*, August 2001, paper No. AIAA 2001-4090.

[48] R. Bhatt, C. P. Tang, and V. Krovi, "Geometric motion planning and formation optimization for a fleet of nonholonomic wheeled mobile robots," *Proceedings of the 2004 IEEE International Conference on Robotics and Automation*, pp. 3276–3281, 2004.

[49] F. Bullo and R. M. Murray, *Proportional Derivative (PD) Control on the Euclidean Group*. California Institute of Technology, 1995, cDS Technical Report 95-010.

[50] A. L. Onishchik and E. B. Vinberg, *Lie Groups and Lie Algebras I*, ser. Encyclopedia of Mathematical Sciences. Berlin, Germany: Springer-Verlag, 1991, vol. 20, ch. Foundations of Lie Theory.

[51] F. Bullo and A. D. Lewis, *Geometric Control of Mechanical Systems*. Springer-Verlag, 2004.

[52] F. Warner, *Foundations of Differentiable Manifolds and Lie Groups*. Glenview, IL: Scott, Foresman, 1973.

[53] I. I. Hussein and A. M. Bloch, "Optimal control of under-actuated systems: A coordinate-free approach," *2005 American Control Conference*, 2005, to appear.

[54] I. I. Hussein, D. J. Scheeres, and D. C. Hyland, "Formation path planning for optimal fuel and image quality for a class of interferometric imaging missions," *2003 AAS/AIAA Space Flight Mechanics Meeting*, February 9–13 2003.

[55] M. Camarinha, "The geometry of cubic polynomials in riemannian manifolds," Ph.D. dissertation, Universidade de Coimbra, 1996.

[56] D. C. Hyland, "Formation control for optimal image reconstruction in space imaging systems," *International Symposium on Formation Flying*, October 29–31 2001.

[57] ——, "Self-reliant control systems for space optics applications," Universities Space Research Association, Albuquerque, NM, Tech. Rep., September 2001.

[58] A. Bloch and P. Crouch, "Nonholonomic and vakonomic control systems on riemannian manifolds," *Fields Institute Communications*, vol. 1, pp. 25–52, 1993.

[59] M. Spivak, *A Comprehensive Introduction to Differential Geometry*. Oxford: Publish or Perish Inc., 1979, vol. 1.

[60] W. M. Boothby, *An Introduction to Differentiable Manifolds and Riemannian Geometry*. Orlando, FL: Academic Press Inc., 1975.

[61] F. Y. Hsiao and D. J. Scheeres, "Design of spacecraft formation orbits relative to a stabilized trajectory," *2003 AAS/AIAA Space Flight Mechanics Meeting*, February 9-13 2003.

[62] L. Mandel and E. Wolf, *Optical Coherence and Quantum Optics*. New York, NY: Cambridge University Press, 1995.

[63] J. H. Ginsberg, *Advanced Engineering Dynamics*. Cambridge, United Kingdom: Cambridge University Press, 1998.

[64] E. B. Lee and L. Markus, *Foundations of Optimal Control Theory*. New York, NY: John Wiley & Sons, Inc., 1967.

[65] V. I. Shalashilin and E. B. Kuznetsov, *Parametric Continuation and Optimal Parametrization in Applied Mathematics and Mechanics*. Dordrecht, The Netherlands: Kluwer Academic Publishers, 2003.

[66] S. E. Gano and et. al, "A baseline study of a low-cost, high-resolution, imaging system using wavefront reconstruction," *AIAA Space 2001 Conference*, August 2001.

[67] Y. J. Cao, L. Jiang, and Q. H. Wu, "An evolutionary programming approach to mixed-variable optimization problems," *Applied Mathematical Modeling*, vol. 24, pp. 931–942, April 2000.

[68] W. A. Sutherland, *Introduction to Metric and Topological Spaces.* Oxford: Oxford Science Publications, 1975.

[69] A. E. Roy, *Orbital Motion.* Philadelphia, PA: Institute of Physics Publishing, 1998.

[70] C. Chen, *Linear System Theory and Design.* New York: Oxford University Press, 1984.

[71] H. Townes, "Noise and sensitivity in interferometry," in *Principles of Long Baseline Interferometry*, P. Lawson, Ed. JPL Publication 00-009, 2000, ch. 4.

[72] R. H. Kingston, "Detection of optical and infrared radiation," *The Journal of Optical Society of America B*, vol. 4, pp. 1450–1741, 1978.

[73] L. Lepetit, G. Chériaux, and M. Joffre, "Linear techniques of phase measurement by femtosecond spectral interferometry for applications in spectroscopy," *The Journal of Optical Society of America B*, vol. 12, no. 12, December 1995.

[74] C. Iaconis and I. Walmsley, "Self-referencing spectral interferometry for measuring ultrashort optical pulses," *IEEE Journal of Quantum Mechanics*, vol. 35, no. 4, April 1999.

[75] H. O. Fattorini, *Infinite Dimensional Optimization and Control Theory.* New York, NY: Cambridge University Press, 1999.

[76] J. E. Marsden, G. Misiolek, J. Ortega, M. Perlmutter, and T. S. Ratiu, "Hamiltonian reduction by stages," http://www.cds.caltech.edu/~marsden/volume/big_stages/Big_Stages_4-13-03.pdf.

[77] J. C. Simo, N. Tarnow, and K. K. Wong, "Exact energy-momentum conservinng algorithms and symplectic schemes for nonlinear dynamics," *Computatioonal Methods in Applied Mechanics and Engineering*, pp. 63–116, 1992.

[78] R. I. McLachlan and G. R. Quispel, "Six lectures on the geometric integration of odes," in *Foundations of Computational Mathematics*, R. Devore, A. Iserles, and E. Sli, Eds. Cambridge University Press, 2001, ch. 7.

[79] O. Junge, J. E. Marsden, and O. B. Sina, "Discrete mechanics and optimal control," *IFAC Congress, Praha*, 2005.

[80] R. Abraham, J. E. Marsden, and T. S. Ratiu, *Manifolds, Tensors Analysis, and Applications*. New York, NY: Springer-Verlag, 1988.

[81] W. L. Burke, *Applied Differential Geometry*. New York, NY: Cambridge University Press, 1985.

[82] M. Crampin and F. A. E. Pirani, *Applicable Differential Geometry*. Cambridge: Cambridges University Press, 1986.

[83] M. P. do Carmo, *Differential Geometry of Curves and Surfaces*. New Jersey: Prentice-Hall, Inc., 1976.

[84] ——, *Riemannian Geometry*. Boston, MA: Birkhauser, 1992.

[85] S. Kobayashi and K. Nomizu, *Foundations of Differential Geometry*. New York, NY: Interscience Publishers, 1963.

[86] R. Abraham and J. E. Marsden, *Foundations of Mechanics*. New York, NY: W. A. Benjamin, Inc., 1967.

[87] V. I. Arnold, *Mathematical Methods for Classical Mechanics*. New York, NY: Springer-Verlag, 1978.

[88] J. C. Monforte, *Geometric, Control and Numerical Aspects of Nonholonomic Systems*. Berlin, Germany: Springer-Verlag, 2002.

[89] J. E. Marsden, *Lectures on Mechanics*. Cambridge: Cambridge University Press, 1992.

[90] A. A. Agrachev and Y. Sachkov, *Control Theory from the Geometric Viewpoint*. New York, NY: Springer-Verlag, 2004.

[91] V. Jurdjevic, *Geometric Control Theory*. New York, NY: Cambridge University Press, 1997.

[92] J. E. Marsden and T. S. Ratiu, *Introduction to Mechanics and Symmetry*. New York, NY: Springer-Verlag, 1999.

[93] R. M. Murray, Z. X. Li, and S. S. Sastry, *A Mathematical Introduction to Robotic Manipulation*. Boca Raton, FL: CRC Press, 1994.

[94] F. Silva-Leite, M. Camarinha, and P. Crouch, "Elastic curves as solutions of riemannian and sub-riemannian control problems," *Mathematics of Control, Signals and Systems*, vol. 13, pp. 140–155, 2000.

[95] C. W. Misner, K. S. Thorne, and J. A. Wheeler, *Gravitation*. New York, NY: W. H. Freeman and Company, 1973.

[96] M. Žefran, V. Kumar, and C. Croke, "Metrics and connections for rigid-body kinematics," *the International Journal of Robotics Research*, vol. 18, no. 2, 1999.

[97] F. Bullo, R. M. Murray, and A. Sarti, *Control on the Sphere and Reduced Attitude Stabilization*. California Institute of Technology, 1995, cDS Technical Report 95-005.

[98] R. Brockett, "Control theory and singular riemannian geometry," in *New Directions in Applied Mathematics*, P. J. Hilton and G. S. Young, Eds. Springer-Verlag, 1981, pp. 11–27.

[99] A. Bloch, P. Crouch, and T. Ratiu, "Sub-riemannian optimal control problems," *Fields Institute Communications*, vol. 3, pp. 35–48, 1994.